# RÉSUMÉ

Les matériaux terrigènes du flysch « syn-orogènique » de Zoumi, se sont mise en place dans un bassin transporté de type « Thrust-top basin » au toit du prisme d'accrétion du Rif Externe au cours du Miocène inférieur-moyen. Les dépôts flyschoides syn-orogéniques du bassin ont été examinés par des études pétrographiques et géochimiques afin de définir les conditions paléoclimatiques de la zone source, l'intensité de l'érosion des roches mères et les effets de tri physique et de recyclage, et caractériser la composition, le système de routage et le cadre géodynamique du bassin de Zoumi. Quarante-trois échantillons de grès et quarante-cinq échantillons de marnes ont été prélevés à partir de six sections stratigraphiques mesurées. Ces échantillons ont été analysés en utilisant XRD, XRF, la spectrométrie de masse à plasma à couplage inductif (ICP-MS) pour les marnes et l'analyse modale pétrographique pour les grès. Les flyschs du Miocène inférieur-moyen du bassin de zoumi ont été défini, selon leur teneur minéralogique comme des sublitharénites et des quartzarénites. Les grains détritiques sont généralement sub-angulaires à subarrondis, faiblement triés et riches en grains de quartz. Les résultats de l'analyse modale par comptage de points a conduit à une provenance mixte des matériaux térrigènes alimentant le bassin de Zoumi :1) de l'intérieur du craton et ; 2) du recyclage de la chaîne orogénique, avec un apport important de sédiments à faible maturité (first cycle supply) et un faible recyclage sédimentaire.

D'après les analyses géochimiques, les marnes sont enrichies en $Al_2O_3$, $Fe_2O_3$, CaO et $TiO_2$ et très appauvries en d'autres oxides majeurs par rapport à la composition des Argiles Australiennes Post-Archéennes (PAAS prise comme référence). Selon les diagrammes de Harker, les courbes régressives montrent une très forte corrélation positive entre $SiO_2$, $Al_2O_3$, et $TiO_2$, et une corrélation négative entre $SiO_2$ et CaO. Les marnes sont classées géochimiquement comme des argiles, des argiles riches en fer et des wackes. Différents diagrammes discriminatoires ont été utilisés pour révéler le cadre géodynamique du bassin, les conditions paléoclimatiques et l'intensité d'altération qui caractérisent les zones nourricières. L'indice chimique d'altération (CIA) et l'indice chimique d'érosion (CIW) du Miocène inférieur-moyen varient de 50 à 80%, indiquant un degré d'altération faible à modéré dans les zones sources compatible avec un état d'altération non stationnaire sous des conditions paléoclimatiques humides et pluvieuses. Localement, les valeurs de CIA sont plus élevées (>80) caractéristiques d'une érosion intense dans les zones nourricières, pouvant être attribuée à une intensification de l'activité tectonique au niveau de l'arrière-pays et à des conditions climatiques plus humides et pluvieuses.

La combinaison des valeurs ICV-CIA, Al2O3-Zr-TiO2 et Th/Sc - Zr/Sc suggère que les matériaux terrigènes déposés dans le bassin sont chimiquement immatures et qu'elles ont subi un tri physique et un recyclage modeste reflétant qu'elles ont été peu transportées à destination finale de dépôt et leur accumulation dans le bassin. Plusieurs rapports géochimiques ($Al_2O_3/TiO_2$, La/Th, Cr/Th, Th/Sc, Zr/Sc) ainsi que les courbes de normalisation des terres rares (REE) par rapport aux valeurs de celles des Chondrites qui présentent une allure horizontale pour les terres rares lourdes, un enrichissement des terres rares légères et une anomalie négative très notable de l'Europium (Eu) suggérant, par conséquent, une source d'apport à dominante felsique (affinité crustale). Cependant, les diagrammes V-Ni-La*4, V-Ni-Th*10 et Th/Sc vs. Cr/Th n'excluent pas la contribution d'une source de nature mafique matérialisée par l'existence de plusieurs affleurements ophiolitiques parsemés le long du Mesorif (i.e. la suture Ophiolitique Mésorifaine de Michard et al., 2014).

**Mots clés** : Oxides majeurs, Eléments traces, Terres rares (REE), , altération, Tri physique et recyclage, conditions paléoclimatiques, Provenance, Cadre géodynamique, Rif Externe, Chaîne du Rif, Maroc


**N°d'ordre : 170 / 2018**

**« Unravelling source-to-sink processes in lower-middle Miocene Zoumi thrust-top basin (External Rif, Morocco): new constraints from sedimentary petrology, sedimentology and geodynamic implications »**

**EL MOURABET MOHAMED**

**N° d'ordre : 170 / 2018**


**UNIVERSITE SULTAN MOULAY SLIMANE**

**Faculté des Sciences et Techniques**

**Béni-Mellal**

*Centre d'Études Doctorales : Sciences et Techniques*

*Formation Doctorale :* **Ressources Naturelles Environnement et santé**


**THÈSE**

Présentée par

**EL MOURABET MOHAMED**

Pour l'obtention du grade de

**DOCTEUR**

*Spécialité : Géologie*

*Option : Pétrographie-Géochimie*

**« Unravelling source-to-sink processes in lower-middle Miocene Zoumi thrust-top basin (External Rif, Morocco): new constraints from sedimentary petrology, sedimentology and geodynamic implications».**

**Soutenue le 23/06/2018 à 10h devant la commission d'examen:**

| | | |
|---|---|---|
| **M. EL BAGHDADI** | Professeur, Université Sultan Moulay Slimane, F.S.T. Beni-Mellal, Maroc | Président |
| **E. BACHAOUI** | Professeur, Université Sultan Moulay Slimane, F.S.T. Beni-Mellal, Maroc | Rapporteur |
| **M. RHALMI** | Professeur, Université Sultan Moulay Slimane, F.S.T. Beni-Mellal, Maroc | Rapporteur |
| **D. CHAFIKI** | Professeur, Université Cadi Ayyad, F.S.T. Semlalia-Marrakech, Maroc | Examinateur |
| **A. BARAKAT** | Professeur, Université Sultan Moulay Slimane, F.S.T. Beni-Mellal, Maroc | Directeur de thèse |
| **J. RAIS** | Professeur, Université Sultan Moulay Slimane, F.S.T. Beni-Mellal, Maroc | Co-Directeur de thèse |

***"In memory of my father"***

# TABLE OF CONTENTS

# PAPERS AND ORAL COMMUNICATIONS

## I/ Published Papers:

1. El Mourabet M., Barakat A., Mohamed Najib Zaghloul, El Baghdadi M. (2018a) Geochemistry of the Miocene Zoumi flysch thrust-top basin (External Rif, Morocco): new constraints on source area weathering, recycling processes, and paleoclimate conditins. Arabian Journal of Geosciences, 11:126, https://doi.org/10.1007/s12517-018-3465-y

2. El Mourabet M., Ahmed Barakat A., Jamila Rais J., Zaghloul M.N. & Atouabat A. (2018b) Petrology of lower-middle Miocene Zoumi Flysch Fm. (Mesorif sub-domain, Rif belt, Morocco): first evidence of mixed mode provenance and geodynamic setting. Arabian Journal of Geosciences, 11:209, https://doi.org/10.1007/s12517-018-3485-7

3. Frizon de Lamotte D., Zaghloul M.N., Haissen F., Mohn G., Leprêtre R., Gimeno-Vives O., Atouabat A., El Mourabet M., Abassi A. (2017) Rif externe : comment comprendre et expliquer le chaos apparent ? Géologues, 2017, 194.

## II/ Oral communications:

1. El Mourabet M., Barakat A., Rais R., Zaghloul M.N. (2017a) New petrographic constraints for a mixed mode provenance of Middle Miocene syn-orogenic Zoumi Sandstone suites (External Rif, Mesorif Sub-Domain, Morocco): Implication for paleoclimate and geodynamic context. The First International ASRO Geological Congress [ASRO – GC – 2017], El Jadida, Morocco.

2. El Mourabet M., Barakat A., El Baghdadi M., Zaghloul M.N. (2017b) Geochemistry of fine-grained syn-orogenic Zoumi flysch (External Rif, Mesorif sub-Domain, Morocco): New constraints for paleoweathering, geological processes and geodynamic setting. The First International ASRO Geological Congress [ASRO – GC – 2017], El Jadida, Morocco.

3. El Mourabet M., Ahmed Barakat A., Rais J., Zaghloul M.N. (2017c) Sedimentology of Middle Miocene syn-orogenic Zoumi Flysch (External Rif, Mesorif Sub-Domain, Morocco): Sedimentary processes and Depositional palaeoenvironments. The First International ASRO Geological Congress [ASRO – GC – 2017], El Jadida, Morocco.

# AKNOWLEDGEMENTS

Firstly, I would like to thank Pr. Ahmed Zeghay, Dean of Faculty of Sciences and Techniques of Beni Mellal for giving me the opportunity to undertake this PHD research project at the Faculty of Sciences and Techniques of Beni Mellal.

I would like to acknowledge the support and dedication I have received from my supervisors Professor Ahmed BARAKAT and Professor Jamila RAISS. Pr BARAKAT, from the first meeting to the end of this project, your enthusiasm and tireless efforts in helping to put this project together have been inspirational. Thanks for providing an excellent topic at the drop of a hat and allowing me to undertake all of the aspects I wanted in this project. Pr RAIS, thank you for all of the time and effort you have provided throughout. Your encouragement and expert knowledge have helped me greatly and your input to this project has been invaluable.

My great Thanks to Pr. Khalid Habbari Scientific Research vice Dean of the Faculty of Sciences and Techniques of Beni Mellal for his help, great support and make me believe on the challenge.

Warm thanks to Pr. Mohamed EL BAGHDADI, thank you for all of your help over the duration of this project and for taking the time to Share and discuss with me.

Professor Zaghloul Mohamed Najib, on the behalf of our old memories on worldwide regional geology (Shankar Mitra, Suppe, Medwedeff, Dahrlstrom,…….). Believe me, our long and tedious discussions have faster updated my geological background on the Rif cordillera and the alpine Mediterranean Belts as well. Be sur, it was a big challenge and we managed it well.

I would like to thank members of my PhD Committee: Pr Mohamed EL BAGHDADI, Pr El Mostapha BACHAOUI, Pr Faouzia Haissen, Pr Mohamed RHALMI, Pr Driss CHAFIKI for their thorough and incredibly helpful review of my work and for contributing timely and healthy criticism and inspirations. Their insight was very much appreciated.

Thanks to Pr. Sajieddine for all of the help provided in XRD laboratory analyses of my samples.

I am very grateful to the staff from the Department of Earth Sciences who helped me out during all stages of this project.

I am greatly appreciative to Lhou MAACHA, MANAGEM GROUP Head Manager and Pr Faouzia Haissen for all of the help provided in Trace and Rare Earth Elements laboratory analyses of my samples.

Finally, I would also like to acknowledge and thank my family, who has always been a constant source of support and inspiration: mom, Fatima, Loubna, Anass, Rim and My Uncle Al Moundir, Samir, Karim, Mohamed. And most of all, I'd like to thank my lovely wife and best friend, Fatima, for her consistent love and support over the years. Fatima has walked beside me every step of the way and has blessed my life beyond description.

# ABSTRACT

The Zoumi Basin was generated in a collisional tectonic setting during the Lower-Middle Miocene. The syn-orogenic flysch deposits of the basin have been well investigated by petrographic and geochemical studies to infer source area palaeoclimatic conditions, the intensity of source rocks palaeoweathering and mechanical sorting and recycling effects and to characterize the composition, source to sink routing system, and tectonic setting of the Zoumi flysch. Forty-three sandstone samples and forty-five mudstone samples have been gathered from six measured stratigraphic sections. These samples have been analyzed using XRD, XRF, Inductively Coupled Plasma-Mass Spectrometry (ICP-MS) for mudrocks and petrographic investigation for sandstones. The Lower-Middle Miocene Zoumi flysch is defined as sublitharenites and quartzarenites according to mineralogical content. Detrital grains are commonly subangular to subrounded, poorly sorted, and rich in quartz grains. Point counting modal analysis leads to craton interior and recycled orogen provenance with significant first-cycle sediment supply, and low sedimentary recycling.

The mudrocks are enriched in $Al_2O_3$, $Fe_2O_3$, CaO and $TiO_2$ relative to PAAS and depleted in the other mobile major elements. There are high positive correlations between $SiO_2$, $Al_2O_3$, and $TiO_2$, and negative correlations between $SiO_2$ and CaO. Geochemically, the mudstones are mainly classified as shales, Fe-shales and wackes. Various discriminant diagrams were used to reveal the inferred tectonics, source area palaeoweathering intensity and palaeoclimatic conditions. Chemical index of alteration (CIA) and chemical index of weathering (CIW) values for Lower-Middle Miocene vary from *50 to 80 %* indicating low- to moderate degree of source area weathering compatible with non-steady-state weathering under wet and humid palaeoclimatic conditions. Locally (Zoumi mid-section) CIA values are higher (>80) reflecting intense source area weathering, which may be attributed to high tectonic impulses and more humid conditions during deposition.

The combination of ICV-CIA, $Al_2O_3$-Zr-$TiO_2$ and Th/Sc-Zr/Sc values suggests the bulk rock is chemically immature and has experienced modest physical sorting and recycling reflecting little transportation until the final deposition. Several chemical ratios ($Al_2O_3/TiO_2$, La/Th, Cr/Th, Th/Sc, Zr/Sc) as well as chondrite-normalized REE patterns with flat HREE, LREE enrichment, and negative Eu anomaly, suggest a dominant felsic rock sources. However, V-Ni-La*4; V-Ni-Th*10 and Th/Sc vs. Cr/Th plots don't exclude a mafic supply source nature which is evidenced by numerous ophiolitic outcrops scattered throughout the Mesorifan Subdomain (Mesorifan Ophiolitic Suture Zone).

**Key words**: Trace elements, REE, Major oxides, Source area weathering, sorting and recycling, palaeoclimate conditions, Provenance, Geodynamic setting, External Rif, Rif belt, Morocco

# RESUME ETENDU

## « *Identification des processus géologiques dans le bassin « transporté » de Zoumi (Miocène inférieur-moyen) (Rif externe, Maroc) : Nouvelles contraintes de la pétrologie sédimentaire, sédimentologie et implications géodynamiques »*

Les matériaux terrigènes du flysch « syn-orogènique » de Zoumi, se sont mise en place dans un bassin transporté de type « Thrust-top basin » au toit du prisme d'accrétion du Rif Externe au cours du Miocène inférieur-moyen. Ce bassin a fait l'objet d'une analyse sédimentologique combinée à une investigation pétrologique fine (i.e. pétrographique et géochimique) afin de : ***i)*** définir leur composition et de bien comprendre les divers processus géologiques intervenus au cours de leur parcours depuis la source jusqu'à leur mise en place dans le bassin. ***ii)*** retracer une telle évolution reconnue comme *« source to sink processes »* des auteurs anglo-saxons est de nos jours l'une des approches multidisciplinaires la plus fréquente dans la littérature scientifique internationale.

Une telle approche inclusive permet une analyse « multi-layers » des divers proxies chimiques, minéralogiques, pétrographiques et physiques pour mieux cerner et comprendre la problématique compliquée des processus de surface terrestre. Ces derniers nécessitent une reconstruction des variations paléoclimatiques de l'archive sédimentaire ancien en relation avec la géographie physique et modelage des reliefs suite aux divers interactions tectono-morphologiques contrôlant les fluctuations de l'intensité de l'érosion à la source. Celles-ci sont elle-même tributaires des divers processus d'altération chimique et physique entretenant l'acheminement du produit de l'érosion, son tri, recyclage et son routage vers le bassin. L'interaction entre processus géodynamiques crustaux et processus de surface résulterait de l'inversion des bassins suite à des changements paléogéographiques du premier ordre (Rifting/Drifting *versus* Subduction/Collision) suivis des implications du second ordre, à l'échelle régionale, tel que la mise en place et l'empilement des nappes tectoniques dans un prisme orogénique progressant vers l'ouest et le sud-ouest depuis le Miocène inférieur. Cette évolution est contemporaine de l'extension progressive de la Mer *Algéro-provençale* et son extrémité occidentale (i.e Mer *d'Alboran*) depuis le début du Miocène moyen. Durant cette période, le raccourcissement horizontal du Rif externe induira d'une part une réactivation tectonique et la création des reliefs à l'arrière-pays de la chaine et d'autre part une mise en place des bassins transportés du type *« Thrust-top basin »* au toit du prisme structuré (i.e. nappes structurées intra-rifaines et celles qui formaient l'avant Fosse Mésorifaine d'âge Jurassique-Oligocène supérieur), et ce probablement dès l'Eocène supérieur?. Néanmoins, cette structuration précoce reste encore mal définie, d'où la nécessité pour mieux comprendre le timing de la chaine, de préciser l'âge exacte de la déformation de « l'avant fosse » du rif externe et celui du début de sédimentation dans les bassins satellitaires transportés (e.g. Bassin de Zoumi) au toit du prisme d'accrétion formé de dépôts de l'avant Fosse mésorifaine structurée avant le Miocène inferieur âge du premier dépôt du bassin type «Thrust-top basin » sus-jacent.

L'analyse verticale des séquences turbiditiques de Zoumi a été effectuée sur des sections lithostratigraphiques mesurées. La nature lithologique, l'architecture et l'épaisseur des bancs, les structures sédimentaires primaires et secondaires ainsi que l'orientation des marqueurs de courant. La totalité de la section a été par la suite subdivisée selon la récurrence des lithofaciès en considérant que chaque groupe de bancs similaires est attribué à un lithofaciès bien défini. Les environnements de dépôt ont été définis, par la suite, sur la base des associations de faciès et la comparaison des attributs sédimentaires (lithofaciès, association de faciès, cyclicité, les relations verticales, etc...) avec les faciès prédéfinis pour les différents modèles de cônes sous-marins. Cinq principales associations de faciès ont été identifiées à partir de l'analyse sédimentologique des quatre sections étudiées dans le bassin de Zoumi : 1) associations de plaine du bassin ; 2) associations de bordure de lobe ; 3) associations de lobe ; 4) associations de chenal :

- L'association de *dépôts de plaine de bassin* est caractérisée par des sédiments à granulométrie fine, organisés selon des paquets de 3 à 5 m d'épaisseur avec alternance de bancs gréseux minces et des marnes argileuses massives et nodulaires, de couleur gris clair et des grés silteux à horizons glauconieux. Les bancs de grés présentent des séquences de Bouma à base et sommet tronqués. Les structures primaires fréquentes sont les lamines parallèles, ondulées, obliques, entrecroisées, ou sous forme de rides. Le rapport sable/argile est de **1/4,** et montre une prédominance des marnes et argiles. Cette association a été déposée par gravité suite à un courant turbiditique de faible densité. Les dépôts marnoargileux se sont déposées par accumulation lente des marnes et matériaux biogéniques.

- L'association de dépôts de *bordure de lobe* représente le prolongement distal des lobes à bacs gréseux à granulométrie moyenne ou la partie proximale des dépôts de plaine de bassin assurant la transition entre les deux environnements dépositionnels. Cette association présente une rythmicité cyclique verticale marquée par une variation stratale des épaisseurs de bancs gréseux et marneux. Le rapport sable/argile dominant est de **2/3**. Les bancs de grés sont centimétriques (10-40 cm) et exceptionnellement métriques (1-2.5m). Les bancs gréseux massifs peuvent éventuellement montrer un granoclassement diffus, et s'organisent selon des bancs amalgamés (*Homolithic packages*) avec des épaisseurs de bancs entre 25cm à 50cm. Les structures primaires les plus fréquentes sont le granoclassement, les laminations parallèles, obliques, convolutées et sinusoïdales. Les bancs gréseux présentent des séquences de Bouma à bases tronquées et rarement complètes. Les dépôts de cette association s'organisent selon des séquences positives grano-stratocroissantes. Le processus de dépôt des couplets grés/marnes à bancs moyens à épais (C2 de Pickering et al. 1986, 2015) s'est effectué selon des courants turbiditiques de moyenne à forte densité. Les bancs épais massifs se sont déposés soit par des courants turbiditiques forts avec des vitesses très rapide de dépôt empêchant le développement des lamines (Lowe 1988; Arnott and Hand 1989; Allen 1991; Hiscott et al. 1997a), soit à partir de courants turbiditiques très concentrés (*Concentrated density flows* de Pickering et al., 1986a, 1989, 2015).
- L'association de dépôts de *Lobe* est représentée par des bancs gréseux massifs, décimétriques à métriques empilés dans des paquets décamétriques à hectométriques avec ou sans intercalations de niveaux minces marno-silteux. Le rapport gés/argile est de **4/1**. Les bacs massifs gréseux présentent généralement une abondance à leurs bases ou au sommet d'un intense remaniement de galets mous marneux. Les structures sédimentaires secondaires sont représentées par des « *dish* » et « *pipe* » reconnues comme structure d'échappement d'eau. Les dépôts de lobes sont organisés selon des rythmes strato-granocroissants reflétant une réactivation tectonique avec excès de reliefs et une forte érosion dans

l'arrière-pays non compensée par la subsidence dont résulte un système depositionel progradant vers le bassin. L'architecture des lobes dans le bassin serait contrôlée par deux facteurs majeurs : (1) l'irrégularité du substratum due à l'activité des chevauchements majeurs responsables de la mise en place des nappes de l'avant fosse du Mesorif au mur du bassin de Zoumi; (2) la proximité de la source d'apport des matériaux terrigènes. Ces dépôts de lobes reflètent l'évolution des courants turbiditiques de haute densité (Mutti, 1992, Pickering et al., 2015), ou les structures massives sont interprétées comme les produits du dépôt en masse rapide d'une suspension non cohésive dense d'un courant turbiditique très chargé en matériaux terrigènes (Middleton and Hampton 1976; Walker 1978; Lowe 1982; Mutti 1992). La présence des ravinements et du granoclassement normal peuvent être interprétés comme l'empreinte de la turbulence du courant où le tassement rapide des grains justifie le développement des structures d'échappement d'eau (Lowe et al., 1974; Lowe 1976; Pickering et al 1982, 1989, 2015). La présence de galets mous peut avoir plusieurs interprétations hydrodynamiques soit faisant intervenir la concentration du courant (Postma et al., 1988) ; ou au contraire comme produit des courants à débris de type « *Sandy Debris Flows* » (Shanmugam et al. 1995) ou par traction de clastes argileux sur un fond sableux (Hiscott et al. 1997a).

- L'association de dépôt de chenal consiste en un remplissage de chenaux par des bancs gréseux épais à grains moyens à grossiers, surmontés subitement ou de manière progressive par une alternance de bancs gréseux minces et des niveaux marneux. Le rapport grés/argile est de **4.5/0.5**. Les bancs gréseux sont irréguliers, lenticulaires et amalgamés avec les contacts basaux des bancs ravinant. Les bancs gréseux grossiers sont organisés en rythmes grano-stratodécroissants. Il s'agit surtout de dépôts des écoulements de débris remaniant des galets sableux et mous centimétriques à décimétriques dans une matrice sableuse.

Un échantillonnage dense a été effectué à travers le bassin le long des sections lithostratigraphiques mesurées, et ceci aussi bien pour les grés (43 échantillons) que pour les marnes (45 échantillons). Ces échantillons ont été analysées par Diffraction aux Rayons X (XRD), Fluorescence aux Rayons X (XRF) et aussi par Plasma spectrométrie de masse à couplage inductif (*Inductively Coupled Plasma-Mass Spectrometry*- ICP-MS) pour les marnes.

Les échantillons de grés ont été analysés en microscopie optique en lumière polarisant. Les grés de Zoumi sont définis comme des sublitharénites et des quartzarénites après analyse modale pétrographique. Les grains détritiques sont généralement sub-angulaires à sub-arrondis, mal classés et à dominance de quartz. L'analyse modale de ces grés terrigènes utilisant les proxies pétrographiques standards (QFL, $Q_mFL_t$, $Q_pL_vL_s$) indique une provenance mixte du bassin transporté de zoumi, issue à la fois du recyclage de la chaîne rifaine en surrection et à degré moindre de la dénudation du craton africain livrant des matériaux à faible maturité. Il semble que le drainage a eu lieu parallèlement à l'axe majeur du bassin et parallèlement aux bordures des marges de zones nourricières si l'on se réfère aux directions initiales des indicateurs de courants (i.e. après restauration de la structure arquée de la chaine).

D'après les analyses géochimiques, les marnes sont enrichies en $Al_2O_3$, $Fe_2O_3$, CaO et $TiO_2$ et très appauvries en d'autres oxides majeurs par rapport à la composition des Argiles Australiennes Post-Archéennes (PAAS pris comme référence). Selon les diagrammes de Harker, les courbes régressives montrent une très forte corrélation positive entre $SiO_2$, $Al_2O_3$, et $TiO_2$, et une corrélation négative entre $SiO_2$ et CaO. Les marnes sont classées géochimiquement comme des argiles, des argiles riches en fer et des wackes. Afin de caractériser le cadre tectonique, l'intensité de l'altération des zones nourricières et les conditions paléoclimatiques, plusieurs diagrammes discriminatoires ont été utilisés. Les valeurs de l'indice chimique de l'altération (CIA) et l'indice chimique de l'érosion (CIW) déduits de l'analyse des dépôts miocènes de Zoumi indiquent une intensité d'érosion faible à moyenne (50%à 80%) dans les zones nourricières reflétant un état d'érosion non stationnaire sous des conditions climatiques humides et pluvieuses.

Localement, les valeurs de CIA sont plus élevées (>80) caractéristiques d'une érosion intense dans les zones nourricières, pouvant être attribuée à une intensification de l'activité tectonique et des conditions climatiques plus humides et pluvieuses.

La combinaison des valeurs issues de certaines proxies géochimiques, à savoir, ICV (indice des variations des compositions chimiques), CIA, $Al_2O_3$-Zr-$TiO_2$ et Th/Sc-Zr/Sc indiquent une nature immature des dépôts qui ont subi un tri physique et un recyclage relativement modeste durant un faible transport à destination finale de dépôt et son accumulation dans le bassin. Plusieurs rapports géochimiques ($Al_2O_3/TiO_2$, La/Th, Cr/Th, Th/Sc, Zr/Sc) ainsi que les courbes de normalisation des terres rares (REE) par rapport aux valeurs de celles des Chondrites qui présentent une allure horizontale pour les terres rares lourdes, un enrichissement des terres rares légères et une anomalie négative très notable de l'Europium (Eu) suggérant, par conséquent, une source d'apport à dominante felsique. Cependant, les diagrammes V-Ni-La*4, V-Ni-Th*10 et Th/Sc vs. Cr/Th n'excluent pas une contribution d'une source de nature mafique matérialisée par l'existence de plusieurs affleurements ophiolitiques parsemés le long du Mesorif (i.e. la suture Ophiolitique Mésorifaine de Michard et al., 2014).

L'application des résultats de l'analyse modale pétrographique et leur report sur les diagrammes ternaires QFL et $Q_mFL_t$ de Dickinson (Dickinson et Suczek 1979; Dickinson 1985), révisés par la suite par Weltje (2006), démontre que les matériaux terrigènes sont les produits de recyclage de la chaîne orogénique rifaine avec une influence mineure des produits issues de l'altération du craton africain. Afin de mieux cerner l'influence conjuguée de plusieurs cadres tectoniques, le diagramme ternaire $Q_pL_vL_s$ (Ingersoll and Suczek 1979) tient compte de la présence simultanée de plusieurs types de fragments de roches et par conséquent, de plusieurs zones nourricières correspondantes, allant des marges passives continentales aux zones orogéniques de collision. Il est important de signaler l'enrichissent notable en grains de quartz dans les secteurs de Khakha et de Taourda par rapport aux parties sud-orientales du bassin (les localités de Zoumi et Dmani). La présence simultanée de caractères variés de provenance correspond à une provenance mixte qui reflète clairement que le bassin de Zoumi évolue dans un cadre tectonique complexe avec des apports terrigènes de sources variées, qui évoluent probablement avec le temps durant la croissance du prisme d'accrétion orogénique externe et la progression de la déformation vers l'extérieure de la chaîne.

L'examen des données de la pétrographie optique a permis de distinguer les produits terrigènes provenant des roches plutoniques et ceux issus des roches métamorphiques. Ainsi, les caractéristiques optiques et texturales des grains de quartz, en particulier, l'extinction roulante des grains monocristallins et la foliation des grains polycristallins expliquent clairement que les matériaux terrigènes comblant le bassin de Zoumi proviennent en partie de roches métamorphiques. Les données de l'analyse modale pétrographique reportées sur le diagramme de Basu (1975) montrent une provenance des terrains métamorphiques à faible degré. En outre, les âges de 13.9 ± 1.8 et 20.0±2.4 Ma obtenues des traces de fission de l'apatite à partir des massifs métamorphiques de Ketama et Temsamane (Azdimoussa et al. 1998) indiquant l'exhumation et la dénudation de ces massifs dès le Miocène inférieure pourraient correspondre à de potentielles sources d'apport des dépôts terrigènes du bassin de Zoumi.

Les éléments traces et les terres rares peuvent servir également, en tant que proxies de détermination de source de provenance (Taylor and McLennan 1985; Condie et al., 1992; Cullers 1995; Madhavaraju and Ramasamy 2002; Armstrong-Altrin et al. 2004). D'une manière générale, les sources principales qui contribuent dans les apports terrigènes peuvent être soit felsique (croute continentale supérieure) soit mafique/ultramafique (roches d'origine mantellique et de croute océanique). Les rapports La/Sc, Th/Sc, Th/Co, et Th/Cr peuvent être utilisés dans la discrimination des provenances d'origine felsique et mafique (Wronkiewicz et Condie, 1990; Cox et al., 1995; Cullers, 1995). Ces rapports ont été comparés avec ceux ayant été dérivés des roches connues felsiques et mafiques (Table 8), et montrent que les matériaux terrigènes, pour la plupart, ont une provenance d'origine felsique et une faible obédience d'origine mafique principalement alcaline. L'allure des courbes des terres rares de la quasi-totalité des échantillons est similaire à celle des Chondrites des PAAS, indiquant ainsi une provenance d'affinité crustale (i.e. croute continentale supérieure). Tenant compte de l'anomalie de l'Europium, en tant qu'indicateur le plus fiable dans la détermination de la provenance (McLennan et al. 1993; Mongelli et al. 1998; Cullers 2000), les échantillons des marnes de Zoumi montrent une moyenne $Eu/Eu^*=0.67\pm0.07$ très proche de celles de la croute supérieure et des argiles du PAAS ($Eu/Eu^*_{PAAS} = 0.66$) confirmant ainsi que les zone nourricières sont à dominante felsique. Les sources mafiques-ultramafiques ont une très grande abondance en éléments ferromagnésiens (McLennan et al. 1993), une telle provenance présente une diminution de Y/Ni par rapport à une augmentation de Cr/V (Hiscott 1984; McLennan et al. 1993). Pour les marnes de Zoumi les valeurs de Y/Ni sont très faibles (0.22-0.47, moyenne=0.31) et celles de Cr/V sont plus élevées (0.65-0.93 ; moyenne=0.81), et le diagramme Cr/V vs. Y/Ni montre une alimentation détritique à composante mantellique/mafique à côté de la dominance de la composante felsique (Fig. 44).

Les proxies de provenance à relation triangulaire Th-Sc-Zr (Bhatia and Crook 1986; Bahlburg 1998), V-Ni-Th et V-Ni-La (Bracciali et al. 2007) ont été utilisées pour discriminer et faire la part des provenances à obédience felsique et de celles de nature mafique. Ces diagrammes suggèrent une provenance mixte, vu que le report des échantillons des localités de Zoumi, Dmani et Khakha sur ces diagrammes correspondent à des compositions mafiques et felsiques, avec un léger enrichissement en Ni selon un alignement vers le pôle ultramafique confirmant la contribution d'une source mafique dans les produits terrigènes qui aliment le bassin de Zoumi.

Les oxides et les éléments traces constituent des proxies très utiles dans la détermination des processus géologiques qui accompagnent la genèse des chaînes orogéniques et les implications géodynamiques et tectoniques ainsi que les paléoenvironnements de dépôts. Les diagrammes discriminatoires de Roser et Korsch (1986) et de Verma et al. (2013) indiquent la prédominance d'un environnement de marge continentale très active pour tous les échantillons marneux. Les données pétrographiques et géochimiques suggèrent que la mise en place et l'évolution du bassin de Zoumi a eu lieu sur la bordure frontale d'une marge continentale active dans un contexte de collision. Les matériaux détritiques ont démontré qu'ils préservent la signature du recyclage d'une chaîne orogénique plutôt qu'une provenance d'un craton continental. La source dominante des dépôts terrigènes correspond au prisme d'accrétion orogénique du Rif externe (i.e. Intrararif –Mesorif *p.p.*) qui constitue l'arrière-pays des dépôts turbiditiques « syn-orogéniques » du bassin transporté de Zoumi. Ces dépôts sont principalement alimentés par les terrains métamorphiques à faible-moyen degré exhumés et leurs couvertures sédimentaires et qui correspondent aux unités métamorphiques de Temsamane et Ketama. Les nappes de flyschs issues de la structuration du Bassin de Flysch Maghrébin ont aussi contribué à l'alimentation du bassin de Zoumi principalement depuis le Miocène moyen. Le scénario tectono-sédimentaire que nous proposons suggère une provenance d'une marge continentale active pour le bassin de Zoumi combinée à une alimentation de l'avant-pays hercynien qui pourrait fournir des matériaux détritiques mobilisés à partir d'un socle paléozoique Mesetien voire même plus ancien probablement de nature cratonique.

Finalement, à partir du Chattien ? et principalement durant le Miocène inférieur-moyen, le bassin de Zoumi a été le réceptacle d'une provenance mixte de sources opposées situées sur les bordures du bassin. Les apports sédimentaires du bassin proviennent de manière synchrone du drainage et de l'acheminement des produits terrigènes à partir des reliefs septentrionaux issus de l'évolution du prisme d'accrétion Rifain qui a probablement atteint la bordure du Mesorif à partir du Miocène inférieur terminal , et à partir du sud du bassin, où affleure le socle paléozoïque Mesetien et ses successions deltaïques subjacentes probablement soulevées par réajustement de la bordure méridionale du bassin comme réponse mécanique à la flexion crustale du bassin causée par une forte subsidence thermique du bassin de Zoumi. Ce bassin transporté mise en place sur le front externe du prisme d'accrétion du Rif externe *(Intrarif-Mesorif p.p.)* progressant vers le Sud et le Sud-Ouest au cours du recul de la plaque Africaine subduite sous les terrains méso-méditerranéens propulsés vers les avant-pays Ibériques et Africains simultanément au début de l'oceanisation de la mer Algéro-Provençale depuis le Miocène inferieur terminal et principalement au cours du Miocène Moyen (Carminati et al. 2012; Benzagagh et al. 2013; Van Hinsbergen et al. 2014; Michard et al. 2014 ; Zaghloul 2005b, Vitale et al. 2014).

**Mots Clés** : Eléments en Trace, Terres Rares, Oxides majeurs, Altération des zones sources, Tri physique et recyclage, conditions paléoclimatiques, Provenance, Cadre géodynamique, Rif Externe, Rif, Maroc

# الملخص

نشأة حوض زومي تمت في بيئة تكتونية تصاعدية أثناء العصر الميوسيني الأدنى والأوسط. ترسبات هذا الحوض تم التحقيق فيها بشكل مستفيض من خلال الدراسات المجهرية والجيوكيميائية لاستنتاج ظروف المناخات القديمة في منطقة المصدر، كثافة حث صخور المصدر، الفرز الميكانيكي وإعادة تدوير الآثار وذلك للتعرف بشكل دقيق على توصيف التركيبة، ودرجات الحث في المصدر، والإعداد التكتوني لحوض زومي. تم جمع 43 عينة من الحجر الرملي و44عينة من الحجر الطيني من ستة أقسام استراتيجية مقاسة. وقد تم تحليل هذه العينات باستخدام XRD ، XRF، الطيف البلازمي المقرن بالحث الحثّي (ICP-MS) من أجل التحاليل الطينية والتحري عن الصخور الرملية الصخرية. تعرَّف ترسبات المايوسين لحوض زومي على أنها خمائر فرعية و كوارتزارينيت وفقا للمحتوى المعدني. عادة ماتكون الحبيبات (Dettital)على شبه زوايا وشبه دائرية، ضعيفة الفرز، وغنية بحبيبات الكوارتز. أدى تحليل الفرز بالفرز النقطي إلى إضفاء الصبغة الداخلية للكراتون وتدويرصخور ذات سلسلة المنشأ المعاد تدويره مع توريد رواسب أول دورة كبيرة، وإعادة تدوير منخفض رسوبي.

مركبات الطين ثرية ب Al2O3 و Fe2O3 و CaO و TiO2 بالنسبة لـ PAAS وتنضب من العناصر الرئيسية المتحركة الأخرى. جيوكيمائياً هناك ارتباطات موجبة عالية بين SiO2 ، Al2O3 ، وTiO2 ، والارتباطات السلبية بين SiO2 و .CaO ، يتم تصنيف أحجار الطحالب بشكل رئيسي على أنها من الصخر الزيتي ، الصخر-الحديد والأغصان. استُخدمت رسوم بيانية توضيحية مختلفة للكشف عن التكتونيات المستنبطة ، وقوة التجوية في منطقة المصدر (palaeoweathering) وظروف العصر الحسي البالي. المؤشر الكيميائي للتآكل والمؤشر الكيميائي لقيم التجوية (CIW) للميوسيني الأدنى والأوسط يختلف من 50 إلى 80٪ مشيرا إلى درجة منخفضة إلى معتدلة من التجوية في منطقة المصدر المتوافقة مع التجوية غير المستقرة في حالة الطقس الباكر والمناخي الرطب الظروف. محليا ( (Zoumi mid-section قيم CIA أعلى (80< )) التي تعكس تجويفات شديدة في منطقة المصدر ، والتي يمكن أن تعزى إلى نبضات تكتونية عالية وظروف أكثر رطوبة أثناء الترسب.

تشير تركيبة قيم ICV-CIA وAl2O3-Zr-TiO2 و Th / Sc-Zr / Sc إلى أن الصخور الكبيرة غير ناضجة كيميائياً وشهدت عمليات فرز وإعادة تدوير معتدلة تعكس القليل من النقل حتى الترسب النهائي. عدة نسب كيميائية ($Al_2O_3/TiO_2$, La/Th, Cr/Th, Th/Sc, Zr/Sc) فضلا عن تطبيع عناصرالأتربة النادرة () على أنماط العناصر الأرضية النادرة لكوندريت مع ضعف عناصرالأتربة النادرة الثقيلة (HREE)، وإثراء عناصرالأتربة النادرة الخفيفة (LREE)، وسلبية شذوذ الأوروبيوم (Eu)، كل هذه المعطيات تشير إلى

هيمنة صخور ذات مصدر فلزيكي. ومع ذلك، 4 * V-Ni-La؛ Ni-V -10*Th و Th/Scمقابل Cr/Th لا تستبعد مصدر ذات طبيعة إمدادات مافية وهو ما يتضح من خلال العديد من النتوءات الأفيوليتية المنتشرة في جميع أنحاء المجال Mesorifan (Ophiolitic Mesorifan Suture Zone).

**<u>الكلمات الرئيسية:</u>** الأكاسيد الكبرى، العناصر النادرة، عناصرالأتربة النادرة، تجوية مناطق المصدر، الفرز و إعادة التدوير، الظروف المناخية القديمة، المصدر، الإعداد الجيوديناميكي، المنطقة الخارجية لسلسلة جبال الريف، المغرب

# LISTE OF FIGURES

# LISTE OF TABLES

# LISTE OF PLATES



.

# CHAPTER I

# INTRODUCTION & GEOLOGICAL SETTING

# CHAPTER I

# INTRODUCTION & GEOLOGICAL BACKGROUND

## I.1. Introduction and aims of the Thesis:

Detrital rock composition is considered to be a complex function of provenance, sediment transport, depositional, and diagenesis processes (Suttner 1974). The relief growth and related external forcings (i.e. climate, sea level, and tectonics) control sedimentation and main provenance patterns. The latter includes the sediment-routing system and their depositions within an integrated source-to-sink approach. The early works (Dickinson and Suczek 1979; Dickinson et al. 1983; Ingersoll and Suczek 1979; Dickinson and Valloni 1980; Dickinson 1985) indicate that sedimentary successions petrographic modal analysis remains one of the reliable guides to assess worldwide sediment provenance in different tectonic settings. Furthermore, complementary geochemical and mineralogical analyses constraint sediments provenance and related geodynamic settings (Bhatia 1983; Bhatia and Crook 1986; Roser and Korsch 1986, 1988; Cullers, 1994b, 2000; Cullers and Berendsen 1998; McLennan et al. 1993, 1990; McLennan and Taylor 1991; Wronkiewicz and Condie 1989). Recently, source-to-sink approach is widely used for its reliable control of geodynamic setting and provenance patterns; namely for siliciclastic sedimentary successions (Bhatia 1983; Van de Kamp and Leake 1985; Roser and Korsch 1986). In the External Rif belt, except a single work (Zaghloul et al. 2005b) which can be considered as an earliest introduction to source-to-sink approach for some Lower-Middle Miocene siliciclastic successions, data dealing with provenance and petrology of terrigenous sediments are till now lacking.

Vidal (1977), as one of the early Pioneers of the Rif belt suggested two subduction slabs northward deepening for the whole Rif belt. Later, the evidence of MP/LT metamorphic units of the Mesorif sub-Domain (i.e. Temsamane nappes stack) that are related to the late Oligocene-middle Miocene subduction processes (Negro et al. 2007) confirmed the Vidal's early proposed model. The growth of scientific interest in the sedimentary basins geodynamics of External Rif enables us to re-analyze the syn-orogenic Zoumi Flysch Fm. through a source-to-sink approach. The Zoumi Flysch Fm. crops out in a wide sub-meridian sheet of about 100 km² lying between Teroual and Souk El Had villages. The Zoumi Basin was subjected to controversial debates regarding its geodynamic setting.

Morley (1988) suggested a piggy-back basin tectono-sedimentary evolution of the Zoumi Basin, whereas Ben Yaich (1991) considered it as a foredeep basin. On the basis of stratigraphy and structural analyses, Zakir et al. (2004) constraint the tectono-sedimentary evolution of Thrust-top and Foreland basins within the External Rif Domain mainly since Middle Miocene; and proposed a fore-belt setting for the Chattian-Langhian successions of the external Mesorif sub-Domain (*Auct*. internal Prerif) laying in the front of the northwestern Intrarif basin. Moreover, all authors reported at various levels, paleocurrent markers that point to northward and/or NW-ward routing sediments (nowadays references) and subsequently interpreted their source area provenance exclusively as the southern Hercynian Meseta promontory without any additional reliable scientific evidence. These controversial settings and related misinterpretations justify the scientific necessity for detailed source-to-sink investigations involving petrology.

In the upper continental crust, feldspar is by far the most abundant (62% by volume) of labile minerals (Wedepohl 1969); consequently, the dominant process during chemical weathering of the upper crust is the alteration of feldspar and subsequent formation of clay minerals (Nesbitt and Young 1982). Further, the major-element geochemistry and mineralogy of siliciclastic sediments are strongly affected by chemical weathering (e.g. Nesbitt and Young 1982; Johnsson et al. 1988; McLennan 1993). The various reliable geochemical proxies (i.e. chemical index of alteration (CIA; Nesbitt and Young 1982), chemical index of weathering (CIW; Harnois 1988), plagioclase index of alteration (PIA; Fedo et al. 1995) may, however, offer a valuable opportunity to assess weathering intensity and paleoclimate conditions. During weathering processes, high CIA values reflect the removal of labile cations (e.g. $Ca^{2+}$, $Na^{+}$, $K^{+}$) relative to stable residual constituents ($Al^{3+}$, $Ti^{4+}$), (Nesbitt and Young 1982). Conversely, low CIA values indicate the near absence of chemical alteration, reflecting consequently cool and/or arid paleoclimatic conditions (Fedo 1995). However, complex geochemical processes involving potassium metasomatism (Condie 1993) might occur during chemical weathering beside mechanical breakdown, and continued chemical alteration during transport, burial, and diagenesis. Further, mechanical sorting during transport and deposition may affect the chemical composition of terrigenous sediments and, consequently, the distribution of palaeoweathering and provenance proxies (Bauluz et al. 2000; Lepera et al. 2000).

The chemical compositions of sedimentary rocks and paleosols are plotted as molar proportions within $Al_2O_3$, $CaO^*$ -$Na_2O$, $K_2O$ (A-CN-K) compositional space, where $CaO^*$ represents Ca in silicate-bearing minerals only. The A-CN-K system is useful for evaluating fresh rock compositions and examining their weathering trends because the upper crust is dominated by plagioclase- and K-feldspar–rich rocks (Nesbitt and Young 1984, 1989) and their weathering products, the clay minerals. The weathering products might contain considerably more $K_2O$ than expected and therefore the rocks are considered having undergone K-metasomatism (Nesbitt 1992).

Since the pioneering sedimentological and tectonic works of Lespinasse (1975), Suter (1965, 1980) and Ben-yaich (1991) in the Mesorif sub-Domain including the Zoumi flysch, the study of the chemical weathering and palaeoclimatic implications recorded in these Lower-Middle Miocene turbiditic deposits have never been attempted.

This thesis is aimed to apply a source-to-sink approach to the Lower-Middle Miocene Zoumi Flysch Fm. in order to clarify the misinterpretations and to find out some scientific answers dealing with provenance and rooting sediment system. Thus, an integrated investigation, here presented, will merge fine-grained sediments petrology (*i.e.* modal petrography, geochemistry, and mineralogy) to decipher: rocks composition, provenance and to replace the Zoumi Basin within its geodynamic setting during Lower-Middle Miocene. It alsoought to evaluate chemical weathering intensities, sorting and recycling effects and assess, from the sedimentary record, palaeoclimatic conditions prevailing in the source area.

## I.2. Geological setting:

The Rif-Betic orogenic arc is the flanking of the Alboran Sea and represents the western ending of the Apennines, Calabrian-Peloritani Maghrebian belts (Fig 1a). The Rif chain was built during Miocene by the superposition of several thrust sheets clustered into three main tectonic complexes (Fig 1b, Fig 2): Internal Zones (Didon et al. 1973; Kornprobst 1974)***;*** External Zones (Lacoste 1934; Leblanc 1979; Sutter 1980, Vidal 1983), and in between the Maghrebian Flysch Units (Durand-Delga 1980; Guerrera et al. 1993, 2005). The Internal Domain is characterized by three superimposed tectonic Complexes from the top to the bottom: ***i)*** *"Dorsale Calcaire"* Complex (Fallot 1937) consists of Triassic-Lower Jurassic shallow-water carbonates evolving upward to Jurassic-Cretaceous slope and basin deposits (Fallot 1937; Mattauer 1960; Wildi et al. 1977; Wildi 1983; Nold et al. 1981; El Hatimi et al. 1991; El Kadiri 1992; Maate 1996).

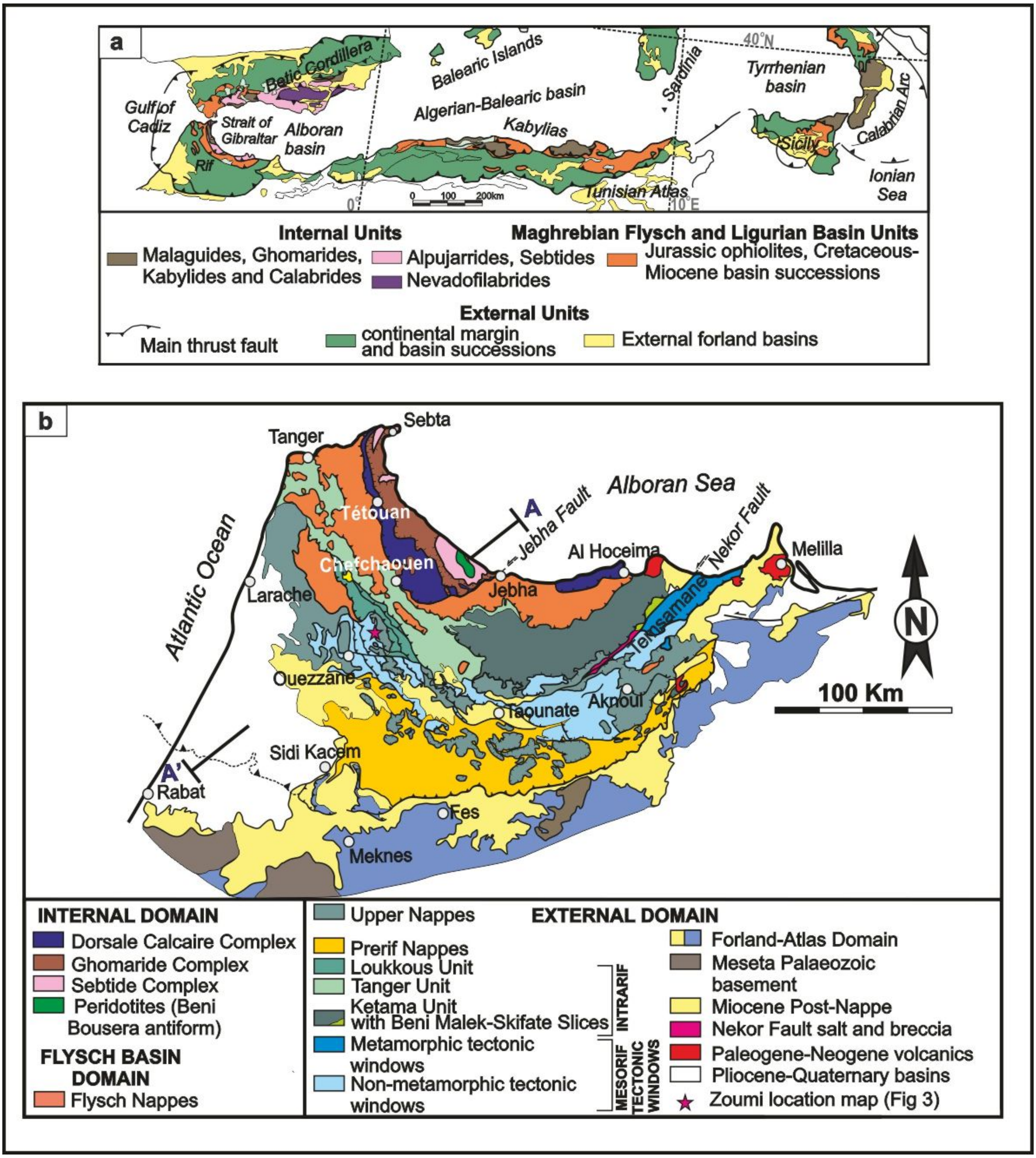


**Figure 1:** Geological setting of the ZoumiBasin. **a** Alpine belts of the West Mediterranean Alpine chains (from Vitale and Ciarcia, 2013, modified). **b** Geological setting of the Rif Cordillera with location of the Zoumi basin (from Frizon de Lamotte et al. 2017, modified).

Upward, the succession is topped by terrigenous successions known as *"syn-orogenic flysch-type"* which is of Aquitanian to Late Burdigalian in age (Zaghloul et al. 2005b, 2007; Hlila et al. 1994); ***ii)*** Ghomaride Complex is organized into four stacked Palaeozoic nappes that are affected by Variscan orogeny (Chalouan 1986; Chalouan and Michard 1990) interleaved with their Triassic–Cenozoic sedimentary cover (Durand-Delga and Kornprobst 1963; Wildi 1983; Chalouan 1986; Michard et al. 1991); and ***iii)*** Sebtide Complex with polymetamorphic crystalline units (Milliard 1959; Kornprobst 1974).

The Maghrebian Flysch Basin Domain (Bouillin et al. 1986; Durand-Delga 1980, 2006; Durand-Delga and Fontboté 1980; Wildi 1983) is classically subdivided into two palaeogeographic realms known as Mauretanian and Massylian sub-Domains, located on the southern Meso-mediterranean and northern African margins, respectively (Bouillin et al. 1970, Dercourt et al. 1986) where it is mainly made of Cretaceous-Lower Miocene turbiditic successions.

The External Domain, classically divided into Prerif, Mesorif and Intrarif sub-Domains, consists of Mesozoic-Cenozoic successions (Durand-Delga et al. 1960; Suter 1965, 1980; Andrieux 1971; Didon et al. 1973; Durand-Delga 1980, 2006; Durand-Delga and Fontboté 1980; Wildi 1983) mainly deposited on the southern African margin and related oceanic basin. Their initial successions were completely rooted from their ophiolitic and/or subcontinental mantelic basements (Michard et al. 1992, 2007, 2014; Benzaggagh et al. 2014).

The Intrarif Unit regroups the Ketamathrust sheets with mainly terrigenous Triassic to Albian facies and the Tangerthrust sheets with mostly marly and clayey Upper Cretaceous and Cenozoic sediments. The Ketama thrust sheet has been affected by an alpine metamorphism and the formation of two sets of cleavages with unclear ages (Andrieux 1973; Frizon de Lamotte and Leikine 1982). The Loukkos Unit is a part of the Intrarif sub-Domain and comprises sedimentary sequences indicative of a shallower environment than the Ketama/Tangerthrust sheets. The Intrarif thrust sheets *"Auct. Nappes rifaines*" are thought to root in the transition between Intrarif and Mesorif because sedimentary facies contain typical features of both (Zaghloul et al. 2005a). These units tectonically cover the

Intrarif, Mesorif and Prerif. Their internal structure is simple and characterized by open folds and, locally, a pre-nappe schistosity (Leblanc 1979).

The Mesorifthrust sheets are overthrusted by the Intrarif ones and the contact towards the Prerif is rather variable, ranging from a continuous transition to large overthrusts (Suter 1980). The sedimentary sequence comprises Liassic to Dogger carbonate platform rocks, followed by thick Upper Jurassic - Lower Cretaceous siliciclastic successions similar to those of KetamaUnit (Andrieux 1971; Frizon de Lamotte 1985; Favre and Stampfli 1992). Resedimentation phenomena are well-known within Mesorif Cretaceous successions.

The Mesorif thrust sheets mainly involve Jurassic to Middle Miocene successions and the whole is sealed by thick Upper Miocene (namely Upper Tortonian) siliciclastic successions (Leblanc 1979; Suter 1980; Frizon de lamotte 1985). The Unit shows upper allochthonous Mesorif thrust sheets Auct. "*External Rif Nappes*" thrust over lower thrust sheets observed in tectonic windows (Michard et al. 2014). The Aknoul thrust sheet is of Intrarif origin and rooted from the upper part of Ketama thrust sheet (Frizon de Lamotte 1985) and it is composed mainly of Upper Cretaceous to Oligocene fine-grained sediments. The Senhadja and Bou Haddoud thrust sheets, of controversial origin, comprise Lower-Middle Jurassic to Middle Miocene sediments (Wildi 1983). The Bou Haddoud thrust sheet begins with thick quartzarenitic turbidites of Lower-Middle Jurassic and Upper Jurassic, respectively (*Auct*. "Ferrysch" of Wildi 1983). The latter is followed by Upper Jurassic-Berriasian carbonates bearing frequent E-MORB basalts flows (Benyaïch et al. 1989; Benzaggagh 2011; Benzaggagh et al. 2014). Upward, succession evolves to Cretaceous marls and sandstones overlain locally by Lower-Middle Miocene conglomerates and marls. The Senhadja thrust sheet (Lacoste and Marçais, 1938) is made of Lower-Middle Jurassic carbonates slices and Upper Jurassic quartzarenitic turbidites (*Auct*."Ferrysch"; Wildi1983). The latter overthrust directly either Mesorif windows or Bou Haddoud thrust sheets (Leblanc 1979,1983).

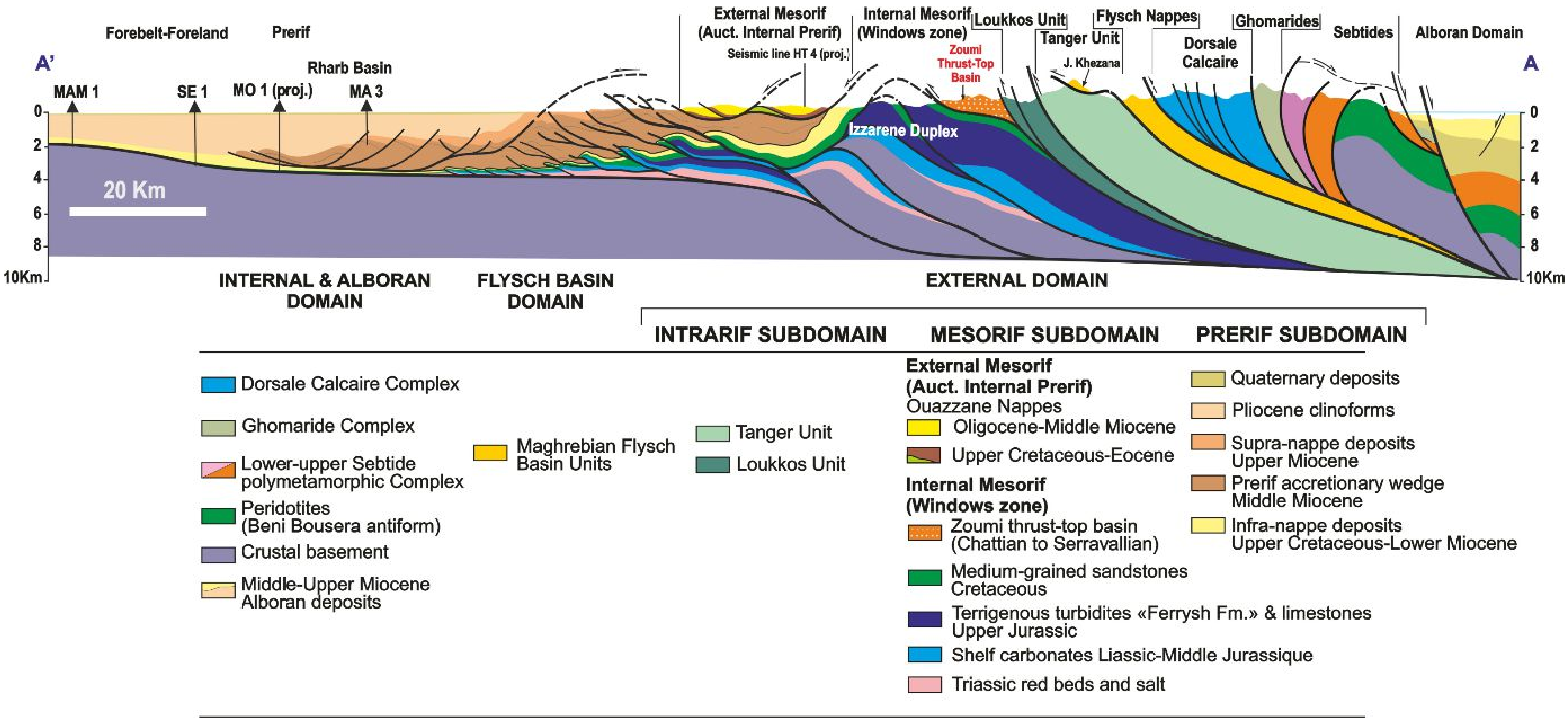


**Figure 2:** Rif cross section (Rharb basin and External Prerif after subsurface data interpretation (after Flinch 1993 and El Mourabet 1996).

The deepest Mesorif basement crop out along the Mesorif Corridor and is made of wide gabbroic massifs (e.g. Bouadel, Klayaa, Tainest-Kef El Ghar outcrops) and ultramafic serpentinized peridotites (BeniMalek and skifate outcrops). The Beni Malek serpentinites, underlying the Ketama thrust sheets, are interpreted as relict mantle units that are exhumed during the Tethyan rifting (Michard et al. 1992, 2014). The Mesorif metamorphic basement is mainly represented by thrust sheets of the Temsamane unit (Fig. 1b), which recorded alpine MP/LT metamorphism evolved to retrograde greenschist facies (Frizon de Lamotte 1985; Michard et al. 2007, 2014; Negro et al. 2007; Jabaloy-Sánchez et al. 2015).

The Prerifsub-Domain consists of Triassic to Miocene thick series and is defined on the basis of its Cretaceous marly lithofacies along with a large number of stratigraphic gaps due to erosion and resedimentation events. The Jurassic carbonates and quartzarenitic thick turbiditic successions crop out in the internal Prerif, defining the emerged so-called "*Sofs*" line, whereas the Cretaceous-Eocene and Miocene marly successions are rooted and transported southward (Michard et al. 2014). The front of the Prerif thrust sheet is interstratified within external Upper Miocene foredeep gritty marls (Gharb basin, Prerif ridges) (El Mourabet 1996; Michard et al. 2014). The Prerif sedimentary series are mainly rooted and detached by means of Triassic-evaporitic level systematically set on the top of sole thrust and in-between stacked thrust sheets. Triassic evaporitic formations are scattered in tectonic contacts within Mesorif thrust sheets as well as into Mesorif windows diapiric intrusions. Evaporites are frequently associated with weathered basalts or "*Auct. Ophites*", while Triassic diapirs are scattered in the whole area, displaying with the overlain Lower-Middle Jurassic sequence the collapsed upper limbs of the regional folds (El Mourabet 1996).

The studied Zoumi Basin (formerly the 'internal Mesorif unit', Suter 1980a, 1980b) is one of the several Tertiary flysch basins of the western Rif of Morocco (Fig. 1b; Fig. 2; Fig. 3). This syn-orogenic Flysch Fm. became involved in the Neogene Alpine deformation as a thrust sheet occupying a tectonic position inbetween lower, external Mesorif thrust sheets) and higher Intrarif thrust sheets (Morley 1988). Thrust stacking started since early Miocene (Kornprobst 1974; Wildi 1983; Leblanc & Oliver 1984). The age of syn-orogenic Zoumi Flysch Fm. span is during Lower-Middle Miocene (Ben Yaich, 1991).

Since deformation prior to thrusting of the Zoumi Flysch Fm. can be found in the Jurassic-Cretaceous Mesorif thick-bedded terrigenous "Ferrych" sequences and overlying limestones thrust pile, usually stacked as regional Duplex strcture (see cross section, Fig. 2) beneath the Zoumi Flysch Thrust-Top basin. Thus, it is evident that Zoumi Flysch Fm. can then be stated as a piggy-back basin *sensu* Ori & Friend 1984. Generally, thrust pattern of some Thrust-Top basins like Zoumi basin did not follow a simple in-sequence foreland-propagating pattern (Morley 1988). Instead, thrusting of both Intrarif and Mesorif units appears to have been synchronous, but perhaps separated by long tectonically quiet periods that allowed the Thrust-Top basin filling (Morley 1988). Hence, the Lower-Middle Miocene Zoumi Flysch Fm. was probably incorporated later into the leading edge of the Intrarif, and the basin was inverted and thrust over older stacked Mesorif thrust sheet following an out-sequence pattern.

It should be emphasized that the Intra-Rif sub-Domain (Tanger and Ketama Units) is marked by a Lower Miocene unconformable coarse-grained deposits (conglomerates) sealing the Jurassic-Neocomian Tifelouest Mesorif successions (Favre and Stampfli, 1992) located in the more external areas of the Ketama Unit. Meanwhile, the sedimentation is continuous synchronously up to the Serravallian within the External Intrarif-sub Domain (Zaghloul et al., 2005). This unconformity occurring within the External Domain could be interpreted as the echo of an earliest onset of the Maghrebian subduction, where the African paleomargin and the related “oceanic” Crust (Benzeggagh et al. 2014; Michard et al. 2014) start to be subducted beneath the Inner Intrarif sub-Domain before the Late Oligocene considered as early Metamorphism age of the subducted Mesorif units (i.e. Temsamane Units) (Negro et al. 2007). Later, the paroxysmal deformation phase leading to the closure of the Maghrebian Flysch Basin and to the Flysch nappes stacking and thrusting onto the External Domain mainly occurred during Langhian-Serravallian (Vitale et al. 2014, 2015; El Ouaragli et al. 2016). This main compressive phase is post-dated by the Upper Miocene “post-nappes” BenIssef Formation (Di Staso et al. 2010). Moreover, we can assume that the final thrust and the overriding of the Intrarif onto the Mesorif has occurred after Serravallian as younger age of the Zoumi Flysch Fm. and before Late-Tortonian as younger age of the overlying thrust top basin (BenYaich et al. 1989; Ben Yaich 1991; Tejera de Leon 1993; Favre 1995; Chalouan et al. 2001; Tejera de Leon & Duée 2003). Finally, both Mesorif and Intrarif thrust piled-up sheets were westward and southward transported as a fold and thrust-belt forming the new backstop of the external Prerif Foreland since late Miocene (Ben Yaich 1991; Zaghloul et al. 2005; El Mourabet 1996).

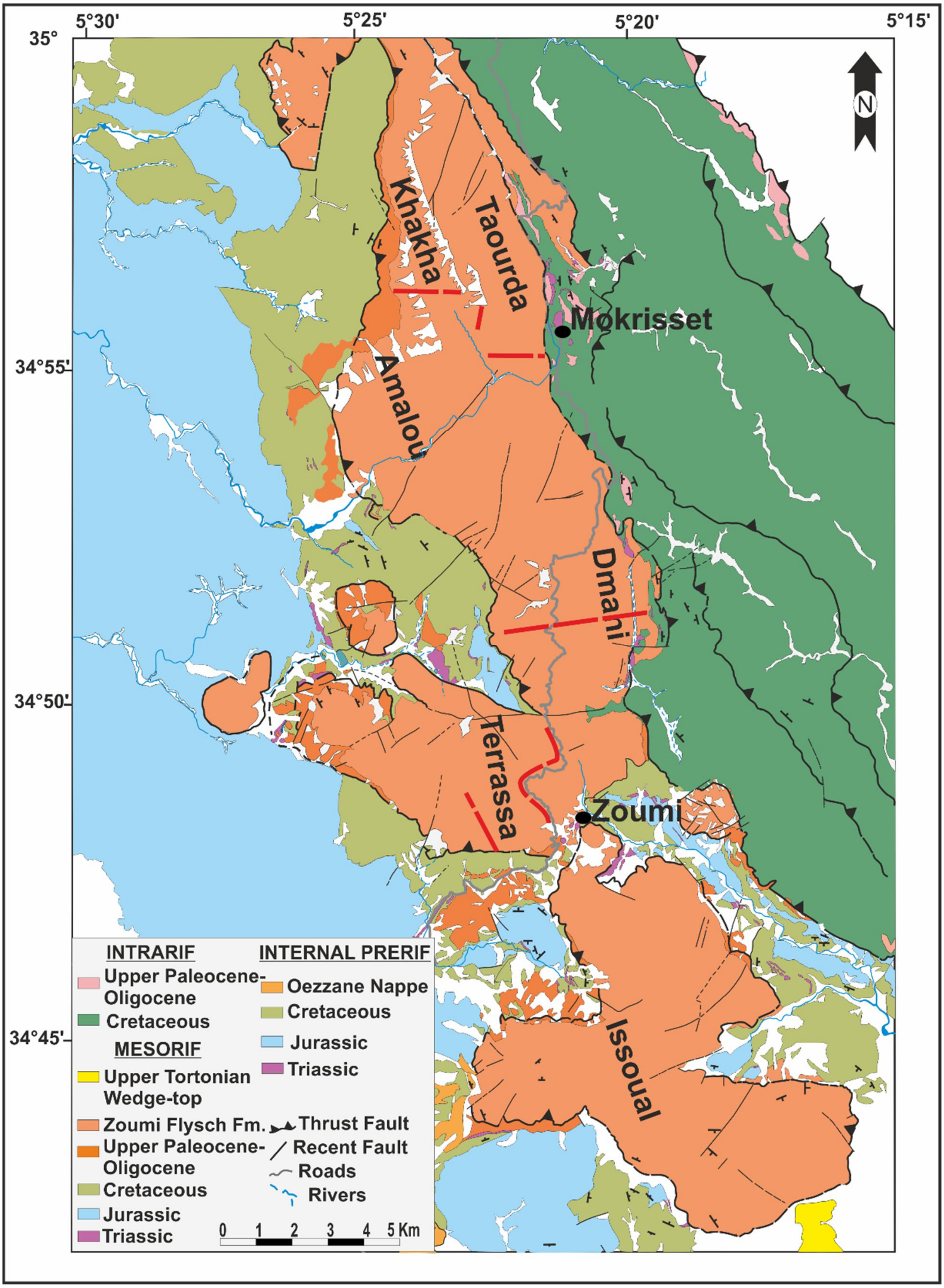


**Figure 3**: Geological map of the Zoumi Basin with stratigraphic sections locations (red lines) (Modified from Bouhdadi 1999).

## I.3. Data source and methodology:

Sedimentologic field data were collected from measured Oligo-miocenelithostratigraphic successions throughout the Zoumi Flysch Basin (ZFB). Internal sedimentary structures, bedthickeness measurement, sand/clay ratio and rhythmicity analysis, have been reported. Latter will be, namely, used for: ***i)*** Facies analysis and interpretation to restore main depositional systems; ***ii)*** Sandstones modal analysison thin sections; and ***iii)*** Mudrock geochemical analysisof ZFB's collected samples.

The analyzed Sandstone and marl/clay samples are covering the whole Zoumi basin. The southern area is located near Zoumi village (***Terrassa section)*** where marls/clays and *Zoumi sandstone suite* samples have been collected. The northwestern area is divided into two sub-areas: the neighboring Mokrisset village sub-area at the western side of JbelTaourda ***(Jbel Tawarda section***), and the second sub-area set located at the base of JbelKhakha where marls/clays and*Khakha sandstone suite samples* have been gathered ***(Jbel Khakha section)***. Eastward, marls/clays and *Dmani sandstone suite* samples have been collected near Dmani village in the oriental part of the Zoumi Basin (***Dmani section***) (Fig. 3).

Along four measured stratigraphic sections of the Zoumi Flysch Fm, a total of 43 medium-grained sandstone samples have been gathered for petrographic modal analysis and 45 mudrocks samples have been collected for geochemical and mineralogical analysis. Thin sections have been etched with HF and stained by immersion in *sodium cobaltinitrite* solution to allow the identification of feldspars, impregnated with *rodasine* to differentiate plagioclase if it is not twined. The sandstone composition, texture, and fabric have been studied. A total of 400 grains have been counted per thin section for modal analysis according to the Gazzi-Dickinson method to minimize the dependence of rock composition on grain size (Gazzi 1966; Dickinson 1970; Ingersoll et al. 1984; Zuffa 1985). Matrix and cement have not been counted (Dickinson 1970). Recalculated grain parameters defined according to Dickinson (1970), Ingersoll and Suczek (1979), Zuffa (1985), Critelli and Le Pera (1994, 1995), and Critelli and Ingersoll (1995) are given in Tables 2 and 3.

Sampled mudrocks were crushed and milled in an agate mill. The quantitative mineralogical composition of the whole-mudrock powder was obtained by X-ray diffraction (XRD) spectra using a Bruker D8 Advance diffractometer (CuKa radiation, graphite secondary monochromator, sample spinner; step size 0.02; speed 1s for step) at the University of

*Sultan MoulaySlimane* (BeniMellal, Morocco). Data collection range was from 2ϴ=5 to 2ϴ=80 with a step size of 0.04° for all samples. Semi-quantitative mineralogical analysis of the bulk rock was carried out on random powders measuring peak areas using the *DIFFRACT EVA V3* computer program.

Major oxides and minor elements have been obtained using X-ray Fluorescence (XRF) spectrometry technique on pressed powder disks of whole mudrock samples at *King Abdul Aziz University*, *Faculty of Earth Sciences, Department of Mineral resources and Rocks (Saudi Arabia)*. Trace elements data have been obtained using laser-ablation–inductively coupled plasma–mass spectrometry *(ICP-MS) at MANAGEM Group, Morocco*. These data were compared to international standard-rock analyses of the *United States Geological Survey* (Flanagan 1976). The estimated precision and accuracy for trace element determinations are better than 5% for the major oxides and 7% for minor elements. Total loss on ignition (L.O.I.) was determined after heating the samples for 3h at 900°C. Geochemical data were visualized and modeled by PetroGraph Software (Petrelli et al. 2005).

# CHAPTER II

# SEDIMENTOLOGY OUTLINE OF ZOUMI TURBIDITIC DEPOSITS

# CHAPTER II

# SEDIMENTOLOGY OUTLINE OF ZOUMI TURBIDITIC DEPOSITS

## II.1. Introduction

This chapter describes processes monitoring transport and deposition of deep-sea sediment gravity flow (SGF). We have elaborated extended thematic introduction and it integrates different sediment gravity flow models and main factors influencing this sedimentation for different deep-sea depositional systems. Three main processes can influence transporting and depositing sediments seaward of the continental shelve edges:

(i) bottom-hugging sediment gravity flows (e.g., turbidity currents and debris flows);
(ii) thermohaline bottom-currents that form oceans deep circulation
(iii) surface wind-driven currents or river plumes that carry suspended sediment off continental shelves.

Tidal currents, waves at ocean density interfaces seem to be just of limited importance as transport agent on the upper parts of slopes and in the heads of some submarine canyons. In order to focus on deep-marine sands and gravels deposition, it is essential to understand sediment gravity flow dynamics.

A *sediment gravity flow* (**SGF**; Middleton and Hampton 1973) is defined as a bottom-hugging density underflow carrying suspended mineral and rock particles, mixed together with ambient fluid (most commonly seawater). A *sediment gravity flow* is thus a special type of *particulate gravity current* (McCaffrey *et al*. 2001). The particles in **SGFs** spend most of their time in suspension rather than in contact with the seafloor. When the **SGFs** become more dilute, particles in suspension eventually settle to the seafloor where they accumulate, either with or without a phase of traction transport. This phenomenon is called *selective deposition* (Ricci Lucchi 1995 or *incremental deposition* of Talling *et al*. 2012), because particles are deposited one by one according to their size, shape, density or some other intrinsic property.

In cohesive debris flows, the particles are not fully free to move independently of one another and therefore accumulate by massive deposition (Ricci Lucchi 1995; *en masse* deposition of Talling *et al*. 2012). The distinction between *selective deposition* and *massive deposition* (or *"en masse"* deposition) is that the former deposits are commonly laminated and the latter ones are commonly structureless, poorly organized, plastically deformed, or contain evidence of intense particle interaction and/or pore-fluid escape. The ultimate end-member example of *"en masse"* deposition is *coherent sliding* in which masses of semi-consolidated material move downslope while retaining some of the organization and stratigraphy of the original failed successions (Pickering et al. 2015).

Basinward sediment transport events along a continental margin can be divided into four phases:

(i) a phase of flow initiation;
(ii) a period during the early history of the flow when characteristics of the transporting current change quickly to a quasi-stable equilibrium state;
(iii) a phase of long-distance transport to the base of the continental slope or beyond
(iv) a final depositional phase.

In each of the aforementioned cases, the concentration of solid particles changes systematically along the flow path. This concentration is an important variable because mixtures of sediment and water can only become fully turbulent if the concentration is low. Without turbulence, it is difficult to suspend and transport particles for long distances, and tractional sedimentary structures like current-ripple cross-lamination cannot form (Pickering et al. 1989, 2015).

Sediment suspended by a storm event on a continental shelf or by tidal currents in the head of a submarine canyon forms low-concentration suspensions that might continue to move downslope as turbidity currents, transporting sediments tens to hundreds of kilometers farther seaward. Other initiation processes, like the disintegration of sediment slides on steep slopes, can generate more concentrated **SGFs** such as submarine debris flows (Pickering et al., 1986a, 1989, 2015).

When a highly concentrated **SGF** decelerates, the internal resistance to flow (*e.g.,* friction between adjacent particles, or electrostatic cohesive forces between clay minerals) eventually exceeds the gradually decreasing gravitational driving force. When this happens, the flowing mass ceases to travel basinward and is deposited. Turbulent **SGFs** can decelerate and deposit their load selectively, grain by grain, during a period when solid particles rain downward to the base of the flow. This deposition 'from the base upward'; with the result that many deposits of this type show graded bedding because of a progressive flow energy decay during the depositional phase (Pickering et al., 1986a, 1989, 2015).

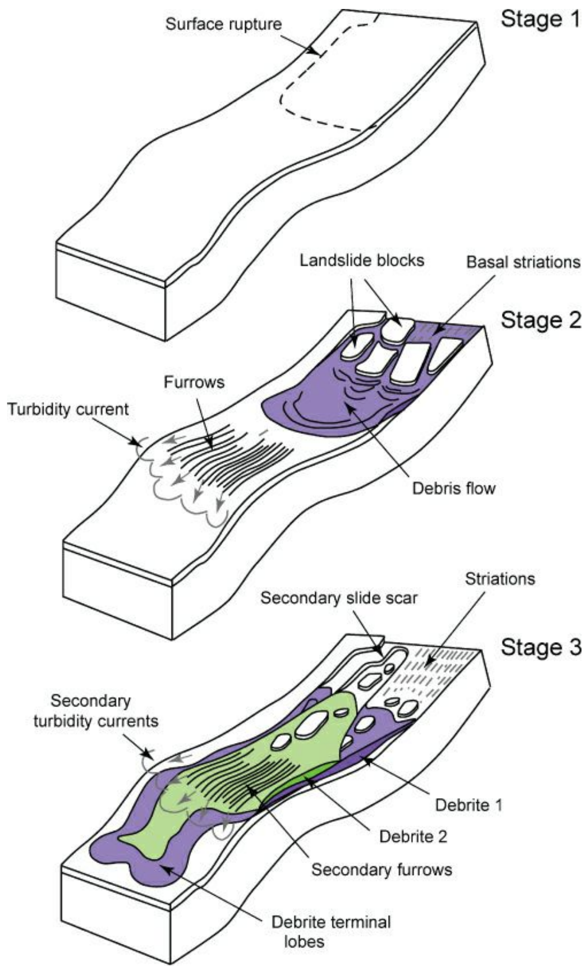


Figure 4: Conceptual model of submarine slide evolution (*Gee et al. 2006*). Stage 1 shows seafloor rupture. Stage 2 shows tabular blocks, basal striations, debris flow and a turbidity current generated in the headwall area. Downslope of the headwall area, turbidity currents erode furrows in the seafloor. Stage 3 shows the development of secondary slide events within the headwall, triggering secondary debris flows and turbidity currents.

### II.1.1. Sediment slides and mass transport complexes (MTCs)

Sediment masses previously deposited on a delta front or on the upper continental slope can move into deeper water because of downslope component of gravity. This happens either by increments or during a single episode. Slow downslope movement without slip along a single detachment surface without failure, is referred to as *creep.* No structures in ancient successions have been attributed to creep, but features in seismic profiles have been interpreted to have been formed by this mechanism (Hill *et al*. 1982; Mulder and Cochonat 1996). More rapid downslope movements following failure events generate sediment slides and submarine debris flows. Sediment slides can result in little-deformed to intensely folded, faulted and brecciated masses (Barnes and Lewis 1991) that have translated downslope from the original site of deposition. If the primary bedding is entirely destroyed by internal mixing, with soft muds and/or water mixed into the slide, then a slide may transform into a cohesive debris flow (Fig. 4) (Gee et al. 2006).

A spectrum of deposits can be generated by mass movements which, when intimately associated with one another, are best referred to as *mass transport*.: "Mass transport complexes include chaotic deposits, typically with visco-plastically deformed and disrupted bedding, cobble-pebble conglomerates, pebbly mudstones, mud-flake breccias, and pebbly sandstones (Pickering and Corregidor, 2005). These deposits represent a range of processes, including slides, slumps, turbidity currents and debris flows".

### II.1.2. Deep, thermohaline, clear-water currents

Geostrophic currents are well known in large parts of the deep ocean basins, especially the Atlantic Ocean (McCave *et al*. 1980; Hollister and McCave 1984). In the North Atlantic Ocean, for example, dense cold water sinks off the coast of Greenland and in the Norwegian Sea and moves southward as a bottom current (Worthington 1976).

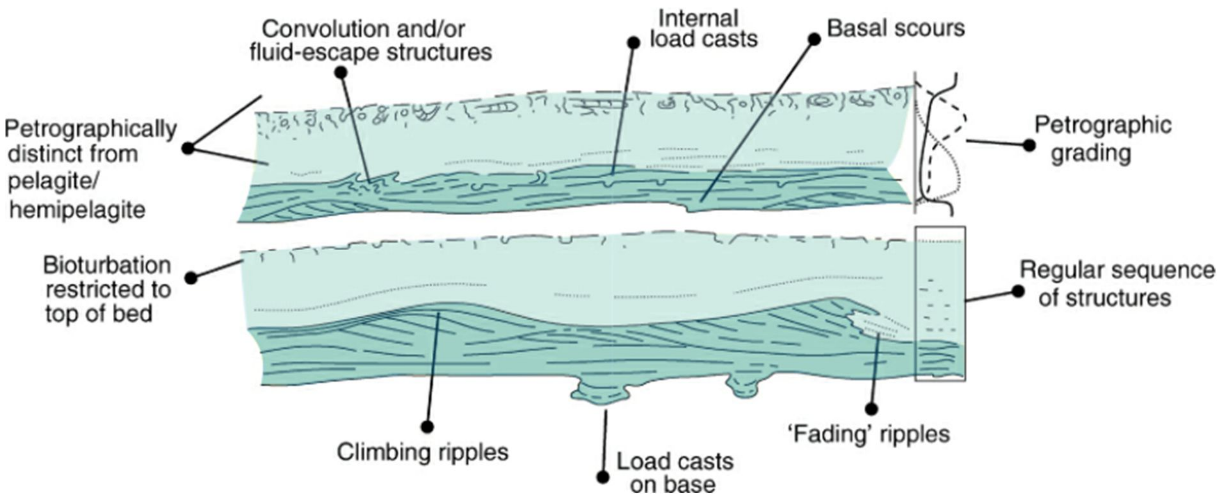


Figure 5: Diagnostic criteria for the recognition of fine-grained turbidites. Rapid deposition from a decelerating **SGF** produces both wet-sediment deformation structures like load casts, and climbing ripples. Accumulation rates under thermohaline currents are much lower, preventing the development of these types of sedimentary structures. The co-occurrence of several of these

structures is sufficient to rule out deposition by clear-water bottom currents (contour currents). (Redrawn from Piper and Stow 1991).

These currents carry a dilute suspended load – generally <0.1–0.2 g.m$^{-3}$ – that forms the thick bottom *nepheloid layer* (Ewing and Thorndike 1965; Biscaye and Eittreim 1977). Sandy contourites can form and comprise thin irregular layers (<5 cm) that are either structureless and thoroughly bioturbated or may possess some primary parallel or cross-lamination which may be accentuated by heavy minerals or foraminiferal tests (Bouma and Hollister 1973; Stow and Faugères 2008). Grain size ranges from coarse silt to, rarely, medium sand, with poor to moderate sorting. In particular cases, it may be difficult to distinguish between mud turbidites and muddy contourites (Bouma 1972; Stow 1979). Moreover, sand turbidites can be reworked and result in bottom-current modified turbidite sands, believed to be common on continental slopes and rises (Pickering et al. 1986a, 1989, 2015).

Since the early 1990s, a number of authors have clamed that rhythmically interbedded sands or large and well-sorted sand lenses in oilfields were emplaced, or largely reworked, by bottom currents (Mutti 1992; Shanmugam *et al*. 1993a, b, 1995; Shanmugam 2008). Some of the supposed bottom-current deposits are coarse grained climbing ripples that always require rapid deposition from suspension during ripple migration (Allen 1971; Jobe *et al*. 2012), consistent with deposition from turbidity currents (Fig. 5).

### II.1.3. Density currents and sediment gravity flows:

A density current results when a denser fluid moves beneath a less dense material under the influence of gravity. The density contrast with the ambient fluid might result from compositional differences (e.g., oil flowing beneath water), from temperature differences (e.g., cold air entering a warm room), from the presence of suspended material (e.g., particulate gravity currents), or where there are strong salinity contrasts (Di Iorio et al. 1999; Hiscott et al. 2013).

In **SGFs**, particles and water move down slopes because the mixtures have a density greater than that of the seawater. Initially, gravity acts solely on the solid particles in the mixture, inducing downslope flow; the admixed water is a passive partner in this process.

Gravity pulls the grains, and the grains pull the water. If sufficient potential energy is converted into kinetic energy in the evolving flow, then the flow may become turbulent and the particles in the fluid phase then become fundamental to the maintenance of the suspension. The flow will continue to move if the following conditions are satisfied:

(i) the shear stress generated by the downslope gravity component acting on the excess density of the mixture exceeds frictional resistance to flow;

(ii) the grains are inhibited from settling by one of several support mechanisms.

Some support mechanisms are believed to be responsible for maintaining sediment in suspension on seafloor slopes of a few degrees or less (Pickering et al., 2015):

1. ***Turbulence*** characterizes low-viscosity fluids in which inertial forces dominate viscous forces. Turbulence is the superimposition of swirling eddies and seemingly random velocity fluctuations on the average downstream velocity. The upward components of the velocity fluctuations diffuse sedimentary particles into the flow according to their settling velocity, so that the finest particles are evenly distributed throughout the flow, even though they are denser than the turbulent fluid.
2. ***Buoyancy*** is the support provided to an object by a dense surrounding fluid phase. If the surrounding fluid has the same density as the object, then the object has no immersed weight and seems to float aimlessly in the fluid. If the fluid is denser, then buoyancy is positive and the object floats on its surface. If the fluid is less dense than the object but denser than water, then the downward gravitational forces on the object are reduced and are equivalent to the gravitational forces on a much smaller object in clear water. Buoyancy permits relatively dense sediment–water mixtures like debris flows to carry large clasts even at low velocities.
3. ***Grain collisions and near-collisions*** (also called *grain interaction*) transfer some of the downstream moving particles to an upwardly oriented dispersive pressure (Bagnold 1956) as faster moving grains ricochet off more slowly moving grains beneath them. The moving mass of grains dilates (expands), thus increasing the vertical spacing between the particles and reducing grain-to-grain friction. This support mechanism only operates at high particle concentrations and cannot alone maintain a **SGF** on low slopes.

4. ***Excess pore pressure* and *pore-fluid escape*** results when a dispersion of grains settles too quickly to allow the interstitial pore-fluid to escape upwards. Instead, low permeability obstructs the upward flow of escaping pore-water, causing fluid pressures in the pore spaces to significantly exceed the expected hydrostatic pressure. This excess pore pressure keeps the grains separated (as if separated by an inflated pillow) so that friction is reduced and the grains can continue to move relative to one another. In local areas, the pressured pore-fluid can escape rapidly along preferred ways, potentially elutriating fine matrix material and forming porous fluid-escape pillars.
5. ***Matrix strength*** is a property of concentrated mixtures of fine grained or poorly sorted sediment and water. Small shear stresses do not cause such mixtures to flow because internal deformation is resisted by friction between adjacent grains (*frictional strength*) and electrostatic attraction between clay and silt particles (*cohesive strength*). This is different to the Newtonian fluids behavior, where the applied shear stress 'τ', is proportional to the fluid viscosity 'μ' x velocity gradient '*du/dy*'. An example is water, which deforms (i.e., flows) no matter how small the applied shear stress. For materials with matrix strength, some critical shear stress must be applied before they will move – likewise, these materials will cease to move even on low slopes if the downslope component of gravity is not sufficient to generate the required shear stress along the basal surface of the flow. Once a material of this type is moving, matrix strength is believed to play a roll in reducing the tendency for large clasts to settle, because in order to do so they have to push cohesive and/or granular material out of the way and overcome a certain amount of residual frictional and cohesive strength.

### II.1.3. 1.Classification

There has been a recent improvement in the understanding of features and behaviour of **SGFs** (e.g., Talling *et al*. 2012). This has resulted from ***i)*** improved hindcast analysis of recent **SGFs** in the oceans (a method for testing a mathematical model, where known or estimated inputs for past events are input into the model to see how well the output matches the known result); ***ii)*** a post-1995 revitalization of research into the flow dynamics and depositional mechanisms of such currents and ***iii)*** completion of a number of relevant experiments on concentrated flows. New classifications of flow processes have resulted.

The classification of Mulder and Alexander (2001) is that **SGFs** are subdivided according to their rheological behavior into predominantly *cohesive flows* and *frictional flows*. Approximate ranges for the volume concentrations of solids are shown in Figure 6. *Cohesive flows* have matrix strength resulting from electrostatic attraction between fine particles in the mud fraction. In contrast, frictional (non-cohesive) flows are made up of discrete particles dispersed in water.

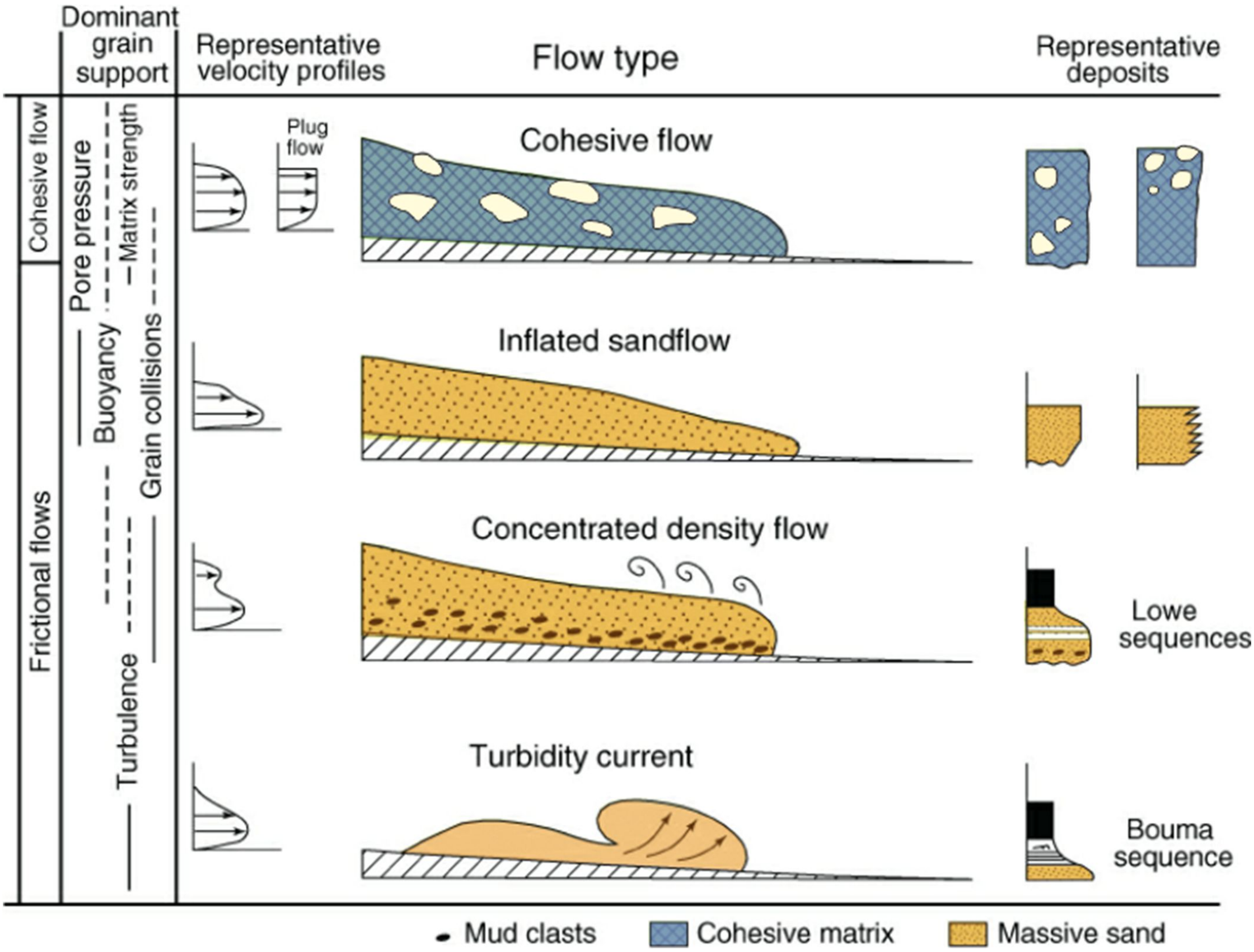


Figure 6: Summary of flow characteristics, typical deposits, and grain-support mechanisms for cohesive and frictional (non-cohesive) **SGFs**, (modified from Mulder and Alexander (2001).

The behavior of frictional flows is related directly to the relative proportion of grains and water. In general, frictional flows are characterized by selective deposition and cohesive flows by "en masse" deposition. Debris flows consist of more poorly sorted sediment (>5% gravel with a variable sand proportion) and may transport boulder-sized clasts of soft sediment or rock and very large rafts or olistoliths. In cases of very coarse-grained material and so little mud that cohesion is insignificant, the alternative terms *inflated sand/gravel flows*, or *inflated gravel flows* can be used.

All four flow types are capable of long distance transport of particulate sediments into the deep sea on relatively gentle slopes (<5°). *Cohesive-flow* deposits and inferred inflated *sand-flow* deposits are common on slopes less than 1° (Prior and Coleman 1982; Damuth and Flood 1984; Simm and Kidd 1983; Thornton 1984; Nelson *et al*. 1992; Aksu and Hiscott 1992; Masson *et al*. 1993; Schwab *et al*. 1996); the flows are capable of travelling for hundreds of kilometers from upper continental slopes to abyssal plains (Embley 1980). Chough and Hesse (1976) suggest that turbidity currents flow for 4000 km in the Northwest Atlantic Mid-Ocean Channel. Similarly, structureless*T*a-divisions of turbidity-current deposits can form whenever the suspension fallout rate is too high to allow sufficient grain traction to form lamination (Lowe 1988; Arnott and Hand 1989; Allen 1991; Hiscott *et al*. 1997)

### II.1.3.2. Transformations between flow types:

Density currents might become stratified, with discontinuities in concentration (Fig. 7), or might change their character dramatically while moving downslope as a result of *flow transformations*. Four varieties of flow transformation are recognized:

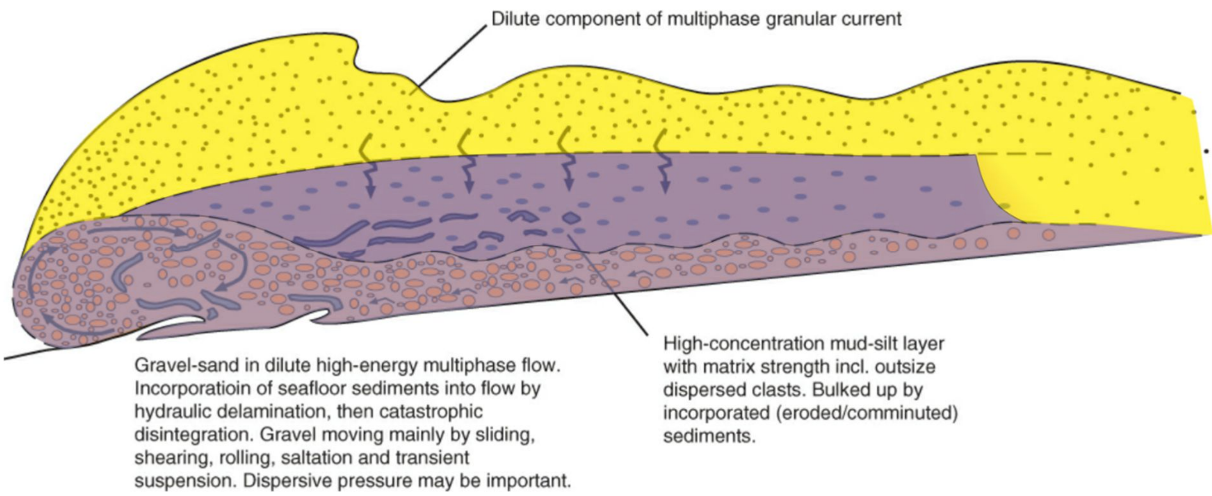


Figure 7: Multiphase hybrid **SGF** proposed by Pickering and Corregidor (2005) to explain certain disorganized beds in the Ainsa Basin, southern Pyrenees.

1. As defined by Fisher (1983), *body transformations* involve down current changes between turbulent and laminar flow, or between a coherent slide and a debris flow as

seawater is incorporated (McCave and Jones 1988; Jones *et al*. 1992; Talling *et al*. 2004; Pickering and Corregidor 2005; Strachan 2008; Haughton *et al*. 2009; Talling *et al*. 2010).

2. *Gravity transformations* involve gravitational segregation into a lower, laminar, highly concentrated part and an upper, turbulent, less concentrated part (Postma *et al*. 1988).
3. *Surface transformations* occur where the front or top of a highly concentrated flow is eroded by shear beneath the overlying ambient fluid, creating a more dilute, turbulent daughter current (e.g., as described from experiments by Hampton 1972 and Talling *et al*. 2002, and inferred for an ancient deposit by Strachan 2008).
4. *Fluidization transformations* occur mainly above highly concentrated pyroclastic flows as a dilute cloud of elutriated material forms a secondary, less concentrated, and turbulent flow (elutriation = the upward flushing out of fine particles by escaping fluids).

Gravity flows that undergo transformations along their path is termed *composite flows* by Haughton *et al*. (2009), with the deposits referred to as *hybrid event beds*. These authors propose a classification (Fig. 8a) that includes these composite flows and their deposits. Contrary to the better-understood case of gradual flow dilution and deposition of progressively more organized and finer-grained deposits in the downdip direction (Fig. 8b1), composite flows increase in concentration distally and transform, in part, into mudflows or debris flows (Fig. 8b2). Three processes can force an increase in concentration and suppression of turbulence (Haughton *et al*. 2010; Fig. 9):

(i) deceleration of a clay-rich flow so that viscous effects become dominant;

(ii) segregation of clay components into trailing and lateral parts of a flow so that turbulence intensity is damped;

(iii) addition of clay to the suspension by disintegration of soft clasts eroded along the travel path – a process referred to as ‘bulking’.

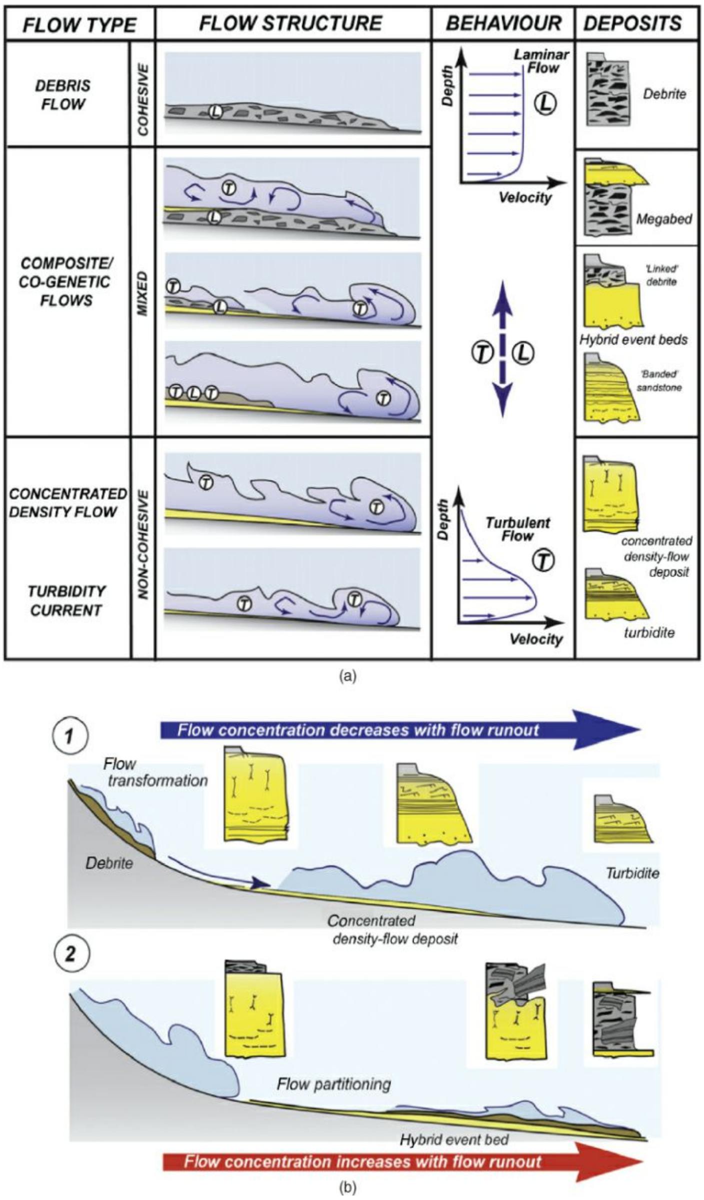


Figure 8 : (a) Haughton *et al*. (2009) classification scheme for event beds emplaced by subaqueous sediment gravity flows. (b1) Debrites, concentrated density-flow deposits and turbidites dominate the record of many deep-water systems and record increasing downdip dilution of the flow (debrites passing to concentrated density-flow deposits and eventually turbidites). (b2) In some systems there is instead a downdip progression from non-cohesive flows (depositing concentrated density-flow deposits and turbidites) to flows transformed into components with radically different rheology, with the deposits of the cohesive flow components increasingly dominant distally. From Haughton *et al*. (2009) who used 'high- and low-density turbidity currents' instead of 'concentrated density-flows and turbidity currents', (in Pickering et al., 2015).

The first of these processes has been studied experimentally by Sumner *et al*. (2009) and Baas *et al*. (2011). With rapid deceleration of a flow carrying ~10% suspended clay, silt and sand, Baas *et al*. (2011) hypothesize that a basal relatively clean sand division can accumulate rapidly because of a sharp decay in the total transport capacity for sand. This decrease results from a decline in turbulence support that occurs more quickly than the parallel increase in cohesive support.

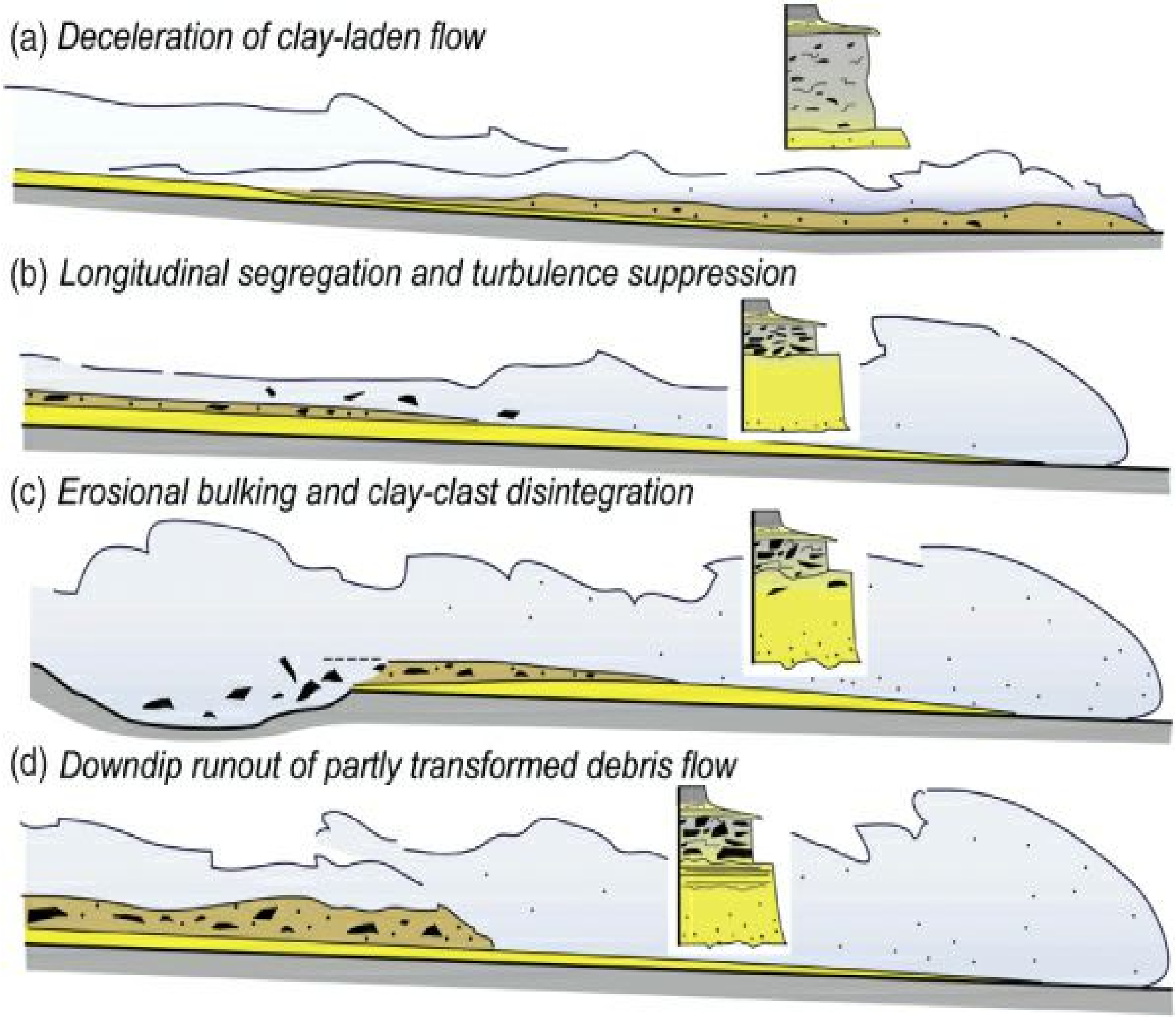


Figure 9 : Summary of depositional origin for hybrid event beds as a result of (a) loss of turbulence and deceleration of a clay-rich flow, (b) longitudinal segregation of clays and clay flakes to suppress turbulence in the rear and margins of an otherwise turbulent flow, (c) bulking and disintegration of clay clasts to release clay near-bed in an otherwise turbulent flow and (d) downdip runout of a flow that was either synchronously triggered with a concentrated density flow, or that partially transformed to generate a forerunning concentrated density flow. From Haughton *et al*. (2010), (in Pickering et al., 2015).

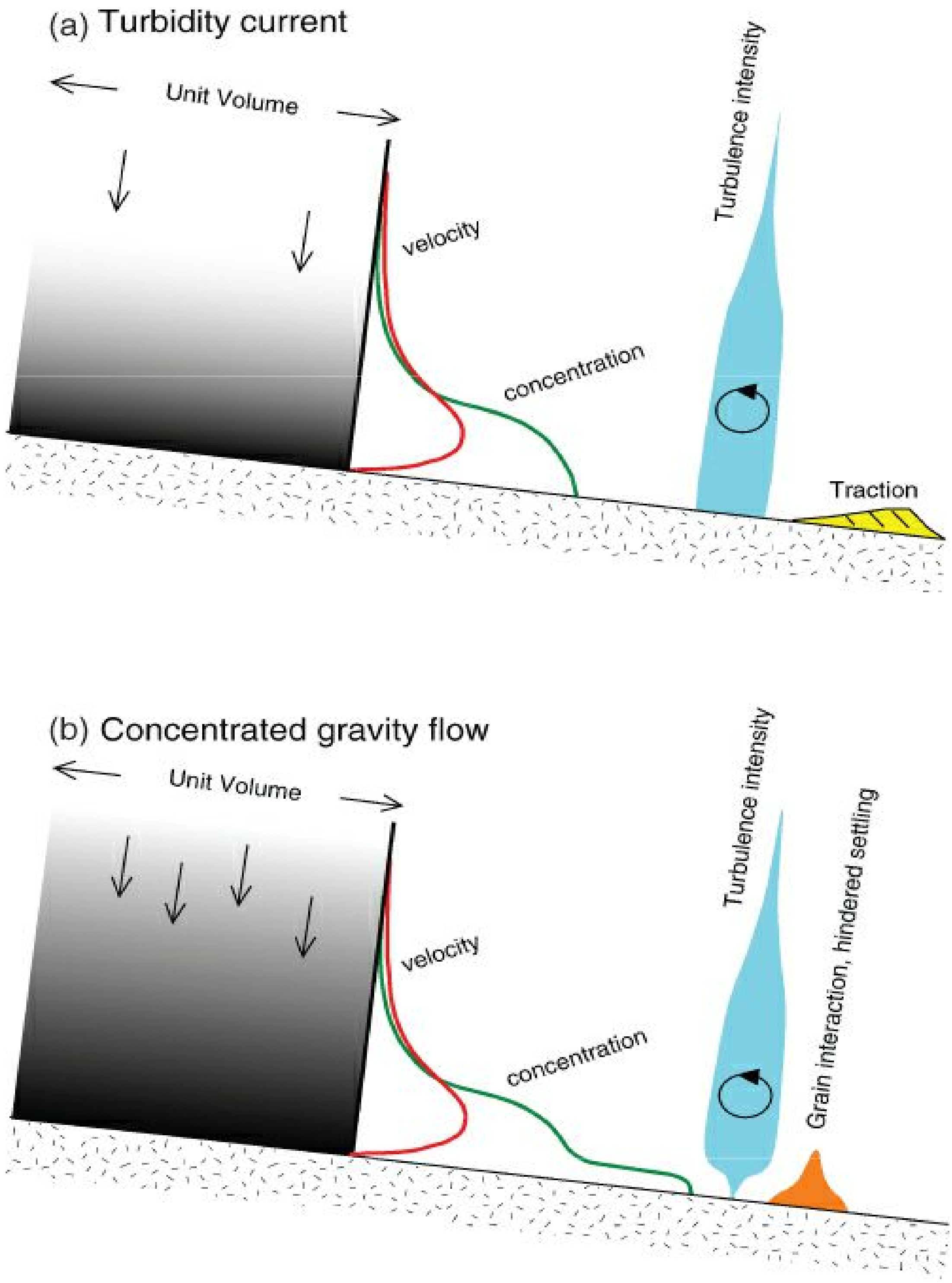


Figure 10: Contrasting near-bed grain support between a turbidity current and a concentrated density flow. Although both types of **SGF** are turbulent away from the sedimentation surface, the latter has strong grain interaction at the aggrading bed, and turbulence is sufficiently damped to prevent the development of tractional sedimentary structures (Pickering et al. 2015).

## II.2. Turbidity currents and turbidites:

### II.2.1. Definition and equations of flow:

Turbidity currents are density currents in which the denser fluid is a grain suspension, with particles supported largely by the upward velocity fluctuations associated with turbulent eddies (Bagnold 1966; Leeder 1983).

Entrained sediment diffuses throughout the flow thickness, but the highest particle concentrations are at the base of the flow (Stacey and Bowen 1988; Middleton 1993; Felix 2001) the coarsest size fractions carried toward the lower part of the flow of the turbidity current may be ***i)*** relatively short, quickly passing an observation point on the seafloor (*surge-type flow*); or ***ii)*** relatively long with steady discharge due to prolonged input from a long-lived source (steady and uniform discharge – generally river-fed as '*hyperpycnal*' flows) (Mulder and Syvitski 1995; Mulder et al. 2001, 2003; Alexander and Mulder 2002; Felix et al. 2006).

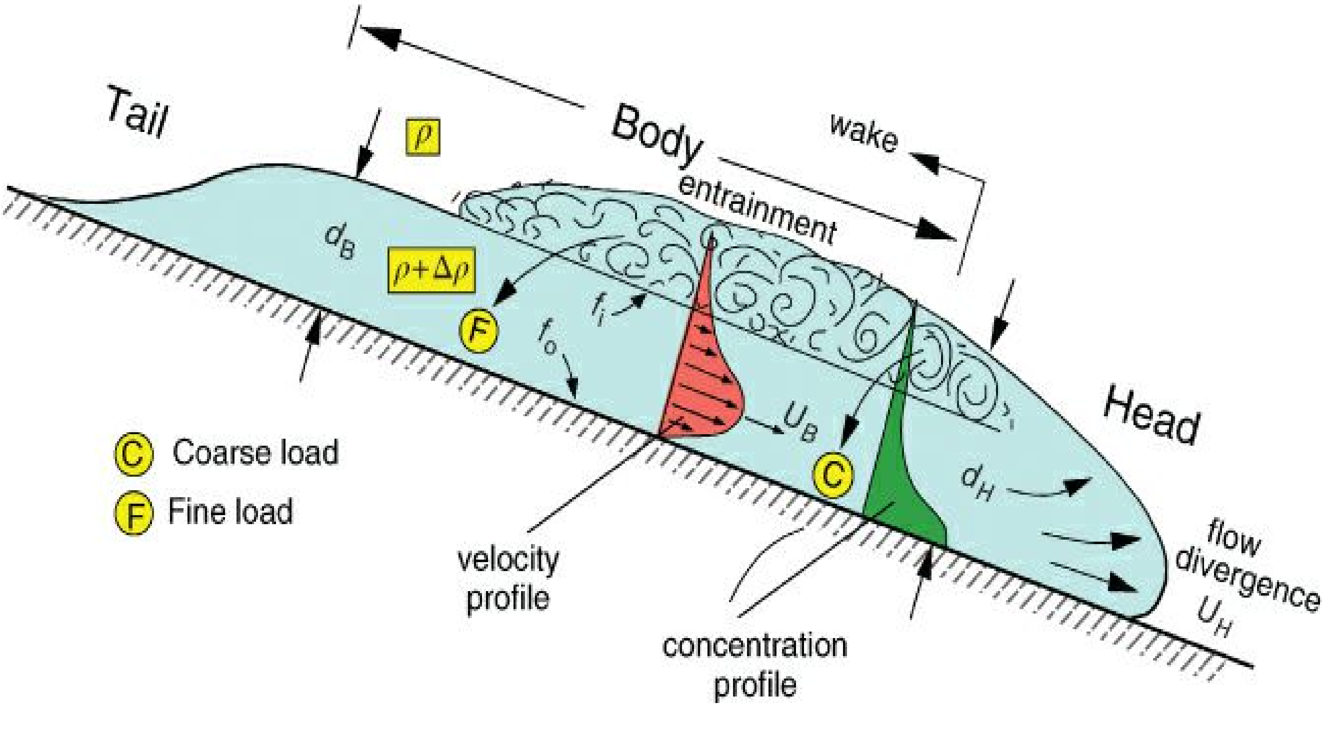


Figure 11**:** Idealized streamwise cross-section of a turbidity current, divided into head, body and tail regions. Settling from the wake behind the head produces a lateral size grading in the flow (Pickering et al. 2015).

The near-bed concentration controls settling rates, intensity of turbulence and the formation of sedimentary structures. Concentration influences flow density and viscosity but has little effect on the flow mechanics of a turbidity current until particle concentrations become so high that ***I)*** interparticle collisions become an important component of grain support even well above the bed (Fig. 7), or ***ii)*** turbulence, particularly near the bed, becomes damped (Fig. 10).

The Properties of the evolving flow are controlled by numerous critical parameters such as the rates of sediment loss through deposition, and dilution of the suspension through seawater entrainment. For continuously-fed flows, the maximum velocity is in the lower part of the body of the current (Fig. 11) and is ∼1.6 times the mean velocity (Felix 2004). The finest grain sizes have a uniform concentration throughout the flow, whereas the coarsest grain sizes are mostly concentrated near the base of the flow (Hiscott 1994a). There is differential transport rate triggered by differences in flow velocity between which is lower near the base of the flow than in the vicinity of the velocity maximum. This differential velocity makes coarse size fractions lagging behind fine fractions and may lead to basal inverse grading in the deposits of turbidity currents (Hand and Ellison 1985; Hand 1997). In most cases, the lower part of the flow will contain coarser sediment. If it also has a higher concentration, then the coarse fractions may outpace the upper part of the same flow with its finer sediment load (opposite to the predictions of Hand 1997). Sequential deposition as the flow passes will produce a graded bed, with the smoothness of the grading depending on the initial density structure of the flow.

### II.2.2. Natural variations and triggering processes of turbidity currents:

Initially, the theory of flow and deposition of turbidity-currents was based mainly on observations from simple, small-scale experiments (Middleton 1993), leading to predicted facies characteristics simpler than those encountered in nature. Natural currents, however, are strongly stratified (Gladstone *et al*. 2004) and are deepely influenced by irregular seabed topography, opposing slopes, or are confined within meandering channels, all of which modify flow behavior and direction.

Various processes can trigger natural turbidity currents (Normark and Piper 1991; Van den Berg *et al*. 2002): ***i)*** hyperpycnal flow from rivers and glacial meltwater (Heezen *et al*. 1964); ***ii)*** sand liquefaction (Seed and Lee 1966; Andresen and Bjerrum 1967) in canyon heads, triggered by storms, earthquakes or local failures, followed by water entrainment and acceleration; ***iii)*** breach failure which results from gradual backsapping (retrogression) of an over-steepened slope in cohesionless material after an initial failure (Van den Berg *et al*. 2004; Mastbergen and Van den Berg 2003); ***iv)*** erosion of the front of a moving debris flow (Hampton 1972; Talling *et al*. 2002) or thickening and dilution of a debris flow as it undergoes an hydraulic jump (Weirich 1988); ***v)*** dilution of sediment slides (Ricci Lucchi 1975b; Cita *et al*. 1984; Hughes Clarke *et al*. 1990); ***vi)*** suspension of sediments in canyon heads by edge waves associated with storms (Inman *et al*. 1976, Fukushima *et al*. 1985); ***vii)*** ignitive flow of shelf suspensions that descend a basin slope and ***viii)*** ignitive flow of ash from pyroclastic falls.

***Hyperpycnal flow*** is the term used to describe river discharge which, because of a high suspended load, is denser than seawater so travels along the seabed as an underflow. The key to this process is the presence of a downward-increasing dominant gradient in salinity, and an upward-increasing gradient in temperature. The term *ignition* (Parker 1982) refers to a state in which an accelerating density current entrains more sediment along its path, which causes it to continue to accelerate and grow in size.

According to Normark and Piper (1991), ignition is favored by initial volume concentrations of particles of about 0.01, initial velocities of about 1 m $s^{-1}$ (fine-grained sand) to 1.2 m $s^{-1}$ (medium-grained sand), and slopes exceeding 3°. Pratson *et al*. (2000) instead explain that ignition is most effective on slopes of 2–2.5°; below this range the turbidity current will decay and die, whereas on higher slopes the quantity of entrained sediment is less and the turbidity current smaller.

Earthquakes are commonly used to be famous triggers for turbidity currents (Hiscott *et al*. 1993; Beattie and Dade 1996). Earthquake recurrence intervals follow a power law, as do many turbidite bed thicknesses (Hiscott *et al*. 1993; Rothman *et al*. 1994; Drummond and Wilkinson 1996). According to Kuribayashi and Tatsuoka (1977) and Keefer (1984), only earthquakes with magnitudes greater than about 5.0 can cause significant sand liquefaction and, as the distance from the epicentre increases, so does the minimum magnitude required for liquefaction. Frequent earthquakes would be capable of liquefying sediment and triggering sediment gravity flows over a wide area (Keefer 1984).

### II.2.3. Supercritical flow of turbidity currents:

A fundamental distinction can be made between turbidity currents that are subcritical (Froude Number, $F < 1.0$) and those that are supercritical ($F > 1.0$). The transition to subcritical flow occurs as the bottom gradient declines, and may involve a hydraulic jump with intense turbulence and flow homogenization (Middleton 1970; Komar 1971). Hydraulic jumps have considerable effect on the formation of widespread scours and lenticular deposits of all scales (Mutti and Normark 1987 1991; Garcia and Parker 1989; Alexander and Morris 1994; Vicente Bravo and Robles 1995).

### II.2.4. Autosuspension in turbidity currents:

It is frequently claimed that turbidity currents can effectively carry sand-sized detritus across basin-margin slopes without leaving a deposit: there may even be net erosion in these areas (i.e., flow *ignition*). Weaver (1994) demonstrated slope bypassing by large mud-rich turbidity currents entering the Madeira Abyssal Plain (*cf*. Stevenson *et al*. 2013) by examining their reworked coccolith assemblages. Such 'bypassing' requires that the turbidity current remain at the least self-sustaining on the slope, or while flowing through slope channels. This process of 'self maintenance' (Southard and Mackintosh 1981) was named *autosuspension* by Bagnold (1962). The excess density of the grain suspension, combined with the downslope component of gravitational acceleration, induces basinward flow. The turbulence generated by the flow maintains the grains in suspension (Middleton 1976; Eggenhuisen and McCaffrey 2012), and the suspension maintains its density contrast with the overlying seawater, allowing continued flow, turbulence generation and effective grain suspension. According to Allen (1982) and Pantin (1979), true autosuspension is probably not common in nature, except for thick turbidity currents carrying fine particles on steep slopes. For all other cases, some of the suspended load settles and is deposited (Alexander and Mulder, 2002).

### II.2.5. Turbidites:

Deposits of turbidity currents are called *turbidites*. They show evidence of grain-by-grain deposition from evolved currents. Such evidence includes size grading, presence of lamination, or organized grain fabric with moderate to low angles of imbrication (Hiscott and

Middleton 1980; Arnott and Hand 1989). As explained by Mulder and Alexander (2001), the imprint of fluid turbulence and grain-by-grain behavior should be stronger in these deposits than the imprint of grain-to-grain interactions (Fig. 6). The character of turbidites depends on the mode of deposition than on the long-distance transport mechanism. Depositional process is mainly a function of: ***i)*** flow concentration near the sediment bed and ***ii)*** rate of deposition. The latter is dependent on the rate of decrease of both *flow competence* – the coarsest particle that can be transported, and *flow capacity* – the sediment discharge over the cross-section of the flow. Competence and capacity both decrease as mean velocity decreases (Hiscott 1994a). Any of the following reasons may make flow velocity decreases: **i)** decreasing bottom slope; **ii)** flow divergence; **iii)** increased bed friction; **iv)** increased particle interaction (intergranular friction); **v)** decreasing flow density due to deposition; or **vi)** deflection of slow, mud-rich flows by contour currents or by the Coriolis effect so that they are constrained to move roughly parallel to the slope contours rather than down the slope (Hill 1984a). High proportion of suspended mud can make flows move for a greater distance than mud-poor flows without suffering a crippling degree of sediment loss, even on quite gentle slopes (Salaheldin *et al*. 2000). Such flows are therefore more 'efficient' in moving both their mud- and sand-size loads into the basin.

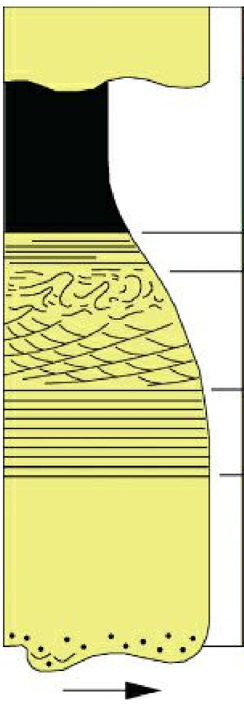

| GRAIN SIZE | BOUMA (1962) DIVISIONS | INTERPRETATION |
|---|---|---|
| Mud | ***e*** Laminated to homogeneous mud | Deposition from low-density tail of turbidity current + settling of pelagic or hemipelagic particles |
| Silt | ***d*** Upper mud/silt laminae | Shear sorting of grains and flocs |
| Sand | ***c*** Ripples, climbing ripples, wavy/convolute laminae | Lower part of lower flow regime of Simons *et al.* (1965) |
| Sand | ***b*** Plane laminae | Upper flow regime plane bed |
| Coarse Sand | ***a*** Structureless or graded sand to granule | Rapid deposition with no traction transport, possible quick (liquefied) bed |

Figure 12: Ideal sequence of sedimentary structures in a turbidite bed (from Bouma 1962, with interpretation from Harms and Fahnestock 1965; Walker 1965; Stow and Bowen 1980).

The Bouma sequence (Bouma 1962) (Fig. 12) represents a summary of the transitions observed in 1061 beds in the Grès de Peïra-Cava in the Maritime Alps of southern France. In a complete Bouma-type turbidite, the $T_a$ division is probably deposited during a phase of rapid fallout from suspension, without traction. Other divisions have been interpreted in relation to the progression of bedforms observed during deceleration of flow in flumes (Harms and Fahnestock 1965; Walker 1965), but with omission of dunes. Most natural turbidites do not contain all five Bouma divisions, but instead are missing one or more basal division. Beds lacking upper divisions and dominated by structureless sand are more likely the deposits of concentrated density flows.

The Bouma sequence is considered a good model for medium-grained deposits of many surge-type turbidity currents (Mulder and Alexander 2001), but can not clearly explain fine-grained turbidites that consist entirely of Bouma's $T_d$ and $T_e$ divisions. As a completely contrary opinion on the genesis of the Bouma (1962) divisions $T_b$–$T_d$, Shanmugam (2000; 2008) attributes the laminated nature of these divisions to reworking of the tops of sand beds by deep-water bottom currents generated by thermohaline circulation, ocean tides, shoaling internal waves or atmospheric winds.

In his view, the original sand beds are more likely to have been deposited by sandy debris flows (our inflated sandflows) than by turbidity currents. Shanmugam (2000) only attributes the normally graded parts of a basal $T_a$ division to direct accumulation beneath a turbidity current. Shanmugam (2000) argument points to the uncommon occurrence of complete Bouma sequences in nature, and extends this argument further to suggest that if turbidity currents are responsible for the lamination, then there should be documented examples of beds possessing all 16 divisions of the Lowe (1982), Bouma (1962) and Stow and Shanmugam (1980; Fig. 13) idealized structural sequences, which those authors have attributed to accumulation beneath decelerating turbulent density currents.

Let us consider a **SGF** that descends the upper slope as an inflated sandflow, transforming along the trend of water entrainment and dilution into first a concentrated density flow and then a turbidity current. The first deposits would consist of the coarsest grain-size fractions, either structureless because of the high rate of fallout, or with structures indicative of particle interaction (e.g., spaced stratification of Hiscott 1994b). This material would be left behind, perhaps covered by a thin level of fine fallout of sediment from a residual dilute cloud, and the remainder of the flow would bypass this area and move farther downslope to deposit finer sediment with different sedimentary structures and different structural divisions. Hence, Shanmugam (2000) might be theoretically correct that a single **SGF** could deposit all 16 structural divisions if it had a sufficiently broad range of grain sizes in suspension, but these divisions would logically be strung out for tens to hundreds (or even thousands) of kilometers along the path of the evolving flow, and so would never be found at a single locality.

### II.2.6. Cross-stratification in turbidites:

Many individual graded beds have sole markings and divisions of cross-stratification or ripple lamination indicating flow reversals during deposition. Grain fabric data obtained by Pickering and Hiscott (1985) from the bedforms described by Skipper (1971) indicate that the depositing current flowed in a direction opposite to that indicated by most flutes in the sequence. Prave and Duke (1990) and Yagishita (1994) described wavy bedforms with lengths of about 1 m from turbidites and interpreted these as antidunes.

### II.2.7. Turbidites from low-concentration flows:

The deposits of low-concentration, mud-load turbidity currents have been widely described by Piper (1978), Stow (1979), Stow and Shanmugam (1980) and Stow and Piper (1984b). As many beds contain only Bouma's $T_d$ and $T_e$ divisions, the Bouma divisions for sandy turbidites are too general for mud turbidites; to further subdivide mud turbidites, several schemes have been proposed and are outlined in Figure 13. Stow and Shanmugam (1980) recognized nine divisions, numbered $T_0$ to $T_8$. The physical structures in these nine divisions are believed to result from suspension fall-out and traction ($T_0$–$T_2$), shear sorting of silt grains and clay floccules in the bottom boundary layer ($T_3$–$T_5$) and suspension fall-out with no traction ($T_6$–$T_8$). Division $T_0$ corresponds to $T_c$ Bouma's division. As with Bouma-type turbidites, complete structure sequences are unusual; top-absent, base-absent and middle-absent sequences are also common (Stow and Piper 1984b).

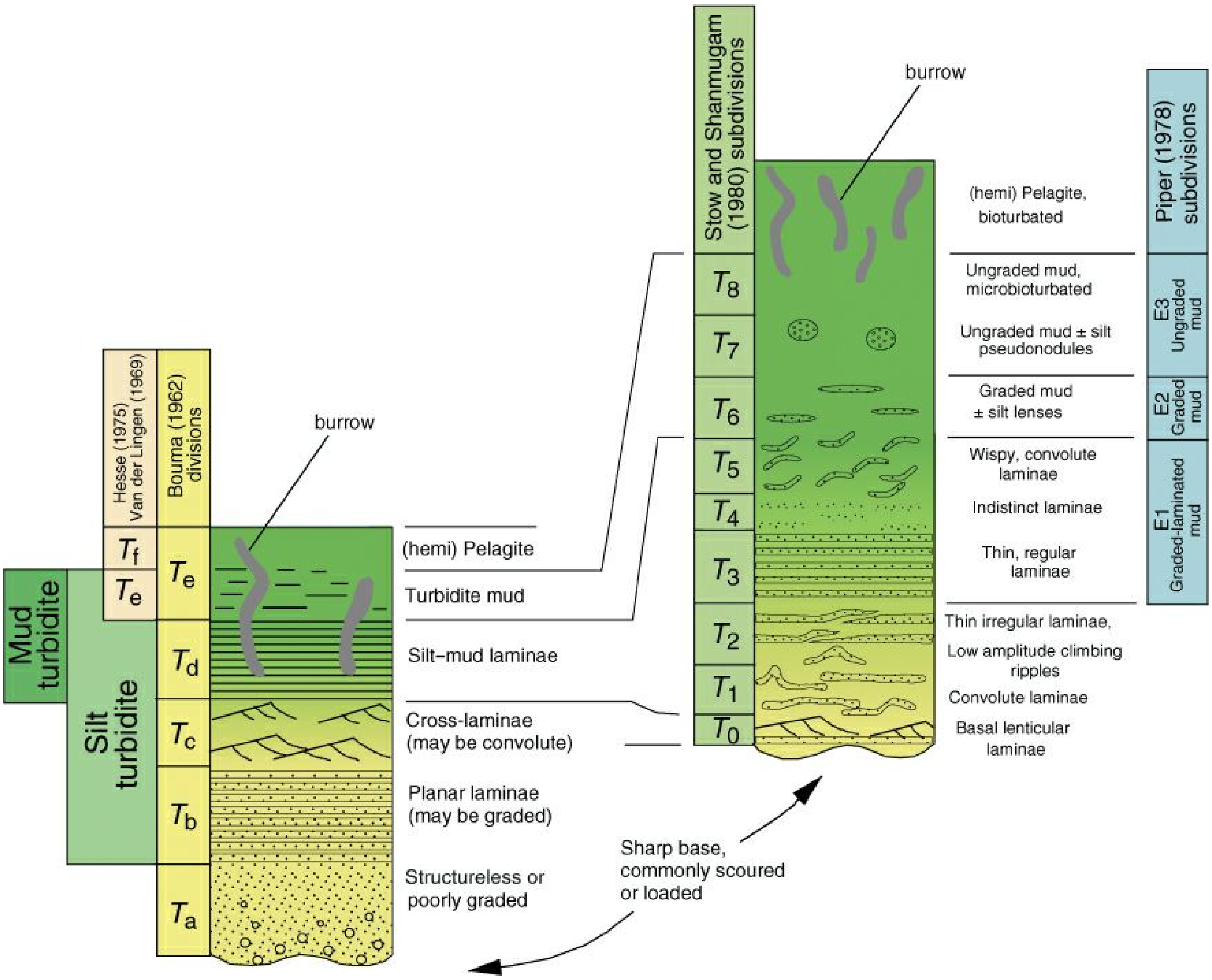


Figure 13: Summary of schemes for subdivision of fine-grained turbidites, based on Bouma (1962), van der Lingen (1969), Piper (1978) and Stow and Shanmugam (1980).

The very thin, regular laminations of division $T_3$ have been attributed to shear sorting near the base of the flow and then alternating deposition of silt grains and clay particles by settling through the viscous sublayer (Stow and Bowen 1980).

### II.2.8. Downcurrent grain size – bed thickness trends in turbidites:

Turbidites derived from a single source with a consistent range of grain sizes have been shown to exhibit a well-defined relationship between bed thickness and grain size (Fig. 14) (Sadler 1982). Sadler's curves indicate a downslope trend from ***i)*** proximal, relatively thin, medium-grained beds, to ***ii)*** intermediate, relatively thick, somewhat coarser grained beds, to ***iii)*** progressively finer-grained and thinner beds with increasing distal transport. The 'distal limb' of this trend is relatively easy to explain. Sadler (1982) calculated that 'for a given flow density and slope and with a uniform grain-size distribution, bed thickness becomes proportional to the square root of bed shear stress cubed'. Hence the decrease of both competence and capacity as turbidity currents decelerate leads to a related decrease of both grain size and bed thickness.

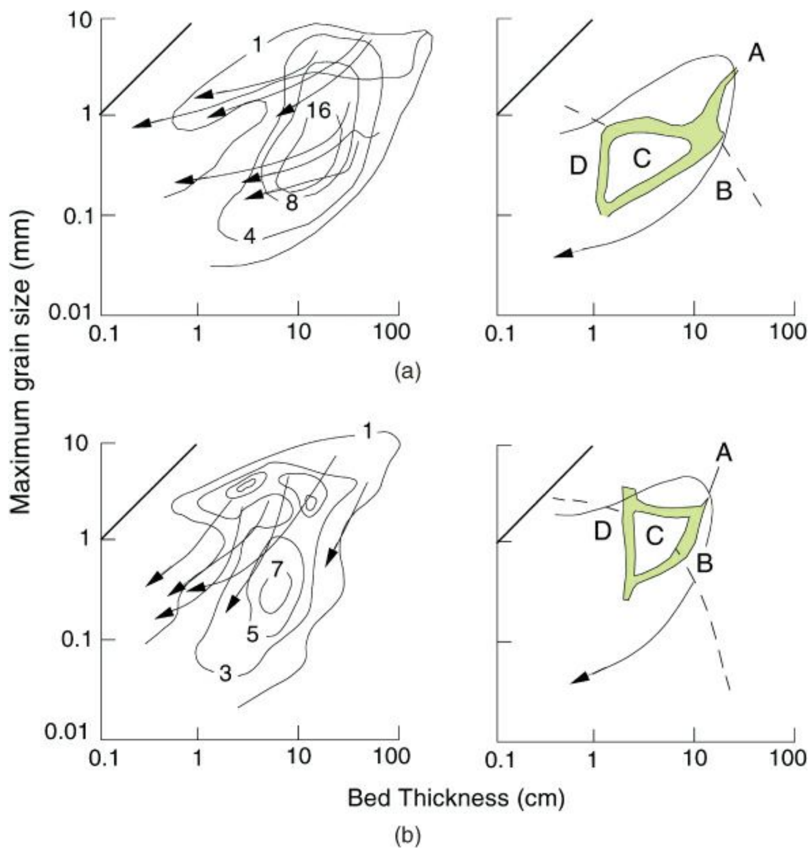


Figure 14: Maximum grain size plotted against bed thickness for Lower Carboniferous turbidites of (a) the RhenaerKalk (498 beds), and (b) the Posidonienkalk (235 beds), from Sadler (1982). The left-hand diagrams show contours of density of data points representing total bed thickness and corresponding maximum grain size. Arrows are selected vertical grading curves using the x-axis scale as a 'distance to top of bed'. The right-hand diagrams show fields for Bouma divisions $T_a$ through $T_d$ found at the base of the beds for which maximum size was determined. Green zones = overlap of fields for divisions $T_b$, $T_c$ and $T_d$. Dashed line = lower limit of field for division $T_a$, which has extensive overlap with the other fields. Arrow = modal horizontal grading curve, based on contour pattern in left-hand diagram.

The 'proximal limb' of the trend involves a temporary downslope increase in both grain size and bed thickness and requires a special explanation. Sadler points to experiments of Kuenen (1951) that show a longitudinal decline of density and competence from the head to the tail of a turbidity current. As a flow that is in a state of autosuspension decelerates, deposition will begin beneath the tail of the current where competence and flow density are relatively low. 'The most proximal part of the deposit will therefore thicken and coarsen downcurrent until the point at which all of the flow, except a small region near the head, will be depositing sediment' (Sadler 1982).

## II.3. Concentrated density flows and their deposits:

The high concentrations of flows that lead to distinctive deposits might be limited to the lower parts of stratified flows which, farther above the bed, are less dense and more turbulent (Pickering et al. 2015). The features seen in the deposits of these flows certainly demonstrate significant grain-to-grain interaction and imply a suppression of turbulence near the sediment bed. According to Mulder and Alexander (2001), depositional processes include: ***i)*** rapid "en masse" deposition of a quick bed (Middleton 1967) due to an increase of intergranular friction; ***ii)*** generation of inverse grading at the base of the flow because of grain collisions and dispersive pressure; ***iii)*** formation of *spaced stratification* (formerly called *traction carpets*) under unsteady flows (Hiscott and Middleton 1979 1980; Hiscott 1994b; Sohn 1997); ***iv)*** grain-by-grain deposition with little subsequent traction transport (Arnott and Hand 1989); ***v)*** alternate deposition of bedload and suspended load (Walker 1975a); ***vi)*** deposition of mudclasts well above the base of the bed and ***vii)*** expulsion of pore-fluids when the primary, unstable, open-grain packing collapses, generating fluid-escape structures (Lowe and LoPiccolo 1974).

Because the transition between turbidity current and a concentrated density flow depends on the relative importance of fluid turbulence and other mechanisms in providing particle support, it is possible for a single current to undergo one or more transition between these flow types during its history. This might occur if an undulatory seabed, or variable amount of flow confinement, leads to alternating increases and decreases in speed along the flow path (Kneller and Branney 1995; Fig. 15).

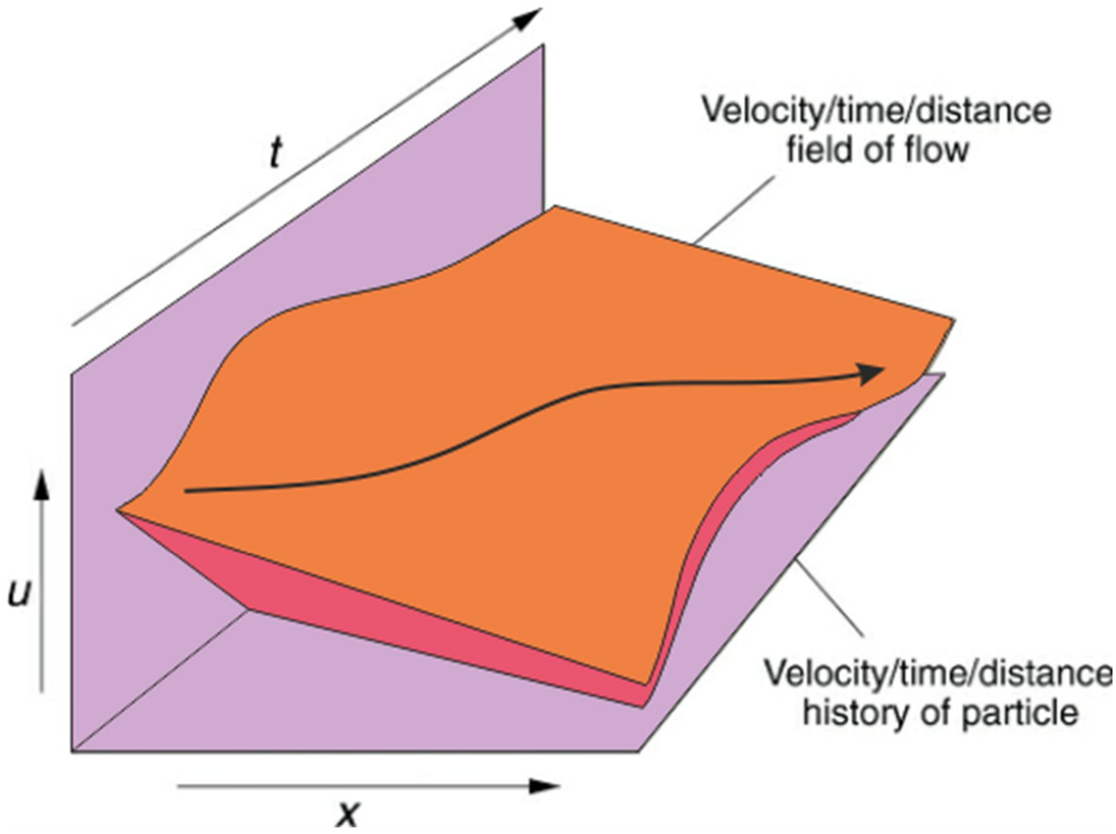


Figure 15: Graphical representation of the velocity history of a turbidity current (arrow) as it changes with time (*t*) and distance along the flow path (*x*). Redrawn from Kneller and Branney (1995).

Sharp decreases in speed would induce higher rates of particle fallout and intensified grain-to-grain interactions in the lower part of the flow. If these alternative support mechanisms dominate the depositional phase, then the deposits will reveal structures characteristic of deposition from a concentrated density flow rather than a turbidity current. Hence, it should always be remembered that these two flow types might be transitional when making interpretations about depositional environment and deposit distribution.

### II.3.1. Deposits from concentrated density flows:

Field studies have revealed sedimentary structures not present in the Bouma sequence for turbidites. One of these was initially called traction-carpet stratification but has since been renamed *spaced stratification* by Hiscott (1994b). The term *traction carpet* (Lowe 1982 division S2) was used to describe generally 5–10 cm-thick, inversely graded stratification found in some concentrated density-flow deposits. As originally envisioned, clasts in such carpets were believed to be sheared as a dense dispersion just above the bed, maintained by dispersive pressure (Bagnold 1956), until a critical thickness was reached that prompted “en masse” deposition. Within each such deposit, intense grain interaction was believed to be responsible for both a basal inverse grading, and a strong alignment of grains with imbrication angles commonly >20° (Hiscott and Middleton 1979) and Legros (2002).

Sedimentary structure sequences for the deposits of concentrated density flows have been presented by Aalto (1976), Hiscott and Middleton (1979), Hein (1982), Lowe (1982) and Mulder and Alexander (2001). From the analysis of Hiscott and Middleton (1979), except for some basal scour-and-fill structures, the first deposits accumulated by rapid “en masse” deposition, producing either a division of structureless coarse- to medium-grained sand or, in the case of highly unsteady flow, a division of spaced stratification. There is no evidence of grain-by-grain traction on the bed during the early stages of deposition, perhaps because the development of planar stratification is suppressed if the rate of bed aggradation exceeds ~4 cm $min^{-1}$ (Arnott and Hand 1989). At the top of most beds, deceleration of the more dilute tail of the current produced a sequence of structures like the Bouma sequence. In other examples, the dilute tail of the current reworked the sandy top of the initial deposit into large ripples or dunes, and then presumably continued down the fan surface to deposit its fine load at more distal sites (cf. Lowe 1982).

Structural divisions were produced either by rapid mass deposition (‘*freezing*’) or by selective grain-by-grain deposition with traction transport. In some cases, post-depositional reworking of the top of the bed is indicated by medium-scale cross-stratification.

Important additional divisions recognized by Hein (1982) are those bearing the imprint of syn- and post-depositional fluid escape; dish structures are particularly abundant in these rocks. Also, the pebbly sandstones of Hein (1982) contain more cross-stratification than was observed in finer deposits by Hiscott and Middleton (1979). Hein (1982) interpreted some of this cross-stratification as the product of reworking of the tops of the deposits by dilute flows that spilled into the submarine channel from other, nearby channels.

### II.3.2. Large mud clasts in concentrated density-flow deposits:

Many concentrated density-flow deposits contain large mud clasts, either dispersed well above the base of the bed, or concentrated into clusters or trains (Walker 1985; Postma et al. 1988; Shanmugam et al. 1995). Such clasts are commonly described to be ‘floating’ in the bed, and for this reason proposals have been made to explain how shale clasts can be suspended by sediment gravity flows, or by stratified two-layer flows.

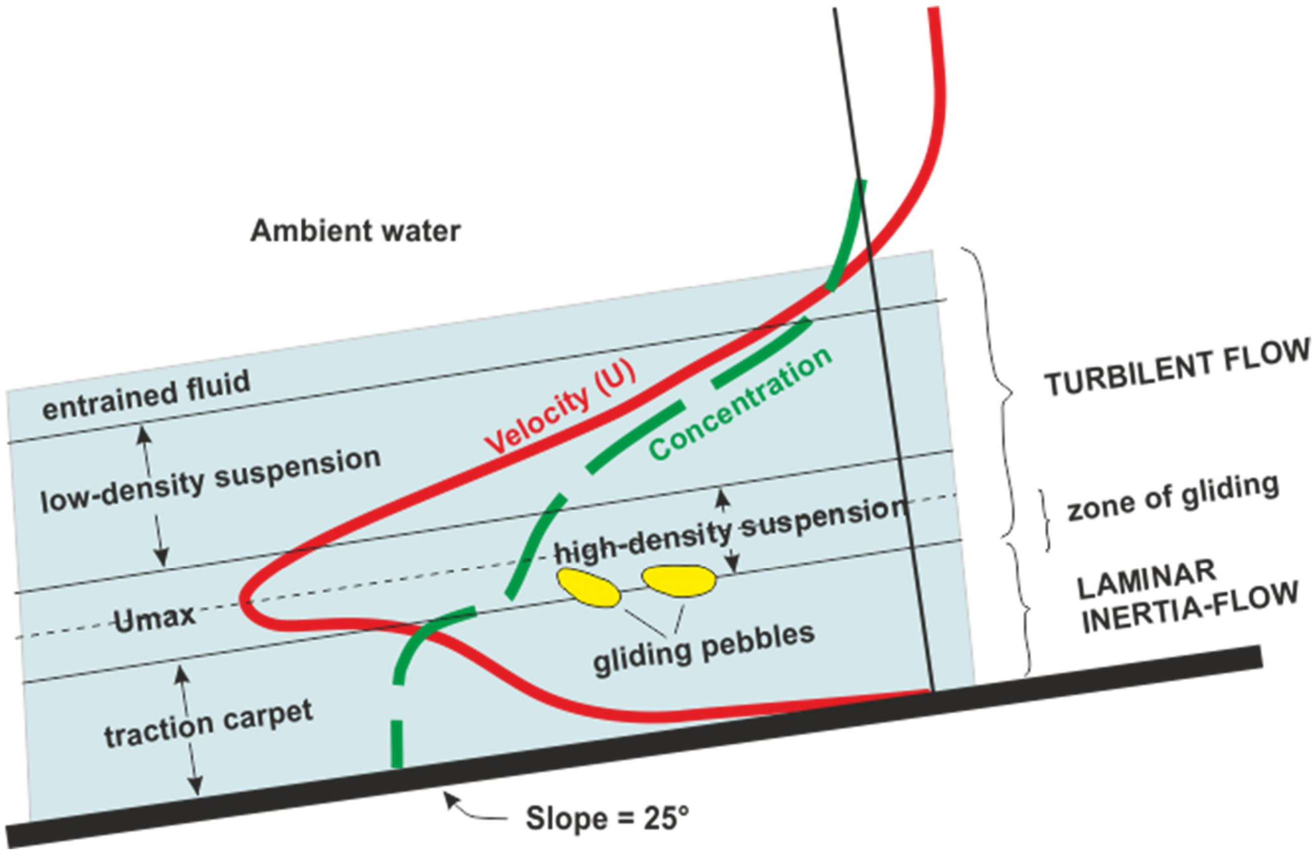


Figure 16: Mechanism proposed by Postma et al. (1988) for the transport of large mud clasts within a strongly stratified SGF. At 25°, the slope for the experimental demonstration of this effect is unreasonably high for natural SGFs.

Postma et al. (1988) employed flume experiments on high slopes of 25° to show how large clasts can be carried along the interface between a highly concentrated, laminar, basal inertia-flow, and a less concentrated, fully turbulent overriding flow (Fig. 16). They proposed that larger natural two-layer flows could operate in the same way on much lower slopes after undergoing a ‘gravity transformation’ (Fisher 1983). Shanmugam et al. (1995) instead interpreted ‘floating’ clasts in structureless sands as a strong indicator that the deposits were emplaced by inflated sandflows (his sandy debris flows), not turbidity currents or concentrated density flows. Hiscott et al. (1997a) disputed this generalisation, noting that concentrated density flows are deposited from the base upward through progressive aggradation (Kneller and Branney 1995), so that part way through the depositional phase the seafloor corresponds to some level well above the base of the eventual deposit. If a mud clast is rolling or sliding along the bed and then ceases to move, it will subsequently be buried by sand and will appear to be suspended in sand. Outsized mud clasts rolling and sliding beneath a concentrated density flow might be expected to reach their final resting place well after deposition of some thickness of sand, because they would travel much more slowly than the mean velocity of the current (Hand and Ellison 1985).

Recent interpretations of 'hybrid event beds' (Haughton *et al*. 2009) explain large floating clasts in deposits having a graded sandy basal division as the product of flow transformation ('gravity transformation') from a turbulent density flow to a debris flow. The basal part of such deposits records accumulation from a turbulent flow, so is organized and graded (Fig. 8a). The clast-rich interval is more muddy and disorganized, because it was deposited from as a concentrated density flow (Fig. 9), leading to stacked deposits comprising a single event bed with large mud clasts in the upper part (Haughton *et al*. 2010). Alternatively, the large clasts might have been carried by a co-genetic debris flow that was triggered at the same time as a concentrated density flow (Fig. 9), leading to stacked deposits comprising a single event bed with large mud clasts in the upper part (Haughton *et al*. 2010).

### II.4. Inflated sandflows and their deposits:

Inflated sandflows are envisaged to range in density from ~40% to 70% by, most of which is coarse silt or larger in size, and the bulk of which is sand. Variable amounts of gravel can also be present. Cohesion is minor (Fig. 6 ), and voids between particles are well connected. Mulder and Alexander (2001) explain that this facilitates the ingesting of seawater and therefore the transition of many inflated sandflows to concentrated density flows. Inflated sandflows lack significant cohesive strength but do possess frictional strength because of grain-to-grain interlocking when concentrations become very high, for example as velocity decreases and deposition starts. As a result, deposition from inflated sandflows takes place by frictional '*freezing'*.

Even though cohesion is not a significant contributor to particle support, a small amount of interstitial mud, or very poor sorting, are required to permit these sandflows to operate on low slopes. Mud, or the very small pore throats that characterize poorly sorted sand, will dramatically reduce the permeability of the mobile sediment and therefore slow the dissipation of excess pore-fluid pressures that contribute to particle support. Without the elevated pore-fluid pressures or cohesion provided by small amounts of clay, inflated sandflows would depend entirely on grain interaction for maintenance of the suspension, and would be pure grain flows. As pointed out by Mulder and Alexander (2001), grain flows cannot operate on slopes less than ∼13°, and as little as 2% by volume clay will permit flow on low slopes if the remaining sediment is fine-grained sand. A maximum of ∼20–25% by volume clay is required at water contents of 25–40% by volume if the rest of the sediment is coarse-grained sand ± gravel (Hampton 1975; Marr *et al*. 2001). In natural poorly sorted mixtures of sand, the fine-grained sand between any larger sand grains will ensure that no more than ∼2% by volume clay is required to significantly reduce the rate of pore-fluid escape.

When clay content is low and the sandy sediment is poorly sorted, the mobility of inflated sandflows is facilitated by the extended persistence of elevated pore-fluid pressures, and by grain-to-grain interactions. When mud forms ∼10–25% of the detrital fraction, the flows may resemble the 'slurry flows' described by Lowe *et al*. (2003). As an explanation for the long runout distances seen in the more muddysandflows, Mulder and Alexander (2001) point to the increased coherence of the flow mass that results from the presence of cohesive particles (i.e., clays). 'Coherence' is the ability of a mixture to hold together and support sediment (Marr *et al*. 2001). For flows with low coherence (i.e., low clay contents), the rheological strength of the material is unable to fully resist the dynamic stresses generated by the flow (Marr *et al*. 2001), leading to uninhibited internal deformation.

Inflated sandflows are more susceptible to 'shear mixing' with ambient seawater than clay-rich cohesive flows, because of their lower coherence and connected voids (Marr *et al*. 2001; Talling *et al*. 2002). Shear mixing is the erosion of the front and top of a SGF because of its movement beneath ambient fluid. This erosion produces a secondary dilute turbidity current (Hampton 1972).

The high particle concentrations do not permit selective deposition and the formation of lamination by traction transport. Grain sorting cannot occur by the differential settling of coarser and finer grains (Mulder and Alexander 2001); hence, deposits lack normal grading or only show poor coarse-tail grading (Marr *et al*. 2001). They may be inversely graded, however, because of grain-to-grain interactions or because the base of the flow undergoes greatest and most prolonged shear, leading to reduced competence (Hampton 1975). The dissipation of elevated pore-fluid pressures often produces fluid-escape structures like dish structures and fluid-escape pillars. In more muddy deposits, a minor but significant amount of cohesion facilitates the development and preservation of a variety of shear laminae and banding, and deformation structures (Lowe *et al*. 2003). If a turbidity current is generated by shear mixing at the upper interface of the inflated sandflow, an organized turbidite might directly overlie the primary deposit, but more likely will accumulate more distally on lower slopes (Marr *et al*. 2001).

Although frictional 'freezing' is the cause of deposition, Mulder and Alexander (2001) conclude that the entire flow does not deposit "en masse". However, thick subaqueous flows might behave differently, and 'freeze' from the top downward as shear stress drops below the frictional strength of the material. Because the shear stress is lowest toward the flow top, the first grain interlocking and arrested internal motion might take place there, leading to the formation of a semi-rigid plug which would thicken downward as deceleration continues. The main variables that distinguish the flows responsible for these deposits are flow concentration, shear rate and deposition rate (Fig. 17) (Branney and Kokelaar (2002)). For relatively low concentrations in turbidity currents, high shear rates produce tractional structures whereas low shear rates with fine-gained suspensions can lead to little traction and structureless deposits. For relatively high concentrations, high shear rates at the accumulating bed produce a sharp interface and strong grain fabrics, whereas low shear rates across a diffuse depositional boundary (perhaps because of strong pore-fluid escape and elutriation) lead to weak fabrics in deposits with signs of syn-depositional liquefaction and fluid escape.

## II.5. Cohesive flows and their deposits:

### II.5.1. Definitions and equations of flow:

*Cohesive flows* are characterised by strong coherence, so that they hold together while flowing along the seabed (Marr *et al*. 2001). The coherence is created by cohesive forces between electrostatically charged clay minerals. Mulder and Alexander (2001) distinguish between *mudflows* and *debris flows*. The mudflow deposits have less than 5% by volume gravel and more mud than sand.

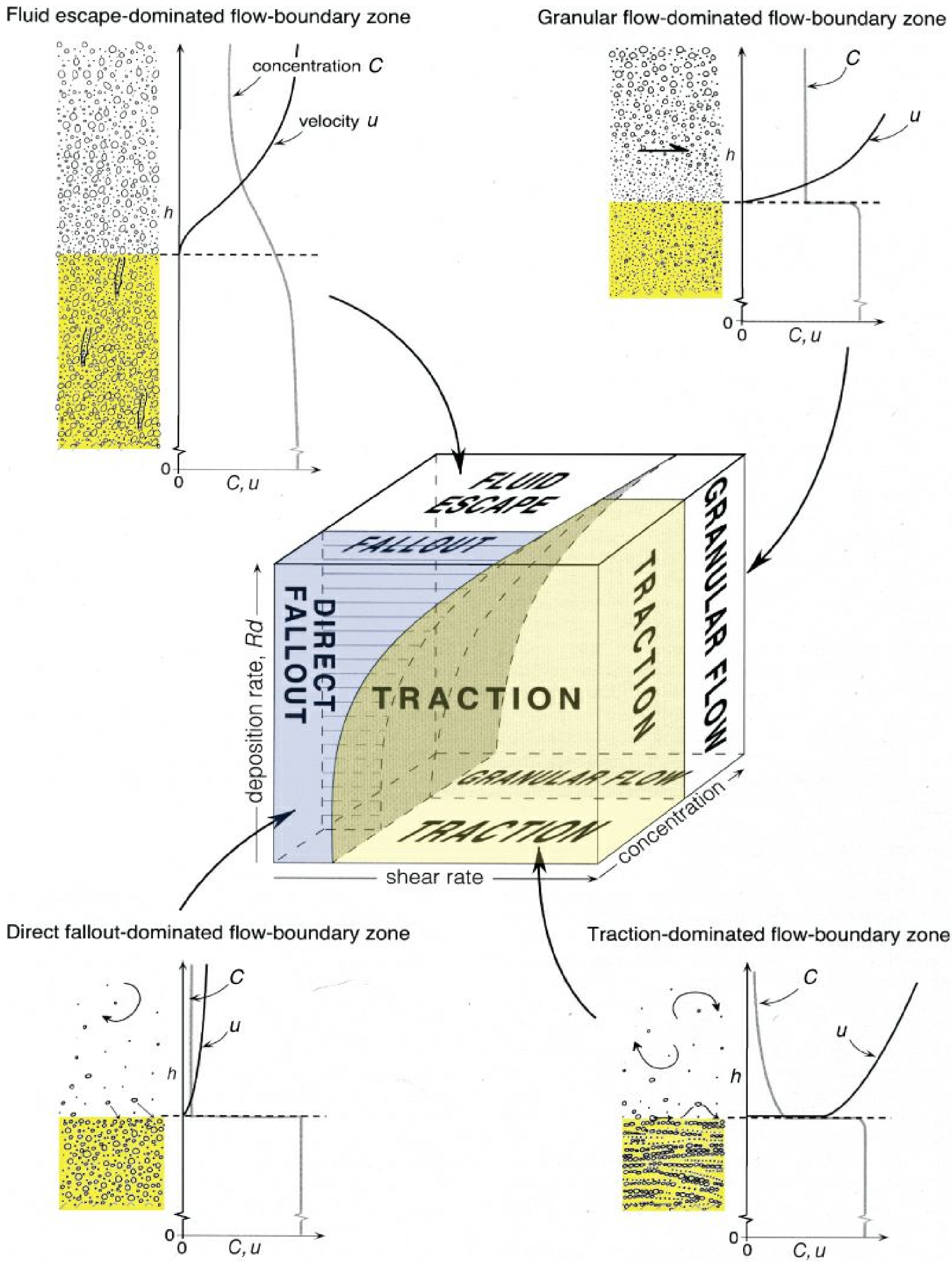


Figure 17: Process cube to explain deposits from sandload **SGFs**. High concentrations (the two upper scenarios) form typical deposits of inflated sandflows and some concentrated density flows. From Branney and Kokelaar (2002), (in Pickering et al., 2015).

The debris-flow deposits consist of more poorly sorted sediment (>5% by volume gravel with variable sand proportion) and may include boulder-sized clasts of soft sediment or rock and very large sediment rafts. The name 'debris flow' commonly is used for both a flow process and a deposit. For clarity, however, the term 'debris flow' is used **for the process** only, and *debrite* **for the deposit**.

Cohesive flows are only well described from modern subaerial settings (Pierson 1981; Takahashi 1981; Middleton and Wilcock 1994). According to Takahashi (1981), cohesive flows are flows 'in which the grains are dispersed in a water or clay slurry with the concentration a little thinner than in a stable sediment accumulation.

In terms of rheology, cohesive flows encompass wet concrete and exhibit *strength*, which can be divided into two components: (1) cohesive strength due to electrostatic attractions between clay-size particles, and (2) frictional strength due to interlocking and surface contacts between clasts and between the flow and its bed. According to Pierson (1981), frictional strength far exceeds cohesive strength as a mechanism of clast support. Strength, and buoyancy of clasts in the matrix, permits the flow to carry clasts above the bed that are more dense than the bulk density of the flow itself.

Although cohesion is a primary support mechanism in both mudflows and debris flows, natural flows exhibit a wide variation in the relative importance of grain-support mechanisms. In particular, elevated pore-fluid pressures are important in explaining the mobility of many cohesive flows (Pierson 1981; Ilstad *et al*. 2004a). Once mud-rich sediments fail and the electrostatic forces responsible for cohesion are broken, the material tends to remain mobile throughout its downslope flow, even on low slopes.

### II.5.2. Turbulence of cohesive flows:

Most cohesive flows are laminar, with no fluid mixing across streamlines. Large flows may be turbulent (Enos 1977; Middleton and Southard 1984), but should not be classified as turbidity currents or concentrated density flows because they lack the strong vertical concentration gradients of more dilute currents, and because they re-acquire laminar behavior and develop a semi-rigid plug with deceleration. Even in laminar flows devoid of eddies, secondary circulation due to clast rotations, or due to flow meandering, may cause churning and internal mixing. For Bingham plastics, the criterion for turbulence is based on both the *Reynolds Number, R*. and the *Bingham Number, B*. Basal scour beneath fully freighted laminar cohesive flows generally is insignificant (Takahashi 1981), possibly because in cases where hydroplaning results this allows the flow to ride along on top of a thin sheet of overpressured water or wet, low-viscosity, mud (Mohrig *et al*. 1998; Ilstad *et al*. 2004b). Also, the lack of turbulence decreases the chance of erosion because fluid scour is inoperative. Nevertheless, underlying sediments may be plucked up and incorporated into the flow because of high shear stresses along the basal interface (Hiscott and James 1985; Dakin *et al*. 2013). Where large cohesive flows impinge upon the base of submarine slopes, they can gouge and disrupt the underlying strata (e.g., Hiscott and Aksu 1994) and produce 10–30 m-deep erosional channels, grooves and scour pits, perhaps facilitated by partial liquefaction of the rapidly loaded substratum of unconsolidated or weakly lithified sediments (Dakin *et al*. 2013). Cohesive-flow deposits also may occur in channels cut by other processes, as these flows seek out bathymetric lows.

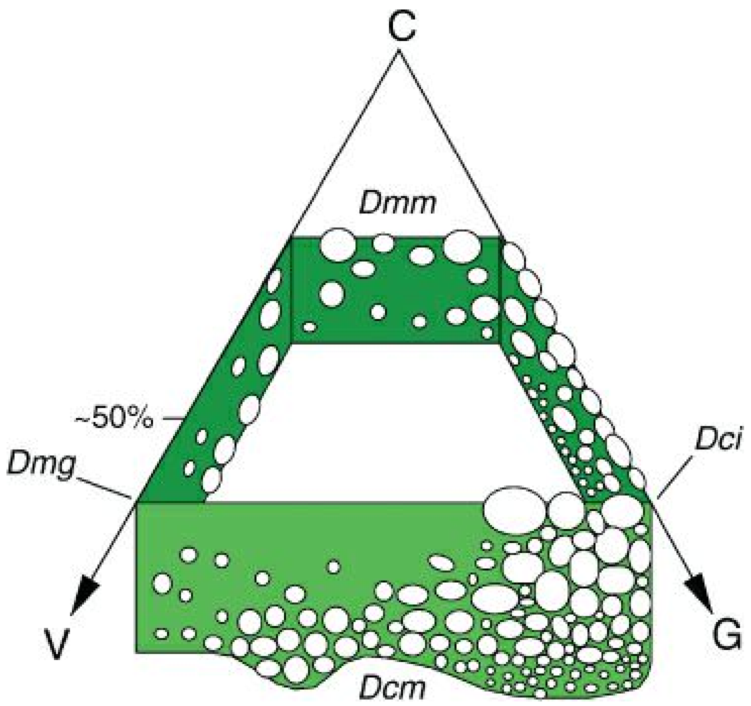


Figure 18: Schematic diagram of relationships among debrite types. See text for abbreviations. Redrawn from Shultz (1984): intermediate in character between four distinct end-member facies: *Dmm* = 'massive' (structureless) matrix-supported debrite, *Dmg* = graded matrix-supported debrite, *Dci* = inversely graded clast-supported debrite, and *Dcm* = 'massive' (structureless) clast-supported debrite (Shultz 1984), (in Pickering et al., 2015).

### II.5.3. Deposits of cohesive flows, including debrites:

Cohesive-flow deposits are poorly sorted, lack distinct internal layering but may have crude stratification due to non-uniform migration through the flow of the base of the semi-rigid plug during deceleration (Hampton 1975; Thornton 1984; Aksu 1984), have a poorly developed clast fabric (Aksu 1984; Hiscott and James 1985), irregular mounded tops and tapered flow margins or snouts. Grading is generally poor, but both normal and inverse grading may occur (Naylor 1980; Aksu 1984; Shultz 1984). Inverse grading may develop because the base of the flow undergoes the greatest and most prolonged shear, leading to reduced competence (Hampton 1975). Individual cohesive-flow events may deposit separate tongues or lobes of material that have quite different textural characteristics, making it difficult to distinguish separate flows in the geological record. Shultz (1984) attributed grading style and volume concentration of matrix in debrites to the relative importance of cohesion, clast interaction (dispersive pressure) and fluid behavior. The result is a continuum of deposit characteristics (Fig. 18): The larger clasts – cobbles and boulders – of some cohesive-flow deposits are concentrated near the base or in the middle of the deposit. Some large boulders may be grounded on the underlying substrate (Masson *et al*. 1993), whilst others project from the tops of the beds, allowing a quantitative assessment of rheological strength using a Bingham plastic.

## II.6. Submarine fans and related depositional systems:

A *submarine fan* is a cone of sediment at the base of a submarine slope, consisting mostly of the deposits of turbidity currents that travelled into deep water through a submarine canyon from an adjacent shelf area.

*Submarine canyons* are features with complex erosional and depositional histories that indent the edges of continental shelves, but that can extend almost to the shoreline in the case of narrow shelves along active continental margins. Canyons, as suggested by their name, are commonly hundreds of metres deep with steep rocky walls. Although submarine fans are described routinely in terms of upper (inner), middle, and lower (outer) divisions, there is no agreement as to the application of these terms

Sophisticated studies of modern fans using deeply towed instruments, including side-scan sonar, began with the work of Normark (1970), with similar techniques subsequently applied to numerous modern fans worldwide (Barnes & Normark 1984; Shanmugam and Moiola 1988). These fans can, in most cases, be described in terms of : (i) an *upper fan* just downslope from the feeder channel, or canyon, and characterised by a single deep channel with levées, (ii) a *middle fan* characterised by updip multiple distributary channels (most inactive) and downdip relatively smooth depositional lobes with shallow channels and relatively high sand content and (iii) a *lower fan* with few if any channels and a smooth surface with low gradient (Fig. 19). For ancient fans, some authors (Mutti and Ricci Lucchi, 1972) consider the presence of "depositional lobes" to be indicative of the lower fan, whereas the presence of "suprafan lobes" is believed to be indicative of the middle fan by others (Walker, 1978).

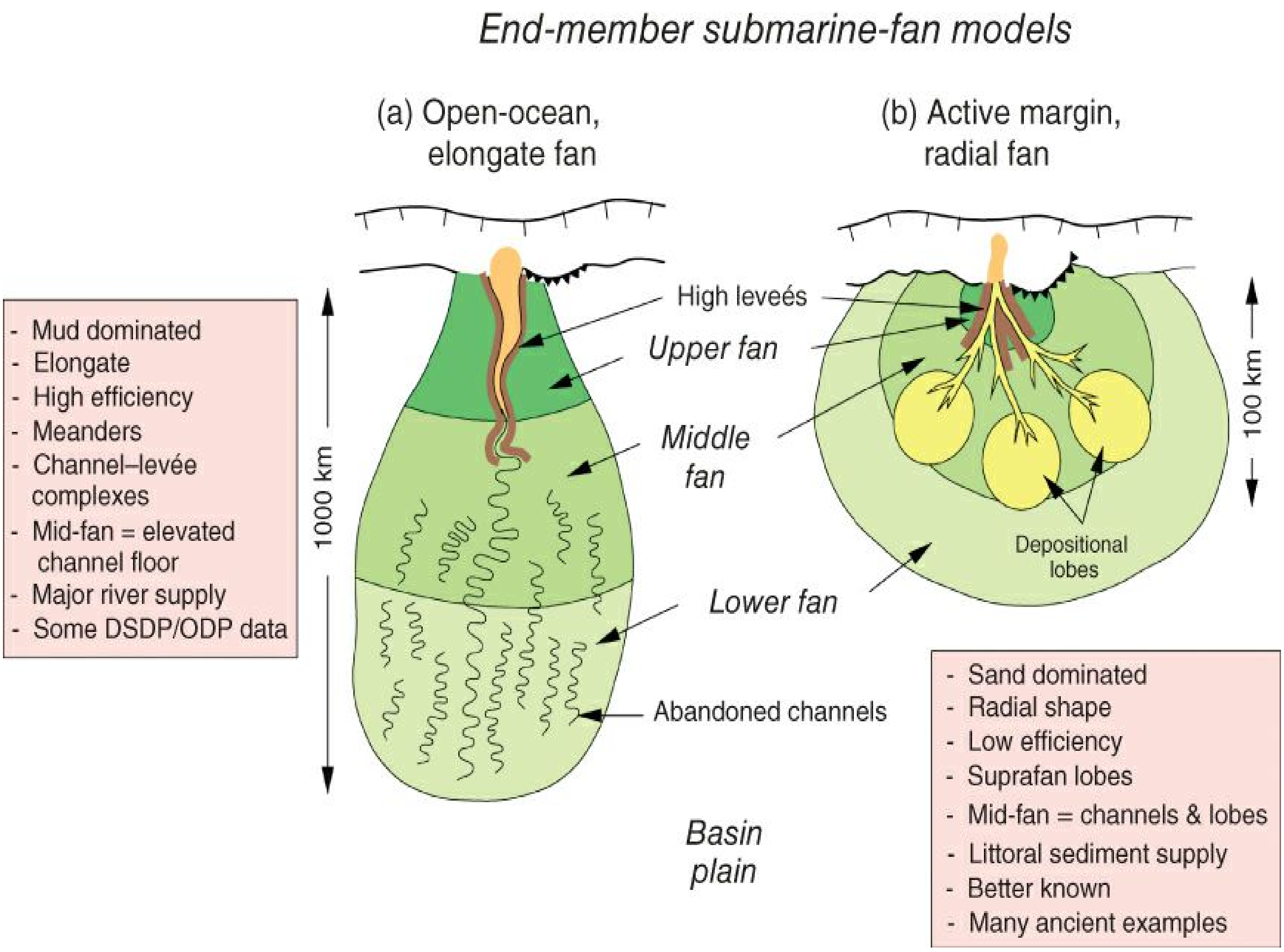


Figure 19: End-member submarine-fan plan-view models, styled after the summary models of Shanmugam and Moiola (1988), who called (a) a 'mature passive-margin fan' and (b) a 'mature active-margin fan'. Open-ocean submarine fans accumulate mainly on oceanic crust, whereas active-margin radial fans accumulate in strike-slip basins, foreland basins and rifts (in Pickering et al., 2015).

Geoscientists now appreciate the variability in size, shape, physiography and facies composition of modern fans (Normark *et al*. 1993b), and much current research is focussed on evaluating the relative importance of the controlling variables such as tectonics, sea-level changes and climate (e.g., Normark *et al*. 2006; Knudson and Hendy 2009). Reading and Richards (1994) and Richards *et al*. (1998) integrated the complexity of sediment sources and grain size into a second-generation classification of submarine fans.

Depositional models that incorporate sequence-stratigraphic concepts can be classified as third-generation models. These models try to differentiate base-level controls from autocyclic controls on the growth and stacking pattern of **SGF** facies in submarine fans and related environments. The *lower fan* and *basin plain* are both underlain by thin-bedded, sheet-like turbidites, so are indistinguishable in ancient deposits. In natural settings, the shapes of submarine fans are rarely simple because of their impingement on irregular basin margins and bathymetric highs.

## II.6.1. Major controls on submarine fans:

### II.6.1.1. Sediment type:

Submarine fans span a spectrum from sand/gravel-rich, to mixed sand–mud systems, to mud-rich systems (Reading and Richards 1994; Richards *et al*. 1998). Sand/gravel-rich and mixed sand–mud fans are widely recognised in ancient successions. These are small, typically radial fans sourced from either relatively small, steep rivers, or from littoral currents that transport sand and silt along an adjacent shelf and into the heads of submarine canyons. For fans supplied by littoral longshore currents, a paucity of mud at the source ensures that sediment gravity flows (**SGFs**) reaching the fan lack a quasi-continuous fluid phase that is significantly denser than seawater, and therefore decelerate more rapidly as sand load is lost through deposition. The **SGFs** are, therefore, less efficient in transporting sand and silt load away from the canyon than they would be if they contained more suspended mud. For this reason, sand-rich fans have been called *low-efficiency fans* by Mutti (1979).

In contrast, mud-rich submarine fans tend to be large, elongate tongues of sediment extending well out onto oceanic crust beyond continental margins, and fed by major rivers draining areas of high sediment yield, particularly areas with a humid climate or active continental glaciation, both conducive to the production of large quantities of mud (Wetzel 1993).

### II.6.1.2. Tectonic setting and activity:

Tectonic setting directly affects basin size and shape, bottom gradients, type and rate of sediment supply and longevity of an individual fan. On mature passive continental margins, the main tectonic process is slow thermal subsidence, which has little effect on the development of large, mature fans with low surface gradients. Many of these large, generally elongate and mud-dominated fans derive their sediment from orogenic belts on the opposite side of the continent. The major rivers that supply the fans flow away from these orogens down a topographic gradient toward the distant passive margins (Potter 1978).

At active margins, which include convergent, oblique-slip and young rifted margins with rapidly tilting fault blocks (e.g., Surlyk 1978; Normark *et al*. 1998; Nakajima *et al*. 1998), depositional basins may be small and irregular in shape (**Zoumi basin case**), so that fans, particularly if they are of the delta-fed high-efficiency type, will be constrained by the basin geometry and will not be able to develop the elongate shape typical of unconfined mud-rich fans (*cf*. Pickering 1982c). Fans at active margins are also often transient, because active vertical and horizontal movements of the crust along faults may cut off sediment supply.

### II.6.1.3. Sea-level fluctuations:

Sea-level variations may be ***i)*** eustatic (global) or ***ii)*** regional or relatively local events caused by tectonic processes. Regardless of cause, relative highstands of sea level generally result in reduced supply of terrigenous sediment to fans due to preferential deposition in coastal systems (e.g., estuarine embayments) and on a relatively broad shelf. Major fan processes during the highstand and early subsequent falling stage then become: ***i)*** slow deposition of hemipelagites (Facies Class E, e.g., Amazon Fan, Flood et al., 1997); ***ii)*** reworking of surface sediments by bottom currents (e.g., distal Mississippi Fan, Kenyon *et al*.

2002) and ***iii)*** mass wasting, producing chaotic deposits of Facies Class F (e.g., Amazon Fan, Piper *et al*. 1997; Rhône Fan, Normark *et al*. 1984).

Relative lowstands in sea level produce deposits that are generally much thicker and coarser than their highstand counterparts, particularly if the rate of sea-level fall is sufficiently high to promote river entrenchment right to the shelf edge (Normark *et al*. 2006). A fall in relative sea level leads to the effective narrowing of shallow-marine shelves and forces fluvial/coastal systems to shift toward the shelf-slope break. Additionally, under conditions of lowered sea level, shallow-marine processes, such as severe storm-wave pounding, are more likely to enhance sediment failure along basin slopes and, therefore, further increase sediment delivery rates into deep-marine environments.

Exceptions to the rule that higher fluxes of sediment are delivered to the deep sea during lowstands occur in carbonate-sourced systems, and in rare cases along active margins where tectonic uplift, climatic changes or enhanced littoral supply to canyon heads may contribute to highstand fluxes of coarser detritus.

### II.6.1.4. Submarine canyons:

Submarine canyons are common features along continental margins, and may cut into crystalline rock, consolidated and under-consolidated sediments, and even evaporites. Canyons may be tens of metres to hundreds of metres deep, have widths varying from tens of metres to tens of kilometres, lengths from kilometres to hundreds of kilometres, and show considerable variability in cross-sectional profile.

Canyons were explained as **i)** formerly subaerial river valleys now submerged by elevated sea level (Spencer 1903; Bourcart 1938); ***ii)*** glaciated valleys now below sea level (Shepard 1933); **(iii)** marine erosional features cut by turbidity currents (Daly 1936); **(iv)** dissolution features caused by circulation of underground water at continental margins (Johnson 1967); **(v)** tsunami-cut depressions (Bucher 1940); and **(vi)** structurally weak areas like faults that are exploited by erosive processes (Kenyon *et al*. 1978; Ediger *et al*. 1993; Harris *et al*. 2014).

The main overarching process in all canyons is erosion and deposition by sediment gravity flows, modulated by rising and falling relative sea level (Mulder *et al*. 1997; von Rad and Tahir 1997; Wonham *et al*. 2000; Popescu *et al*. 2004). Episodic triggering of sediment gravity flows provides a mechanism for the emptying of canyon heads. In recent years, research has emphasised the manner in which sediment reaches the deep sea through canyons, including the detailed analysis of events that have culminated in the triggering of large turbidity currents and concentrated density flows in canyons. Most submarine canyons show the following features (Shepard 1977): ***i)*** sinuous courses, partly true meanders; ii) canyon floors deepen quite consistently seaward; ***iii)*** canyons loose their deep V-shaped profiles at about the same distance from the shore as the adjacent continental slope shows a marked decrease in slope gradient, transitioning to the continental rise; ***iv)*** canyons are rarely found where the continental slopes are gentle; ***v)*** canyons are cut into rocks of all degrees of hardness as well as into unconsolidated sediments; and ***vi)*** they have tributaries, better developed at the canyon heads than in their lower reaches.

## II.7. Zoumi Flysch Facies associations:

Four stratigraphic sections have been measured and sampled within the Lower-Middle Miocene Zoumi Flysch Fm. These sections encompasse all facies associations from where sandstones suite samples have been selected. The sections are vertically organized, according to the field observations, into stratigraphic intervals gathering facies associations related to different depositional palaeoenvironments (Figs: 20, 21, 22, 23, 24 and 25).

The chronostratigraphical data for the measured Zoumi Flysch Fm. successions was based on lateral and vertical facies correlation of the present work and Ben Yaich's intervals (1991), (Zoumi synthetic section, Fig. 20); namely regarding planktonic foraminifers biostratigraphic data (Table 1). The planktonic foraminiferal assemblage consists of *globigerinids*, *Globigerinoides sp*. *Orbiluna sp*. and *Globorotalia sp*. The first occurrence of *Globigerinita* and *Globigerina* genus are assigned to Burdigalian and attributes an age not older than Late early Miocene for the first and second intervals (i.e Intervals "A" and "B" according to Ben Yaich's nomenclature, 1991). The third interval (interval "C" according to Ben Yaich 1991) displays the first occurrence of *Globigerinoidessicanus*andis attributed to Langhian age. While the first occurrence of *Orbiluna*, *Globorotalia* and *Praeorbulina* genus characterize a Late Langhian-Early Serravallian age to the fourth interval (i.e. interval "D" of Ben Yaich 1991).

The vertical sequence analysis of the Zoumi turbidites was carried out by measuring detailed sections along continuously exposed rocks. Bed by bed thickness, rock type, bed contacts, internal primary structures as well as orientation of paleocurrent indicators were noted. All beds were measured individually, described, and numbered. The entire section was then subdivided into a number of recurrent lithofacies. The term 'lithofacies' is used here to refer to individual beds or groups of beds with similar sedimentological attributes (Pickering, 1979, 1986a, 1989, 2015). Following the criteria introduced by Mutti and Ghibaudo (1972) and Ricci-Lucchi (1975a) and Ghibaudo (1992), a group of similar beds was considered as a distinct lithofacies only when thicker than 2 m. Each lithofacies consists, therefore, of a group of beds with similar sedimentary attributes with only minor intercalations of different beds. The complete section was subsequently graphically plotted to show the internal organization of different lithofacies. Depositional environments were interpreted from facies associations through comparison of their sedimentary attributes (rock type, facies associations, cyclicity, vertical relationships, etc.) with the inferred facies distribution from the available fan models.

Five main facies associations have been depicted from lithofacies analysis of four measured lithostratigraphic logs collected from the Zoumi Basin: **(1)** Basin plain; **(2)** lobe fringe; **(3)** lobe; **(4)** channel; and **(5)** matrice-supported conglomerate facies associations:

## II.7.1. Basin Plain facies association:

### II.7.1.1. Analysis:

This facies association is characterized by a fine-grained facies association (150 m thick), represented by 3 to 5 m thick bundles containing thin-bedded calcareous sandstones alternating with nodular and massive white-green hemipelagic marly-clayey strata, and siltstone bearing-glauconite horizons (Zoumi synthetic section (Fig 20), Zoumi section (Fig. 21), Plate 1a). The thin-bedded sandstones are mainly fine- to very fine-grained, flat floored and sharp-topped, and base-missing Bouma sequences (Plate 1e). Usually, the observed primary sedimentary structures are parallel, wavy, planar, trough-cross and ripple-drift laminations. Thin-bedded calcareous sandstones are structureless or thinly-laminated bedforms, nodular or flat and display normal and rarely reverse grading (Plate 1b, c, d). The main Bouma sequences are top or base missing, namely Ta/c; Tb-e, Tc-e and Td-e. The sand:mud ratio 1:4 in these deposits is very low and mud predominates (Zoumi synthetic section (Fig.20); Zoumi sections (Fig 21; 22); Dmani section (Fig. 23); Khakha section (Fig. 24); Taourda section (Fig. 25) and Plate 1a, b, c, d, e).

#### II.7.1.2. Interpretation:

The depositional process5for the n-bedded sand/mud couplets is interpreted as suspension fall-out for low concentration turbidity currents. The fine-grained mud-clay deposits are interpreted as due to slow accumulation of mud and biogenic materials (Stanley & Maldonado 1981; Pickering et al. 1989). These facies present the product of dilute and low concentration turbidity currents, thus corresponding to the D2 facies group of Pickering et al. (1985, 1989, 2015) and also, to the T0-T8 divisions of Stow &Shanmugam (1980).

### II.7.2. Lobe-fringe facies association:

#### II.7.2.1. Analysis:

Lobe-fringe deposits form a well-defined facies association (Zoumi synthetic section (Fig. 20); Zoumi sections (Fig. 21; 22); Dmani section (Fig. 23); Khakha section (Fig. 24); Taourda section (Fig. 25) and Plate 2a). They represent the downcurrent equivalents of the thick-bedded lobes and are deposited in a transitional area between the lobes and the basin-plain (Jacka et al. (1968); Mutti and Ghibaudo (1972); Ghibaudo (1992); Mutti and Ricci-Lucchi (1972, 1975); Ricci-Lucchi (1975a, b); Mutti (1977 and 1992); Mutti and Johns (1979)). This facies association includes cyclic vertical variations depicted by the vertical change in sandstone bed thickness versus marly beds. The 2:3 Sand/Mud ratio is prevailing. Sandstone strata are mainly decimeter-thick (10- 40 cm) and exceptionally meter-thick sized (1m to 2.5m) (Plate 2a). The beds are structureless, graded and massive debrites, locally medium-to coarse-grained sandstones are organized into homolithic packages with typical bed thicknesses ranging between 25 and 50 cm up to 150 cm. Beds are normally-graded with uneven base and top surfaces. Common primary sedimentary structures are grading, parallel, convoluted, ripple-drift laminations, and wavy ripples (Plate 2b, c, d, e). Sandstone strata are base-missing Bouma sequences with occasionally complete Ta-e sequences and single Ta sequences lacking upper divisions are randomly scattered through the stratigraphic interval (Plate 2a). Sequences display small-scale thickening-upward cycles or, subordinately, symmetric cycles, resulting from systematic variations in sandstone bed thickness (Plate 2a). Such sediments represent the final depositional stage of the fan-related turbidity currents (Mutti and Johnes 1979).

#### II.7.2.2. Interpretation:

Medium- to thick-bedded sand/mud couplets (C2 of Pickering et al. 1986, 2015) deposition is from turbidity currents ranging from high to moderate concentrations, namely suspension fall-out and traction (Tc-d Bouma (1962) divisions) and ($T_0$–$T_5$ Stow and Shanmugam 1980 divisions), shear sorting of silt grains and clay floccules in the bottom boundary layer ($T_d$ Bouma (1962) division) and ($T_3$–$T_5$ Stow and Shanmugam 1980) divisions) and suspension fall-out with no traction ($T_e$ Bouma (1962) division) and (T6-8 Stow and Shanmugam 1980 divisions) . The basal structureless Ta division (Bouma 1962) of turbidity-current deposits forms whenever the suspension fallout rate is too high to allow sufficient grain traction to form lamination (Lowe 1988; Arnott and Hand 1989; Allen 1991; Hiscott *et al*. 1997a). Moreover, single coarsest grain-size fractions structureless *T*a-divisions are more likely the deposits of concentrated density flows (Pickering et al. 1986a, 1989, 2015).

### II.7.3. Lobe facies association:

#### II.7.3.1. Analysis:

Mainly represented by medium- to coarse-grained massive, structureless and normally and sometimes reverse gradded (Plate 3e), flat-floored sandstone beds. Bed thickness is mainly decimeter thick (10 to 80 cm) and can reach meter-thick strata amalgamated in bundles up to 4 m of the total thickness with flat bases and tops, and the main vertical trend of cyclic sequences is thickening-coarsening upward, with or without intercalations of silty-clayey and marly levels (Plate 3a). The Sand:Mud ratio is 4:1. The massive sandstone strata usually present scours and gutters structures (Plate 3c) and rework at/or near the strata tops abundant mudclasts (Plate 3b). Main observed secondary structures are water escape structures as dish, centimeter- to decimeter-sized pipe and pillar structures (Plate 3d). Beds lacking upper divisions and dominated by structureless sand are more likely the deposits of concentrated Sandy Density Flows (SDF) (Pickering et al., 1989, 2015).

Throughout the Zoumi basin, lobes are sheet-like, constructional sandstone bodies organized in thickening- and coarsening-upward megasequences reflecting basinward progradation (Mutti and Ghibaudo, 1972) and Ghibaudo (1992). Two major parameters monitor lobe architecture downcurrent and laterally: (1) substratum instability as a consequence of mesorif sole-thrust activity and (2) proximality from sand source area supply.

***II.7.3.1.1. Proximal Lobe Deposits:*** (Zoumi synthetic section (Fig. 20); Zoumi section (Figs. 21; 22) and Plate 3a)*:* consist primarily of thick-to very thick-bedded, medium-to coarse-grained, "classical" turbidites and minor amounts of thin-bedded sandstone. The thick-bedded turbidites are characterized by classical Bouma sequences. Complete sequences are rare, and most beds consist of a lower graded interval capped by few centimeters of current-laminated siltstone and by very thin, locally discontinuous, turbiditic shale. Most of the beds can be described as $T_{a/c/e}$, $T_{a/e}$, $T_{a/c}$ Bouma sequences, whereas b and d divisions are rarely observed. Grading in the basal Ta division is relatively good, primarily coarse-tail grading, and faint, crude parallel laminae may be present in this lower interval. The sandstone/mud ratio 4:1 of these deposits is very high, and they correspond to $C_1$ facies of Mutti and Ricci-Lucchi (1975), deposited by high-concentration turbidity currents characterized by mass deposition followed by reworking of top surfaces by the entrained layer. Thickening- and coarsening-upward cycles are well developed in the proximal lobe deposits and range in thickness from 3 to 15 m (Plate 3a). Sandstone beds in the upper part of the cycles can be as thick as 4 m and amalgamated. Unlike the distal lobe facies, intercalations of thin-bedded turbidites are very rare and mostly concentrated in the lower, thinner bedded parts of the cycles. Major differences from distal lobe deposits include higher sandstone/mud ratio, thicker sandstone beds, frequent amalgamations, and lesser amounts of dilution by thin-bedded turbidites.

***II.7.3.1.2. Distal Lobe Deposits:*** (Dmani section (Fig. 23); Khakha section (Fig. 24) and Taourda section (Fig. 25)**:** consist of prevailing thick-bedded, coarse- to fine-grained "classical" turbidites associated with notable amounts of thinner bedded and finer grained deposits. They pass gradually downcurrent and laterally into equivalent thin bedded lobe-fringe deposits, and the progradation of depositional lobes onto fringe sediments results in coarsening-upward cycles. Medium to thick-bedded, coarse to fine-grained, "classical" turbidites organized in thickening and coarsening-upward cycles are well represented in the Zoumi Flysch sections (Figs. 23, 24, 25). Lobe deposits consist mainly of medium to thick-bedded, fine-to medium-grained turbidites, associated with minor amounts of thin-bedded turbidites. The medium-to thick-bedded turbidites typically contain base-missing Bouma sequences and consist predominantly of $T_{b-e}$ beds. Distal lobe deposits show internal organization in repeated thickening-upward cycles; each cycle consists of a lower part composed of medium-bedded (10-30 cm) $T_{c-e}$ sandstone beds and an upper part composed of thicker (30-100 cm) $T_{b-e}$ sandstone beds. Individual thickening-upward cycles have thicknesses usually comprised between 2 and 12 m and, as shown on Figures 22, 23, 24 and 25 they are diluted by small intercalations of monotonous thin-bedded turbidites.

#### IV.7.3.2. Interpretation

The lobe deposits are related to the evolution of a high-density turbidity currents (Mutti, 1992), where massive structures are interpreted as the results of very quick deposition for freezing of a dense cohesionless suspension apparently lacking post-depositional liquefaction/fluidization (Lowe 1982), under a highly concentrated flow (Middleton & Hampton 1976; Walker 1978; Lowe 1982; Mutti 1992). The occurrence of scouring and normal grading could be interpreted as turbulent imprint of turbidity current where quick packing of grains justifies the fluid escape (Lowe et al. 1974; Lowe 1976; Pickering et al 1982, 1989, 2015). The presence of mud clast horizons within strata could have the following interpretations: (1) mud clasts carried along the interface between a highly concentrated, laminar, basal inertia-flow, and a less concentrated, fully turbulent overriding flow (Postma et al. 1988); (2) Shanmugam et al. (1995) instead interpreted 'floating' clasts in structureless sands as a strong indicator that the deposits were emplaced by inflated sandflows (his sandy debris flows), not turbidity currents or concentrated density flows; (3) For Hiscott et al. (1997) mud clast is rolling or sliding along the bed and then ceases to move and will subsequently be buried by sand.

### II.7.4. Channel facies association:

#### II.7.4.1. Analysis:

This association consists mainly of coarse-grained and thick-bedded strata that are gradationally or abruptly topped by fine-grained and thin-bedded beds and very thin marly-clayey interval. The commonly observed lithofacies consist of sandy debris flow strata bearing sandy matrix and reworking frequents centimeter- to decimeter-sized mud and rip-up clasts (Plate 4d). The sandy beds are medium- to coarse-grained with interstratified hyper concentrated flow deposits and pebbly sandstones beds, lensoid to rough shape (Plate 4a, b, c, d). The Sand/Mud ration is about 4.5:0.5. Beds are bounded by irregular surfaces, and virtually no pelitic interbedding is present due to ubiquitous amalgamations (Plate 4c, d). Lower erosional surfaces cutting down are common. As shown in Figures 20, 21 and 22 massive sandstone and pebbly sandstone are organized in a fining-thinning upward cycle and markedly contrast with the thickening-upward trends of underlying depositional lobe sediments.

#### II.7.4.2. Interpretation

Channel deposits are characterised by discrete packets of coarse-grained, medium to thick-bedded, amalgamated sandy debris flow beds of mass-flow deposits and sandstone turbiditic beds, generally 2 to 3 m thick. There is often lateral depositional lensing or erosional wedging-out of individual beds and packets of beds. Channel deposits comprise thinning-and-fining-upward sequences, overlain by thin and very thin bedded Bouma Tc-e siltstones and mudstones. Towards the channel margin, there is a lateral thinning and fining of deposits. The tops of channel fills are arbitrarily fixed where predominantly sandy beds are replaced by silty beds.

The thinning- and-fining-upward sequences associated with channel infilling, can be explained by gradual channel abandonment.  In deep sea channel model, a thinning-and-fining-upward sequence is believed to be primarily a consequence of vertical accretion and is interpreted as showing the gradual infilling of a channel by successive *depositing currents* (Pickering, 1982).

### II.7.5. Matrice-supported conglomerate facies association:

#### II.7.5.1. Analysis:

Some matrix-supported conglomerate can be observed locally with nodular marls, lenticular beds, rounded medium to fine boulders (10 to 60 cm) of calcareous sandstones (Figs. 20, 22; Plate 5a, b). The conglomerate, 8-m-thick, is capped by tens meters of hemipelagic blue gray marls which, in turn, intercalated within thin-bedded fine-grained sandstone deposits.

#### II.7.5.2. Interpretation

This facies can be interpreted as single events reflecting intense tectonic activity in the hinterland and notable movement of the underlying Mesorif sole-thrust. This tectonic instability is recorded by the presence in the topmost part of the Zoumi section of matrice-supported conglomerate directly superposed on the top of an actively progradating distal lobe.

## II.8. Conclusion on Zoumi flysch lithostratigraphic logs description and vertical evolution:

The stratigraphic evolution of the Zoumi flysch Formation is shown on Figures 20, 21, 22, 23, 24. The sections record the deposition of distinct lobes complexes separated by a period of fine-grained sedimentation. The clastic material was supplied from the east (Fig. 50), and dispersal followed the longitudinal west to northwest-oriented paleoslope of the basin. The coarse clastic sedimentation in the Zoumi basin was preceded by deposition of a 10 to 20-m-thick level of glauconitic rich muds deposited as chattian pre-orogenic level (level 1, Fig. 20). The input of clastic sediment to the basin was rather slow as basin plain deposits overlie the chattian level with development of lobe fringe sediments.

The Zoumi Flysch deposits record four major progradational cycles. A complete cycle starts with basin plain deposits, lobe fringe deposits, lobe deposits and terminates with channel-fill sediments in its upper part. Each progradational cycle constitutes an overall thickening and coarsening upward sequence. In fact, thin to medium-bedded "classical" turbidites in the lower part change upward into thick-bedded "classical" turbidites and, finally, into massive sandstone and pebbly sandstone (Figs. 20, 21, 22, 23, 24, 25). The thickening and coarsening upward cycles reflect succession of periods of intense compressive tectonic activity in the hinterland (namely the Internal Rif domain and the Intrarif sub-domain). This high relieves due to this tectonic activity with humid and wet paleoclimatic conditions triggered intense weathering and runoff/runout of clastic material and its routing to the Zoumi basin.

The basin was subject to a very notable tectonic subsidence, and the accommodated space was completely compensated by the important input of clastic material. Later, during the Late Middle Miocene (Serravallian), Zoumi Sections display thining and fining upward cycles. The accommodated space due to the important subsidence triggered by the weight of huge clastic material deposited in the basin was not compensated by the input of clastic material. On the contrary, the final denudation stage of the hinterland leads to weak release of clastic material and the predominance of fine-grained marly-clayey sedimentation.

The superposition of progradational cycles, ranging from fringe sediments up to lobe deposits, probably reflects repeated shifting in position of the inner fan valley (Walker, 1978) as a consequence of nappes stacking and uplift of intrarif subdomain. Each lateral migration would result in the abandonment of a particular main locus of deposition on the fan surface and the starting of sedimentation and progradation in adjacent areas. The repetition of this mechanism through time led to the superposition and/or juxtaposition of discrete, major progradational sandstone bodies. However, because of multisource input of clastic Zoumi deposits and incomplete and imprecise available biostratigraphic data; we cannot confirm the superposed/juxtaposed stacking or synchronous/diachronous deposition and growth of the Zoumi turbiditic lobes. This can be subject to the future research perspectives on detailed sedimentologic and biostratigraphic study of the Zoumi basin.

Two important events have been noticed in the vertical/lateral facies evolution: (1) the downcurrent proximal/distal bed-thickeness and grain-size evolution; (2) the imprint of basin morphology on the bed-thickeness. The Zoumi basin morphology seems greatly influenced by the mesorif sole-thrust. The mesorif sole-thrust cut up and down the Mesozoic-Cenozoic underlying pre-orogenic substratum and created deep sub-basin (i.e. Zoumi and Amalou localities) receiving the thickest sandstone deposits. Elsewhere, in the shallower and distal areas, the transition between the proximal lobe deposits and the distal fringe lobe and basin plain deposits is probably related to a progressive decrease of sand/shale ratio of sediment supplied which result in a reduction of sandstone bed thickeness and progressive pintchout of these sandstone beds downcurrent into shale.

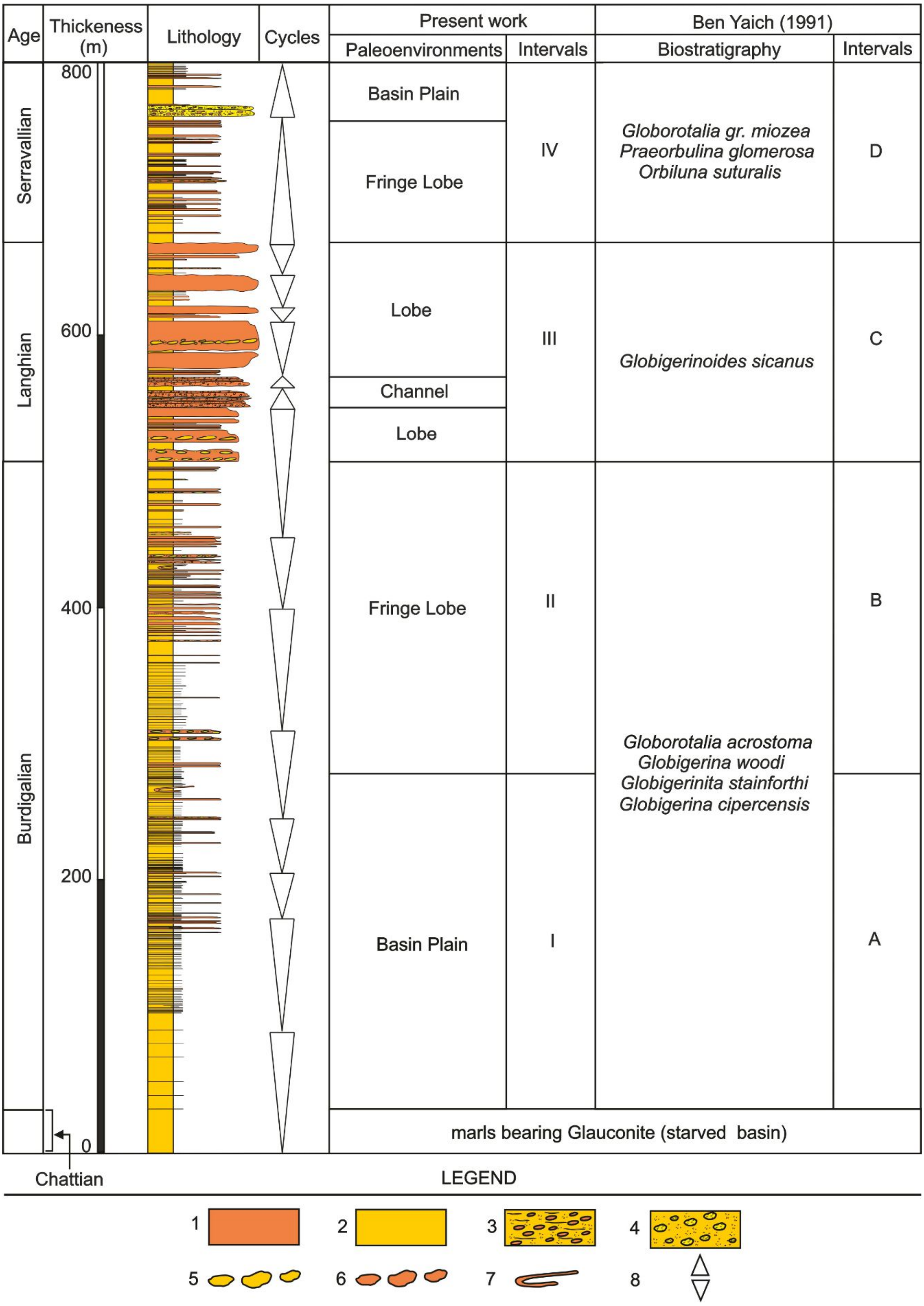


Figure 20 : Zoumi synthetic stratigraphic section. Ages are based on foraminifers data after Ben Yaich (1991). **1**- sandstone, **2** – mudstone, **3** – matrice supported conglomerate, **4** – reworked matrice supported conglomerate, **5** – mud clasts, **6** – sand clasts, **7** – contorted bed, **8** – negative and positive cycles.

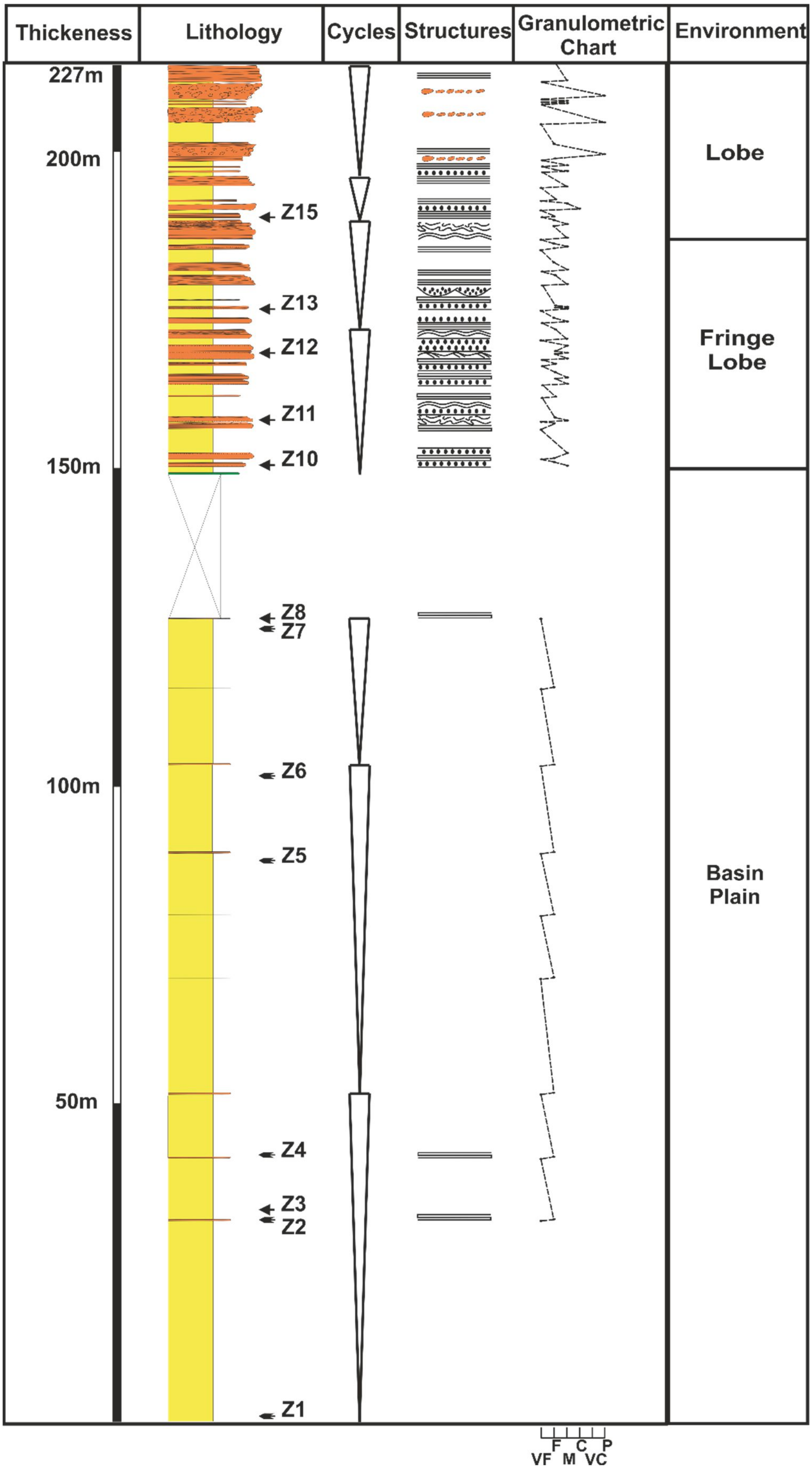


**Figure 21 :** Zoumi 1 lithostratigraphic section.

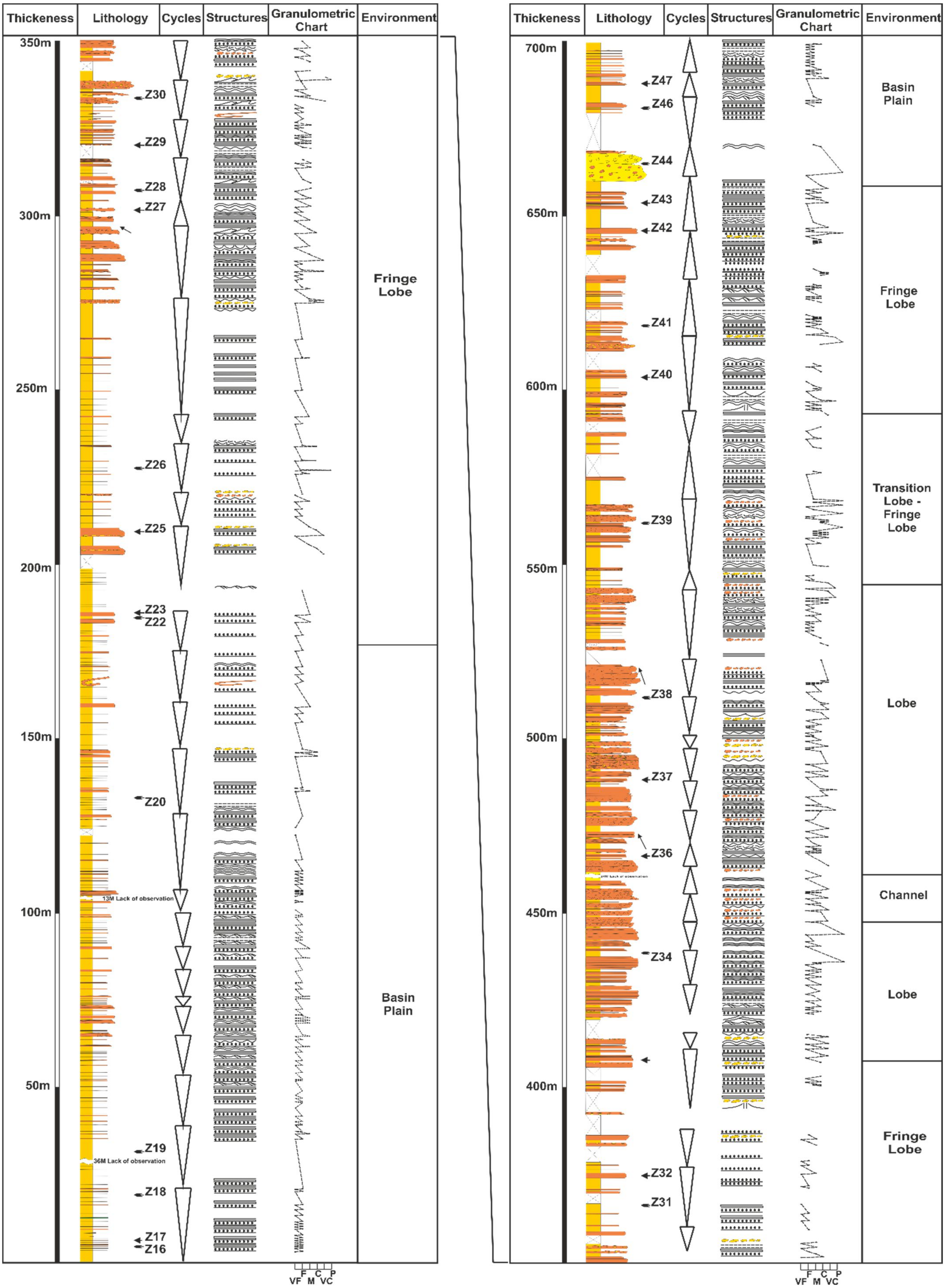


**Figure 22** : Zoumi 2 lithostratigraphic section

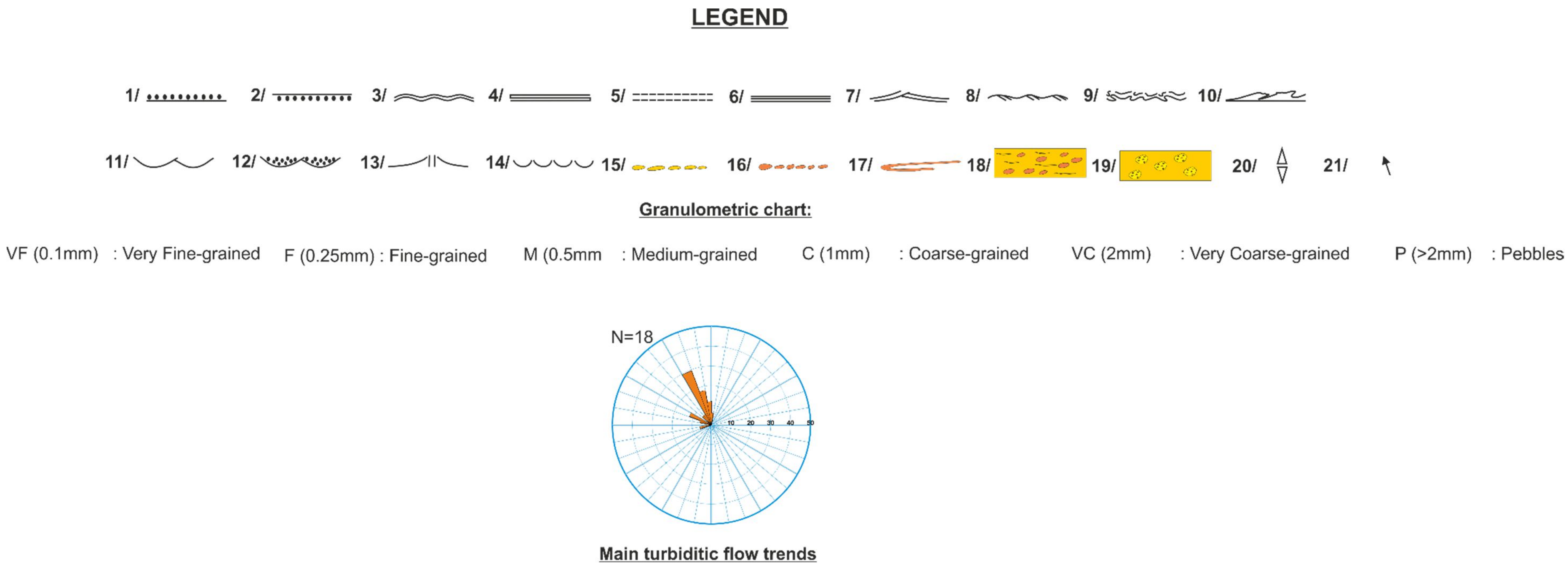


**Figure 22 (continued)**: Legend for Zoumi basin stratigraphic sections:1. Normal grading; 2. Reverse grading; 3. undulouse laminae; 4. parallel laminae; 5. Sil/mud laminae; 6. parallel Strata; 7. Oblic cross laminae; 8. Ripples; 9. Convoluted laminae; 10. Slumped strata; 11. Scours; 12. Scours and fills; 13. Pillar water escape structures; 14. Dishes structures; 15. Mud clasts; 16. Sandstones clasts; 17. Contorted bed; 18. Matrice-supported conglomerate; 19. Reworked matrice-supported conglomerate; 20 positive and negative cycles; 21. Paleocurrents trends.

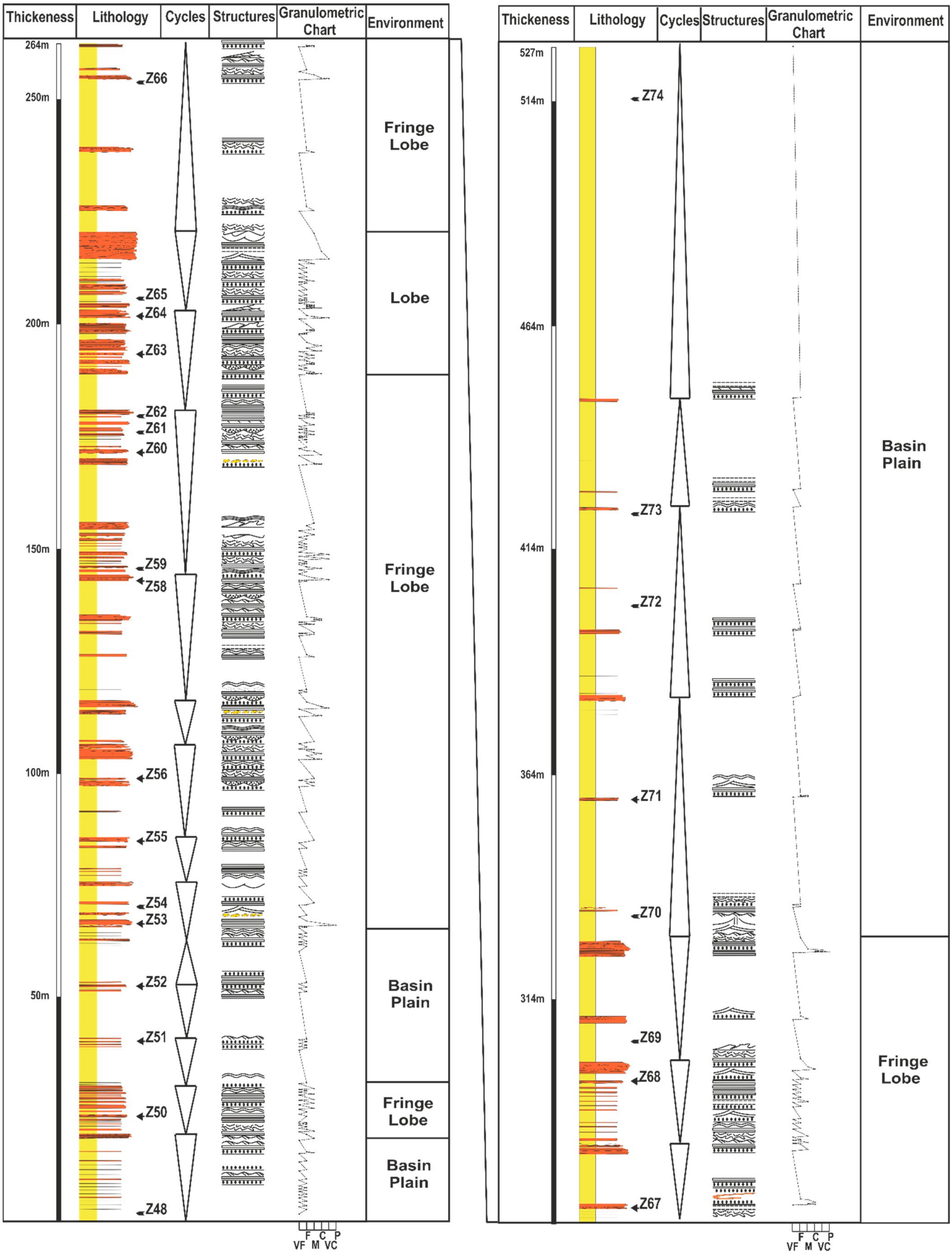


**Figure 23** : Dmani stratigraphic section (see Fig. 21 for legend).

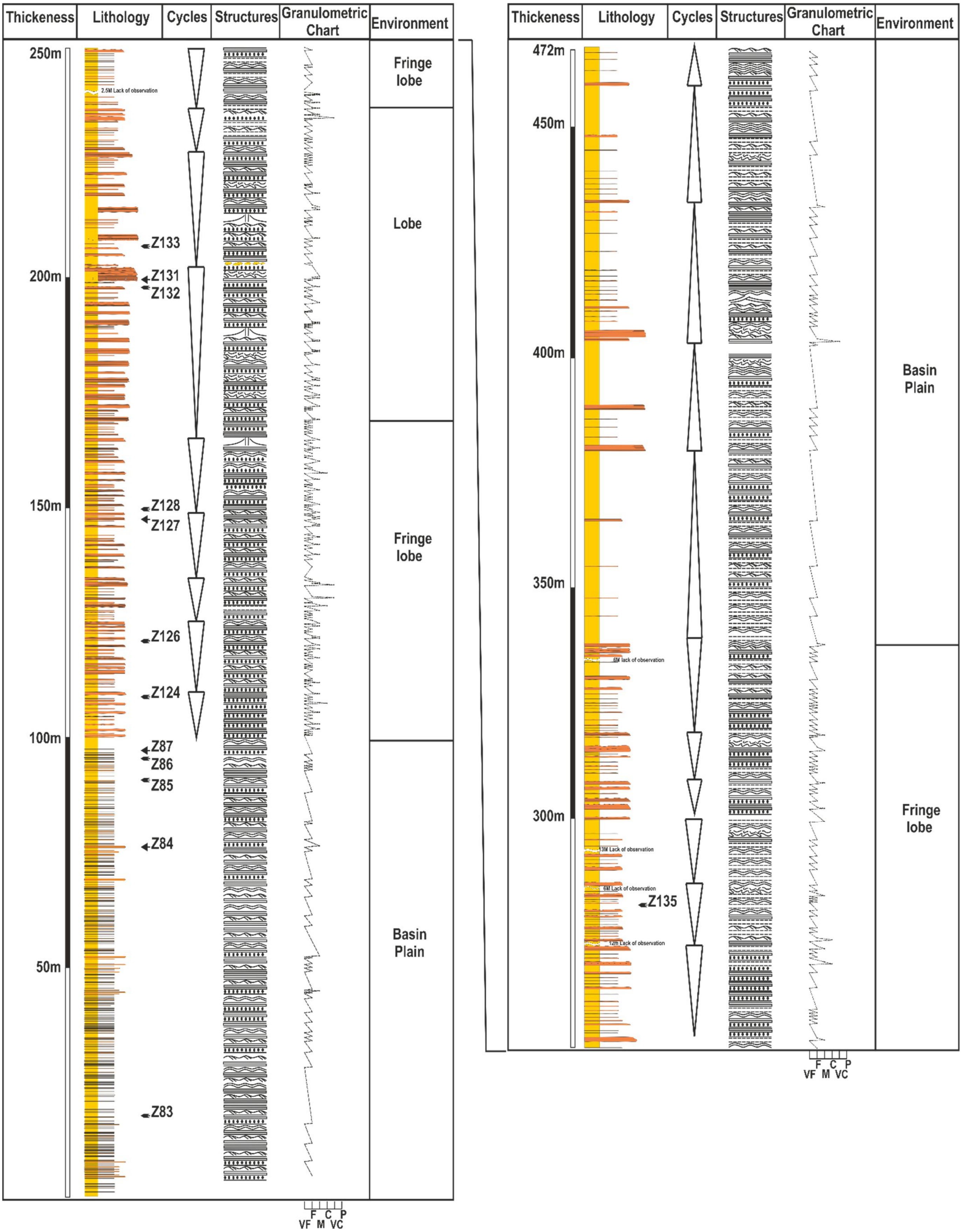


**Figure 24 :** Taourda stratigraphic section (see Fig. 21 for legend).

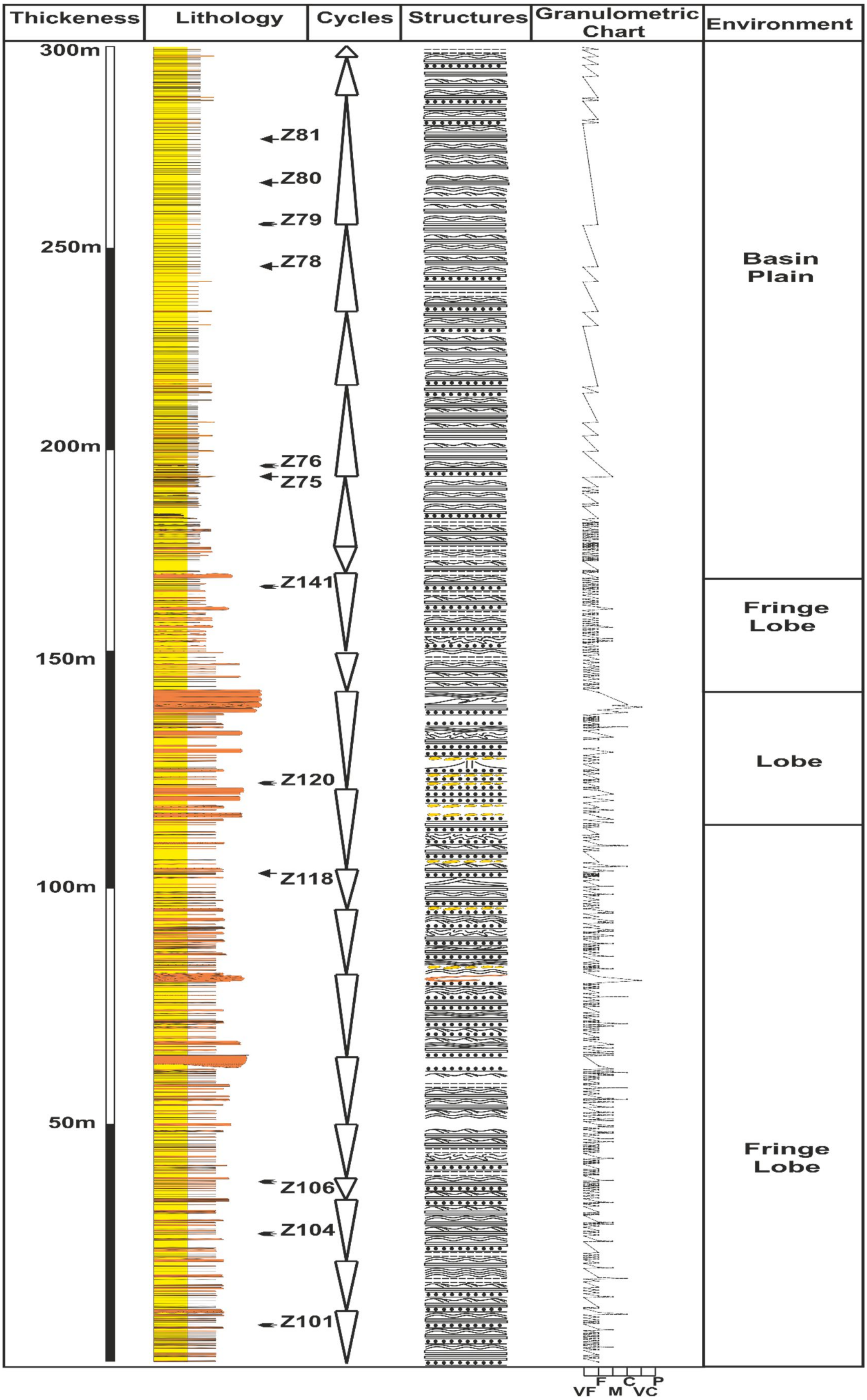


**Figure 25** : Khakha stratigraphic section(see Fig. 21 for legend).

# CHAPTER III

# PETROGRAPHIC MODAL ANALYSIS

# CHAPTER III

# PETROGRAPHIC MODAL ANALYSIS

## III.1. Petrographic Modal Analysis Method:

It is widely accepted that accurate detrital modes of sandstone suites can yield specific information on provenance and reflect the different tectonic settings of provenance terranes, although various other sedimentologic factors also influence sandstone compositions Dickinson (1970, 1985). The Gazzi-Dickinson method of point counting was developed to maximize source-rock data, while minimizing the time, effort, and expense of gathering such data. Use of the method minimizes variation of composition with grain size, thus eliminating the need for sieving and multiple counts of different size fractions (Ingersoll et al., 1984).

The unique aspect of the Gazzi-Dickinson method of point counting is the assignment of sand-sized crystals and grains within larger fragments to the category of the crystal or grain, rather than to the category of larger fragment. In addition, every attempt is made to reconstruct original detrital compositions in spite of subsequent alterations. Compositions of detrital sediments are controlled by four factors: provenance, transportation, depositional environment, and diagenesis (Suttner, 1974). Study of ancient sediments commonly has the goal of understanding one or more of these factors. Study of diagenesis commonly is most straightforward because it is the most recent process affecting given sediment (Ingersoll et al., 1984).

The apparent dependence of sandstone detrital modes on grain size has been demonstrated by several workers (Blatt, 1967; Young, 1976; Basu et al., 1975; Mack and Suttner, 1977). However, there are two basic schools of thought concerning the subject: **1)** that which believes that there is a fundamental dependence of modal composition on grain size (Suttner, 1974; Basu, 1976; Mack and Suttner, 1977;); and **2)** that which believes that modal composition can be determined independently of grain size (Gazzi, 1966; Dickinson, 1970).Less traditional methods (Gazzi, 1966; Dickinson, 1970; Gazzi et al., 1973; Graham et al., 1976; Ingersoll, 1978; Ingersoll and Suczek, 1979) place greater emphasis on using petrographic techniques to reconstruct original detrital compositions independent of grain size. Dickinson (1970) argues that the identification and recording of mineral crystals of sand size, whether within coarse-grained lithic fragments or not, reduces compositional dependence on grain size. Additionally, careful petrographic techniques (applied by both schools of methodologists) allow the recognition of grains severely altered because of physical or chemical diagenetic effects. Thus, alterations such as those described by Walker et al. (1978) do not change detrital modes significantly. The Gazzi-Dickinson method reduces the effect of grain size and alteration on composition and thereby allows accurate determination of original detrital mode and provenance.

Sandstone suites can be described adequately using six numerical grain parameters plotted as $Q_xF_yL_z$, ternary diagram where Q is total quartzose grains, F is total feldspar grains, and L is total unstable lithic fragments in the framework. Three secondary parameters in the form of ratios permit desirable refinement within each primary parameter. Stable grains, whose sum is the parameter Qinclude both monocrystalline quartz and polycrystalline lithic fragments.

Lithic fragments are subdivided at two levels into four main categories within which are various subcategories: (a) volcanic fragments include felsic, microlitic, lathwork, and vitric types; (b) clastic fragments include silty-sandy and argillaceous types; (c) tectonite fragments include metasedimentary quartzose types and metavolcanic feldspathic or ferromagnesian types; and (d) microgranular fragments include hypabyssal, hornfelsic, and indurated sedimentary types.

Interstitial materials include (a) exotic cements like calcite or zeolite; (b) homogeneous, monominerallic phyllosilicate cement displaying textures indicative of pore-filling; (c) clayey detrital latum called protomatrix; (d) recrystallized latum or protomarix called orthomatrix with relict detrital texture; (e) murky, polyminerallic, diagenetic pore-filling called epimatrix, whose growth is accompagned by alteration of framework grains; and (f) deformed and recrystallized lithic fragments called pseudomatrix. Extensive albitisation and other alterations complicate the interpretation of detrital modes in many rocks, but potential errors can be ovoided by close attention to mineralogy and relict texture except where tectonite fabrics disrupt or transpose the original detrital framework.

Many subquartzose sandstones were derived from one, or a mixture, of three salient provenance types: (a) volcanic terranes, yielding feldspatholithic rocks nearly free of quartz, (b) plutonic terranes, yielding feldspathic rocks with few lithic fragments, and (c) uplifted sedimentary and metasedimentary “tectonite” terranes, yielding “chert-grain” lithic rocks with few quartz and feldspar grains except where recycled volcanic or plutonic detritus is abundant.

### III.1.1. Stable grain types:

The dominant stable grains (Q) in many graywackes and arkoses are monocrystalline quartz grains of common plutonic type (Folk, 1968) with trains of vacuoles and slightly undulose extinction. Clear, unstrained volcanic quartz with bipyramidal habit, resorbed margins, or bleb inclusions (originally glassy) can be identified in some rocks and is the dominant quartz type in quartz-poor volcanic sandstones.

### III.1.2. Lithic grain types:

Lithic grains are classified below according to Ingersoll et al., 1984; Critelli and Lepera (1994); Critelli and Ingersoll (1995):

- Lithic-fragment compositions (Lm, Lv, Ls, Qp) are especially consistent and provide the most useful parameters for relating composition to source rock and, ultimately, to tectonic setting. Four categories can be distinguished (carbonate rock fragments are a fifth):
- Volcanic rock fragments have the textures of igneous aphanites and include altered or recrystallized volcanic rock fragments where relict textures are preserved. Volcanic rock fragments can be divided conveniently into four main types, of which the first two are most important:
- Felsitic grains are an anhedral, microcrystalline mosaic, either granular or seriate, composed mainly of quartz and feldspar, and represent mainly silicic volcanic rocks, either lavas or tuffs.
- Microlitic grains contain subhedral to euhedral feldspar plates and prisms in pilotaxitic, felted, trachytic, or hyalopilitic patterns of microlites, and represent mainly intermediate type of lavas

- Lathwork grains contain plagioclase laths in intergranular and intersertal textures representing mainly basaltic lavas
- Vitric to vitrophyric grains and shards are glass or altered glass, which may be phyllosilicates, zeolites, feldspars, silica minerals, or combinations of these in microcrystalline aggregates.
- Clastic rock fragments have fragmental textures and can be somewhat arbitrarily divided into silty-sandy types lacking clay except interstitially, and argillaceous types in which clay is dominant or prominent. The argillaceous grains include shale with mass extinction from which slatytectonites may not be distinguishable in every case. More massive mudstone and argillite grains are more common in most rocks.
- Tectonite rock fragments have schistose or semischistose fabrics and can be split into two broad classes. Metasedimentary types are characterized by quartz and mica. Metavolcanic types contain abundant feldspar or, more diagnostic, assemblages including chlorite and amphibole.
- Microgrannular rock fragments, whose identity is the most difficult to specify, are made of roughly equant, well-sized grains and include three main types that can be distinguished only with difficulty as sand grains, even though they are quite different kinds of rocks:
- Hypabyssal types are hypidiomorphic igneous rocks commonly low in quartz and rich in feldspar; where they can be recognized, they can be summed with volcanic rock fragments, to which they have a close genetic affinity.
- Hornfelsic types contain a metamorphic mineralogy, commonly including abundant quartz, and can be summed with the tectonites as metamorphic rocks where they can be identified with confidence
- Sedimentary types include pressolved and indurated aggregates whose originally clastic textures have been modified by diagenesis or metamorphism, but they can be summed with clastic rocks where their true nature can be discerned.

### III.1.3. Interstitial constituents:

The interstitial constituents of graywackes and arkoses can be grouped into six categories: although ambiguous interpretations cannot be avoided in all cases. Cement of calcite, chalcedony, Zeolite, or other minerals uncommon in the framework can be recognized with comparative ease.

Phyllosilicate cement is commonly confused with matrix, but a number of criteria, observable singly or in combination, serve to distinguish inhomogeneous matrix from clear-cut phyllosilicate cement whose growth pattern in open pores is reflected by its crystalline habit. Reliable textural indicators of interstitial phyllosilicate cement include the following (Carrigy and Mellon, 1964):

  - Clear transparency indicating absence of minute detritus or murky impurities
  - Monomineralogy indicating restricted compositions
  - Radial arrangement of cystal platelets indicating growth inward from surrounding framework grains toward the centers of interstitial voids,
  - Concentric color zonation indicating successive compositional changes in minerals grown in voids fom interstitial fluids as coasting built on framework grains.
  - Medial sutures within the interstitial phyllosilicates indicating the lines of juncture of pore-filling crystals growing inward from surrounding framework grains.

- **Protomatrix** is a term introduced here for unrecrystallized clayey lutum in weakly consolidated rocks and is as much an idealization as a description in my personal experience.
- **Orthomatrix**is a term introduced here for recrystallized detrital lutul or protomatrix. Definitive recognition of orthomatrix requires the perception of a relict clastic texture within it, and an appropriate inhomogeneity of its composition contrasting, for example, with the homogeneity of phyllosilicatecement. Where orthomatrix is abundant, the framework is visibly poorly sorted and grades imperceptibly into the surrounding detrital paste, not only by intergrowth at grain margins, but by size as well.
- **Epimatrix** is a term introduced here for inhomogeneous interstitial materials grown in originally open interstices during diagenesis but lacking the homogeneity and clear textural evidence of pore-filling needed to classify interstitial paste as phyllosilicate cement. Especially in rocks where diagenetic alteration of the framework grains is

well advanced, these circumstances point to epimatrix as a more plausible interpretation than orthomatrix.

- **Pseudomatrix** is a term introduced here for a discontinuous interstitial paste formed by the deformation of weak detrital grains. In many subquartzose sandstones, grain shapes have been modified extensively by compaction and pressolution. Quartz and feldspar grains are not commonly distorted but are locally fractured. Micas flakes are commonly bent and wrinkled, to display a characteristic crimped appearance megascopically. Less competent lithic fragments, argillaceous and microlitic grains as examples, are commonly mashed and squeezed between more competent grains, chert grains and mineral crystals as examples. There are several reliable criteria for the recognition of pseudomatrix: (a) Flame-like wisps of crushed lithic fragments extend into narrowing orifices between undeformed rigid grains, (b) the pseudofluidal internal fabric of lithic fragments deformed by pseudoplastic flow commonly conforms to the margins of confining rigid grains as concentric drape lines, (c) large “matrix”-filled “graps” in the framework suggest pseudomatrix, and the sug.

### III.1.4. Common alteration textures:

Extensive albitization and other recrystallizations can affect many graywackes and arkoses that appear unmetamorphosed on the outcrop. The habits of the alteration minerals in sandstones fall into three categories (Crook, 1963):

- New growths (cement), which fill pores interstitial to the framework;
- Replacements, which may be pseudomorphs of whole detrital grains, or irregular patches including several remnants of detrital grains, or scattered inclusions within detrital grains;
- Veins, filling quasi-planar structures formed by disruption of the framework.

In assessing the effects of alteration on detrital texture and mineralogy, veins can be discounted as a clearly secondary feature. Cements are visibly distinct from the framework in most cases, although confusions between cement and matrix, as well as between deformed framework and matrix, are common.

### III.1.5. Petrofacies evolution:

Spatial patterns of correlative petrofacies within a sedimentary basin reflect simultaneous contributions of detritus from different sources. Successive time-dependent petrofacies reflect either the evolution of individual provenance terranes or changes in disperal patterns through time. Significant contrasts in petrofacies imply major differences in diagenetic processes within basin fill. Stratigraphic variations in petrofacies within forearc and foreland regions suggest that an integrated view of basin evolution requires attention to petrofacies evolution, both as a record of tectonic events and as a means of understanding diagenetic conditions (Critelli and Lepera (1994); Critelli and Ingersoll (1995)).

Volcaniclastic sandstone suites commonly become more quartzoseupsection, because the normal evolution of many magmatic arcs leads to the eruption of more felsic materials as time passes (Korsch, 1984). Moreover, there is commonly a tendency for uplift and erosion to expose more and more of the plutonic roots of an arc as time passes. Consequently, Forearc sandstones of the volcaniplutonic suite generally become more arkosic and less lithic with time (Dickinson and Rieb, 1972).

Recycled orogenic sources in exposed subduction complexes may influence petrofacies locally (Tennyson and Cole, 1978), and major changes in drainage patterns within arcs may cause abrupt shifts in petrofacies within adjacent forearc basins (Heller and Ryberg, 1983). Petrofacies become on average more quartzofeldspathic and less lithic upward, although some feldspatholithic sandstones occur throughout the section. In many parts of the sequence, lithofeldspathic and feldspatholithicpetrofacies variants are intercalated within the same general horizons. The K-feldspar/plagioclase ratio increases systematically upward, as does mica content somewhat more irregularly. Both trends probably reflect increasing contributions from plutonic source rocks. The Lv/Ls ratio varies geographically as well as stratigraphically and appears to reflect variations in the nature and amount of bed rocksexposed adjacent to batholithic sources as well as the extent of local volcanic cover in the arc.

Foreland basins adjacent to collision orogens experience drastic changes in provenance during their sedimentary history. Prior to collisional tectonics, sediment sources are dominantly within the adjacent continental block. Commonly, arkosicpetrofacies of a rift phase lie at the base of the foreland succession and are overlain by quartzosepetrofacies of platform successions or passive margin sequences. These pre-orogenic strata are then succeeded by quartzolithicpetrofacies derived from recycled orogenic sources developed during collision orogenesis. Arc-derived petrofacies may form a part of the orogenic succession. Foreland petrofacieshave been well constrained is the Apennines, where multiple sources of detritus are inferred for both pre-orogenic and synorogenic phases (i.e., Zuffa et al, 1980; Gandolfi et al, 1983).

An important characteristic of many foreland sandstone suites, including those of the Apennines, is the comparative abundance of detrital limeclasts (Lc) of extrabasinal origin. In the synorogenic flysch of the Alps, for example, individual sandstone units vary widely in petrofacies, but essentially all contain some proportion of limeclasts reworked from deformed and uplifted sedimentary strata exposed as a recycled orogenic provenancewithin the developing collision orogen (Critelli and Lepera (1994); Critelli and Ingersoll (1995)).

## III.2. Sandstone Petrography:

Point count modal analysis and recalculated point-counting data for the analyzed sandstones suite samples are shown in tables 2 and 3 respectively. On the sandstone ternary classification plot (Folk 1980), almost all sandstones are sublitharenites, and only 4 samples fall in quartzarenite field (Fig. 26). The Zoumi sandstone suites show high amount of subangular to subrounded poorly sorted monocrystalline quartz (55% to 98%) (Fig. 27a, Table 2). The latter display undulatory extinction under cross-polarized light and usually show authigenic cement and rimed by quartz overgrowths. Polycrystalline quartz doesn’t exceed 44.6%; mainly display two to three or more than three sub-grains. Their features reflect a transition phase between the original crystals and the new recrystallized ones (Young 1976). The main observed sub-grain features are: ***i)*** polyhedral outlines with smooth boundaries, ***ii)*** elongated original host crystals, ***iii)*** crenulated and sutured boundaries characterized by tectonitic and non-tectonitic fabric (Figs. 27b, c).

Feldspar grains are noticeably scarces ($Qm_{96.9}$ $F_{0.9}$ $Lt_{2.1}$ – $Qm_{71}F_{2.3}$ $Lt_{26.7}$; F = total feldspars), with prevalent K-feldspar ($Qm_{99.4}$ $P_{0.2}$ $K_{0.2}$ - $Qm_{91.8}$ $P_{0.3}$ $K_{7.8}$). K-feldspar grains are represented by highly weathered orthoclase and microcline including sericiticepimatrix derived from altered K-feldspar (Figs 27d, e; Fig. 27m). K-feldspar can also show albitized domains as secondary porosity (Fig. 27n). Plagioclase grains are Na-plagioclases, mainly fresh and display polysynthetic twins (Fig. 27f). Lithoclasts are mainly seldom sedimentary and low-grade metamorphic clasts. The metamorphic rock fragments (with semischistose fabrics) are elongate quartz layered with white micas and seldom chlorites (Fig. 27g). Volcaniclastic fraction is very scarce characterized by quartz embayment and well-crystallized feldspars (Fig. 27h). The matrix is phyllosilicates-rich and cement carbonates bearing intrabasinal and extrabasinal clasts both associated with Fe-oxides as pore-filling phase. Few samples provide abundant foraminifera fossils (CI) (Fig. 27K). Quartz cement occurs mainly as syntaxial overgrowths with dust rims around detrital hosts (Fig. 27i). The foremost sedimentary rock fragments are exclusively carbonates, chert, siltstone, and Fe-oxides, as well lithic fragments (Figs. 27g, j, k, l). Carbonate minerals occur both as cement or small pore-filling calcite crystals (Fig. 27j) and as large intergranular calcite crystals showing a poikilotopic-like texture (Fig. 27j); while coarse-grained dolomite clasts rarely occur. The most common accessory minerals are micas (including muscovite and chlorite flakes), light heavy minerals (zircon, tourmaline, rutile) and opaque Fe-oxides.

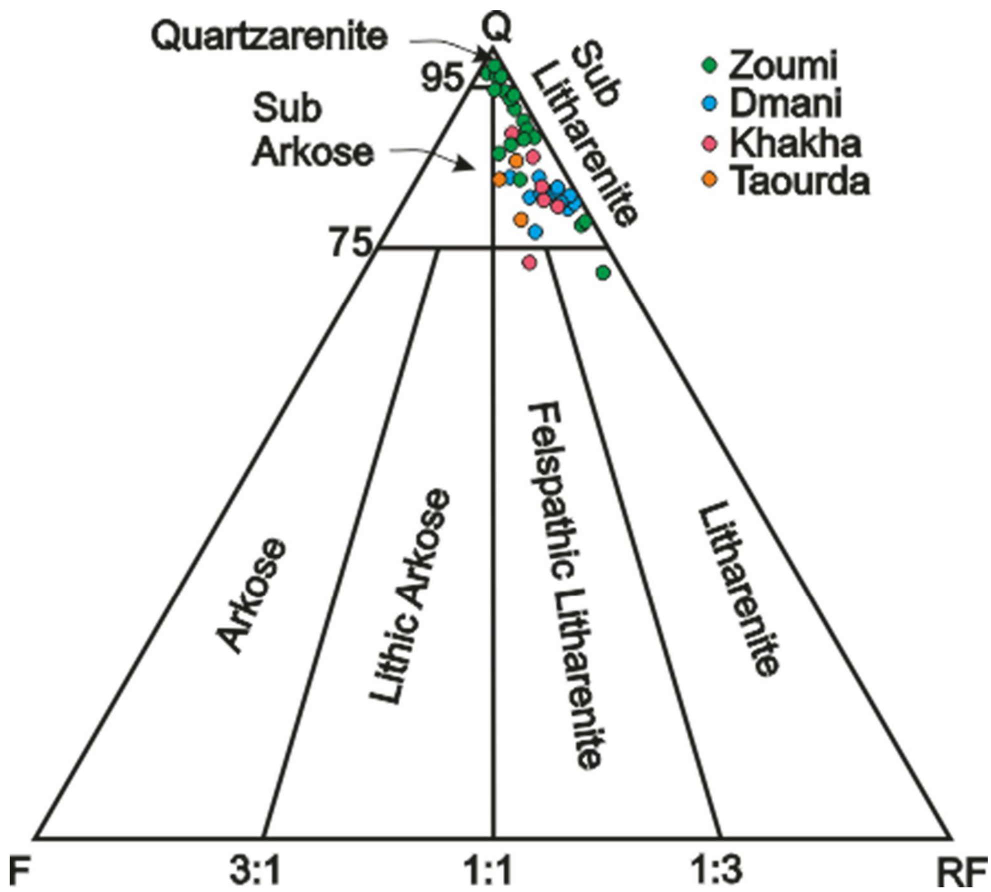


Figure 26: Composition of the Zoumi sandstones (Q: total quartz; F: feldspar; RF: rock fragments after Folk 1980). Samples are mainly composed of sublitharenite and some quartzarenite.

Figure27**:** Thin section photomicrographs of prominent petrologic features within Zoumi Sandstones. **a:** poorly sorted sandstone with plagioclase feldspar (arrows) showing polysynthetic albite twinning (10X). **b:** Polycrystalline, stretched, elongated quartz grains (Qp) of metamorphic origin having Crenuled contact (20X). **c:** Polycrystalline, stretched, elongated quartz grains (Qp) of metamorphic origin having sutured contact (20X). **d:** Sericitized altered K-feldspar (S-k-f) (20X). **e:** Microcline K-feldspar (M-K-f) showing characteristic grid twinning (20X). **f:** plagioclase feldspar (Pl) showing polysynthetic albite twinning(20X). **g:** weakly deformed metamorphic rock fragment (Lm), sedimentary lithics (Ls), and Fe-hydroxides (Fe-ox) (20X). **h:** microlithic texture lithic volcanic (Lv) (20X). **i:** Syntaxial quartz overgrowths (arrows), Clay cement (Cl) (20X). **j:** poikilotopiccalcitic cement with monocrystalline quartz grains (Qm) (20X). **k:** big & smallforaminifers fossils. **l:** Sedimentary lithics (Ls), Chert polycrystalline Quartz grains (Chrt) (20X). **m:** Sericitized k-feldspar (K-f) (20X). **n:** possible Albitized domains and secondary porosity (arrow) within K-feldspar, syntaxial quartz overgrowth (Qo) (20X). **O:** Well rounded monocristalline Quartz grains (20X). **p:** Nummilitic fossils (20X). All examples are in plane polarized light and depicted at the same scale.

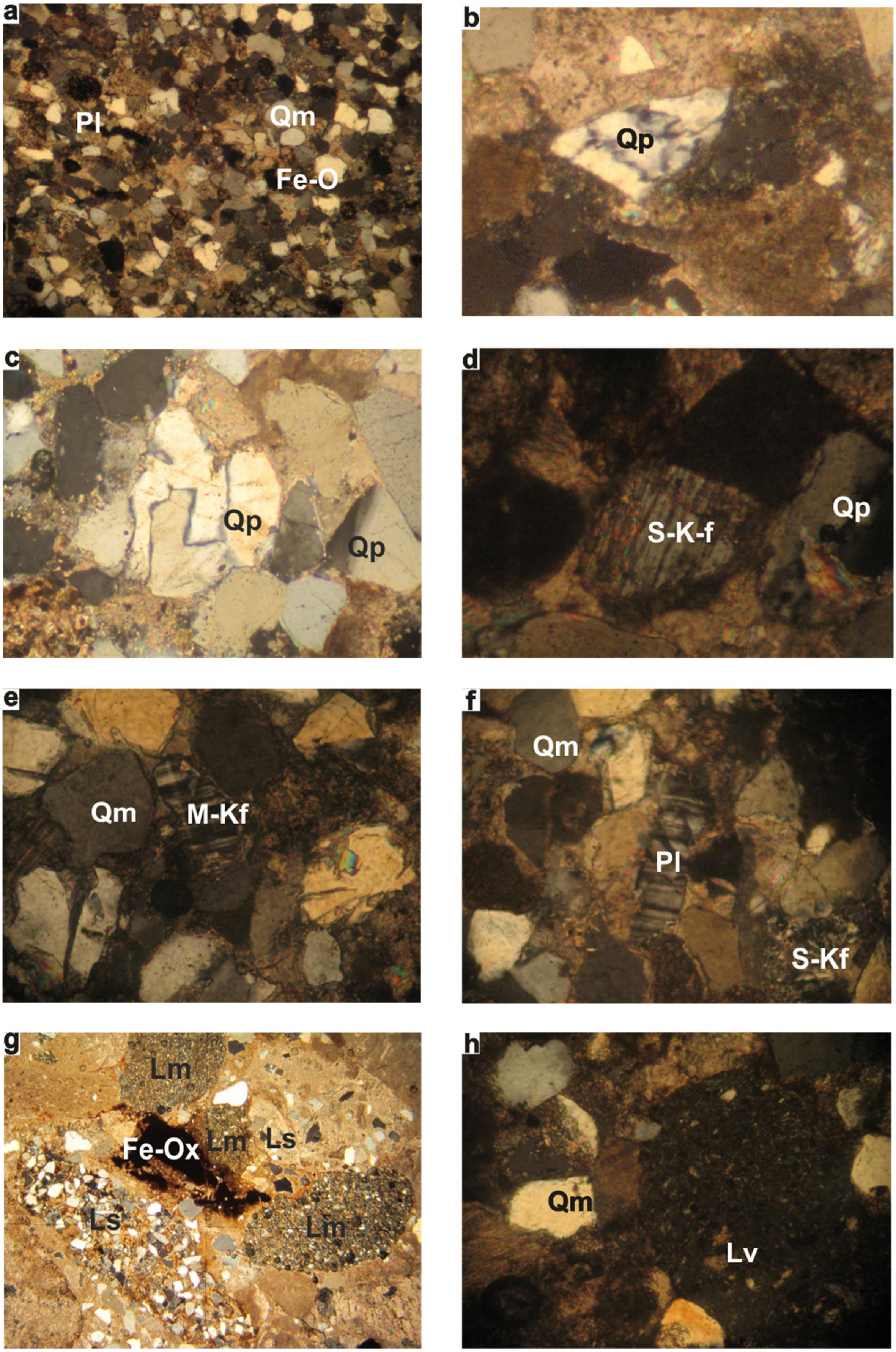
a
Pl
Qm
Fe-O
b
Qp
c
Qp
Qp
d
S-K-f
Qp
e
Qm
M-Kf
f
Qm
Pl
S-Kf
g
Lm
Fe-Ox
Lm
Ls
Ls
Lm
h
Qm
Lv

Figure 27.

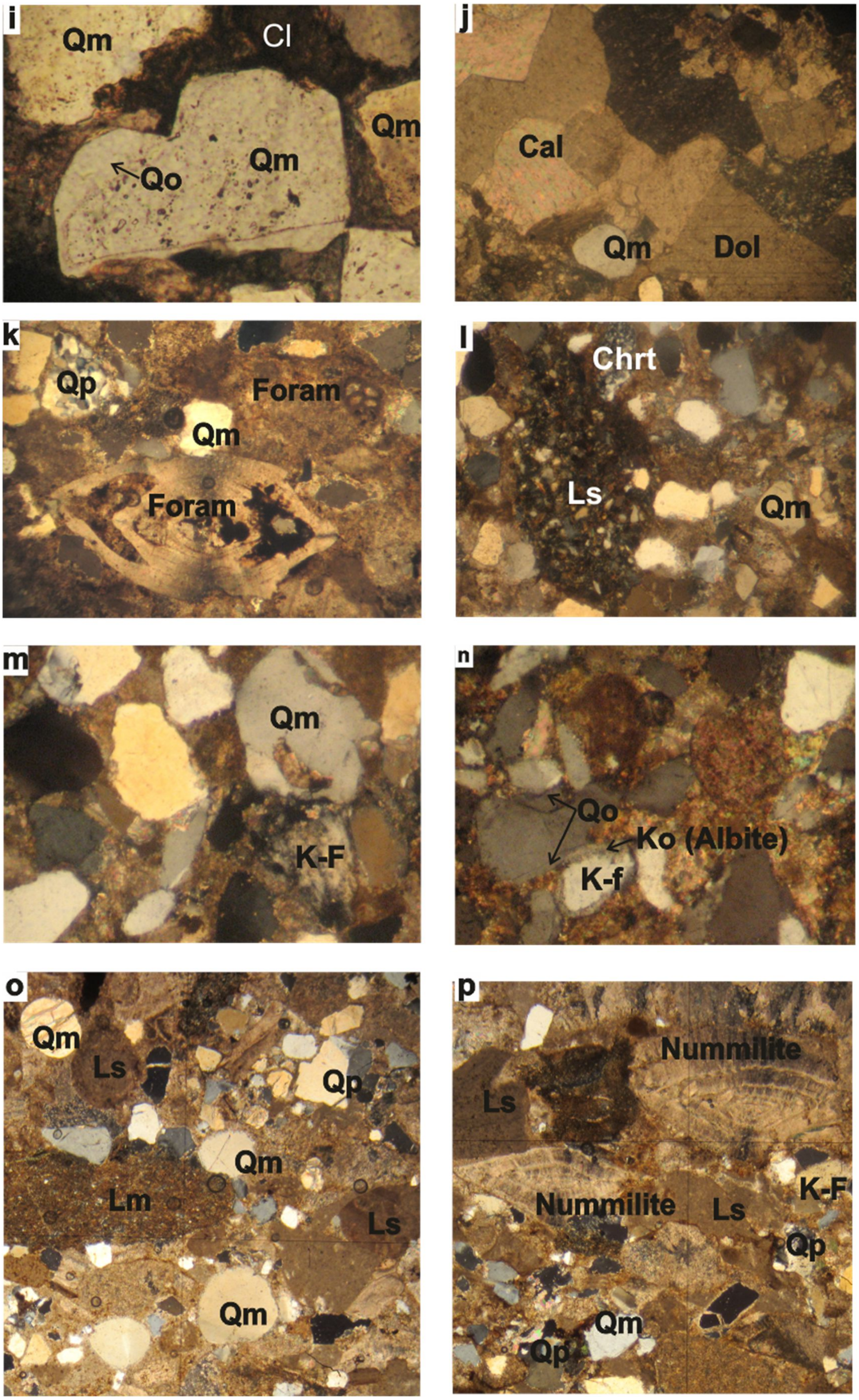

Figure 27: (continued).

# CHAPTER IV

# GEOCHEMISTRY OF ZOUMI MUDROCKS

# SOURCE AREA WEATHERING, PHYSICAL SORTING, RECYCLING PROCESSES AND PALEOCLIMATE CONDITIONS

# CHAPTER IV

# GEOCHEMISTRY OF ZOUMI MUDROCKS

# SOURCE AREA WEATHERING, PHYSICAL SORTING, RECYCLING PROCESSES AND PALEOCLIMATE CONDITIONS

## IV.1. Source area Weathering, Physical sorting and recycling processes:

### IV.1.1. Weathering profiles:

Weathering, Transportation and deposition are three of the most important processes influencing the properties of sediments (Nesbitt and Young 1984). Thorough investigations into physical effects, chemical aspects and chemical properties of the above processes on the bulk chemical composition of siliciclastic sedimentary rocks have received considerable attention as evidenced by important advances in sedimentary petrology.

The upper crust consists of approximately 21% by volume of quartz, 41% plagioclase and 21% potassium feldspar (Wedepohl, 1969). Moreover, Blatt and Jones (1975) determined that approximately a quarter of the exposed crystalline rocks is intrusive, a quarter is extrusive and a half is metamorphic and “Precambrian”. Considering quartz, and the Fe and Ti-bearing oxides as resistates, plagioclase, potash feldspar and volcanic glass constitute 75% of the exposed minerals readily susceptible to chemical weathering (labile minerals) so that studies concerning the weathering of the exposed crust necessarily must emphasize the behavior of these phases (Nesbitt and Young 1984).

Feldspars is by far the most abundant of the reactive (labile) minerals, consequently the dominant process during chemical weathering of the upper crust is the degradation of feldspars and subsequent formation of clay minerals (Nesbitt and Young 1984). Calcium, sodium and potassium generally are removed from the feldspar by aggressive soil solutions so that the proportion of alumina to alkalis typically increases in the weathered product.

Highly aluminous minerals such as kaolinites and beidellites are produced in high quantity during intense weathering and such sediments will have correspondingly high CIA values. High degree of chemical alteration is thus suggestive of weathering in humid, possibly in low latitude under tropical conditions. On the contrary, when chemical weathering is minimal, such as what happen in glacial conditions, fine grained resulted sediment will contain less aluminous clay minerals (illite and smectite) and high proportion of unaltered feldspar.

Feldspars are stable only in natural waters of relatively high cation/$H^+$ values and/or high aqueous silica concentrations. Most of the waters of weathering profiles are derived from rainwater which is made acidic by dissolution of atmospheric CO2 and CO; derived from oxidation of organic materials within weathering profiles. These profiles assume that potassium is more susceptible to leaching from K-feldspar and illite than is Al from the clay minerals. The assumption seems reasonable and the proposed reactions are feasible in that kaolinite is stable in acidic weathering solutions associated with the advanced stages of weathering. A good measure of the degree of weathering can be obtained by calculation of the chemical index of alteration (**CIA**) using molecular proportions (Nesbitt and Young 1982, 1984):

**CIA = [$Al_2O_3$/$Al_2O_3$+CaO*+$Na_2O$+$K_2O$]x100**

Where CaO* is the amount of CaO incorporated only in the silicate fraction of the rock. A correction can be made for carbonate and apatite content. The resultant value is a measure of the proportion of $Al_2O_3$ versus the labile oxides in the analyzed sample. Values of the index are 50 for analtered albite, anortite and K-feldspar, whereas the value for diopside is 0; consequently, fresh basalts have values between about 30 and 45 and granites and granodiorites have higher values, ranging between 45 and 55. Idealized muscovite gives a value of 75 and illite ranges between 75 and 80 as do smectite, kaolinite and chlorite yield the highest values, very close to 100. The changes in CIA reflect thus changes in the proportion of feldspar and the various clay minerals in the weathering profile. Size sorting during transportation and deposition generally results in some degree of mineralogical differentiation which may modify the CIA.

The early stages of weathering are characterized by depletion in CaO and $Na_2O$ and $K_2O$ along a straight line sub-parallel to the (CaO + $Na_2O$)-$A1_2O_3$ join. The late or advanced stage of weathering shows depletion in $K_2O$ as the composition of the leached rocks approaches that of kaolinite and/or gibbsite (Fig. 28). Continued weathering of rocks results in progressive destruction of plagioclase, eventually to the point where little Ca or Na remains in the residue (in either plagioclase or secondary products). For this situation, the bulk compositions of the residues plot close to the A-K join. Since residues plotting along the

A-K join contain little Ca- or Na-bearing phases, the dominant minerals that remain are aluminous phases such as kaolinite and potassic phases such as illite and/or K-feldspar (Nesbitt and Young 1984). In **A-CN-K** ternary plot, the initial trends are sub-parallel to the **A-CN** join, with a second segment following the A-K join toward the $Al_2O_3$ apex. These trends can be used as templates against which the chemical history of ancient profiles can be read. Deviations from these trends generally are the result of diagenesis and metasomatism (Nesbitt and Young 1989). Potassium is generally leached during soil formation, but most Precambrian paleosols are enriched in K, which is possibly a diagenetic feature (Retallack, 1986; 1990). Using these criteria, the proposed **CIW** index is an improved measure of the degree of weathering experienced by a material relative to its source rock (Harnois, 1988):

**CIW = [$A1_2O_3/(A1_2O_3 + CaO + Na_2O)$] X 100**

In the proposed index, $Al_2O_3$ is used as the immobile component. CaO and $Na_2O$ are the mobile components because they are readily leached during weathering. This index does not incorporate potassium because it may be leached or it may accumulate in the residue during weathering.

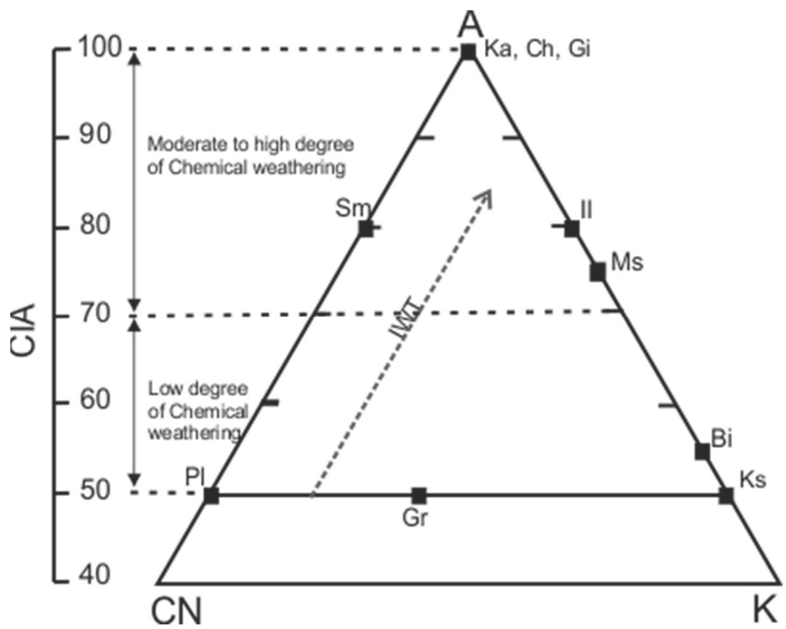


Figure 28: Triangular Diagram for weathering trends calculations (MOLAR PROPORTIONS). Small squares are idealized mineral compositions. CaO* represents CaO associated with only the silicate fraction of the samples (Nesbitt and Young, 1982; McLennan, 1993). Gr, granite; Ms, muscovite; Il, illite; Ka, kaolinite; Ch, chlorite; Gi, gibbsite; Sm, smectite Pl = plagioclase; Ks = alkali feldspar; Ms = muscovite; Ka = kaolinite.

Temperatures affect rates of weathering primarily, and from both equilibrium thermodynamic and kinetic viewpoints, the qualitative aspects of weathering do not change greatly; the same weathering products are produced from the same parent materials, but the proportions of secondary products and their rates of production are affected by temperature, hence climate Nesbitt and Young (1984). Singer (1980) and Nesbitt and Young (1984) discuss the effects of climate on weathering profiles and conclude that the extent of weathering is determined primarily by the amounts of acids introduced into the profile by rain water-derived solutions. The weathering trends of ancient rocks are controlled by the bulk compositions of the parent rocks, and there is no noticeable climatic effect on these trends. We conclude that there is no significant climatic effect on weathering trends within the compositional space represented by various diagrams (**A-CN-k, A-N-K, CIW, PIA** and **A-CNK-FM**).

### IV.1.2. Physical sorting and recycling effect during sediment transportation:

Petrographically, the identification of recycled sedimentary components is straightforward either by recognizing sedimentary rock fragments or abraded quartz overgrowths and may be suggested by the quartz-rich nature of sands (although note Johnsson et al, 1988).

Sedimentary recycling may also be accompanied by fractionation and enrichment of heavy minerals, notably zircon. It is likely inappropriate to use geochemical data alone because most well-sorted sediment and highly reworked first-cycle sediments could also possess enrichments in heavy minerals (Johnsson et al, 1988). The latter effect may be seen in data for loess, where Zr and Hf are strongly enriched over upper crustal abundances. In the sands, a major recycled metasedimentary component may be directly identified from the petrography. Such a component is also observed through the trace element relationships where zircon and other trace minerals are concentrated due both to the sedimentary provenance and further enrichments related to sedimentary transport.

There are several petrographic approaches to examine sorting processes in sedimentary rocks. The most straightforward is to evaluate the textural maturity of the sediment, using characteristic grain sizes and shapes, and mineralogy (e.g., Folk, 1974). The chemical composition of a sedimentary rock may also be helpful in evaluating the influence of sedimentary sorting. With increasing textural maturity in sandstones, there is typically an increase in quartz at the expense of primary clay-sized material, resulting in an elevation of the $SiO_2/Al_2O_3$ ratio and a decrease in the abundances of most trace elements.

Since a number of heavy minerals are dominated by elements that are trace elements in most sedimentary rocks (e.g., Zr in zircon, **REE** in monazite and allanite), it is possible to evaluate the role of heavy mineral concentration during sedimentary sorting (McLennan, 1989a). The ratio Zr/Sc is a useful index of zircon enrichment, since Zr is strongly enriched in zircon, whereas Sc is not enriched but generally preserves a signature of the provenance similar to other REE (McLennan, 1989a). In contrast, Th/Sc is a good overall indicator of igneous chemical differentiation processes since Th is typically an incompatible element, whereas Sc is typically compatible in mafic igneous systems.

In the case of monazite, an **REE** enriched heavy mineral, it is also possible to estimate enrichments from REE patterns (McLennan, 1989a). Since monazite has very high REE abundances and a very steep chondrite normalized heavy REE pattern, even small amounts (<0.01%) result in significant increases in the $Gd_N/Yb_N$ ratio (where subscript N refers to chondrite-normalized values). Monazite enrichments may be recognizable since post-Archean sedimentary REE patterns and most upper crustal igneous rocks rarely have $Gd_N/Yb_N$ outside of the range of 1.0 to 2.0 (McLennan, 1989a; McLennan and Taylor, 1991).

Quantifying sedimentary recycling processes, or the cannibalistic turnover of the sedimentary mass, are becoming increasingly important in understanding issues such as crustal evolution (e.g., Veizer and Jansen, 1979; McLennan, 1988) and the tectonics of sedimentary basins (e.g., Ingersoll, 1988; Johnsson et al, 1988; Johnsson and Meade, 1990; Steidtmann and Schmitt, 1988). Recycled sediment is likely the dominant source of preserved sedimentary rocks, but in detail the extent of any recycled component is highly variable and in many cases is related to tectonic history (Veizer and Janson, 1985).

### IV.I.3. Early and late diagenesis of weathering profiles:

Near-surface ground waters generally are near-neutral to slightly basic (White et al. 1963) and contain significant quantities of dissolved solids. Diagenetic reactions between groundwaters and weathering profiles may occur by transfer of dissolved constituents from solution to the weathering profile (i.e., metasomatism), and form diagenetic products superimposed on previously formed weathering products. Potassium metasomatism is particularly common during post depositional changes, and typically involves the conversion of kaolin (residual weathering product) to illite by reaction with $K^+$-bearing pore waters. Sandstones also undergo K metasomatism, which involves the replacement of plagioclase by potassium feldspar (Fedo et al., 1995). Growing concerns regarding potassium metasomatism in shale (Condie, 1993) point to the complex processes involved in chemical weathering in situ (production of clay minerals), mechanical breakdown, and continued chemical alteration during transport, burial, and diagenesis.

Weathering profiles buried under marine conditions can be expected to suffer Na-metasomatism. Only at low temperatures (T<100°C) might K-metasomatism occur in marine basins, and where temperatures anywhere within the basin exceed approximately 100°C, albite will form in preference to the potassic minerals. In contrast, profiles of continental basins may be subjected to over 200°C without diagenetic albite forming. Wahlstrom (1948) notes that quartz and K-feldspar persisted throughout the profile, and plagioclase weathered more rapidly than did K-feldspar, and biotite and hornblende altered rapidly to vermiculite, iron oxides, and other clay minerals.

Chemical studies of some paleosols indicate that they have been affected significantly by diagenetic reactions, including K-, Mg-, Fe-, or Na-metasomatism. Kaolinite can be converted to illite and chlorite. Partially degraded feldspars of the incipiently weathered zones can be converted to either K-feldspar or albite. These are "late" diagenetic effects. There is evidence of early diagenetic effects in some of the paleosols, for instance, where profiles contain evidence of reaction with perched or permanent ground water, and features preserved in these paleosols help to evaluate ancient climates and palaeogeographic settings.

## IV.2. Results of geochemical and mineralogical analysis:

### IV.2.1. Mudstones geochemistry and mineralogy:

Chemical and mineralogical composition of clastic sediments constitutes a good key element in deciphering source area composition, weathering and subsequent sorting and recycling effects during transport/deposition processes. Chemical weathering can strongly affect mineralogy and major element geochemistry and thus suffer removal of labile cations (e.g., $Ca^{2+}$, $Na^+$, $K^+$) relative to stable residual ones ($Al^{3+}$, $Ti^{4+}$) (Nesbitt and Young, 1982).

The results of whole-rock XRD analyses on Zoumi Flysch mudrocks samples show some mineral assemblages variations (Table 4). They are rich in illite associated with significant amounts of kaolinite, quartz, k-feldspar, plagioclase and other phyllosilicates (micas and chlorite). Minor amounts of iron oxides-hydroxides (such as goethite, siderite, and hematite). The phyllosilicates are the main mineralogical components forming 21.54% to 45.04% of the bulk rock. The feldspar is the most abundant phase in all samples ranging from 31.66% to 76.41%. Illite mineral is ranging from 6.79% to 16.72%. Chlorite occurs in similar proportions in all samples (1–4%). The non-phyllosilicate minerals are represented by minor amount of quartz and negligible ones of iron oxides-hydroxides. In all studied samples the lowest content of quartz occurs with the highest content of kaolinite (Table 4, Fig. 29).

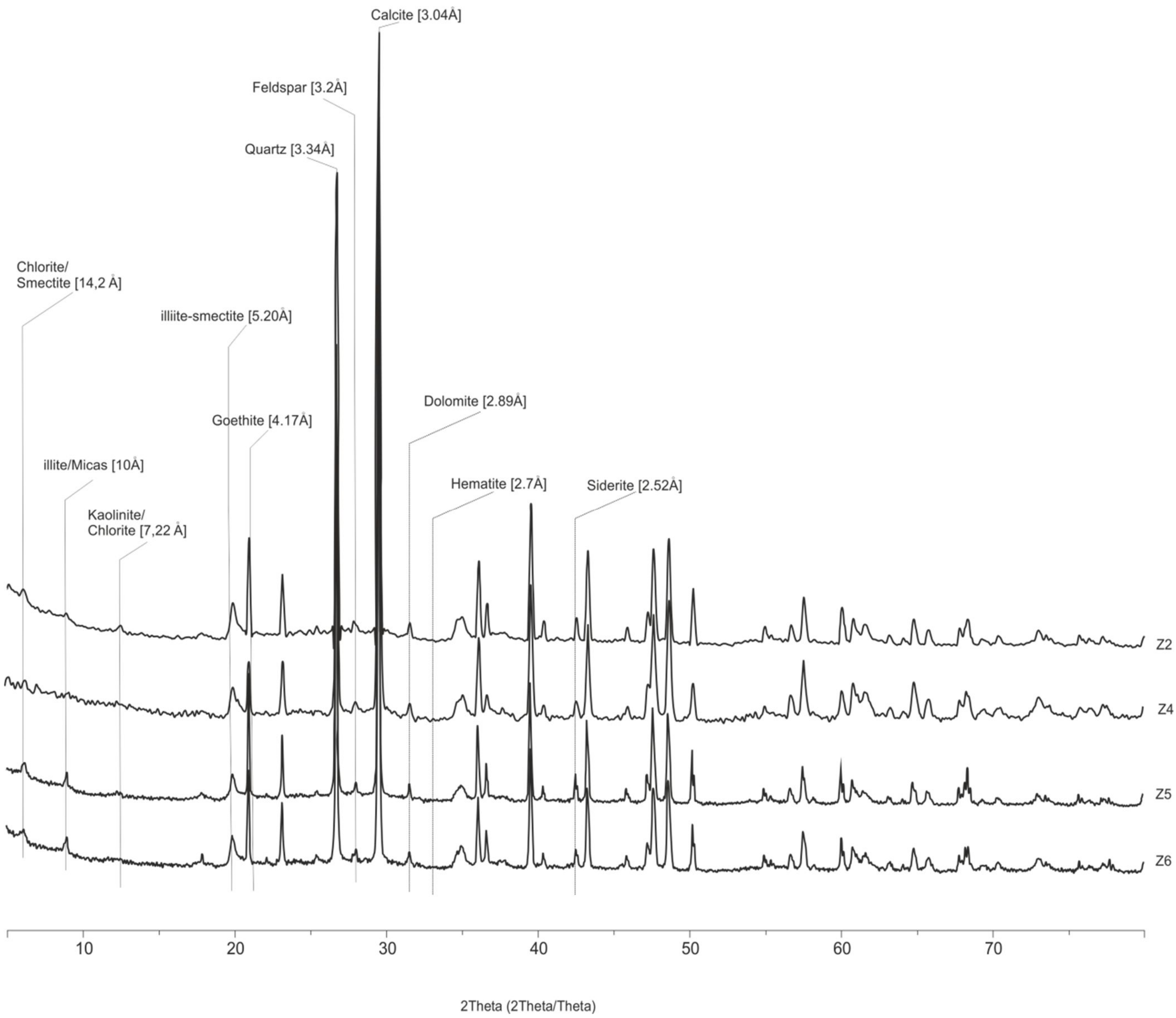


**Figure 29***:* The x-ray diffraction patterns of some Zoumi mudstone whole-rock samples.

Whole-rock geochemical analysis of the studied samples is presented in Table 5. $SiO_2$ content of Zoumi mudrocks is relatively high (ranging from 31% to 58%). Average concentrations of other oxides are 15.25% for CaO, 12.65 % for $Al_2O_3$, 3.23 % for $Fe_2O_3$, 1.65 % for $K_2O$, 0.4 % for $TiO_2$, and 0.46 % for $Na_2O$. Lower concentrations were detected for MnO, and $P_2O_5$ (0.02 %, and 0.16 % respectively). Harker diagrams show mudrocks major elements variation relative to $SiO_2$ (Bhatia 1983; Roser and Korsch 1988). Plots of $TiO_2$, $Al_2O_3$, $Fe_2O_3$, K2Oand MgO against $SiO_2$concentration show positive linear patterns (with R2 values 0.247, 0.341, 0.154, 0.108and 0.187, respectively), whereas, CaO against $SiO_2$ plot shows negative linear patterns (R2 = -0.865), (Fig. 30). Analyses of MnO, and $P_2O_5$ returned very low concentrations with increasing $SiO_2$ while $Al_2O_3$, $Fe_2O_3$, and $K_2O$ returned relatively high values. Further, CaO analysis returns very high values due to a significant enrichment in carbonates in almost all mudrock samples. Moreover, geochemical compositions of the studied mudrocks and the post-Archean Australian shales (PAAS; Taylor and McLennan 1985) normalized to the Upper Continental Crust (UCC; McLennan et al., 2006), and compared with average post-Archean Australian shales (PAAS; Taylor and McLennan 1985), which are considered to be representative of the UCC composition. The general sample trend of observed patterns shows close variations with those observed for the PAAS (Fig. 34a), except a very notable MnO and $Na_2O$ depletion and CaO enrichment.

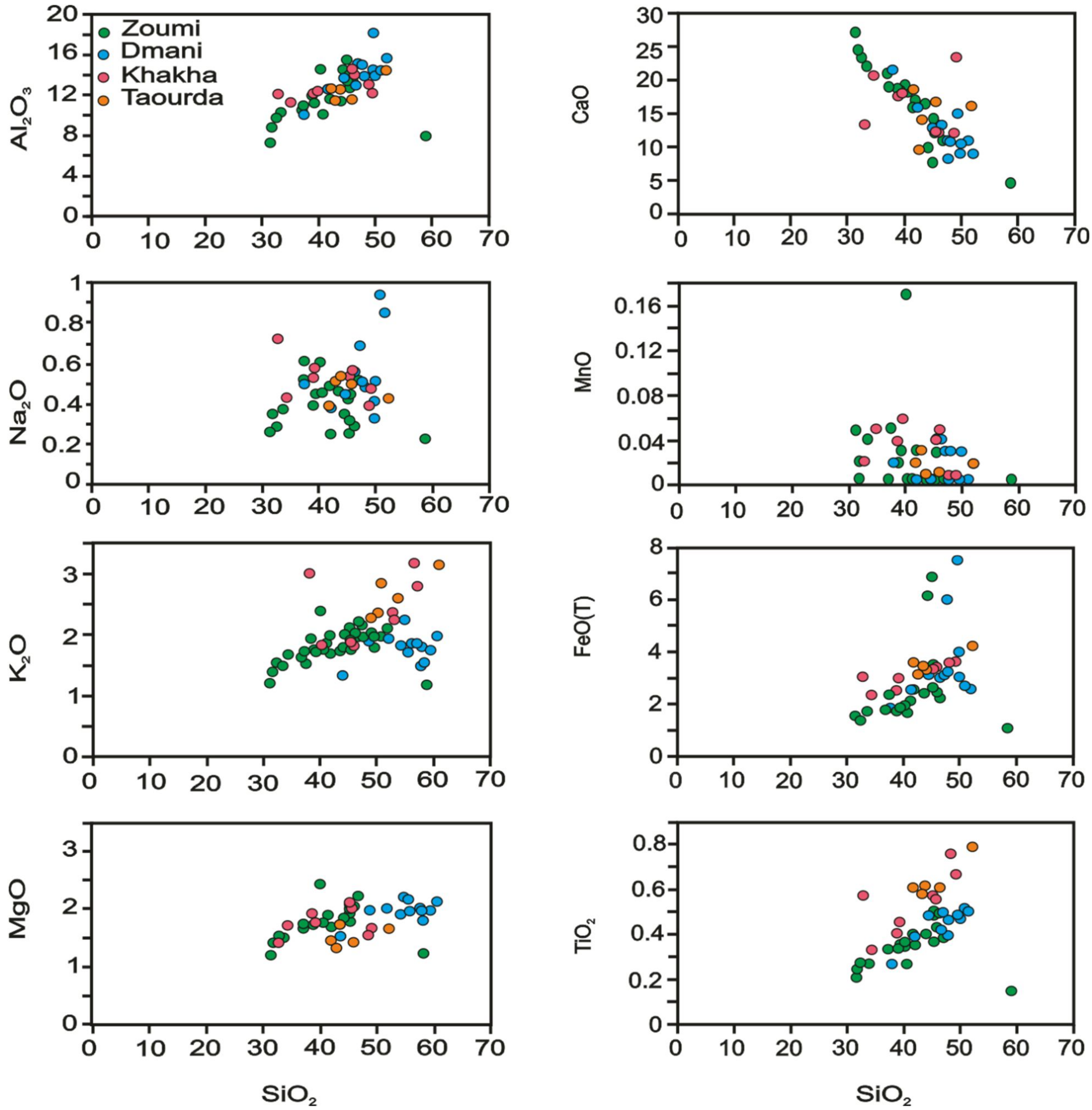


**Figure 30**: Harker variation diagrams for major elements in the Zoumi mudrocks.

According to Herron's diagram (Herron 1988), almost all analyzed Zoumi mudrocks samples fall in the shale and wacke fields (Fig. 31) and rare ones (03) fall in the Fe-shale field since they are characterized by notable concentrations of Fe-oxides, as attested by mineralogical analyses (Table 4). The mudrocks display relative enrichment in $Al_2O_3$ related to high amount of mica, K-feldspar, and clay minerals. The CaO enrichment is probably due to extrabasinal carbonate input resulting from the alteration and erosion of remnants of both Jurassic and/or Eocene-Oligocene limestone slices belonging to previously lost realms carbonate platforms (Ben Yaich 1991, Lespinasse 1975).

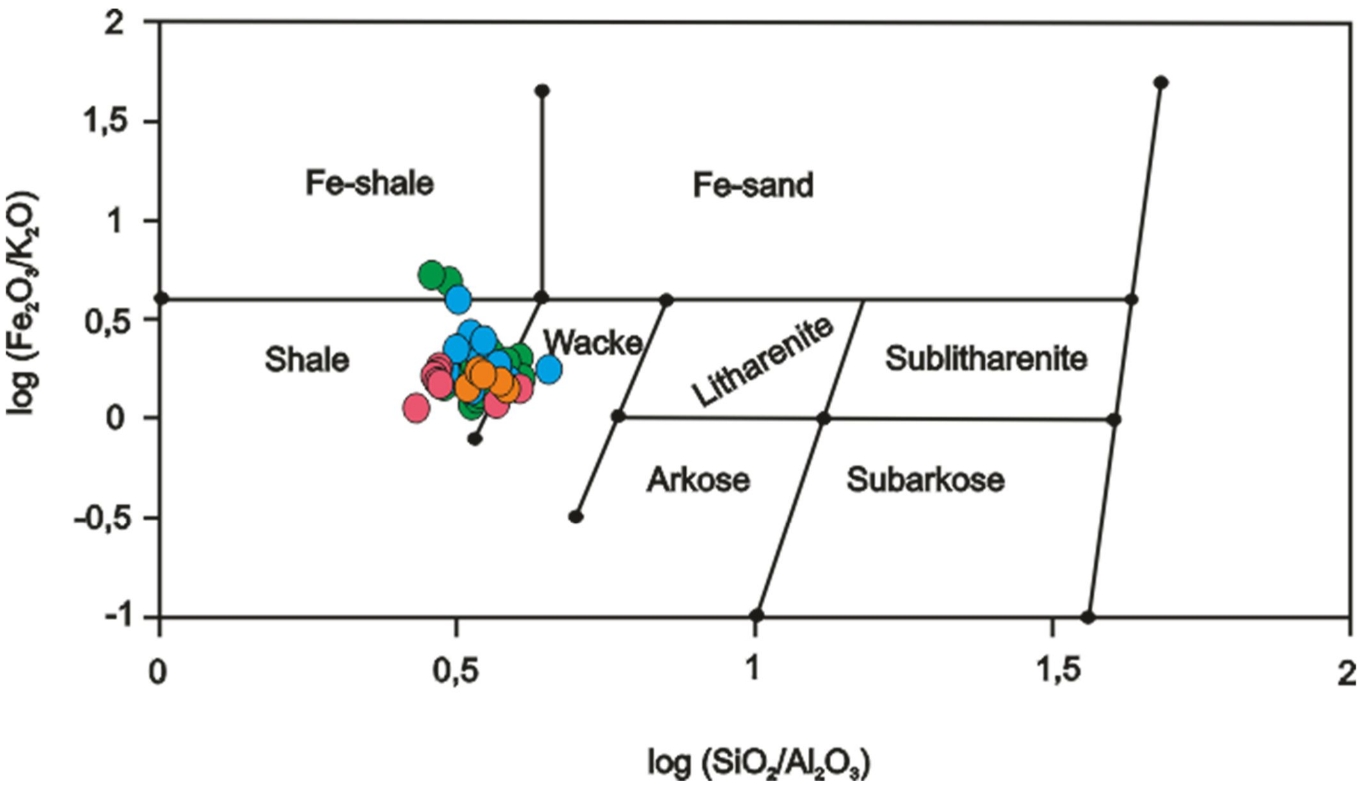


**Figure 31:** Classification diagram for the studied mudrocks samples (Diagram after Heron 1988).

In the $5^*Al_2O_3$-$SiO_2$-$2^*CaO$ ternary plot (Perri et al. 2012), studied sediments can be described as mixtures of aluminosilicates with evident carbonate enrichment (Fig. 32), since the majority of samples display a homogeneous array toward CaO apex consistent with a very pronounced carbonates enrichment. This array falls perpendicular to the $Al_2O_3$-$SiO_2$ join close to the PAAS and UCC. These chemical associations and elemental variations are closely related to sediments mineralogical composition as shown by the mineralogical analyses (Table 4).

Generally, the Si/Al, K/Al and Na/Al ratios (proxies for quartz content in clays, for illite and smectite contents, respectively) are used to identify mineralogical variations within the samples (Hofmann et al. 2001; Hofer et al. 2013; Perri 2016). Si/Al values are 2.98±0.25 in average. Na/Al values are very low (average = 0.05) than K/Al (average = 0.20). K/Al *vs.* Na/Al discrimination plot shows a relative proportion between illite and smectite contents (Hofer et al. 2013). Besides, K/Al ratios are four times higher than Na/Al ones in average (Fig. 33) which suggests a noteworthy illite enrichment relative to smectite for the studied mudrocks (Hofer et al. 2013).

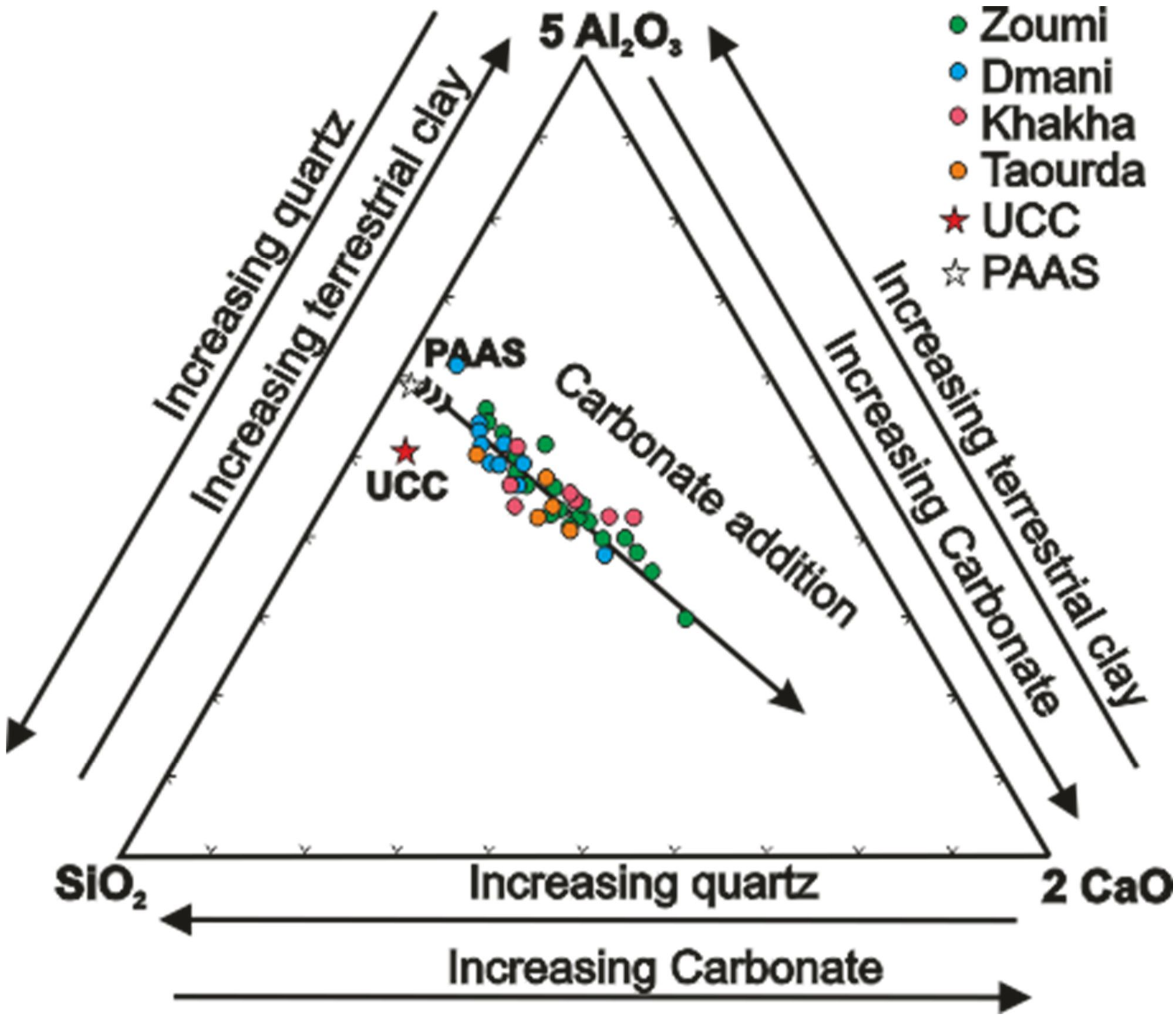


**Figure 32**: Ternary plot showing the relative proportions of SiO2 (representing quartz or opaline silica), Al2O3 (representing mica/clay minerals), and CaO (representing carbonate) for the studied mud samples. (Plot after Perri et al. 2012).

### IV.2.1.1. Major oxides:

The analytical results are presented in Table 2, and Herron's (1988) chemical classification diagram is shown in Figure 4. The studied samples plot in the shale and the wacke fields, thus reflecting variation in the quartz-feldspars/mica ratio in the studied samples. Only three samples plot in the Fe-shale field.

Geochemical compositions of studied mudrocks and the Post-Archean Australian Shales (PAAS; Taylor and McLennan 1985) were normalized to the Upper Continental Crust (UCC; McLennan et al. 2006). The analyzed samples were compared with average Post-Archean Australian shales (PAAS), which are considered to be representative of the UCC composition. The samples general trend shows similar variations with those observed for the PAAS (Fig. 34a), except a very notable MnO and $Na_2O$ depletion and Cao enrichment.

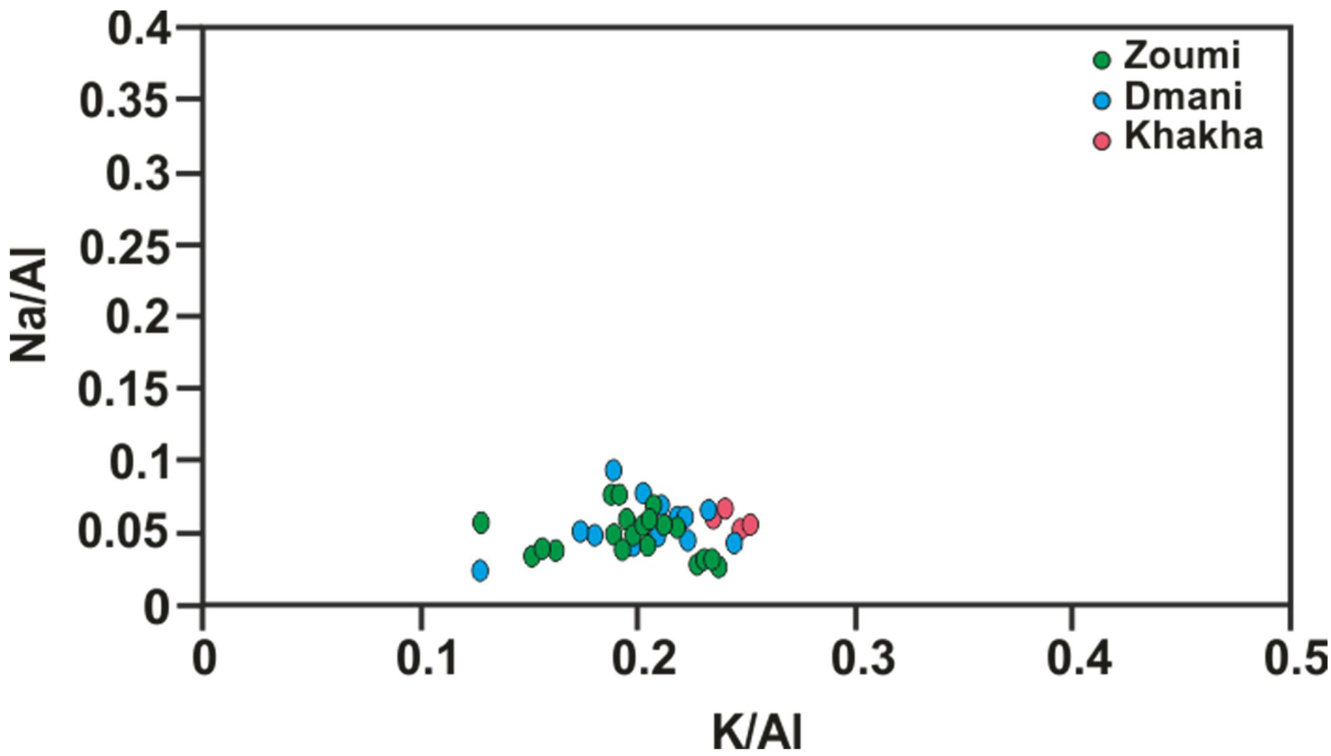


**Figure 33:** K/Al vs. Na/Al discrimination diagram as proxies forsmectite and illite contents (diagram after Hofer et al. 2013).

The studied mudrocks are characterized by compositional ranges for $SiO_2$, $TiO_2$, $Al_2O_3$, $Fe_2O_3$, MgO and $P_2O_5$ close to those of the UCC (McLennan et al. 2006). Almost all mudrocks are enriched in CaO. Although, some samples from Zoumi and Taourda localities compared to the UCC standards are mildly depleted in $SiO_2$, $Al_2O_3$, $Fe_2O_3$, $TiO_2$ and $K_2O$, while MnO, $Na_2O$ and, in a lesser extent, $K_2O$ is strongly depleted.

The $Na_2O$ depletion is likely due to the sediments burial history, which promoted the formation of K-rich, mica-like clay minerals (Amendola et al. 2016). On the other hand, MnO depletion may have multiple causes including both source-area composition and redox chemistry of the element promoting Mn solubility as $Mn^{2+}$ under surface conditions (Mongelli et al. 2006).

The high CaO concentration is related to the carbonate minerals resulting from the exhumation and erosion/alteration of Jurassic and Paleocene-Eocene carbonates and also to post-depositional diagenetic processes.

### IV.2.1.2. Trace elements:

The distribution of large-ion lithophile trace elements is characterized by a marked depletion of these elements with respect to the PAAS and UCC, except for Sr which is slightly enriched (Fig 34b). Zoumi mudrocks are depleted in high-field-strength elements (HFSE), even though some samples are slightly enriched in Nb. The chondrite-normalized REE patterns have a PAAS-like shape (except sample Z135 which is enriched in Eu (Eu/Eu* = 0.94) relative to the PAAS) with LREE/HREE fractionation [average (La/Yb)ch = 10.69±0.85] and negative Eu anomaly (average Eu/Eu* = 0.67±0.07). The average $(La/Yb)_{ch}$ ratio is higher than the $(La/Yb)_{ch}$ of PAAS (9.2), whereas the Eu anomaly is quite similar (Eu/Eu*PAAS = 0.66) (Fig. 35). Concentrations of transition elements (TEs) are relatively depleted in Co, Cr, V, and enriched, for some samples, in Ni relative to the PAAS.

Trace-element concentrations are reported in Table 6. In comparison with UCC average (McLennan et al. 2006) and the PAAS (Taylor and McLennan 1985), concentrations of most trace elements are generally low. The average relative concentration ratios lie between 0.1 and 1, except for Sr, Ni, Cr, Nb are enriched with respect to UCC and PAAS. Ba, Co, Th, Zr, Y and Ce are almost exclusively depleted with respect to UCC and PAAS (Fig. 34b). Zirconium concentrations are clearly lower than UCC values (McLennan et al. 2006) testifying that mudrocks are weakly reworked. Due to a combination of its weathering resistance and its high specific gravity, this mineral does not undergo a very notable sorting related fractionation that, in turn, means that Zr is not affected by a very pronounced gravitative fractionation (Taylor and McLennan 1985).

The concentrations of the transition elements are close to or highly greater than those of UCC, except for Co which is highly depleted relative to UCC (Fig. 34b). High field strength trace elements (HFSE) and light rare earth elements (LREE) have concentrations close to the UCC. Some samples are enriched in Nb, and all samples are highly depleted in Zr relative to the UCC (Fig. 34b).

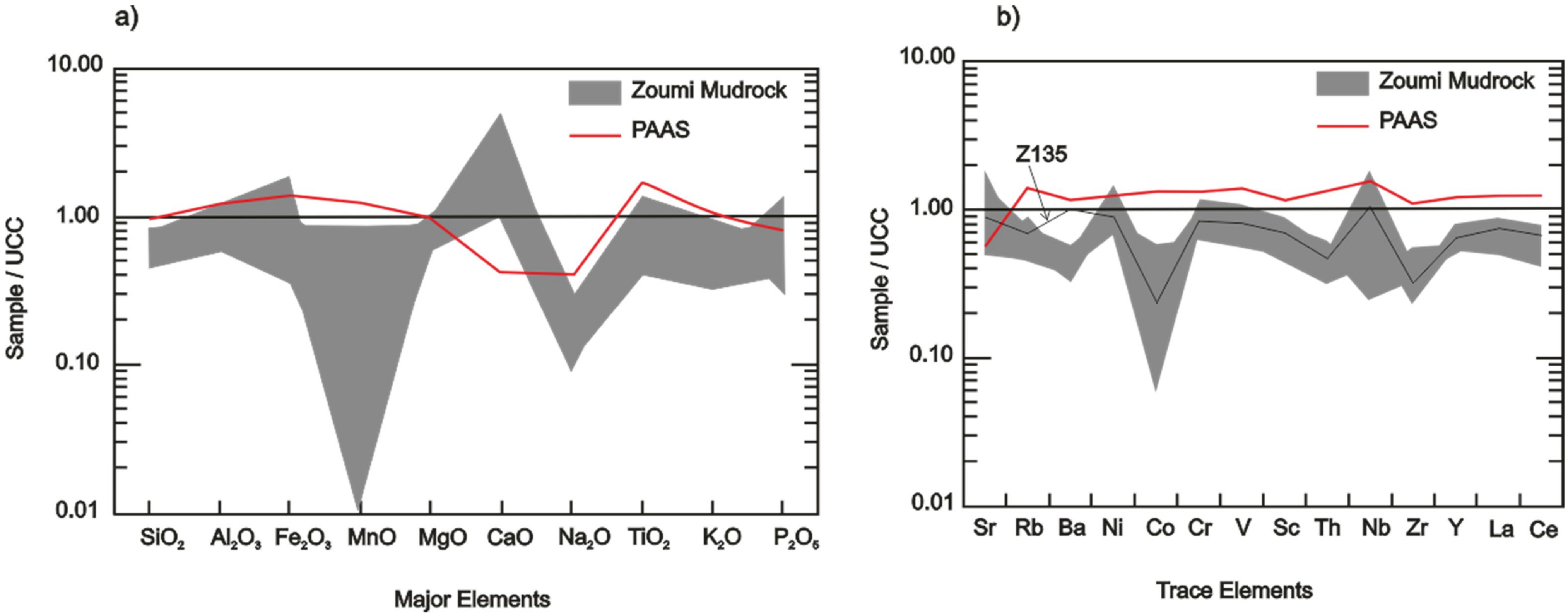


**<u>Figure 34</u>: a**. Normalization of major elements to the upper continental crust (UCC; McLennan et al. 2006). The plot of the Post-Archean Australian Shales (PAAS; Taylor and McLennan 1985) is shown for comparison. **B**. Normalization of trace elements to the upper continental crust (UCC; McLennan et al. 2006). The plot of the Post-Archean Australian Shales (PAAS; Condie 1993) is shown for comparison.

The high CaO concentration is related to the carbonate minerals resulting from the exhumation and erosion/alteration of Jurassic and Paleocene-Eocene carbonates and also to post-depositional diagenetic processes.

### IV.2.1.2. Trace elements:

The distribution of large-ion lithophile trace elements is characterized by a marked depletion of these elements with respect to the PAAS and UCC, except for Sr which is slightly enriched (Fig 34b). Zoumi mudrocks are depleted in high-field-strength elements (HFSE), even though some samples are slightly enriched in Nb. The chondrite-normalized REE patterns have a PAAS-like shape (except sample Z135 which is enriched in Eu (Eu/Eu* = 0.94) relative to the PAAS) with LREE/HREE fractionation [average (La/Yb)ch = 10.69±0.85] and negative Eu anomaly (average Eu/Eu* = 0.67±0.07). The average $(La/Yb)_{ch}$ ratio is higher than the $(La/Yb)_{ch}$ of PAAS (9.2), whereas the Eu anomaly is quite similar (Eu/Eu*PAAS = 0.66) (Fig. 35). Concentrations of transition elements (TEs) are relatively depleted in Co, Cr, V, and enriched, for some samples, in Ni relative to the PAAS.

Trace-element concentrations are reported in Table 6. In comparison with UCC average (McLennan et al. 2006) and the PAAS (Taylor and McLennan 1985), concentrations of most trace elements are generally low. The average relative concentration ratios lie between 0.1 and 1, except for Sr, Ni, Cr, Nb are enriched with respect to UCC and PAAS. Ba, Co, Th, Zr, Y and Ce are almost exclusively depleted with respect to UCC and PAAS (Fig. 34b). Zirconium concentrations are clearly lower than UCC values (McLennan et al. 2006) testifying that mudrocks are weakly reworked. Due to a combination of its weathering resistance and its high specific gravity, this mineral does not undergo a very notable sorting related fractionation that, in turn, means that Zr is not affected by a very pronounced gravitative fractionation (Taylor and McLennan 1985).

The concentrations of the transition elements are close to or highly greater than those of UCC, except for Co which is highly depleted relative to UCC (Fig. 34b). High field strength trace elements (HFSE) and light rare earth elements (LREE) have concentrations close to the UCC. Some samples are enriched in Nb, and all samples are highly depleted in Zr relative to the UCC (Fig. 34b). The chondrite-normalized REE patterns have a close PAAS-like shape (except sample Z135 which is enriched in Eu (Eu/Eu* = 0.94) relative to the PAAS) (Fig.

35), and are characterized by LREE/HREE fractionation (average $La_N/Yb_N$ = 10.69 ± 0.85) (where ''N'' expresses chondritic normalization) and negative Eu-anomaly (average Eu/Eu* = 0.67 ± 0.07). We can notice that trace and rare earth elements for most samples show a moderatedepletion, likely owingto a dilution effect exerted by the detrital carbonatecomponent (e.g. Stevenson, Whittaker & Mountjoy, 2000). The average $La_N/Yb_N$ ratio and the Eu anomaly are similar to the PAAS ($La_N/Yb_N$ = 9.2; $Eu/Eu^*_{PAAS}$ = 0.66). Rare earth elements and Yttrium that behave like heavy rare earth elements (HREE), hasno correlation with $Al_2O_3$; this is congruent with the fact that in fine-grained sediments these elements may be hosted in accessory phases in mudrocks (Slack & Stevens 1994; Mongelli et al. 1996, 2006).

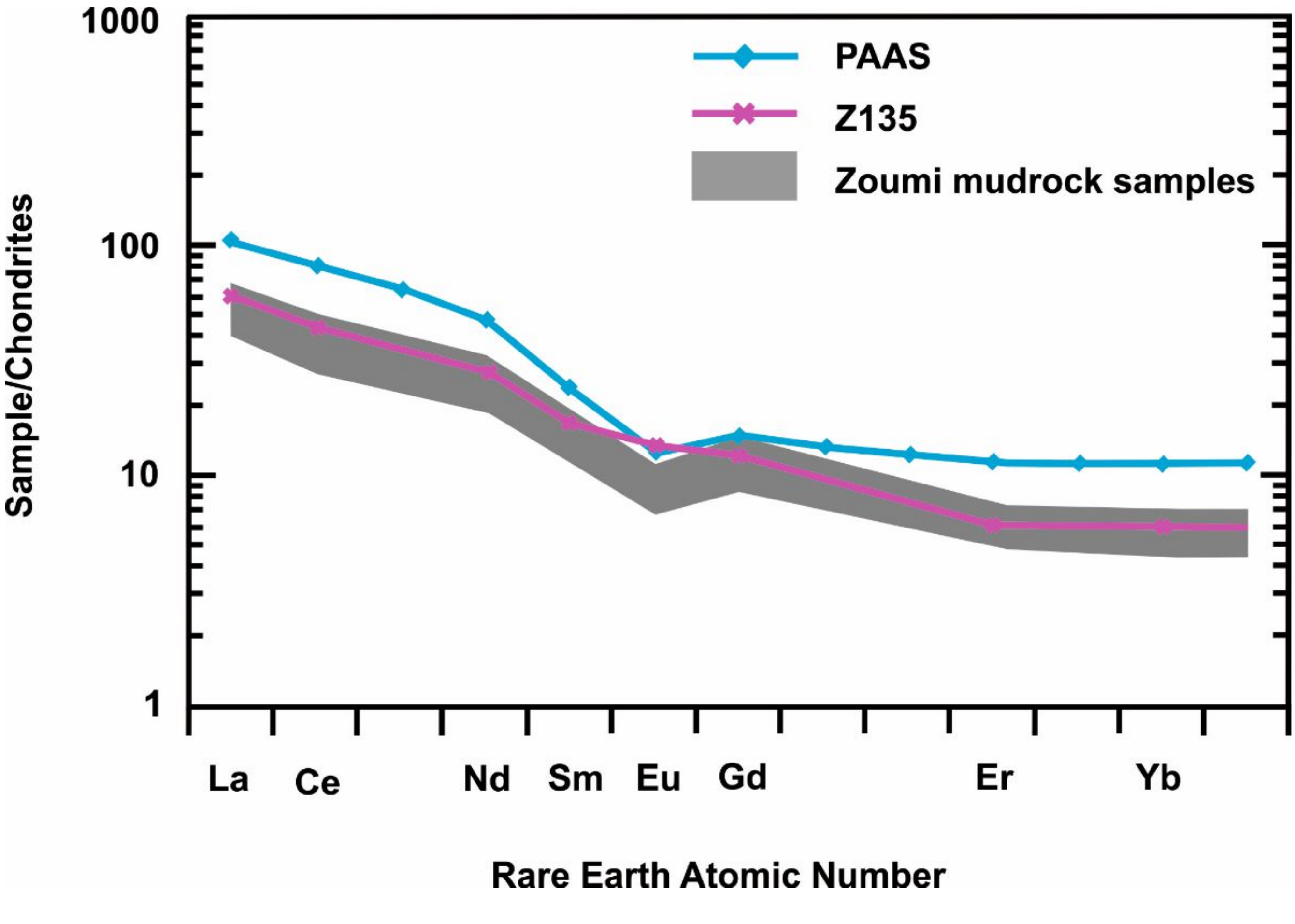


**Figure 35**: Rare earth element compositional ranges, chondrite normalized (Taylor and McLennan 1985). The plot of the Post Archean Australian Shales is shown for comparison.

## IV.3. Discussion:

### IV.3.1. Source-area weathering:

It is widely accepted that chemical weathering strongly affects major-element geochemistry and mineralogy of siliciclastic sediments (Nesbitt and Young 1982; Johnson et al. 1988; McLennan 1993). Quantitative measurement of chemical weathering, such as chemical index of alteration (CIA; Nesbitt and Young 1982), is potentially useful to evaluate the progressive conversion of plagioclase and potassium feldspar into clay minerals (Nesbitt and Young 1982, 1984). CIA is calculated using molecular proportions: $CIA=[Al_2O_3/(Al_2O_3+CaO^*+Na_2O+K_2O)]x100$, where $CaO^*$ represents the fraction residing only in silicate minerals (Nesbitt and Young 1982, 1989). Thus, it is necessary to make a correction to the measured CaO content for the presence of carbonates (calcite, dolomite) and apatite. In this study, the CaO was initially corrected for phosphate using available $P_2O_5$ data ($CaO^*$ = mole CaO - mole $P_2O_5 \times 10/3$). If mole's remaining number is less than that of $Na_2O$, then CaO value is accepted as the $CaO^*$. Otherwise, the $CaO^*$ is assumed to be equivalent to $Na_2O$ (McLennan 1993; Bock et al. 2002; Vital and Stattegger 2000; Roddaz et al. 2006).

The CIA values for unaltered plagioclase and K-feldspar are approximately equal to 50 as are those of unaltered upper crustal rocks. The samples with CIA values below 60 display low chemical weathering, those between 60 and 80 indicate moderate chemical weathering and those with more than 80 exhibit extreme chemical weathering (Fedo et al. 1995). Typical shales (PAAS Shales) CIA average is about 70 to 75 (Nesbitt and Young 1982; McLennan et al. 1993). The weathering trend can be illustrated on $Al_2O_3$-($CaO^*$+$Na_2O$)-$K_2O$ triangular plot (Nesbitt and Young 1984, 1989).

The calculated CIA values for the Zoumi mudrocks are presented in Table 2, CIA values show a gradual progression in alteration from low (CIA = 50–60) to intense (CIA > 80) chemical weathering. In the A-CN-K ternary plot (scale of CIA shown at the left side of the figure for comparison) (Fig. 36a), we can distinguish two sample subsets: The samples of Khakha and Taourda outcrops are characterized by similar CIA values (from 67 to 77, average=73±2.64) and fall close to the A-K join along a linear trend indicating moderate feldspar weathering and subsequent Illite and minor Kaolinite formation (as attested by bulk mudrock mineralogy displaying low amounts of Kaolinite). They form a cluster in a limited area, indicating steady-state weathering conditions which imply that physical and chemical processes balance was similar (Fedo et al. 1995). Whereas, data points from Zoumi and

Dmani outcrops are on a straight line probably deviating from the theoretical trend (IWT Nesbitt and Young 1982; McLennan 1993), and departing from a source intersecting the feldspar join toward the A-K join close to the Illite-Muscovite area. The studied mudrocks have lower average CIA values and a higher variability of the CIA index (from 45 to 84, average=72±11.9 and average=72±9.07 respectively), and hence indicating non-steady state weathering conditions with low to moderate chemical weathering. However, some mudstone samples from the middle Zoumi section show slightly higher CIA values of 81.22 – 84.07. Further, the CIA´ calculated without CaO content and expressed as molar volumes of [Al/(Al+Na+K)]×100 (Perri et al. 2014) have also been used. The CIA' values plotted in the A-N-K diagram (Fig 36b) display a weathering trend similar to the A-CN-K diagram, testifying weak to moderate paleoweathering conditions.

The Chemical Index of Weathering (CIW) proposed by Harnois (1988), which is not sensitive to post-depositional K-enrichments, has been used to constrain palaeoweathering intensity. The Zoumi mudrocks show a wide range of CIW values with two subsets: Zoumi and Dmani localities subset (averages of 84±12.8 and 85±11.5 respectively) and Khakha and Taourda localities subset (averages of 87±2.1 and 88±2.3 respectively). These values, plotted in the A–C–N diagram (Fig. 36b), form for Zoumi and Dmani localities a large array departing from the feldspar join toward the A-apex, indicating weak to moderate and rarely intense weathering under non-steady-state conditions at the source area. On the contrary, Khakha and Taourda plotted values form a tight array close to the A apex indicating moderate to intense weathering under steady-state conditions.

The degree of chemical weathering can be also appraised by using the plagioclase index of alteration (PIA) (Fedo et al., 1995); in molecular proportions: PIA= [($Al_2O_3$-$K_2O$)/($Al_2O_3$+CaO*+$Na_2O$+$K_2O$), where CaO* is the only inherent CaO in silicate fraction. The unweathered plagioclase has PIA value of 50. Khakha and Taourda mudrocks have an average PIA of about 84±2.9 and 86±2.9 respectively, while Zoumi and Dmani mudrocks show PIA averages of 80±15.9 and 82±12.7 respectively.

The degree of weathering of the source region can also be performed by using the Mineralogical Index of Alteration (MIA=[quartz/(quartz+plagioclase+K-feldspar)]×100 using point count modal proportions), (Nesbitt et al. 1996; Rieu et al. 2007). The Zoumi mudrocks MIA values range from 92.8% to 99.7% (El Mourabet et al. 2017a).

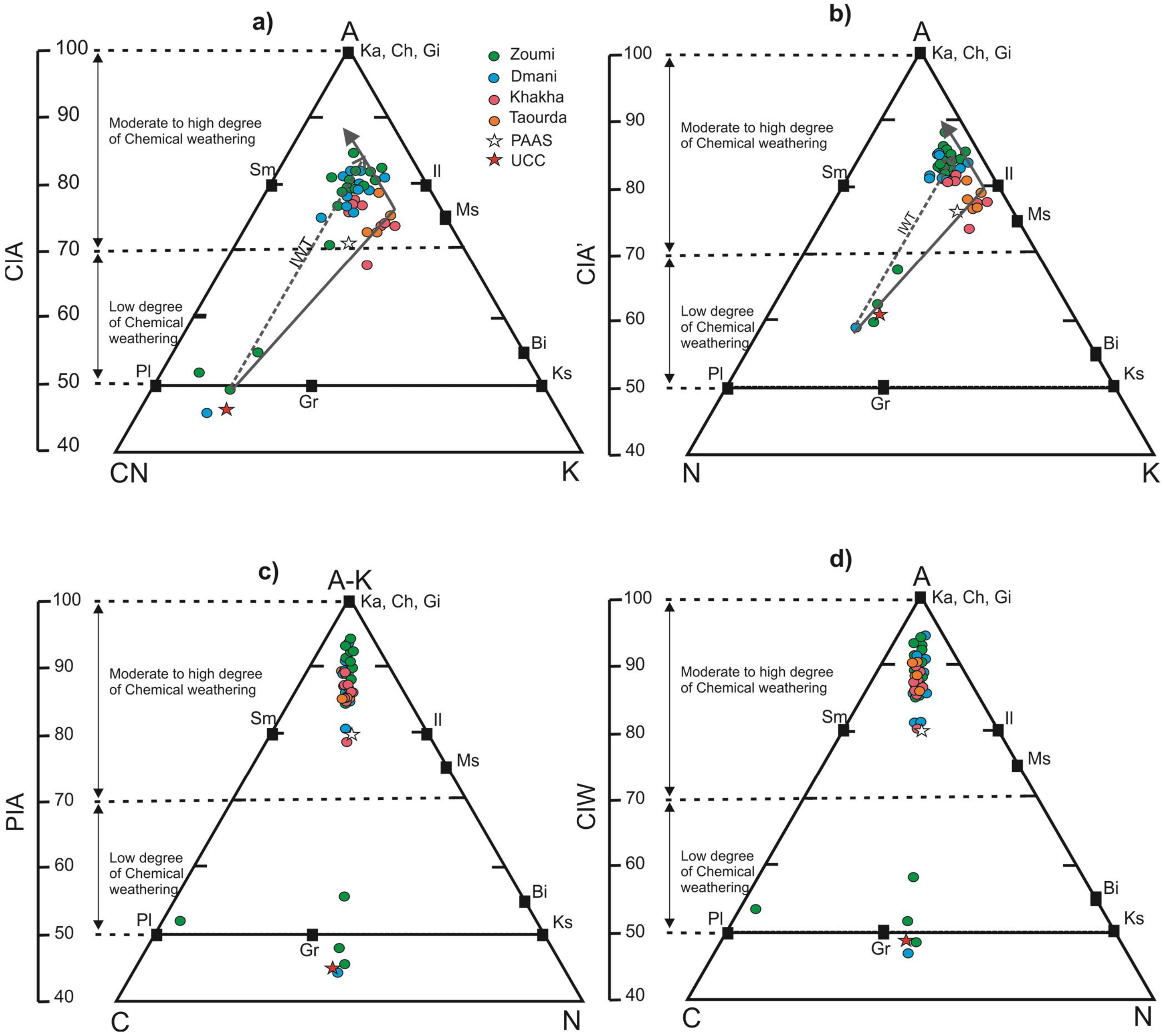


[Figure 36]: Ternary A-CN-K plot. Legend: Gr, granite; Ms, muscovite; Il, illite; Ka, kaolinite; Ch, chlorite; Gi, gibbsite; Sm, smectite. The samples are clustered close to the Ill-Muscovite point indicating a steady-state weathering conditions or fall along a trend sub-parallel to the A-CN join and shifting toward A apex indicating a non-steady-state weathering conditions. b) CIA' (A-N-K) plot. c) PIA ((A-k)-C-N) plot. d) CIW (A-C-N) plot. The samples suggest weak to moderate weathering and rarely strong weathering at the source. IWT: Ideal Weathering Trend. See text for more details.

In order to understand the relationship between the calculated indices of chemical weathering and the elemental ratios of the elements with contrasting mobility in the supra-crustal environment (e.g. Schneider et al. 1997; Roy et al. 2008; Perri 2014), scatter plots of CIA *vs*. Al/Na, Al/K, Ti/Na, K/Na and Rb/K were generated (Fig. 37). These ratios are used as proxies for chemical weathering intensities. CIA values of all the samples are linearly related to their Al/Na, Al/K and Ti/Na. However, CIA lacks linear interrelation with the ratios of K/Na and Rb/K. These elemental ratios can be used to broadly assess source area weathering intensity.

The Al/K ratios are low and constant (average=5.01±0.91) for all analyzed mudrocks. Schneider et al. (1997) interpreted the Al/K ratio as a result of weathering intensity fluctuations, while high Al/K ratios reflect Kaolinite dominance versus feldspar (or other K-bearing minerals) as an important product of intensive weathering. Furthermore, Rb/K ratio can be used to monitor palaeoweathering. During initial fresh rocks weathering both K and Rb are incorporated into clay minerals by adsorption and cations exchanges (Nesbitt et al. 1980), and with increasing weathering, K is preferentially leached compared to Rb (Wronkiewicz and Condie 1989; Peltola et al. 2008; Perri 2014). The $Fe_2O_3/K_2O$ ratio is higher in Zoumi and Dmani mudrocks (average=1.77 and 1.84 respectively) as regard to Khakha and Taourda mudrocks (average=1.37). Source area weathering can also be evaluated by clayeyness (Al/Si ratio), which increases leading to clay production during pedogenesis (Mitchell and Sheldon 2009 and references therein). The analyzed Zoumi mudrocks show an average Al/Si ratio (0.34 ± 0.02) close to the PAAS and UCC averages (0.34 and 0.26 respectively; Taylor and McLennan 1985; McLennan et al. 2006).

The High MIA values recorded within all Zoumi mudrocks reflect a substantial loss of feldspar relative to quartz and due to intense chemical weathering in warm and wet/humid palaeoclimate conditions (Roy el al. 2013).

The higher CIA mudrocks values may be related to episodic influx of intensively weathered detritus from hinterland uplands. This pattern is typical of a source area where active tectonics triggering a strong erosion of rejuvenated high relief with deep weathering profiles within source area (Nesbitt et al. 1997). Further, both Dmani and Zoumi mudrocks display a notable K-depletion through a linear trend toward the A-apex and parallel to the A-K join. As a whole, this weathering trend intersects the feldspar joins at a point that shows high proportion of plagioclase *versus* K-feldspar of the fresh rock. This proportion yields a good proxy to constraint the parent rock type. The high PIA values indicate that almost all plagioclases have been converted to clay minerals (Table 2).

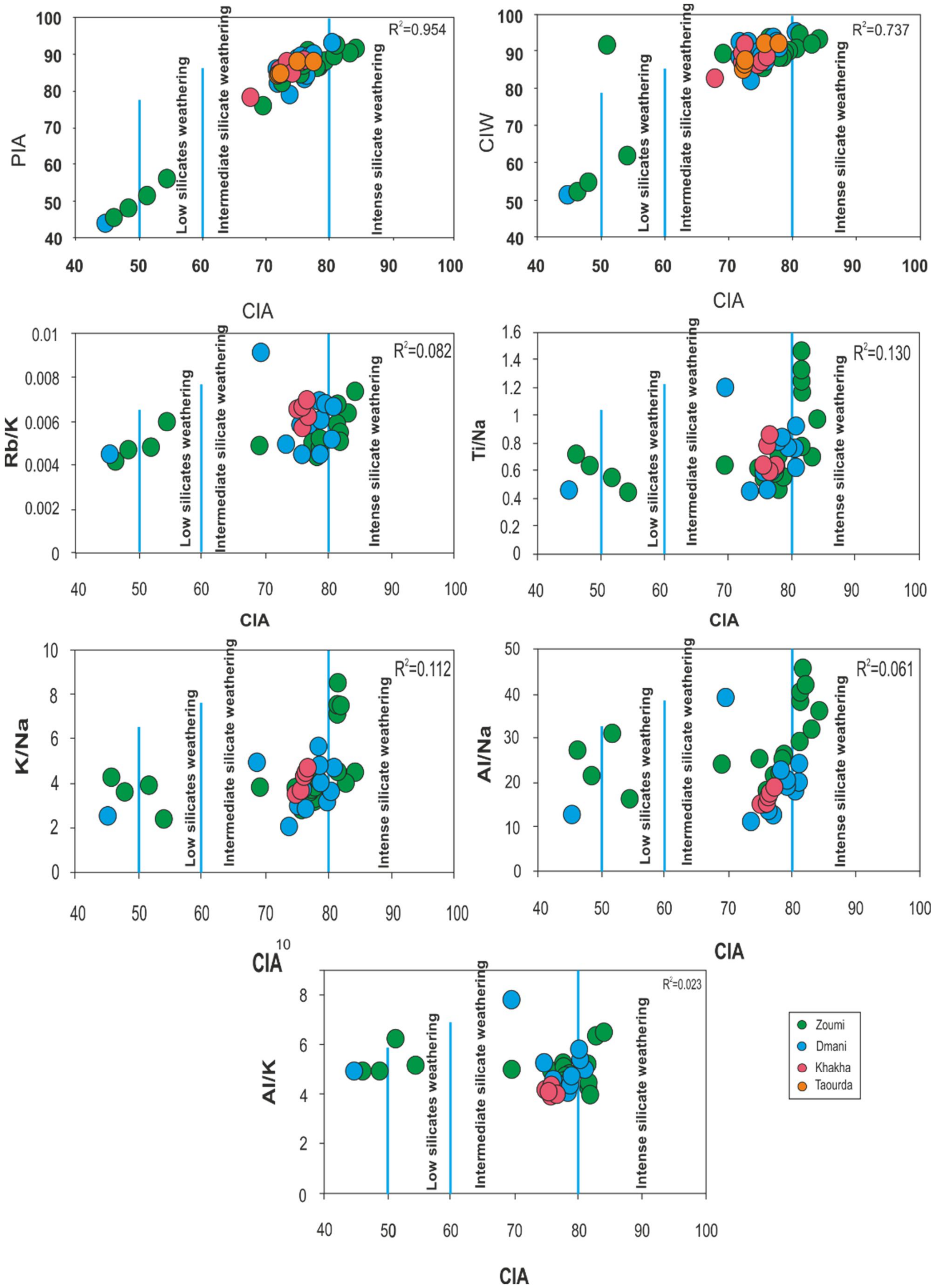


**Figure 37**: Scatter plots of Chemical Index of Alteration (CIA) vs PIA, CIW, Al/Na, Rb/K, K/Na, Al/K and Ti/Na in the Zoumi mudrocks sediments.

Indeed, both CIA, CIA', PIA and CIW indices indicate that Zoumi and Dmani mudrocks were derived from a source area where erosion overcomes chemical weathering, in contrast to Khakha and Taourda mudrocks which were originated from a weathered source area probably under steady-state conditions. Furthermore, the relationship between CIA index and $Fe_2O_3/K_2O$ ratio reflects a strong intense weathering control. Very low and homogeneous values of Rb/K ratios (<0.007), and the low Al/K and Al/Si ratios close to the PAAS and UCC averages for analyzed mudrocks, indicate weak to moderate weathering in a wet-humid climate with restrained shift in weathering intensity.

### IV.3.2. Sediment sorting and recycling:

Generally, terrigenous sediments undergo mechanical sorting during routing, transport, and deposition. These sedimentary processes may affect their chemical compositions and thus, the weathering source area distribution and related provenance proxies (Mongelli et al. 2006; Perri et al. 2011, 2012, 2014). The $Al_2O_3$-$TiO_2$-Zr ternary plot applied to analyzed mudrocks of Zoumi Flysch show immature sediments with a wide to a more limited range of $TiO_2$/Zr variations. They are mainly plotted as a tight clustered area in the middle of the 15*$Al_2O_3$-Zr-300*$TiO_2$ diagram with very limited $TiO_2$/Zr variation range following a Zr enrichment trend (Fig 9). The maturity of clastic sediments is calculated by using the Index of Compositional Variability (ICV; Cox et al. 1995) [ICV=($CaO+K_2O+Na_2O+Fe_2O_3+MgO+MnO+TiO_2$)/$Al_2O_3$], and the $K_2O/Al_2O_3$ ratio (Armstrong-Altrin et al. 2015), where the weight percent of oxides are used rather than moles, $Fe_2O_3$ is the total iron and CaO includes all sources of calcium (Ca). Typical rock-forming minerals (i.e. feldspars, amphiboles, and pyroxenes) show ICV values >0.84, whereas alteration products such as Kaolinite, Illite, and muscovite show ICV values <0.84 (Cox et al. 1995). The ICV value (average=1.90±0.67) of all analyzed mudrocks of Zoumi Flysch deposits fall above of the PAAS (0.85) and point to the mudrocks chemical immaturity. According to McLennan et al. (1993), Th/Sc and Zr/Sc ratios can be used to evaluate the effect of multi-cycle sediments reworking. The Zoumi mudrocks Th/Sc ratio ranges between 0.49 and 0.72 with an average of 0.57, and Eu/Eu* ratio range between 0.60 and 0.94 with an average of 0.67 (Table 6). Further, the sorting-related fractionation can be evaluated by plotting the Zr/Sc ratio (as sediment recycling index) (Cox et al. 1995; Hassan et al. 1999) against the Th/Sc ratio (as an indicator of chemical differentiation) (McLennan et al. 1993) (Fig. 40). The latter also provides a sensitive index of mafic *versus* felsic composition (McLennan et al. 1990).

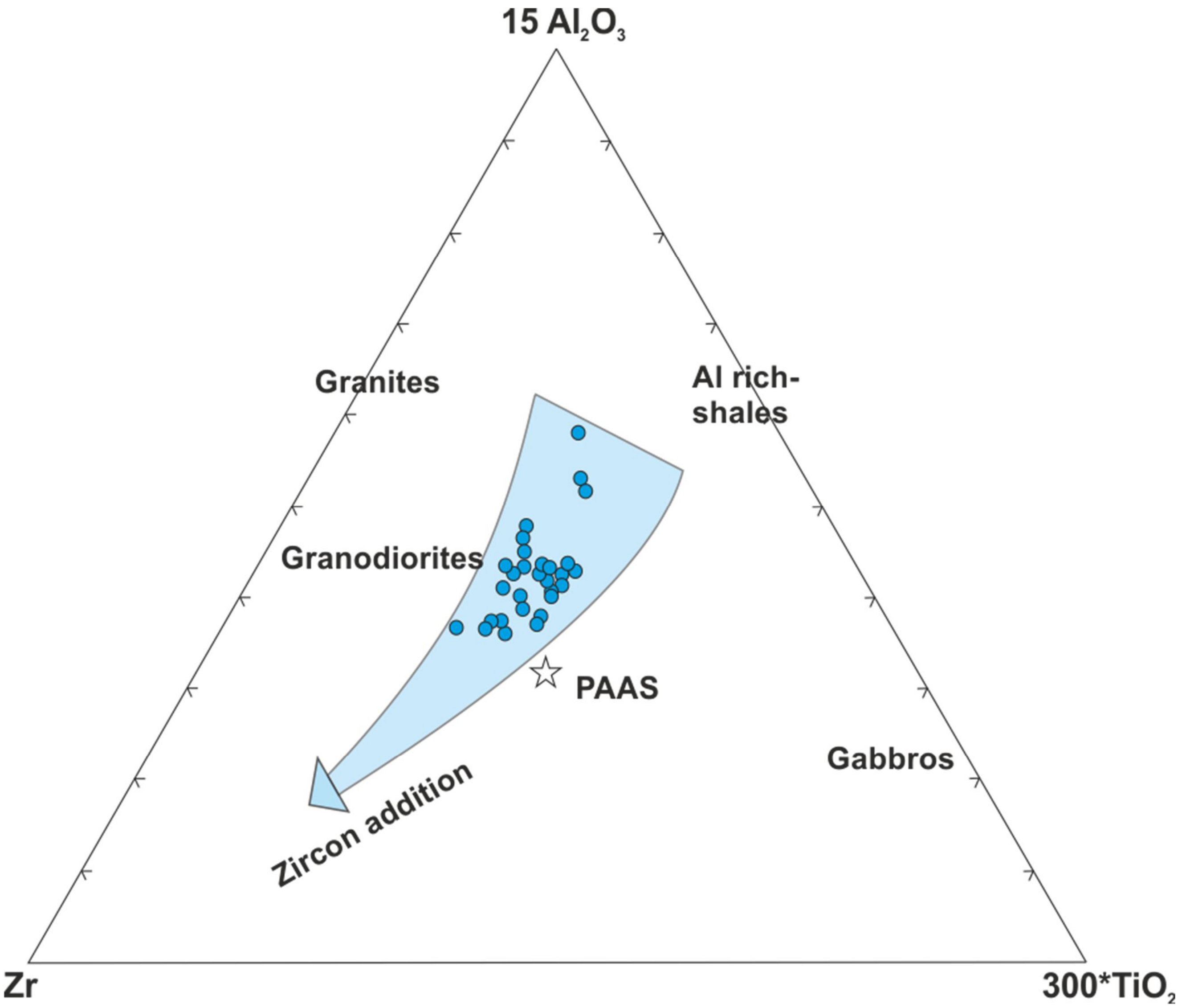


**Figure 38**: Ternary 15*Al2O3–300*TiO2–Zr plot suggesting poor sorting and rapid deposition of the sediments. (Diagram after Garcia et al. 1994; Caracciolo 2011).

Aluminum, Titanium, and Zirconium are considered the least mobile major and minor elements during chemical weathering (Perri et al. 2008). Ti and Zr are usually hosted by resistant minerals such as Zircon, Rutile, and Ilmenite. The $Al_2O_3$-$TiO_2$-Zr ternary plot (Garcia et al. 1994; Caracciolo et al. 2011) eliminates weathering effects and monitors the effect of sorting-related fractionation based on elements proportion (Fig. 38). Indeed, the 15*$Al_2O_3$-Zr-300*$TiO_2$ diagram indicates poor sorting and quick sedimentation for clastic Zoumi deposits. Their immaturity is a consequence of their modification amount by physical and chemical weathering. On the other hand, the $TiO_2$/Zr ratio suggests low Zr enrichment, poor sorting, fast sedimentation and irrelevant recycling processes (Fig. 38). All these facts suggest a causal relationship between building and uplift of the external Rif accretionary prism, subsequent relieves rejuvenation, high mechanical erosion rate and fast accumulation of sedimentary sequences in a basin close to tectonically active source area.

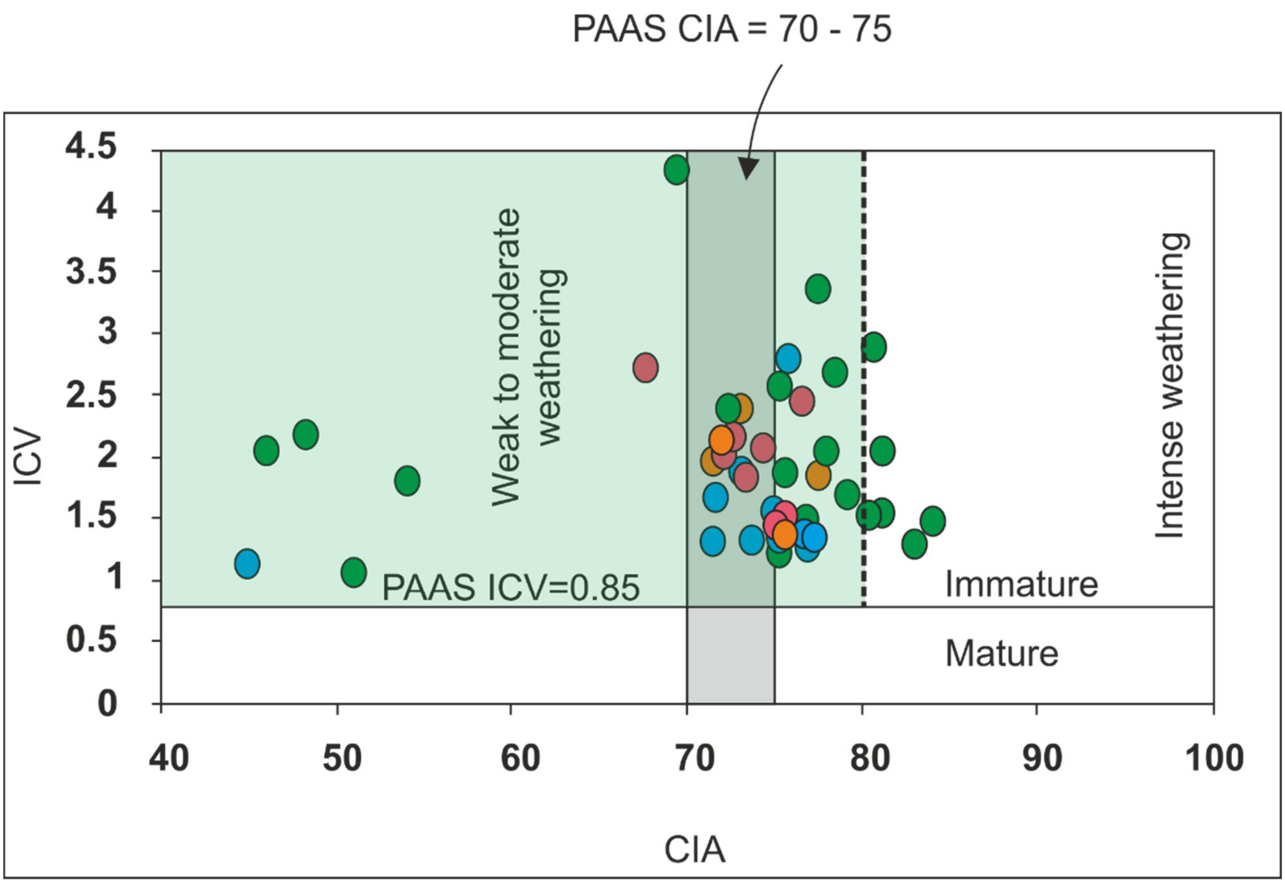


**Figure 39**: CIA versus ICV plot shows the intensity of weathering and maturity of the mudrocks sediments of the Mesorifain Zoumi basin (diagram modified after Long et al., 2012).

The ICV values decrease with increasing intensity of weathering and/or maturity of the clastic sediments. Compositionally immature mudrocks found in tectonically active settings are characteristically first-cycle deposits (Pettijohn et al. 1972; Van De Kamp and Leake 1985). The Zoumi mudrocks have ICV>1 (Table 5; Fig. 39), and are typical of compositionally first-cycle immature sedimentary rocks derived from tectonically active source area, where chemical weathering played a modest role as attested by low to medium CIA and CIA' values.

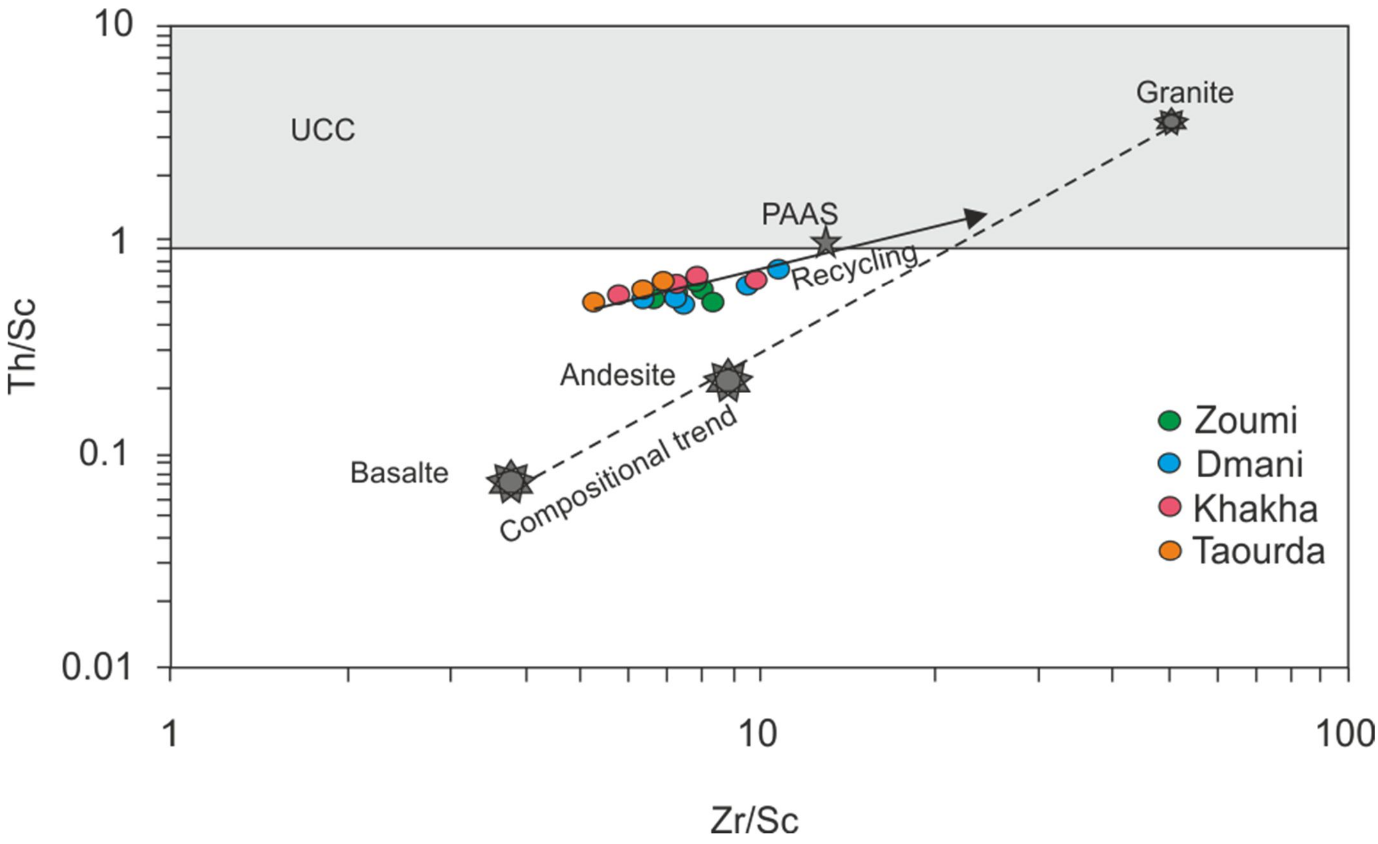


**Figure 40**: Ternary Th/Sc vs. Zr/Sc plot (Diagram after McLennan et al., 1993), samples depart from the comopositional trend indicating weak zircon addition suggestive of a poor recycling effect.

### IV.4. Climatic variations:

Systematic mineralogical and compositional variations observed in the Zoumi mudrocks and Their climatic changes are supported by Qt/(F+RF) *versus*. Qp/(F+RF) relationships (El Mourabet et al. 2017a; Fig. 41a) and defined by CIA and also A–CN–K plots (Fig. 36). The analyzed Zoumi mudrocks show high MIA values (average 97.31% ±1.88%).

The high MIA and moderate CIA ratios for Khakha and Taourda distal clayey successions, and low to moderate CIA ratios and rarely high CIA ratios for sandy-clayey proximal Zoumi and Dmani ones. The combined petrographic and aforementioned geochemical data show that they both clearly indicate mainly low to moderate chemical weathering in the source area occurring under warm and humid/wet palaeoclimate conditions. This fact is corroborated by the Qt/(F+RF) and Qp/(F+RF) high ratios in Zoumi sandstone suites, confirming the semi-humid to humid palaeoclimate conditions in the source area (El Mourabet et al. 2017a) (Fig. 41a).

Ratios of elemental compositions in soil provide useful tools for estimating rainfall and infer palaeotemperature (Marbut 1935). Thus palaeoprecipitation rate and rainfall within the source area can be successfully determined from different climofunctions using alkali and alkaline earth elements (Ca, Mg, Na, K and Al), (Sheldon et al. 2002):

Mean annual precipitation 1 (MAP 1) = 14.265(CIA - K) – 37.632 (Maynard 1992)

Mean annual precipitation 2 (MAP 2) = 259:34 ln(B) + 759.05 (Maynard 1992)

where B = molar ratio of bases ($CaO$, $MgO$, $Na_2O$, $K_2O$) to $Al_2O_3$

Mean annual precipitation 3 (MAP 3) = 130.93 ln(C) + 467.4 (Retallack 2001)

where C = molar ratio of $CaO$ to $Al_2O_3$

For all the studied samples, MAP1 gives palaeoprecipitations values higher than MAP2 and MAP3 resulting probably from substantial amounts of carbonates diagenetic processes. Though, only MAP2 and MAP3 palaeoprecipitations values have been retained. Source area palaeoprecipitation rate and rainfall yield values of mean annual precipitations of 543-400 mm/year (Table 7). The range of calculated precipitation satisfies the prerequisite rate of 200-1600 mm/year for safe application of the palaeoclimate and rainfall climofunctions (Sheldon et al. 2002).

Mean annual temperature can be estimated from the formula:

Mean annual temperature = -18:51(S) + 17.2989 (Sheldon et al. 2002)

Where S is the molecular ratio of $Na_2O$ and $K_2O$ to $Al_2O_3$

The above temperature climofunction for the studied samples yields palaeotemperature average around 14°C (Table 7).

Geochemical climatic proxies based on Ga/Rb–$K_2O/Al_2O_3$ ratios are useful to emulate climatic records (Roy et al. 2013). Ratios between theseelements (Ga/Rb and $K_2O/Al_2O_3$) may be used also as weathering indicesin chemostratigraphy (Roy et al. 2013). For Zoumi mudrocks, all Ga/Rb ratios are high (0.19-0.31) and $K_2O/Al_2O_3$ ratios are low (0.10-0.15). Mudrock samples are clustered between cold/dry and warm/wet climatic conditions (Fig. 41b), suggesting abundance of Illite (average 11.72±2.58), and hence weak to moderate weatheringassociated with fairly humid and wet climatic conditions (Fig. 41b); and substantial amount of Kaolinite (average 2.55±0.94) produced during intense chemical weathering under warm/wet and humid climatic conditions. However, an exception rises for two samples from the base of Khakha and the top of Taourda sections showing predominant proportions of Illite minerals for the former locality, and hence limited weathering under cool/dry climatic conditions and predominance of Kaolinite for the latter one, produced during intense chemical weathering under warm/wet and humid climatic conditions. Aluminum and Ga are mainly associated with the fine-grained aluminosilicate fraction, and are enriched in Kaolinite associated with warm and humid climate (Hieronymus et al. 2001; Beckmann et al. 2005; Ratcliffe et al. 2010), while Potassium andRb are associated with Illite, reflecting weak chemical weathering under dry and cold climatic conditions (Ratcliffe et al. 2004, 2010). Indeed, the analyzed mudrocks exceptionally rich in Illite have low Ga/Rb and high$K_2O/Al_2O_3$ ratios, whereas those rich in Kaolinite have high Ga/Rband low $K_2O/Al_2O_3$ ratios.

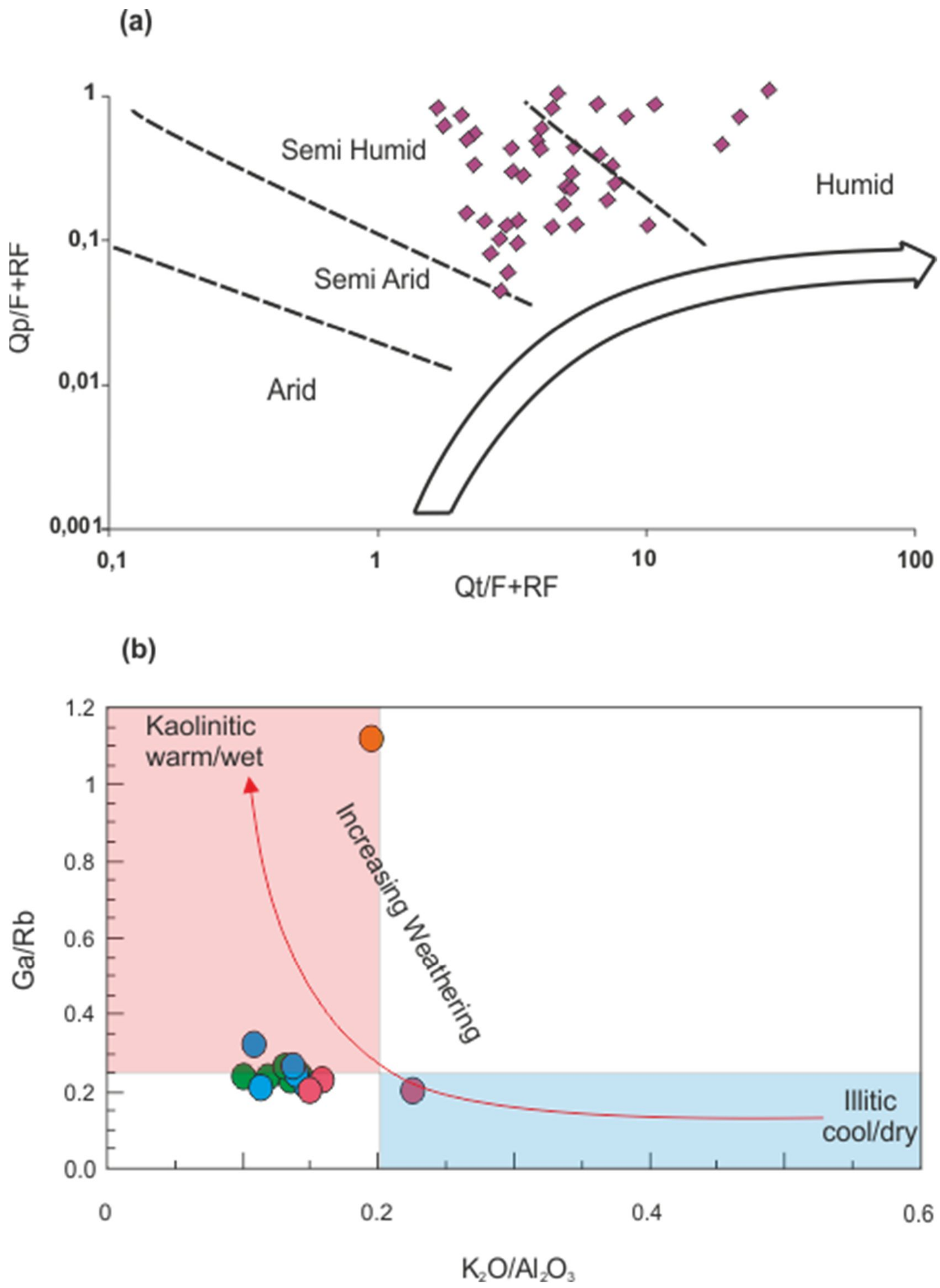


**Figure 41**: a: Bivariat log/log Qt/(F+RF) against Qp/(F+RF) plot and the infered semi humid-humid paleoclimate conditions from the composition of the Zoumi sandstone (bivariate plot after Suttner and Dutta 1986). Qp (polycristallin Quartz), Qt (total Quartz), F (Feldspars), RF (rocks fragments); b: Ga/Rb–K2O/Al2O3 plot for the Zoumi mudrocks emphasizing humid/wet climat (Binary diagram After Roy et al. 2013).

# CHAPTER V

# LOWER-MIDDLE MIOCENE TURBIDITES PROVENANCE AND ZOUMI BASIN GEODYNAMIC SETTING

# CHAPTER V

# LOWER-MIDDLE MIOCENE TURBIDITES PROVENANCE AND ZOUMI BASIN GEODYNAMIC SETTING

## V.1. Introduction to Provenance:

The provenance of a sediment includes all aspects of the source area, including source rocks, climate, and relief (Pettijohn et al. 1972). In areas of intense tectonic/magmatic activity, source-rock type determines sediment composition more than do climate and relief (Dickinson, 1970). Where tectonism/magmatism is absent, climate and relief are more important in determining composition (Basu, 1975). The investigation of the petrographic signatures of sandstones deposits can single out the several factors that control terrigenous materials generation, including weathering and recycling, and monitor the compositional changes caused by chemical and physical processes during fluvial transport from sources to sinks (Garzanti et al., 2005, 2006, 2012, 2013, 2014).An additional complicating factor is that recycling of sediment may have a profound effect on compositions but commonly may be difficult to recognize or quantify (Blatt, 1967). It follows that a good knowledge of the regional geology and stratigraphy thus becomes an essential facet of reconstructions of ancient source/basin systems (Zuffa, 1987).

The major provenance types related to continental sources are stable cratons, basement uplifts, magmatic arcs, and recycled orogens. Each provenance type contributes distinctivedetritus preferentially to associated sedimentary basins that occupy a limited number of characteristic tectonic settings in each case.

Evolutionary trends in sandstone composition within individual basins or sedimentary provinces commonly reflect changes in tectonic setting through time, or erosional modification of provenance terranes (Dickinson 1985). Foreland sandstone suites commonly evolve from rift-related quartzofeldspathicpetrofacies, through quartzosepetrofacies of passive continental margins, to quartzolithicpetrofacies derived from recycled orogens. Sands of composite provenance can be described as mixtures of quartzose sand from stable cratons, quartzofeldspathic sand from basement uplifts or arc plutons, feldspatholithic. Proportions of contributions from different provenance types can be estimated from mean compositions for ideal derivative sands represented by points or restricted areas on triangular plots.

Reliable identification of P and K, and their distinction from quartz, requires routine staining for both feldspars. Systematic replacement of K-feldspar by diagenetic albite may upset attempts to recover the detrital ratio of K-feldspar to plagioclase in some instances (Dickinson et al, 1982; Walker et al., 1984). However, albitization of plagioclase is a much more common process at moderate stages of diagenesis (Boles, 1982; Ramseyer et al., 1992).

Sedimentary and metasedimentary lithic fragments (Ls) include chiefly microclastic siltstone, massive cryptocrystalline argillaceous grains, phyllosilicate-rich shaly or slaty grains showing mass extinction effects, and foliated or microgranular aggregates of quartz and mica from phyllite and/ or hornfels. Firm distinctions between these various subtypes are commonlycomplicated by the presence of texturally and compositionally transitional grains. Gradations from chert (Qp) to argillite (Ls) are also common, and are best resolved by relegating siliceous argillite to Ls. The various Ls subtypes are more quart-zrich and/or phyllosilicate-rich than the various Lv subtypes.

Quantitative information provided by provenance studies of terrigenous deposits can helps to better understand the relationships between sediment composition and plate-tectonic setting (Garzanti et al., 2005, 2006, 2012, 2013, 2014). In determining detrital modes, the effects of diagenesis and outcrop weathering on the framework should be assessed. Every effort should be made to obtain fresh, unweathered samples. Where secondary porosity of any origin has developed allowances for its effect on framework composition must be made in all interpretations of point-count data.

### V.1.1. Provenance types:

Compositional fields characteristic of different provenances is well constrained on four triangular diagrams (Dickinson and Suczek, 1979; Dickinson et al, 1979, 1983a): QtFL, with emphasis on maturity; QmFLt, with emphasis on source rock; QpLvLs, with emphasis on lithic fragments; and QmPK, with emphasis on mineral grains (Fig. 42).

Nominal fields proposed within QtFL/QmFLt diagrams for discrimination of sands derived from various types of provenances in continental blocks, magmatic arcs, and recycled orogens. The latter, include the deformed and uplifted supracrustal strata, dominantly sedimentary but also volcanic in part, exposed in varied fold-thrust belts of orogenic regions.

### V.1.1.1. Stable Cratons provenance:

The main sources for craton-derived quartzose sands are low-lying granitic and gneissic exposures, supplemented by recycling of associated flat-lying platform sediments. The sands either accumulate as platform successions deposited within continental interiors, or are transported chiefly to passive continental margins and the cratonflanks of foreland basins.

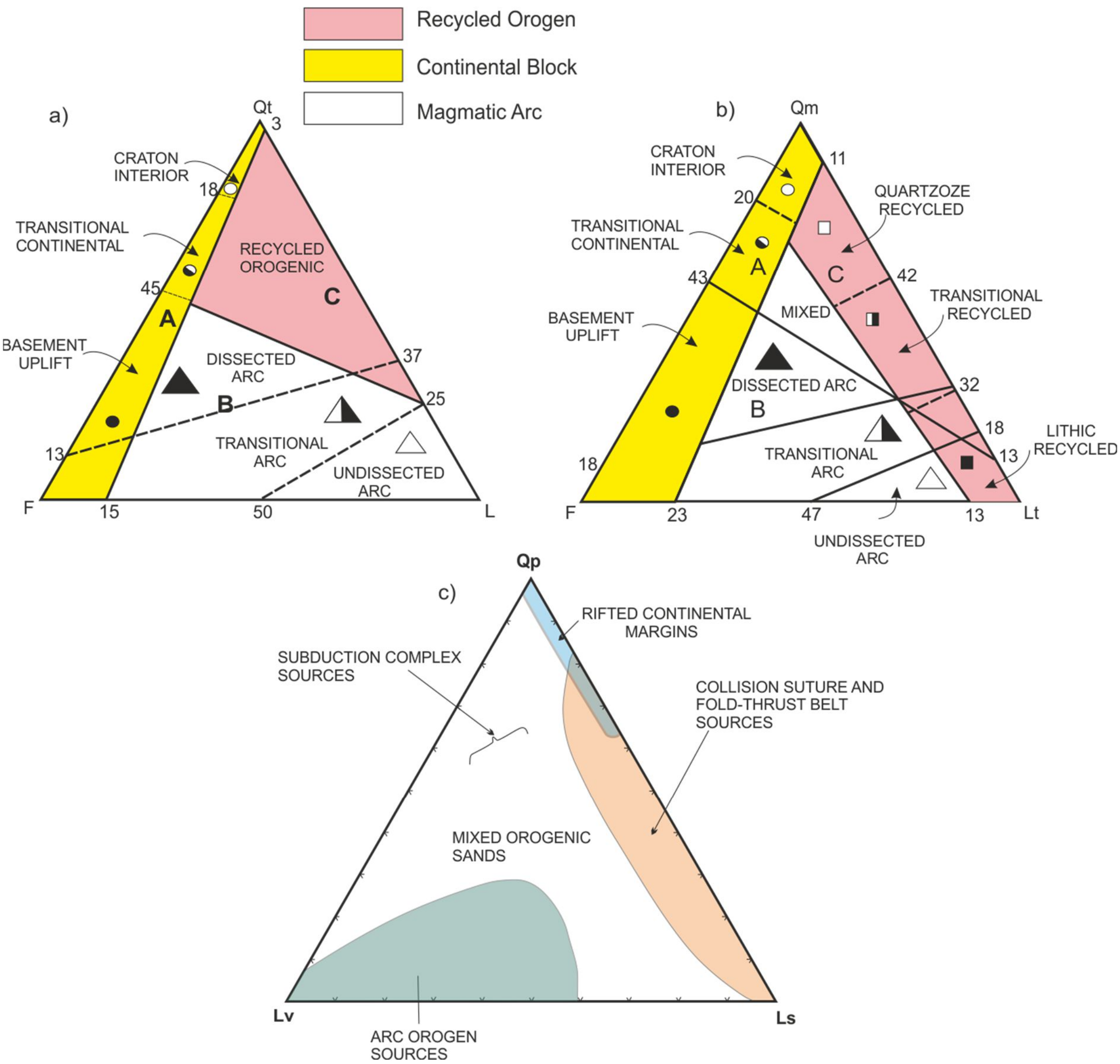


**Figure 42**: QtFL (a); QmFLt (b) and QpLvLs (c) plots for framework modes of terrigenous sandstones showing provisional subdivisions according to inferred provenance types (modified after Dickinson and Suczek (1979) and Dickinson (1983). Geometric symbols (filled, open and half-filled triangles, circles and squares) in various compositional fields indicate inferred provenance type on QFL/QmFLt plots. Numbered ticks on legs of triangle denotes positions of empirical provenance divisions lines in percentage units measured from nearest apical pole.

Ultimate sources for quartz grain populations can be inferred to some degree from the frequency and nature of undulose extinction and polycrystallinity (Basu et al, 1975). However, both properties can be affected markedly by grain deformation during diagenesis (Graham et al, 1976). Textural details of polycrystalline quartzose grains offer more reliable guides to specific source rock types in favorable instances (Young, 1976).

Many have speculated that multi-cyclic reworking on cratons might be required to develop mature quartzose sands. However, recent work has shown conclusively that quartzose sand is being produced as first-cycle sediment from deeply weathered granitic and gneissic bedrock exposed in tropical lowlands of the modern Amazon basin (Franzinelli and Potter, 1983).

The importance of intense weathering for concentrating quartz in relation to feldspar and/or lithic fragments deserves special emphasis. In most cases, fluvial transport alone is apparently ineffective as an influence on the proportion of quartz in sand. More than 600 km of transport on the Platte River in the Great Plains proves insufficient to change either the Q/F or K/P ratio of the stream sands to any significant degree (Breyer and Bart, 1978).

#### V.1.1.2. Basement uplift provenance:

Fault-bounded basement uplifts along incipient rift belts and transform ruptures within continental blocks shed arkosic sands mainly into adjacent linear troughs or local pull-apart basins. Similar detritus can be derived from basement uplifts within broken foreland provinces, and from eroded plutons in deeply dissected magmatic arcs.

A spectrum of lithic-poor quartzofeldspathic sands forms a roughly linear array on QtFL and QmFLT diagrams (Fig. 42) linking these arkosic sands with the craton-derived quartzose sands that plot near the Qt and Qm poles. This spectrum of sands reflects derivation from various tectonic elements of continental blocks where basement rocks are exposed. Where erosion has been insufficient to remove cover rocks from basement, uplifts may shed sands having affinity with detritus derived from magmatic arcs or recycled orogens (Mack, 1984). Although granitic rock fragments may be abundant in coarser size grades, the proportion of true lithic fragments (see discussion above) is generally less than 10% and averages about 5%. Quartz forms about 40-45% of the quartzofeldspathic grain population, and Kspar averages 35-40% of the total feldspar present. These are values appropriate to areas of rugged relief in arid or semiarid climatic zones. The spectrum of sands derived from continental blocks can be viewed as forming a mixing array or evolutionary trend connecting this ideal arkosic composition to the craton quartzose sand composition (Fig. 42).

Humid weathering raises the proportion of quartz relative to feldspar. Plagioclase is less stable than k-feldspar in all climatic regimes, but the disparity is much more marked for humid areas. In stream sands from semiarid regions, the fraction of total feldspar that is plagioclase may be nearly as high as in the parent granitic rock; however, in stream sands from humid regions, the fractional value may fall to only a third of that for the parent rock (James et al, 1981). The tendency for the K-feldspar/plagioclase ratio to rise as the quartz content of typical sands increases is shown by the QmPK diagram.

### V.1.1.3. Magmatic arc provenance:

The most characteristic sands derived from active magmatic arcs constructed parallel to subduction zones are volcaniclastic materials erupted and eroded from stratovolcano chains and associated ignimbrite plateaus. Deep dissection of arc assemblages can expose their batholithic roots, and may give rise to quartzofeldspathic sands indistinguishable from the arkosic debris produced by other basement uplifts. Mixing of volcanic and plutonic contributions results in a spectrum of volcanoplutonic sands (Dickinson, 1982), which range from feldspatholithic to lithofeldspathic in composition, but display consistently high Lv/Lt ratios coupled with low to moderate quartz contents (Fig. 42).

Arc-derived debris is typically deposited in forearc or interarc basins, but may also reach foreland basins locally. Sandstones incorporated into subduction complexes are commonly arc-derived variants of the volcanoplutonic suite deposited in trenches or on trench slopes (Dickinson, 1982).

The mean composition of the volcaniclastic end member of the array of volcanoplutonic sand types can be estimated from data for appropriate first-cycle sand suites from the circum-pacific region. Volcanic rock fragments in the more common andesitic (to basaltic and/or dacitic) sands are dominantly microlitic varieties, whereas those in the rhyodacitic sands have felsitic or pyroclastic textures.

### V.1.1.4. Recycled Orogen provenance:

Orogenic recycling occurs in several tectonic settings where stratified rocks are deformed, uplifted, and eroded:

- subduction complexes, where oceanic and trench slope deposits are exposed as thrust panels, recumbent isoclines, and mélange belts along tectonic ridges between trenches and forearc basins;

- backarc, thrust-belts, where folded sedimentary and metasedimentary strata of continental derivation override the flanks of retroarc, foreland basins; and

- suture belts, where structurally juxtaposed sequences of both oceanic and continental types can provide sources of sediment for transverse dispersal systems that feed adjacent peripheral foreland basins, and for longitudinal dispersal systems that feed nearby remnant ocean basins. Orogenic highlands also give birth to major river systems that can transport recycled orogenic sediment across the surfaces of adjacent continental blocks and into distant basins having a variety of tectonic settings (Potter, 1978).

By its nature, sediment from recycled orogens includes various proportions of materials whose compositions reflect ultimate derivation from cratonic, arkosic, or volcaniclastic sources, modified in part by metamorphic processes. In addition are materials generated by sedimentary processes, acting alone or in combination with diagenesis and metamorphism. These latter are lithic fragments of chert and meta-chert, or pelitic debris such as shale, argillite, slate, and phyllite. As yet there is also no consensus on the way in which detrital limeclasts (Lc) should be treated during recalculation of detrital modes (Mack, 1984).

Sands derived from fold-thrust systems of indurated sedimentary and low-grade metamorphic rocks have consistently low contents of feldspar and volcanic rock fragments (Dickinson and Suczek, 1979). Consequently, they form a quartzolithic array of compositions that plot near the Qt-L, Qm-Lt, and Qp-Ls legs of standard triangular diagrams (Fig. 42). Van Andel (1958) early called attention to the abundance of this type of sand in the orogenic region of western Venezuela. In the modern Andean foreland (Franzinelli and Potter, 1983), the least mature sands derived directly from the adjacent highlands contain roughly equal amounts of quartz grains and rock fragments (with only 5-10% feldspar grains). Relative proportions of resistant quartzose grains and unstable lithic grains are highly variable in recycled orogenic sands.

Clastic sequences in foreland basins commonly display interstratified petrofacies with contrasting Qt/L and/or Qm/Lt ratios (e.g., Putnam, 1983). In some cases, the salient differences can be attributed to the mingling (*mélange*) of contributions from disparate sources. For example, Carboniferous foreland clastics of the Trenchard Group in England are composed of a northern quartzarenitefacies ($Qt_{87}$, $F_8$, $L_5$), derived from the gentle cratonal flank of the basin, and a southern litharenite facies ($Qt_{46}$, $F_5$, $L_{49}$) derived from the orogenic flank (Jones, 1972). In some sequences, recycled sands derived from uplifted quartzose strata cannot be distinguished compositionally from craton-derived sands, especially where humid weathering and intense reworking enhance the quartz content of the sands (Mack et al, 1981; Mack, 1984). Chert-rich sand frameworks are characteristic in some recycled orogenic suites (Dickinson and Suczek, 1979). The supracrustal chert sources are typically either radiolarites within deformed oceanic assemblages, or replacement nodules in platform carbonate successions. The Qm/Qp ratios in derivative sands are largely a function of the extent to which turbidite or platform sandstones are intercalated within the chert-bearing sections (Dickinson and Suczek, 1979).

### V.1.1.5. Composite Provenances:

Triangular compositional diagrams provide a convenient means to plot graphically in a quantitative format. Any point within the plot can obviously be interpreted as a certain mixture of the three entities represented by the poles of the diagram. More generally, any point within the interior of the diagram can be interpreted in terms of mixing of any three compositional end members distributed near the perimeter of the diagram. Of course, any one of such controlling end members may itself be a mixture of two or three other compositions (Dickinson, 1982).

If the compositions of end members that are truly diagnostic of provenance type can be accurately defined, the actual parentage of specific sandstone suites can thus be inferred. In the case of the sands derived from collision belts, for example, the variation in quartz content may be attributed either to different proportions of recycled quartzose sand derived from the orogenic belts in question, or to contrasting climatic influences within those same orogenic belts, rather than literally to an admixture of first-cycle cratonic detritus (Dickinson, 1982).

## V.2. Petrofacies evolution:

Spatial patterns of correlative petrofacies within a sedimentary basin reflect simultaneous contributions of detritus from different sources. Successive time-dependent petrofacies reflect either the evolution of individual provenance terranes or changes in disperal patterns through time. Significant contrasts in petrofacies imply major differences in diagenetic processes within basin fill. Stratigraphic variations in petrofacies within forearc and foreland regions suggest that an integrated view of basin evolution requires attention to petrofacies evolution, both as a record of tectonic events and as a means of understanding diagenetic conditions (Dickinson, 1982).

Volcaniclastic sandstone suites commonly become more quartzose upsection, because the normal evolution of many magmatic arcs leads to the eruption of more felsic materials as time passes (Korsch, 1984). Moreover, there is commonly a tendency for uplift and erosion to expose more and more of the plutonic roots of an arc as time passes. Consequently, Forearc sandstones of the volcaniplutonic suite generally become more arkosic and less lithic with time (Dickinson and Rieb, 1972).

Recycled orogenic sources in exposed subduction complexes may influence petrofacies locally (Tennyson and Cole, 1978), and major changes in drainage patterns within arcs may cause abrupt shifts in petrofacies within adjacent forearc basins (Heller and Ryberg, 1983).

Petrofacies become on average more quartzofeldspathic and less lithic upward, although some feldspatholithic sandstones occur throughout the section. In many parts of the sequence, lithofeldspathic and feldspatholithic petrofacies variants are intercalated within the same general horizons. The K-feldspar/plagioclase ratio increases systematically upward, as does mica content somewhat more irregularly. Both trends probably reflect increasing contributions from plutonic source rocks. The Lv/Ls ratio varies geographically as well as stratigraphically and appears to reflect variations in the nature and amount of bed rocks exposed adjacent to batholithic sources as well as the extent of local volcanic cover in the arc.

Foreland basins adjacent to collision orogens experience drastic changes in provenance during their sedimentary history. Prior to collisional tectonics, sediment sources are dominantly within the adjacent continental block. Commonly, arkosic petrofacies of a rift phase lie at the base of the foreland succession and are overlain by quartzose petrofacies of platform successions or passive margin sequences. These pre-orogenic strata are then succeeded by quartzolithic petrofacies derived from recycled orogenic sources developed during collision orogenesis. Arc-derived petrofacies may form a part of the orogenic succession. Foreland petrofacies have been well constrained in the Apennines, where multiple sources of detritus are inferred for both pre-orogenic and synorogenic phases (i.e., Zuffa et al., 1980; Gandolfi et al., 1983).

An important characteristic of many foreland sandstone suites, including those of the Apennines, is the comparative abundance of detrital limeclasts (Lc) of extrabasinal origin. In the synorogenic flysch of the Alps, for example, individual sandstone units vary widely in petrofacies, but essentially all contain some proportion of limeclasts reworked from deformed and uplifted sedimentary strata exposed as a recycled orogenic provenance within the developing collision orogen (Hubert, 1967).

## V.3. Provenance and geodynamic setting of the Zoumi basin:

To evaluate results of the above presented geochemical provenance analysis we have compared major geochemical provenance statements with common provenance analysis using sediment petrography. The application of the point count data generated for Zoumi sandstone suites to the QFL and QmFLt diagrams of Dickinson (Dickinson and Suczek 1979; Dickinson 1985) and revised later by Weltje (2006) yields source rocks derived from a recycled orogen terrains (Fig 43a) with minor influence of a craton interior ones (Fig 43b) for the lower part of the Zoumi sandstone suites. To better constrain the influence of various geotectonic settings, the ternary QpLvLs-diagram (Ingersoll and Suczek 1979) takes into account the lithics varieties and therefore their related source areas. When plotting Zoumi sandstone suites on QpLvLs-diagram, multiple possible source areas can be deduced, which range from rifted continental margins to collision orogens (Fig 43c). Further, the most significant observation is the relative enrichment of quartz grains in the suite of Khakha-Taourda when compared to the south-eastern part of the Basin. (i.e. Zoumi-Dmani localities). The coexistent varying provenance signals can only be explained by mixed provenances, clearly reflecting a model of complex tectonic settings along with variable source areas, possibly varying in time as the external orogenic prism built and deformation progress outward.

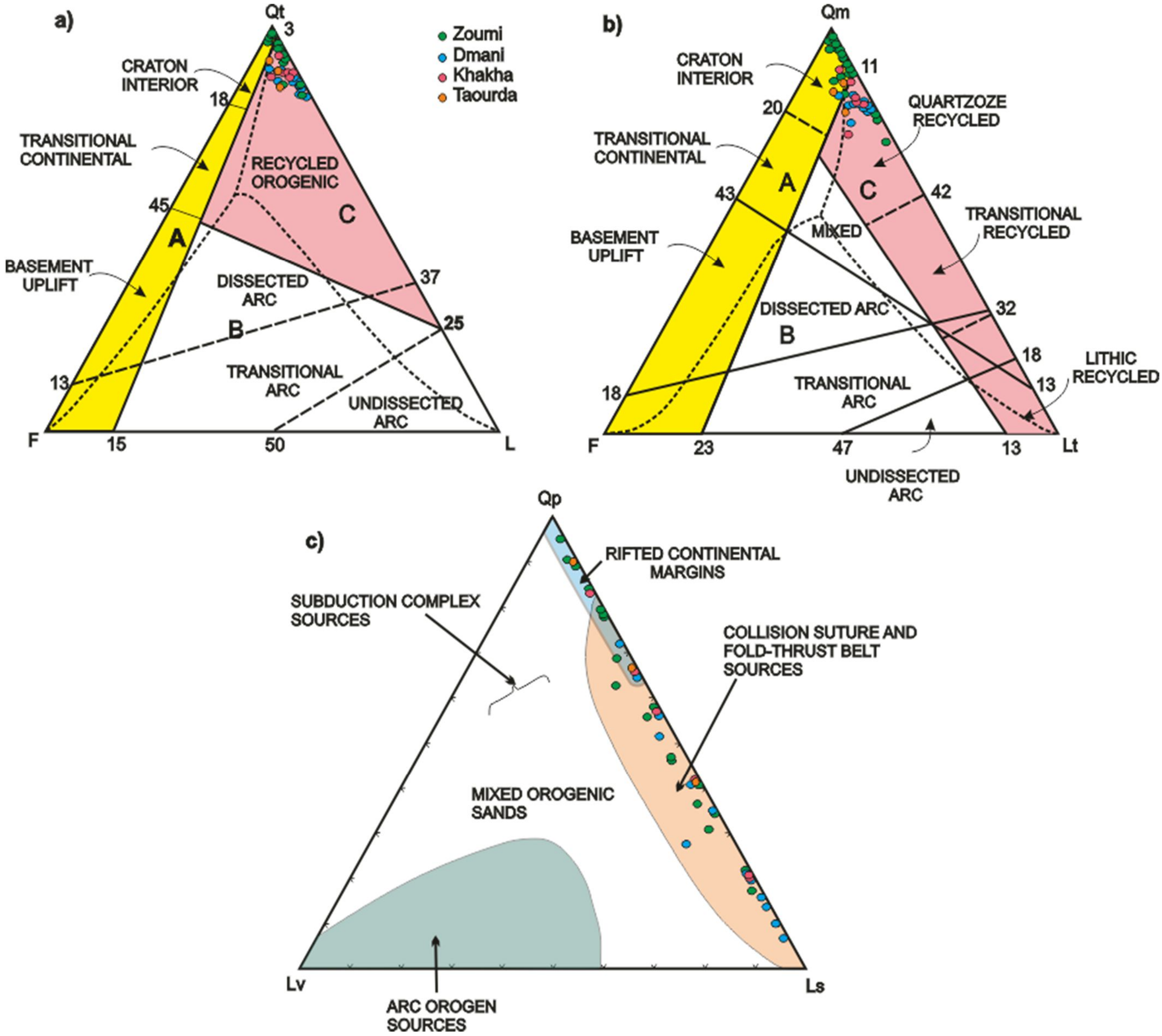


**Figure 43:** Provenance plots of the Zoumi sandstones (provenance fields of **a** and **b** after Dickinson et al. (1983). Dotted lines mark the revaluated provenance fields after Weltje (2006) with A = continental block provenance, B = magmatic arc provenance and C = recycled orogen provenance. Provenance fields of **c** after Dickinson and Suczek (1979) as modified by Dickinson (1982 et al. 1983) plotting the Zoumi sandstone data.

In order to find out metamorphic- and plutonic-provenance sources inferred from sandstones petrographic data, the observed optical and textural features of quartz grains; in particular, undulous extinctions of single grains and the foliated and sutured fabrics of polycrystalline grains are consistent with a derivation from metamorphic rocks. These data plotted in Basu (1975) diamond diagram clearly emphasize a provenance from low-grade metamorphic rocks (Fig. 44). Moreover, the apatite fission track ages 13.9 ± 1.8 and 20.0±2.4 Ma of Ketama-Temsamane metamorphic massifs (Azdimoussa et al. 1998) indicates that uplift and cooling/denudation of these massifs started since Early-Middle Miocene and may constitute *pro-parte* potential metamorphic sources for detrital sediments supplied to the Zoumi Basin.

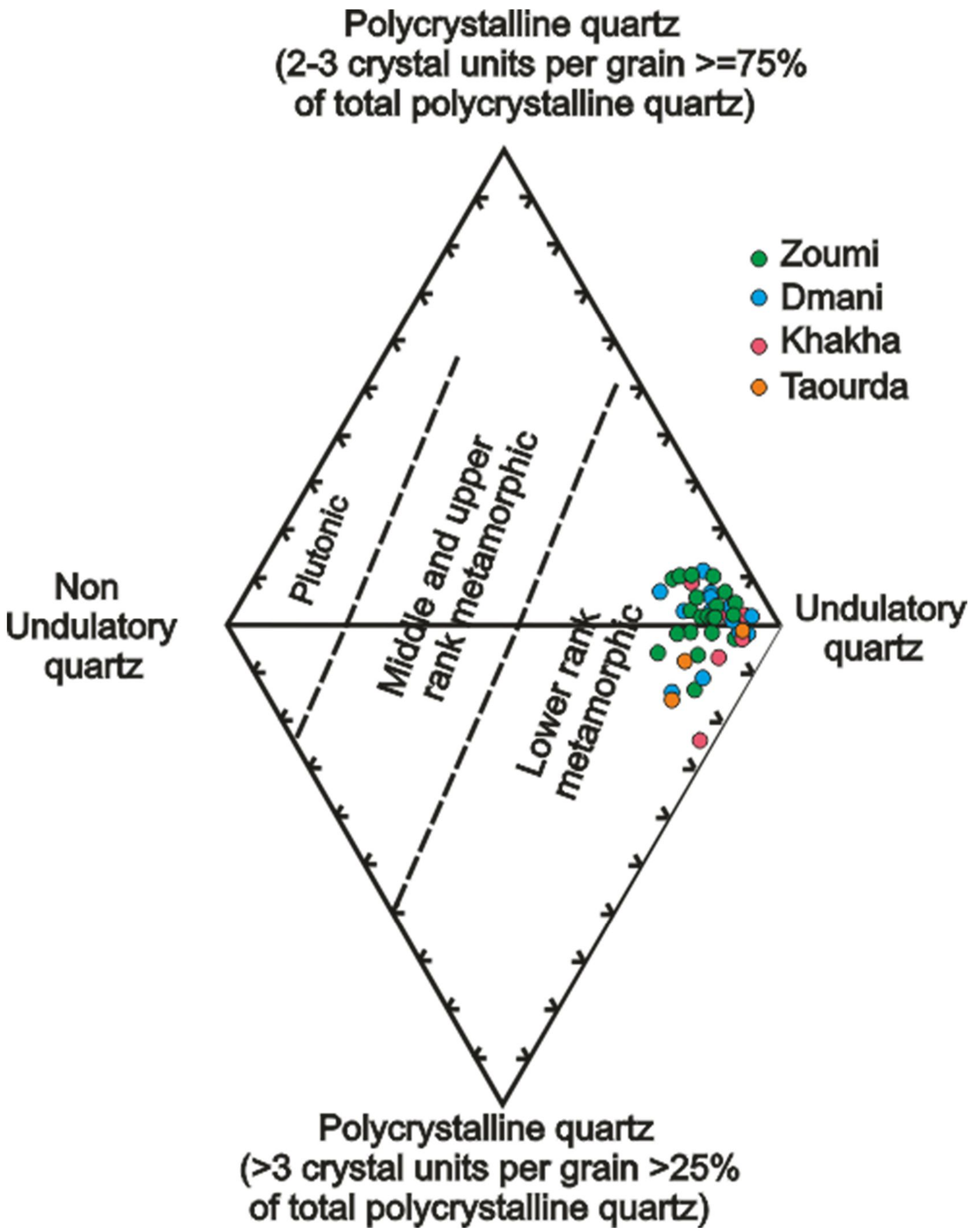


**Figure 44**: Four variable plot of nature of quartz population for Zoumi basin sandstone exclusively derived from lower rank metamorphic source rocks (Diamond diagram after Basu et al. 1975).

Trace elements and REE have been used to find out provenance (Taylor and McLennan 1985; Condie et al. 1992; Cullers 1995; Madhavaraju and Ramasamy 2002; Armstrong-Altrin et al. 2004). Rare earth elements (REE) and Th, among the HFSE (High Field Strength Elements), and some transition elements, including Sc and Cr, can provide an insight into the provenance and are thus useful to constrain the average source-area composition (e.g. Taylor and McLennan 1985; Floyd et al. 1989; McLennan et al. 1993; Fedo et al. 1996; Cullers and Berendsen 1998). Overall, the main chemical types of sources that contribute to the sediment can be grouped as felsic (upper-crustal rocks) and mafic/ultramafic (namely mantle rocks).

Ratios such as La/Sc, Th/Sc, Th/Co, and Th/Cr can be used to discriminate sediments with felsic sources from progressively more mafic sources (Wronkiewicz and Condie 1989; Cox et al. 1995; Cullers 1995). The Th/Sc, Th/Co, Th/Cr, Cr/Th, and La/Sc ratios of Zoumi mudrocks were compared with those of sediments derived from felsic and mafic rocks as well as to UCC and PAAS values (Table 8). All these ratios are within the range of felsic rocks suggesting mainly felsic nature of source rocks with minor mafic supply. Further, the variation among the LREEs (Light Rare Earth Elements; e.g. La and Ce) and the transition elements (e.g. Co, Cr and Ni) is considered a useful indicator for provenance studies (Cullers 2000; Perri et al. 2012). The range of elemental ratios La+Ce/Cr (on average between 0.72 and 1.06), and La+Ce/Ni (on average between 1.05 and 2.11) (Table 6) of studied samples suggests a provenance from felsic rather than fairly mafic source-areas. The REE patterns are closely PAAS-like, thus indicating upper-crustal affinity. Moreover, as the Eu anomaly is considered the more conservative provenance proxy (McLennan et al. 1993; Mongelli et al. 1998; Cullers 2000), the Zoumi mudrocks show average value of Eu/Eu* (average Eu/Eu* = 0.67 ± 0.07) close to those of UCC and PAAS (average $Eu/Eu^*_{PAAS}$ = 0.66), thereby confirming the prevailing provenance from felsic source areas. However, these ratio values do not exclude a supply from a mafic source. Generally, a low concentration of Cr and Ni indicates sediments derived from a felsic provenance (Wrafter and Graham 1989), whereas, higher content of these elements are mainly found in sediments derived from ultramafic rocks (Armstrong-Altrin et al. 2004). Furthermore, the Cr/V ratios indicate enrichment of Cr over other ferromagnesian trace elements, where Y/Ni tests the abundance of ferromagnesian trace elements (McLennan et al. 1993). Mafic-ultramafic sources tend to have high ferromagnesian abundances; such a provenance would result in a decrease in Y/Ni ratios and an increase in Cr/V ratios (Hiscott 1984; McLennan et al. 1993). For the Zoumi mudrocks, Y/Ni ratios are very low (range: 0.22-0.47; average: 0.31) and Cr/V ones are higher (range: 0.65-0.93; average 0.81). Further, Cr/V vs. Y/Ni provenance proxy (Hiscott 1984) indicates mafic–ultramafic detritus input for the studied samples beside main supply from felsic rocks (Fig. 45).

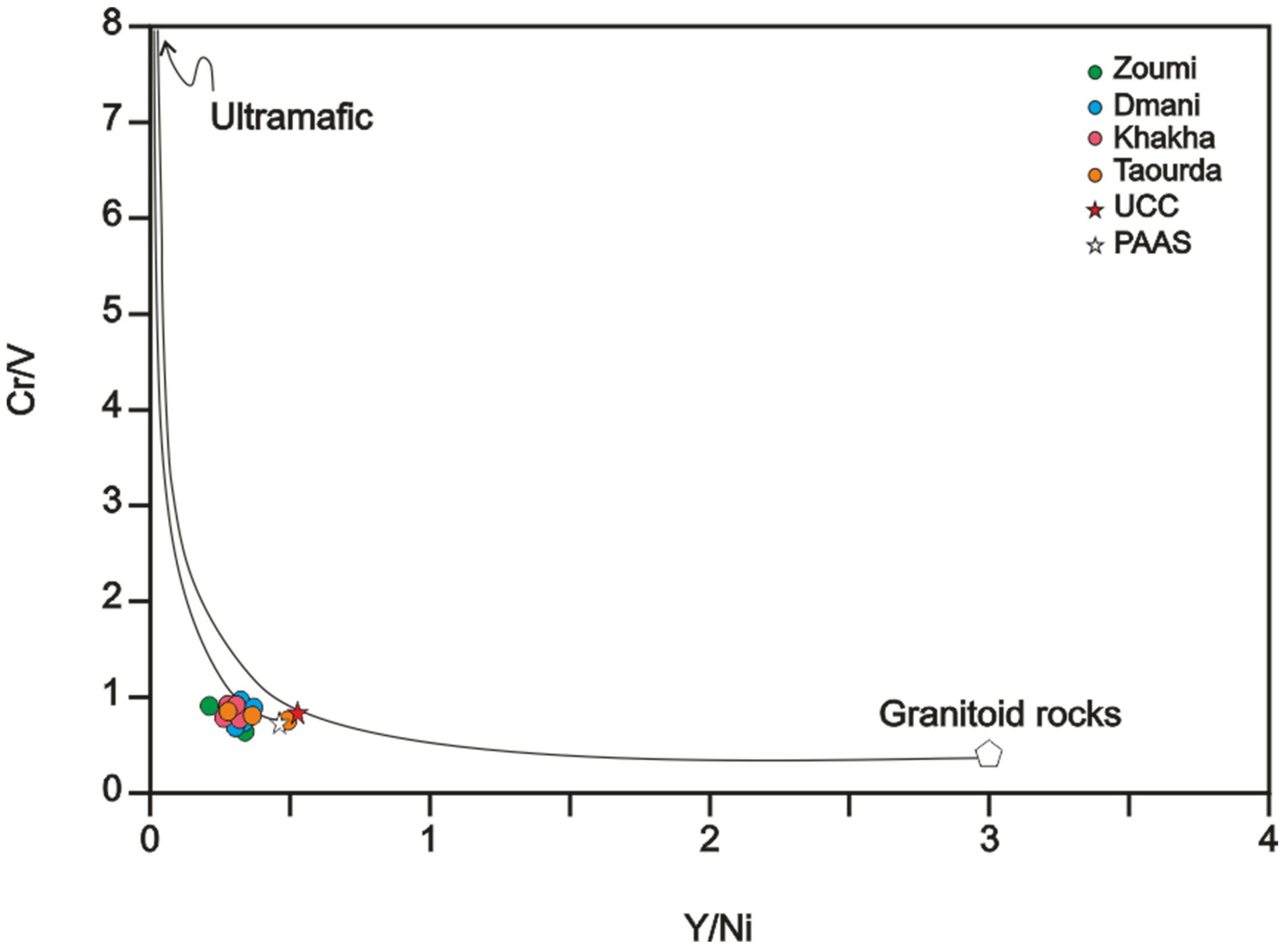


**Figure 45:** Cr/V versus Y/Ni diagram of mudrock samples. Ultramafic sources have very low Y/Ni and high Cr/V ratios. The samples fall in a region close to the Post-Archean Australian Shale (PAAS) point, ruling out mafic supply.

Provenance proxies including triangular relationships of Th-Sc-Zr (Bhatia and Crook 1986; Bahlburg 1998), V-Ni-Th and V-Ni-La (Bracciali et al. 2007) may be used to discriminate sediments from felsic sources to progressively more mafic sources (Bhatia and Crook 1986; Cullers 1994). In Th-Sc-Zr/10 diagram the studied mudrocks plot in the felsic rocks field, close to the PAAS and UCC point (Fig. 46a). Moreover, studied samples follow a trend towards a continental environment, far from the oceanic arc-related field suggesting their mainly felsic source. Also, the occurrence of all mudrocks samples in the area of Continental Island Arc (CIA), could be an additional source area may be related to the subduction of Mesorif slab under Ketama unit since Early Oligocene (Negro et al. 2007) and this arc seems to be made of mainly intermediate magmatic rocks but this CIA and related magmatic setting are nowadays not yet evidenced in the External Rif thrust belt. However, a mafic supply can't be excluded for Zoumi Basin, since the V-Ni-Th*10 and V-Ni-La*4 diagrams (Bracciali et al. 2007; Perri et al. 2011) (Fig 46b, c) suggest a mixed mode provenance, as samples plot between the mafic and the felsic compositions, and the Zoumi, Dmani and Khakha samples display a weak enrichment in Ni through a trend shifted toward the ultramafic apex. Moreover, the diagram based on Cr/Th vs. Th/Sc ratios (Fig. 47) shows that the mudrocks are consistent with a mixing between felsic and mafic end-members, with a significant contribution from a felsic source; the mafic input is lower but not negligible. The mafic-ultramafic supply is probably related to the weathering of the eastward exhumed Mesorifan ophiolitic slices as widely scattered remnants of the main Mesorifan Suture Zone throughout the Mesorifain Sub-Domain (Benzagagh et al. 2014, Michard et al. 2014).

During basin fill stage, tectonic activity can influence the geochemical composition of sediments. Active tectonics and high relieves rejuvenation during the progression of the external Rif accretionary prism allow rapid sediments discharge and routing from source to sink, whereas tectonic quiescence and low relieves permit longer residence times, and hence more weathering and chemical modification during transport (Johnsson 1993).

Major and trace elements are important proxies for inferring geodynamic and tectonic settings as well as sediment depositional palaeoenvironment. A tectonic setting discrimination diagram proposed by Roser and Korsch (1986) uses Log ($K_2O/Na_2O$) against $SiO_2$. Afterward, increasing values of $K_2O/Na_2O$ and $SiO_2$ indicate a change from passive margin (PM) to active continental margin (ACM) (Fig. 48a). High $K_2O/Na_2O$ and $SiO_2$ values indicate a relatively tectonically active continental margin environment for the deposition of almost all analyzed mudrocks.

Verma and Armstrong-Altrin (2013), through an assessment of worldwide older tectonic setting models, recommend two discrimination function diagrams for tectonic setting discrimination of siliciclastic sediments: the first for high-silica content rocks [$(SiO_2)_{adj}$ = 63 % to 95 %] and the second for low-silica content [$(SiO_2)_{adj}$ = 35 % to 63 %].

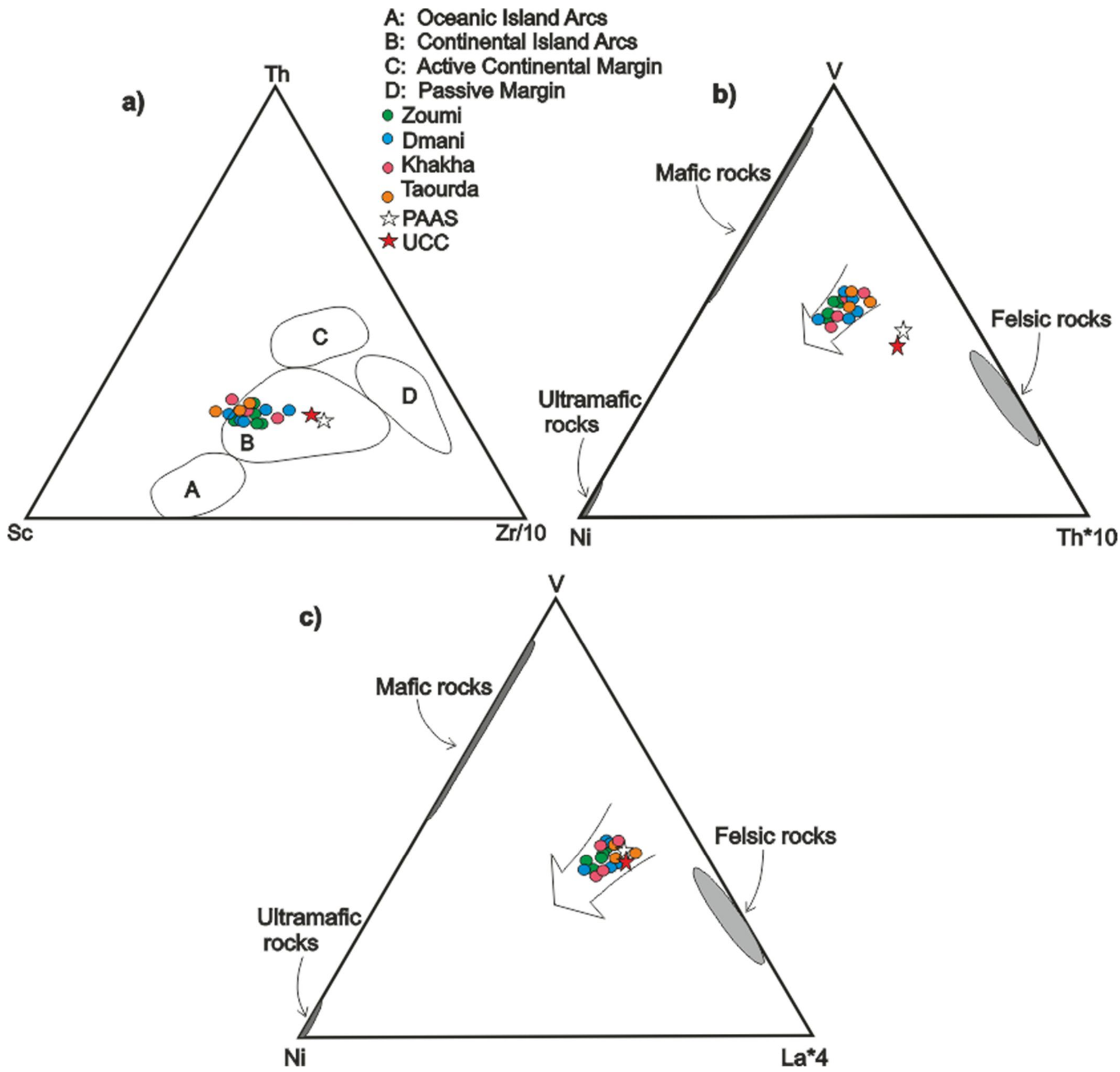


**Figure 46: a.** Th-Sc-Zr/10 diagram (after Bhatia and Crook 1986; Bahlburg 1998) the mudrocks fall in a region close to the PAAS and the UCC points that rule out important mafic supply (A: Oceanic Island Arcs, B: Continental Island Arcs, C: Active Continental Margin, D: Passive Margin). **b** and **c** V-Ni-La*4 and V-Ni-Th*10 plots of mudrocks, concentrations are in ppm, shaded areas represent composition of the same felsic, mafic and ultramafic rocks. The shifting of samples toward the Ni corner suggests an ultramafic component in the detritus derived from the MesorifanOphiolitic Suture Zone (MOSZ of Michard et al.2007 and 2014) of the Mesorif Subdomain.

These diagrams representing new binary plots allow differentiating among three tectonic settings: *i)* island or continental arc (Arc), *ii)* continental rift (Rift), and *iii)* collision (Col) tectonic settings. Except one sample, all analyzed Zoumi sandstone suites show ≤63% $SiO_2$ content, thus the tectonic discrimination diagram for low-silica [$(SiO2)_{adj}$ = 35%–≤ 63%]

has been used. Two discrimination functions ($DF_1$ and $DF_2$) were calculated based on major element concentrations. Obtained results from discriminant functions were plotted on a binary diagram; seldom samples on rift field and almost exclusively all fall on collision orogen field (Fig. 48b).

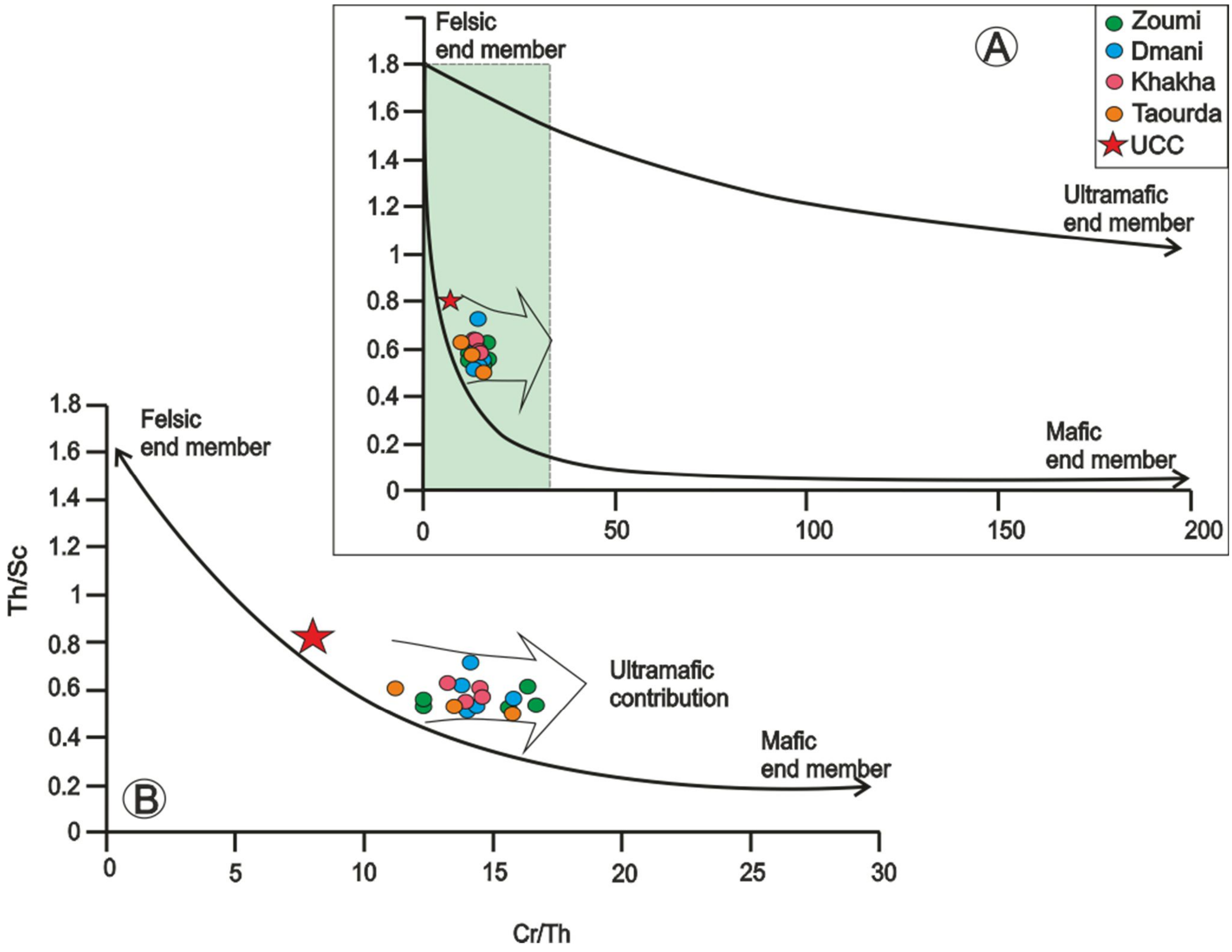


**Figure 47**: Th/Sc versus Cr/Th Plot for mudrocks samples (Condie and Wronkiewicz, 1990; Totten et al. 2000). B is the enlargement of shaded area in A. Zoumi basin mudrocks composition display a mixing between a mafic and a felsic end member, with a major contribution from a felsic source. The large arrow suggests a possible contribution from ultramafic source. The composition of UCC (upper continental crust composition after McLennan et al. 2006) is plotted for comparison.

Such features are thus consistent with an active collisional tectonic setting. Sandstone framework models and geochemical features suggest passive and active continental margins for the Zoumi sandstone suites (i.e southern African margin and northern fold and thrust belt, respectively) and preserve signatures of recycled orogen rather than continental craton provenance. Sediment source deals with the Rif accretionary prism evolved as hinterland areas of the syn-orogenic Zoumi Flysch Fm. The latter is mainly supplied from various exhumed low to middle-grade metamorphic basements and their sedimentary covers (i.e. Ketama and Temsamane units) and also from the stacked Flysch Nappes built by the closure and structuration of the Maghrebian Flysch basin (Fig. 50). The suggested tectono-sedimentary scenario is congruent with the ACM provenance of Zoumi sandstone suites. Whereas, the accretionary prism nappes-stacking load accentuated the thermic subsiding frontal foredeep of the external Rif leading to the uplift of Hercynian promontory forebulg which could then constitute the main basement provenance source assumed to a continental craton source area.

Finally, since late Oligocene? and mainly during Lower-Middle Miocene, the Zoumi Basin underwent a mixed mode provenance from opposite source areas located at the Zoumi Basin borders. The sediments input in the syn-orogenic Zoumi Basin was drained and routed synchronously from both the northern relieves made of the built accretionary prism which reached the Mesorif sub-domain boundary since Lower Miocene, and from the southern side of the basin where uplifted forebulg deltaic successions and the underlying African exhumed Paleozoic basement are cropping out as mechanical readjustment of the highly subsiding Zoumi Basin. The latter could be assigned to a syn-tectonic thrust-top basin laying in the southern front of the External Rif accretionnary prism migrating southward, during the downgoing subducted African slab beneath the dislocated Mesomediterranean Terrane during Miocene time (Carminati et al. 2012; Benzagagh et al. 2014; Van Hinsbergen et al. 2014; Michard et al. 2014).

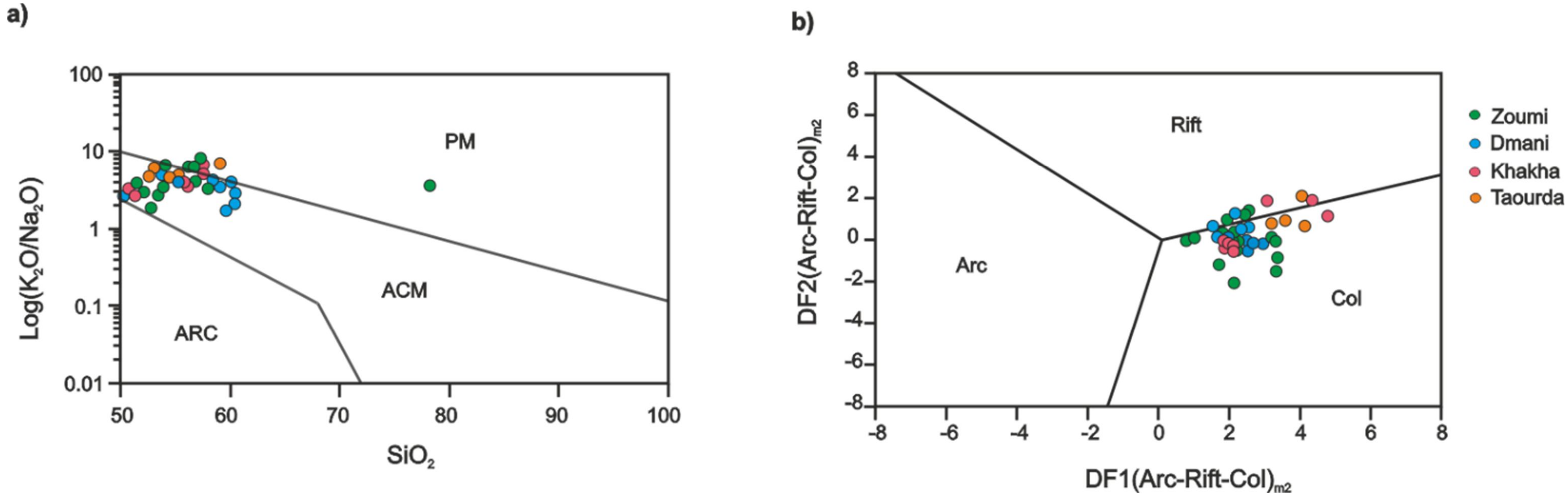


**Figure 48**: **a**. SiO2 vs Log (K2O/Na2O) tectonic setting diagram, PM = Passive margin; ACM = active continental margin; ARC = oceanic island arc margin (Diagram after Roser and Korsh 1986); **b.** Tectonic settings from discriminant-function multi-dimensional diagram for low silica Zoumimudrocks sediments (arc, continental rift, and collision; Diagram after Verma and Armstrong-Altrin (2013). All data were recalculated to 100% volatile-free.

# CONCLUSIONS

# CONCLUSIONS

The Zoumi Basin is a key area laying in front of progressively uplifted and exhumed massifs, constituting the dominant provenance sources for Lower-Middle Miocene syn-orogenic siliciclastic sedimentation whose composition can be examined to check source-to-sink routing and to constrain palaeogeographic and palaeotectonic reconstructions.

The Zoumi sandstone suites are mainly sublitharenites with quartzarenites in small amount. They are coarse-grained mainly characterized by low-grade metamorphic components, and subordinate volcanic lithic fragments displaying higher Qm/Lt ratio than fine-to medium-grained ones. The dominant clastic detritus input is mainly fed by Intrarif and Mesorif metamorphic basement units, their rooted sedimentary successions (Loukkos-Tanger-Aknoul nappes) and carbonate slices imbricated within Mesozoic-Paleogene successions (Fig. 50). The Middle Miocene collision and docking of the Betic-Rifian Internal Units to the Iberian and African margins, the subsequent deformation and erosion of the Maghrebian Flysch Basin foredeep successions provided additional detrital material filling to the Zoumi Flysch Basin since Middle Miocene (Durand Delga 1980; Hoyez 1989; Guerrera et al. 2005; de Capoa et al. 2007; Thomas et al. 2010; Vitale et al. 2015) (Fig. 49(b), (c); Fig. 50).

The prevailing rounded and polycrystalline Quartz with crenulated- and sutured-like quartz-grain contacts, coupled with evidence of WNW-ward current flows, suggest a provenance from low-rank metamorphic massifs set to the NE of the Zoumi Basin (i.e. Ketama and Temsamane massifs) (Fig. 50). Petrographic provenance proxies including QtFL and QmFLt plots suggest a mixed mode provenance with a dominant input from recycled orogen source rocks, with a minor craton source rocks contribution. Moreover, geochemical data indicate also this mixed mode provenance from both passive margin and active continental margin.

The Lower-Middle Miocene syn-orogenic Zoumi flysch Fm. underwent thus a complex Alpine history. Namely, mudrocks show similar concentrations to UCC standards, for Si, Ti, Al, Fe, Mg, K, Rb, Ba, Cs. They are highly enriched in Ca and strongly depleted in Mn, Na and P. The geochemistry of Dmani, Khakha, Taourda and Zoumimudrock suites provide interesting palaeoclimatic and palaeoweathering indications. For the almost majority studied mudrocks, both CIA and the CIA' weathering proxies coupled to A-CN-K and A-N-K plots, suggest low to moderate and rarely intense weathering at the source area. The studied fine-grained sediments seem to come from highly eroded sources and probably affected by brief reworking. These sources ostensibly correspond to tectonically active high elevation coastal ranges connected to braided fluvial drainage network. The latter underwent intense rainfall/runoff processes under wet/humid climate conditions, controlling terrigenous sediments routing, their subsequent quick input to multi-channels marine canyons. This marine network feed longitudinal lobes and their fast accumulation within a narrow and subsiding trough where accommodated space did not exceed the erosion rate in the source area as testified by prevailing thickening-coarsening upward sequence trends (El Mourabet et al. 2017c). The source-to-sink short rooting and poor recycling processes of studied mudrocks are both corroborated by $Al_2O_3$-Zr-$TiO_2$ and Zr/Sc-Th/Sc plots. Moreover, the effect of sorting-related fractionation on the elements proportion seems to be related to sediment alteration by physical and chemical weathering processes. The ICV values are systematically >1 reflecting compositional immaturity of first cycle sediments, which are mainly derived from a tectonically active External Rif accretionary prism. The latter was due to docking of the already structured Internal Zones to the Flysch Nappes that themselves derived from the Maghrebian Flysch basin senescence since early Middle Miocene. Both override the sedimentary and low-grade metamorphic Intrarif units consecutively thrusting the uplifted, exhumated sedimentary and metamorphic Mesorif windows (Frizon de lamotte 1985; Zaghloul et al. 2005b; Azdimousa et al. 1998; Negro et al. 2007) (Fig. 49c, d; Fig. 50). All stacked units build the external Rif accretionary prism during middle Miocene have been coeval with the sedimentation of very thick syn-orogenic successions which are quickly accumulated within narrow thrust-top basins during the same age and usually sealed by upper Tortonian coarse- to fine-grained thick deltaic sequences along the Mesorif corridor.

The source areas were probably characterized by high relieves of the uplifted accretionary prism supporting narrow longitudinal syn-tectonic thrust-top basins. The tectonically active hinterland underwent chemical and mechanical weathering processes under wet and humid paleoclimate conditions as indicated by the aforementioned palaeoclimate proxies. The detritus input was rapidly routed and accumulated in a narrow basin by multichannel feeders. The middle Miocene filling of the syn-tectonic thrust-top basins coeval with runoff/rainfall processes in the bordering high relieves and related source areas could be partly assigned to a global cooling event which seems triggered by a short-lived Miocene glacial events (Lavier et al. 2001; John et al. 2003) known as Mi global events of Miller et al. 1991. The latter events could be responsible for regional increase in rainfall/runoff continental weathering along the North African margin which mainly happened during cooler periods (Thomas et al. 2010).

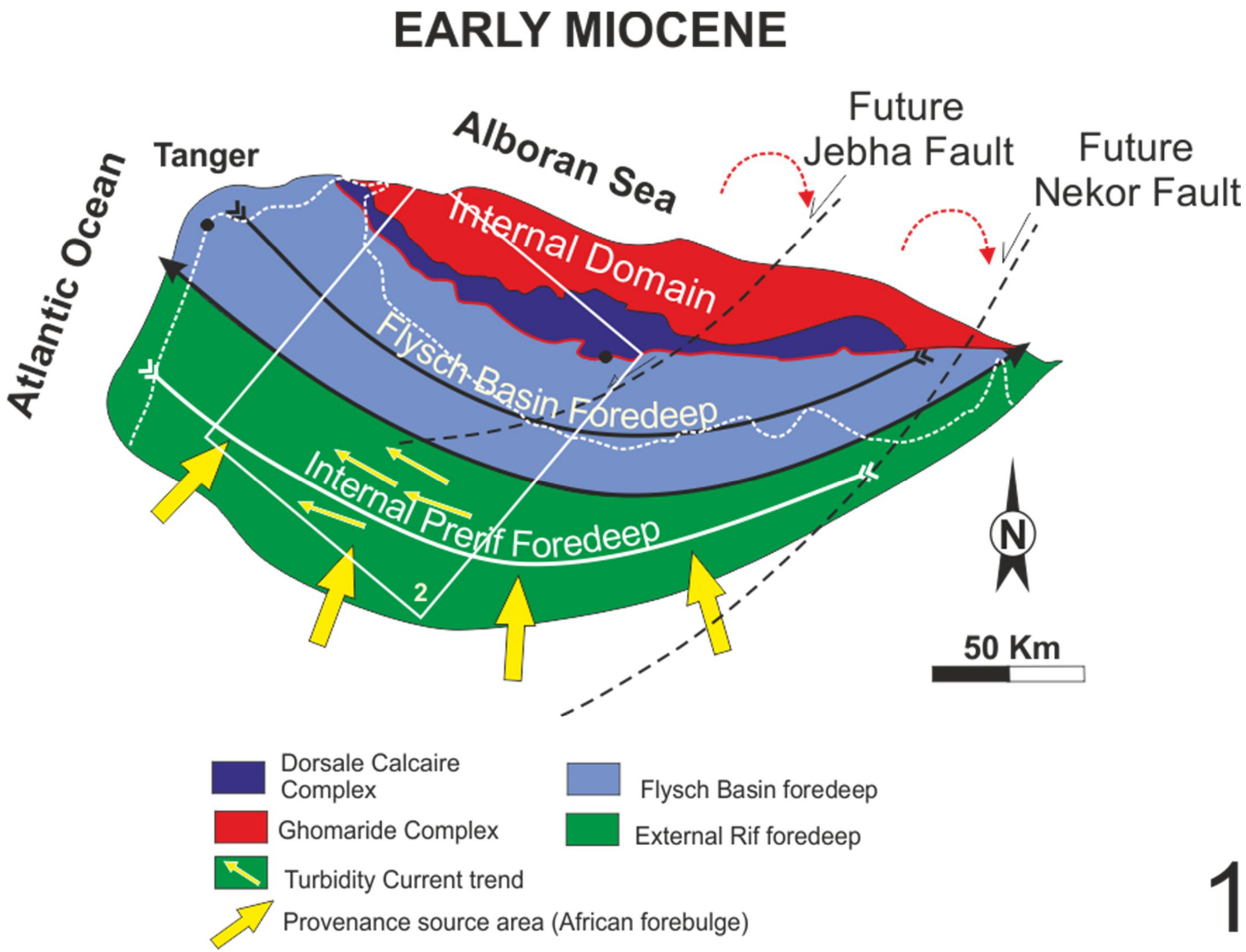


**Figure 49 (a):** Geodynamic evolution scheme of the Zoumi basin: 1/ Early Miocene Flysch and External Rif foredeep

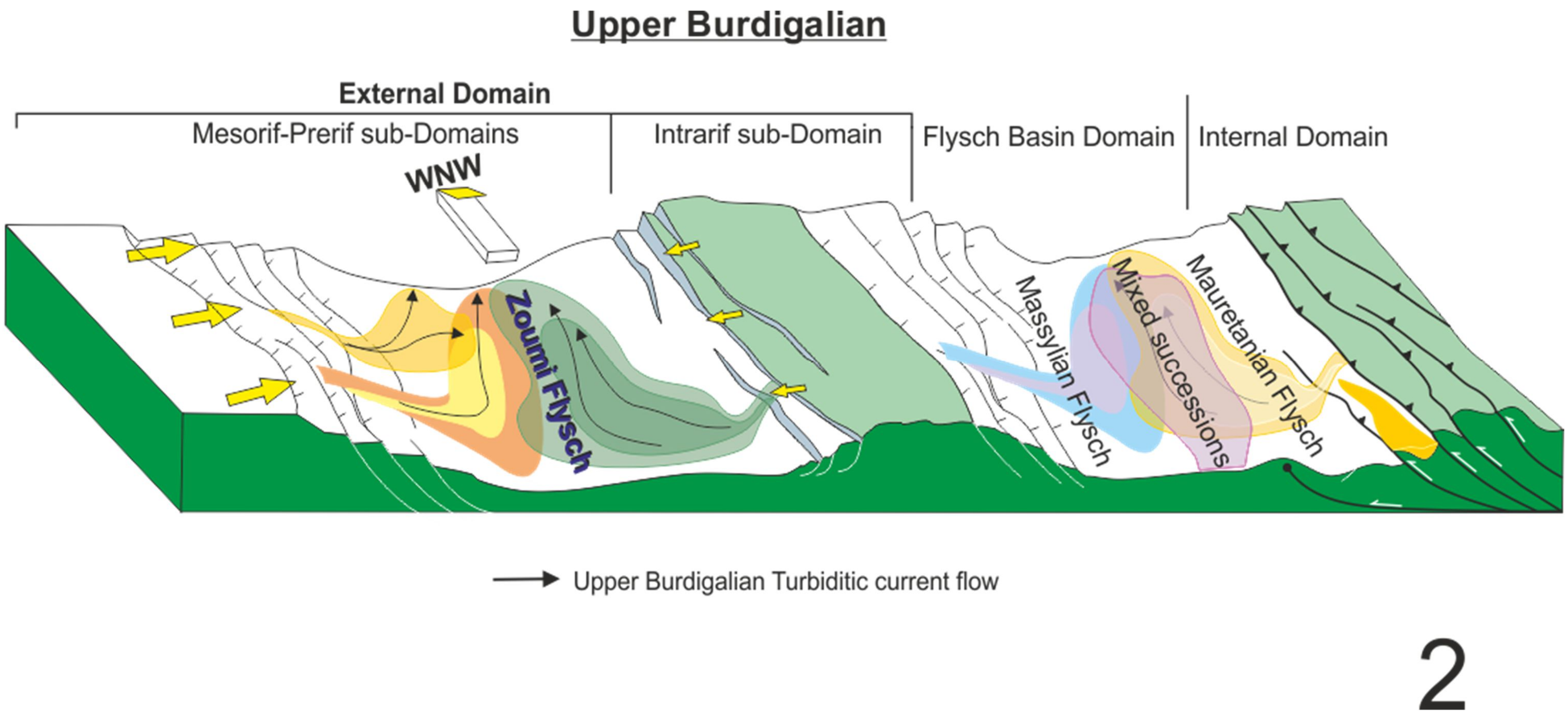


**Figure 49 (b):** Geodynamic evolution scheme of the Zoumi basin: 2/ Two Flysch basin sinks of Zoumi and mauretanian-Massylian and mixed successions.

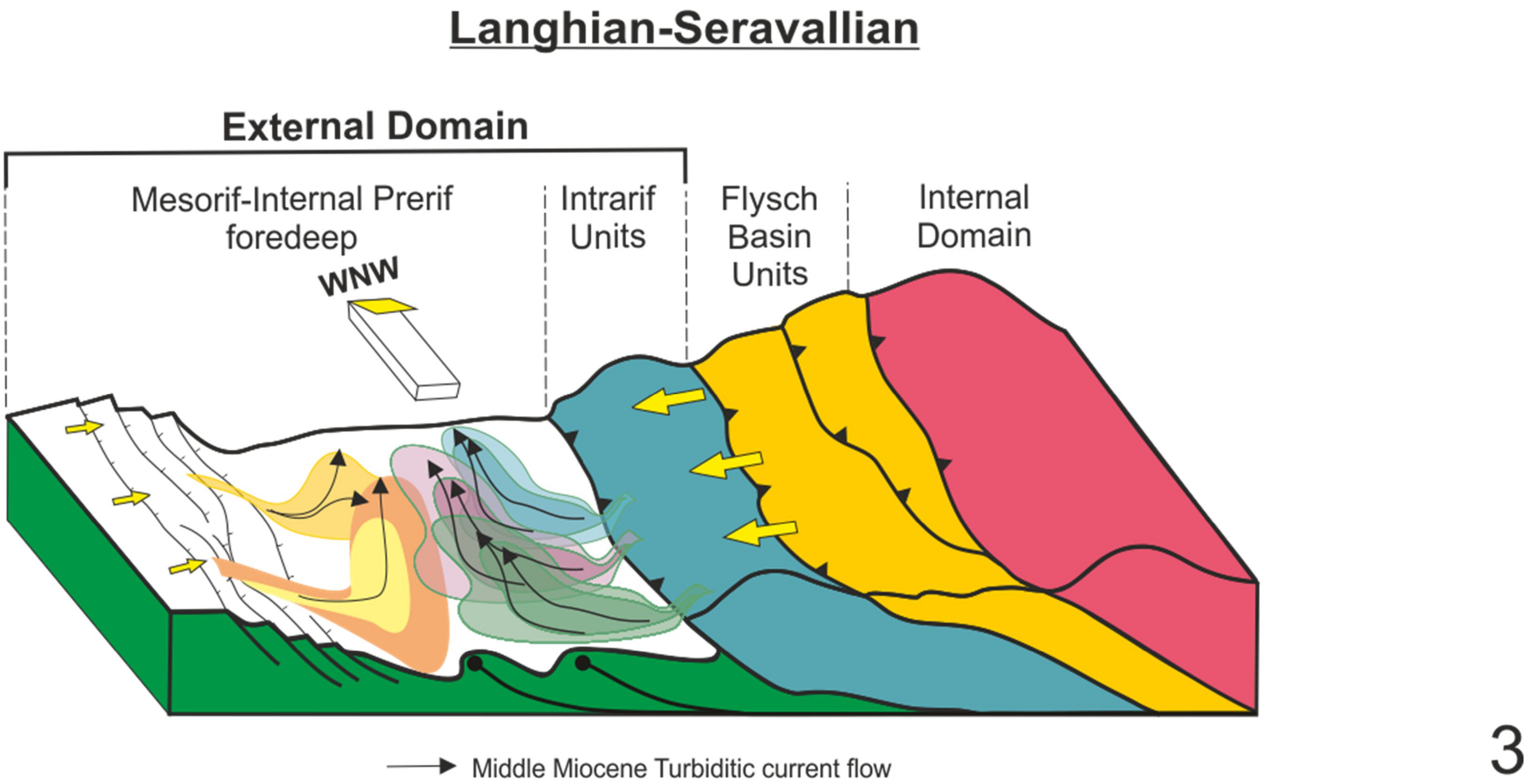


**Figure 49 (c):** Geodynamic evolution scheme of the Zoumi basin: 3/ Langhian-Serravallian Internal domain nappes stacking and intense weathering of High relieves under humid wet paleoclimatic conditions

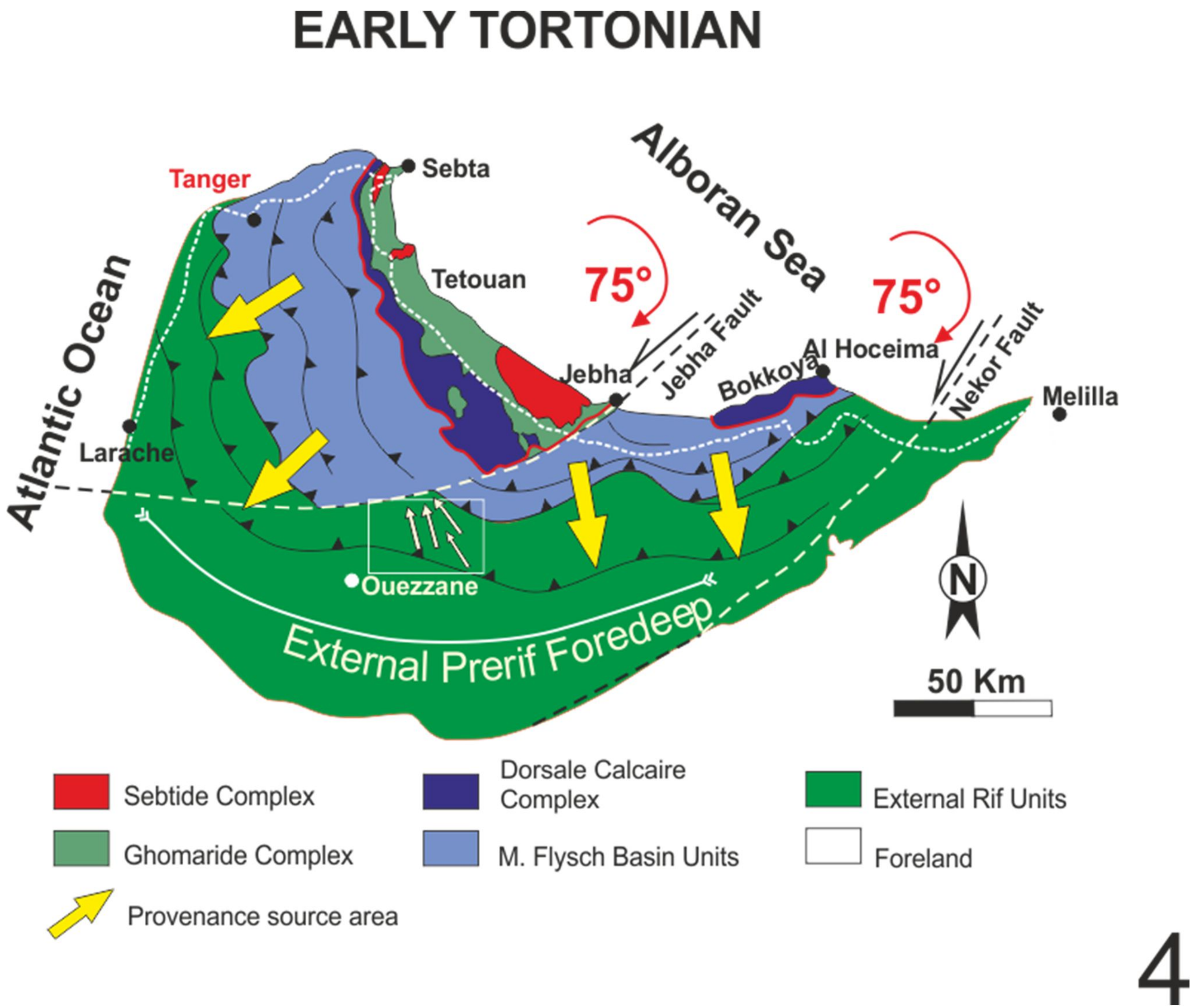


**Figure 49 (d):** Geodynamic evolution scheme of the Zoumi basin: 4/Early Tortonian Blocks rotations of the Rif belt (estimated amounts of blocks rotation after paleomagnetic data of Cifelli et al.; 2008, 2009, 2016).

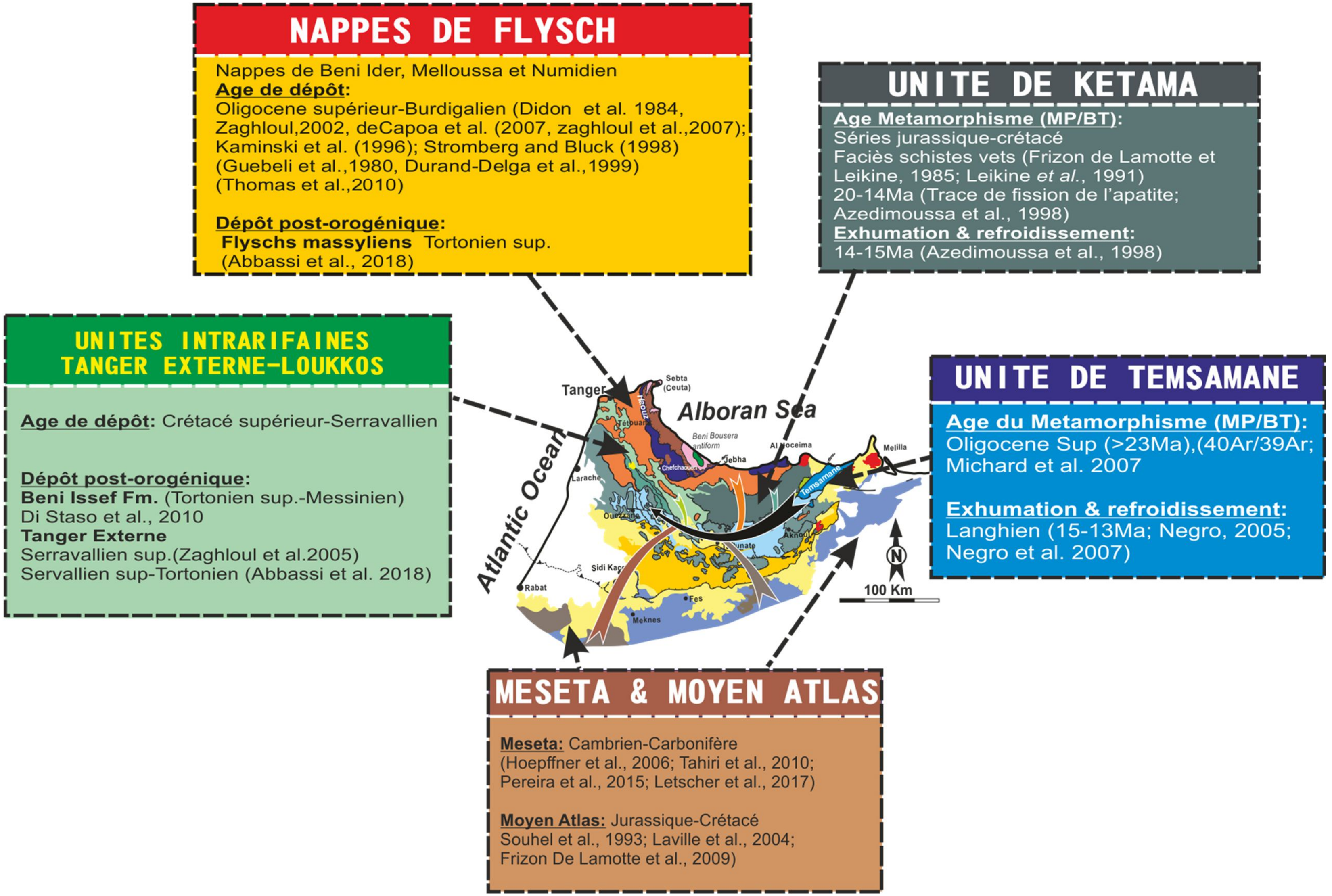


**Figure 50:** Interaction géodynamique Chaîne-Bassin/Evolution thermo-tectonique et processus de surface, Exhumation/Cooling/Denudation and Uplift/Erosion of hinterland source area for terrigenous supply of the Zoumi basin turbiditic deposits.

# REFERENCES

# REFERENCES


Aalto KR (1976) Sedimentology of a melange; Franciscan of Trinidad, California. Journal of Sedimentary Research 46:913–929. doi: 10.1306/212F7090-2B24-11D7-8648000102C1865D

Aksu AE (1984) Subaqueous debris flow deposits in Baffin Bay. Geo-Marine Letters 4:83–90. doi: 10.1007/BF02277077

Aksu AE, Hiscott RN (1992) Shingled Quaternary debris flow lenses on the north-east Newfoundland Slope. Sedimentology 39:193–206. doi: 10.1111/j.1365-3091.1992.tb01034.x

Alexander J, Morris S (1994) Observations on experimental, nonchannelized, high-concentration turbidity currents and variations in deposits around obstacles. Journal of Sedimentary Research 64:899–909. doi: 10.1306/D4267F00-2B26-11D7-8648000102C1865D

Alexander J, Mulder T (2002) Experimental quasi-steady density currents. Marine Geology 186:195–210. doi: 10.1016/S0025-3227(02)00313-4

Allen JRL (1971) Instantaneous sediment deposition rates deduced from climbing-ripple cross-lamination. Journal of the Geological Society 127:553–561. doi: 10.1144/GSL.JGS.1971.127.06.02

Allen JRL (1982) Sedimentary structures, their character and physical basis. Elsevier

Allen JRL (1991) The Bouma division A and the possible duration of turbidity currents. Journal of Sedimentary Research 61:291–295. doi: 10.1306/D42676F4-2B26-11D7-8648000102C1865D

Amendola U, Perri F, Critelli S, et al (2016) Composition and provenance of the Macigno Formation (Late Oligocene–Early Miocene) in the Trasimeno Lake area (northern Apennines). Marine and Petroleum Geology 69:146–167. doi: 10.1016/j.marpetgeo.2015.10.019

Andresen A, Bjerrum L (1967) SLIDES IN SUBAQUEOUS SLOPES IN LOOSE SAND AND SILT. Norwegian Geotechnical Institute Publ 81:221–239

Andrieux J (1973) Sur le metamorphisme des zones externes du Rif. Bulletin de la Société Géologique de France 15:106–107. doi: 10.2113/gssgfbull.S7-XV.2.106

Armstrong-Altrin JS, Lee YI, Verma SP, Ramasamy S (2004) Geochemistry of Sandstones from the Upper Miocene Kudankulam Formation, Southern India: Implications for Provenance, Weathering, and Tectonic Setting. Journal of Sedimentary Research 74:285–297. doi: 10.1306/082803740285

Armstrong-Altrin JS, Machain-Castillo ML, Rosales-Hoz L, et al (2015) Provenance and depositional history of continental slope sediments in the Southwestern Gulf of Mexico unraveled by geochemical analysis. Continental Shelf Research 95:15–26. doi: 10.1016/j.csr.2015.01.003

Arnott RWC, Hand BM (1989) Bedforms, primary structures and grain fabric in the presence of suspended sediment rain. Journal of Sedimentary Research 59:1062–1069. doi: 10.1306/212F90F2-2B24-11D7-8648000102C1865D

Aubouin J, Durand-Delga M (1971) Aire méditerranéenne. EncyclopaediaUniversalis 10:743–745

Azdimousa A, Bourgois J, Poupeau G, Montigny R (1998) Histoire thermique du massif de Kétama (Maroc): sa place en Afrique du Nord et dans les Cordillères bétiques. Comptes Rendus de l'Académie des Sciences - Series IIA - Earth and Planetary Science 326:847–853. doi: 10.1016/S1251-8050(98)80023-2

Baas JH, Best JL, Peakall J (2011) Depositional processes, bedform development and hybrid bed formation in rapidly decelerated cohesive (mud–sand) sediment flows. Sedimentology 58:1953–1987. doi: 10.1111/j.1365-3091.2011.01247.x

Bagnold RA (1956) The flow of cohesionless grains in fluids. Phil Trans R Soc Lond A 249:235–297. doi: 10.1098/rsta.1956.0020

Bagnold RA (1962) Auto-suspension of transported sediment; turbidity currents. Proc R Soc Lond A 265:315–319. doi: 10.1098/rspa.1962.0012

Bagnold RA (1966) An Approach to the Sediment Transport Problem from General Physics. U.S. Geological Survey Professional Paper 422-I, pp. v + 37, with 15 figs, and 1 table. U.S. Government Printing Office, Washington, D.C. Geological Magazine 104:409–446. doi: 10.1017/S0016756800049074

Bahlburg H (1998) The geochemistry and provenance of Ordovician turbidites in the Argentine Puna. Geological Society, London, Special Publications 142:127–142. doi: 10.1144/GSL.SP.1998.142.01.07

Barnes NE, Normark WR (1985) Diagnostic Parameters for Comparing Modern Submarine Fans and Ancient Turbidite Systems. In: Submarine Fans and Related Turbidite Systems. Springer, New York, NY, pp 13–14

Barnes PM, Lewis KB (1991) Sheet slides and rotational failures on a convergent margin: the Kidnappers Slide, New Zealand. Sedimentology 38:205–221. doi: 10.1111/j.1365-3091.1991.tb01257.x

Basu A, Young SW, Suttner LJ, et al (1975) Re-evaluation of the use of undulatory extinction and polycrystallinity in detrital quartz for provenance interpretation. Journal of Sedimentary Research 45:873–882. doi: 10.1306/212F6E6F-2B24-11D7-8648000102C1865D

Bauluz B, Mayayo MJ, Fernandez-Nieto C, Gonzalez Lopez JM (2000) Geochemistry of Precambrian and Paleozoic siliciclastic rocks from the Iberian Range (NE Spain): implications for source-area weathering, sorting, provenance, and tectonic setting. Chemical Geology 168:135–150. doi: 10.1016/S0009-2541(00)00192-3

Beattie PD, Dade WB (1996) Is scaling in turbidite deposition consistent with forcing by earthquakes? Journal of Sedimentary Research 66:909–915. doi: 10.1306/D4268437-2B26-11D7-8648000102C1865D

Beckmann B, Flögel S, Hofmann P, et al (2005a) Orbital forcing of Cretaceous river discharge in tropical Africa and ocean response. Nature 437:241–244. doi: 10.1038/nature03976

Beckmann B, Hofmann P, Wagner T (2005b) Linking Coniacian-Santonian (OAE3) black shale formation to African climate variability: a reference section from the eastern tropical Atlantic at orbital time scales (ODP Site 959, off Ivory Coast/Ghana). The Deposition of Organic Carbon-Rich Sediments: Models, Mechanisms and Consequences 82:125–143. doi: 10.2110/pec.05.82.0125

Benyaich A, Hervouet Y, Duee G, El Hatimi N (1989) Age jurassique et réinterprétation des roches basiques au nord de Ouezzane (Rif externe, Maroc) : significations géodynamiques. Comptes rendus de l'Académie des sciences Série II, Mécanique, physique, chimie, sciences de l'univers, sciences de la terre 309:1197–1202

Benyaich A (1991) Evolution tectono-sédimentaire du Rif externe centre occidental (régions de M'Sila et Ouezzane, Maroc) : la marge africaine du Jurassique au Crétacé; les bassins néogènes d'avant fosse. Thèse Doctorat d'Etat, Univérsité de Pau et Pays de l'Adour

Benzaggagh M (1988) Etude stratigraphique du jurassique superieur dans le Prerif interne (régions de Msila et de Moulay Bouchta, Maroc). Thèse 3ème cycle, Université de Lyon-I

Benzaggagh M (2011) Activités volcaniques sous-marines à la limite Jurassique-Crétacé dans le Rif externe (Maroc). Âge et relation avec la sédimentation et la paléogéographie du sillon rifain externe. Comptes Rendus Geoscience 343:302–311. doi: 10.1016/j.crte.2010.12.009

Benzaggagh M, Mokhtari A, Rossi P, et al (2014) Oceanic units in the core of the External Rif (Morocco): Intramarginhiatus or South-Tethyan remnants? Journal of Geodynamics 77:4–21. doi: 10.1016/j.jog.2013.10.003

Bhatia MR (1983) Plate Tectonics and Geochemical Composition of Sandstones. The Journal of Geology 91:611–627

Bhatia MR, Crook KAW (1986) Trace element characteristics of graywackes and tectonic setting discrimination of sedimentary basins. Contr Mineral and Petrol 92:181–193. doi: 10.1007/BF00375292

Biscaye PE, Eittreim SL (1977) Suspended particulate loads and transports in the nepheloid layer of the abyssal Atlantic Ocean. Marine Geology 23:155–172. doi: 10.1016/0025-3227(77)90087-1

Bock B, Mclennan SM, Hanson GN (2002) Geochemistry and provenance of the Middle Ordovician Austin Glen Member (Normanskill Formation) and the Taconian Orogeny in New England. Sedimentology 45:635–655. doi: 10.1046/j.1365-3091.1998.00168.x

Bonardi G, Cavazza W, Perrone V, Rossi S (2001) Calabria-Peloritani terrane and northern Ionian Sea. In: Anatomy of an Orogen: the Apennines and Adjacent Mediterranean Basins. Springer, Dordrecht, pp 287–306

Bouhdadi S (1999) Carte géologique du Rif, feuille de Zoumi au 1/50.000. Notes et Mémoires du Service géologique du Maroc 386

Bouillin JP, Durand-Delga M, Gélard JP, et al (1970) Définition d'un Flysch massylien et d'un Flysch maurétanien au sein des Flyschs allochtones de l'Algérie. Comptes rendus de l'Académie des sciences Série II, Mécanique, physique, chimie, sciences de l'univers, sciences de la terre 270:2249–2252

Bouillin JP (1986) Le bassin maghrebin; une ancienne limite entre l'Europe et l'Afrique a l'ouest des Alpes. Bulletin de la Société Géologique de France II:547–558. doi: 10.2113/gssgfbull.II.4.547

Bouma AH (1962) Sedimentology of some Flysch deposits; a graphic approach to facies interpretation. Elsevier Pub. Co., Amsterdam

Bouma AH (1972) Recent and Ancient Turbidites and Contourites. 22:205–211

Bouma AH, Hollister CD (1973a) Deep Ocean Basin Sedimentation. In: Middleton, GV & Bouma, AH (eds), Turbidites and Deep Water Sedimentation Pacific Section, Society of Economic Paleontologists and Mineralogists Short Course Notes, Anaheim 79–118

Bouma AH, Hollister CD (1973b) Deep ocean basin sedimentation. In: Middleton, G.V. & Bouma, A.H. (eds), Turbidites and Deep Water Sedimentation. pp 79–118

Bourcart J (1938a) La marge continentale: essai sur les regressions et les transgressions marines. Bulletin de la Société Géologique de France 8:393–474

Bourcart J (1891-1965) (1938b) La marge continentale. Essai sur les régressions et transgressions marines. Bulletin de la société géologique de France 5e série:393–474

Bouybaouene M, Goffé B, Michard A (1995) High-pressure, low-temperature metamorphism in the Sebtides nappes, northern Rif, Morocco. Geogaceta 17:117–119

Bracciali L, Marroni M, Luca P, Sergio R (2007) Geochemistry and petrography of Western Tethys Cretaceous sedimentary covers (Corsica and Northern Apennines): From source areas to configuration of margins. In: Special Paper 420: Sedimentary Provenance and Petrogenesis: Perspectives from Petrography and Geochemistry. Geological Society of America, pp 73–93

Branney M, Kokelaar P (2002) Pyroclastic Density Currents and the Sedimentation of Ignimbrites. Geol Soc London Mem 27:. doi: 10.1144/GSL.MEM.2002.027.01.01

Bucher WH (1940) Submarine valleys and related geologic problems of the North Atlantic. GSA Bulletin 51:489–511. doi: 10.1130/GSAB-51-489

Caracciolo L, Pera EL, Muto F, Perri F (2011) Sandstone petrology and mudstone geochemistry of the Peruc–Korycany Formation (Bohemian Cretaceous Basin, Czech Republic). International Geology Review 53:1003–1031. doi: 10.1080/00206810903429011

Carminati E, Lustrino M, Doglioni C (2012) Geodynamic evolution of the central and western Mediterranean: Tectonics vs. igneous petrology constraints. Tectonophysics 579:173–192. doi: 10.1016/j.tecto.2012.01.026

Chalouan A (1986) LES NAPPES GHOMARIDES (RIF SEPTENTRIONAL, MAROC), UN TERRAIN VARISQUE DANS LA CHAINE ALPINE. Thèse Ès-Sciences, Université Louis Pasteur

Chalouan A, Michard A (1990) The Ghomarides Nappes, Rif Coastal Range, Morocco: A Variscan chip in the Alpine Belt. Tectonics 9:1565–1583. doi: 10.1029/TC009i006p01565

Chalouan A, Michard A, Feinberg H, et al (2001) The Rif mountain building (Morocco); a new tectonic scenario. Bulletin de la Société Géologique de France 172:603–616. doi: 10.2113/172.5.603

Chalouan A, Michard A, Kadiri KE, et al (2008) The Rif Belt. In: Continental Evolution: The Geology of Morocco. Springer, Berlin, Heidelberg, pp 203–302

Chough S, Hesse R (1976) Submarine meandering thalweg and turbidity, currents flowing for 4,000 km in the, Northwest Atlantic Mid-Ocean Channel, Labrador Sea. Geology 4:529–533. doi: 10.1130/0091-7613(1976)4<529:SMTATC>2.0.CO;2

Cifelli F, Mattei M, Porreca M (2008) New paleomagnetic data from Oligocene–upper Miocene sediments in the Rif chain (northern Morocco): Insights on the Neogene tectonic evolution of the Gibraltar arc. Journal of Geophysical Research: Solid Earth 113:1–12. doi: 10.1029/2007JB005271

Cifelli F, Mattei M, Chadima M, et al (2009) The magnetic fabric in “undeformed clays”: AMS and neutron texture analyses from the Rif Chain (Morocco). Tectonophysics 466:79–88. doi: 10.1016/j.tecto.2008.08.008

Cifelli F, Caricchi C, Mattei M (2016) Formation of arc-shaped orogenic belts in the Western and Central Mediterranean: a palaeomagnetic review. Geological Society, London, Special Publications 425:1–27. doi: 10.1144/SP425.12

Cita MB, Beghi C, Camerlenghi A, et al (1984) Turbidites and megaturbidites from the Herodotus abyssal plain (eastern Mediterranean) unrelated to seismic events. Marine Geology 55:79–101. doi: 10.1016/0025-3227(84)90134-8

Comas M, Platt JP, Soto J, Watts A (1999) The origin and Tectonic History of the Alboran Basin: Insights from Leg 161 Results. In: Integrated Ocean Drilling Program: Preliminary Reports. pp 555–580

Condie KC, Wronkiewicz DJ (1990) A New Look at the Archaean-Proterozoic Boundary Sediments and the Tectonic Setting Constraint. In: Naqvi SM (ed) Developments in Precambrian Geology. Elsevier, pp 61–83

Condie KC, Boryta MD, Liu J, Qian X (1992) The origin of khondalites: geochemical evidence from the Archean to Early Proterozoic granulite belt in the North China craton. Precambrian Research 59:207–223. doi: 10.1016/0301-9268(92)90057-U

Condie KC (1993) Chemical composition and evolution of the upper continental crust: Contrasting results from surface samples and shales. Chemical Geology 104:1–37. doi: 10.1016/0009-2541(93)90140-E

Cox R, Lowe DR, Cullers RL (1995) The influence of sediment recycling and basement composition on evolution of mudrock chemistry in the southwestern United States. Geochimica et Cosmochimica Acta 59:2919–2940. doi: 10.1016/0016-7037(95)00185-9

Critelli S, Pera EL (1994) Detrital modes and provenance of Miocene sandstones and modern sands to the Southern Apennines thrust-top basins (Italy). Journal of Sedimentary Research 64:824–835. doi: 10.1306/D4267ED8-2B26-11D7-8648000102C1865D

Critelli S, Ingersoll RV (1995a) Interpretation of neovolcanic versus palaeovolcanic sand grains: an example from Miocene deep-marine sandstone of the Topanga Group (Southern California). Sedimentology 42:783–804. doi: 10.1111/j.1365-3091.1995.tb00409.x

Critelli S, Le Pera E (1995b) Tectonic Evolution of the Southern Apennines Thrust-Belt (Italy) as Reflected in Modal Compositions of Cenozoic Sandstone. The Journal of Geology 103:95–105

Critelli S, Mongelli G, Perri F, et al (2008a) Compositional and Geochemical Signatures for the Sedimentary Evolution of the Middle Triassic–Lower Jurassic Continental Redbeds from Western-Central Mediterranean Alpine Chains. The Journal of Geology 116:375–386. doi: 10.1086/588833

Critelli S, Mongelli G, Perri F, et al (2008b) Sedimentary Evolution of the MiddleTriassic - Lower Jurassic continental redbeds from Western-Central Mediterranean Alpine Chains based on geochemical, mineralogical and petrographical tools. Journal of Geology 116:375–386

Critelli S, Muto F, Perri F, Tripodi V (2017) Interpreting provenance relations from sandstone detrital modes, southern Italy foreland region: Stratigraphic record of the Miocene tectonic evolution. Marine and Petroleum Geology 87:47–59. doi: 10.1016/j.marpetgeo.2017.01.026

Cullers RL (1994) The chemical signature of source rocks in size fractions of Holocene stream sediment derived from metamorphic rocks in the Wet Mountains region, Colorado, U.S.A. Chemical Geology 113:327–343. doi: 10.1016/0009-2541(94)90074-4

Cullers RL (1995) The controls on the major- and trace-element evolution of shales, siltstones and sandstones of Ordovician to tertiary age in the Wet Mountains region, Colorado, U.S.A. Chemical Geology 123:107–131. doi: 10.1016/0009-2541(95)00050-V

Cullers RL, Berendsen P (1998) The provenance and chemical variation of sandstones associated with the Mid-continent Rift System, U.S.A. European Journal of Mineralogy 10:987–1002

Cullers RL (2000) The geochemistry of shales, siltstones and sandstones of Pennsylvanian–Permian age, Colorado, USA: implications for provenance and metamorphic studies. Lithos 51:181–203. doi: 10.1016/S0024-4937(99)00063-8

Cullers RL, Podkovyrov VN (2000) Geochemistry of the Mesoproterozoic Lakhanda shales in southeastern Yakutia, Russia: implications for mineralogical and provenance control, and recycling. Precambrian Research 104:77–93. doi: 10.1016/S0301-9268(00)00090-5

Dakin N, Pickering KT, Mohrig D, Bayliss NJ (2013) Channel-like features created by erosive submarine debris flows: Field evidence from the Middle Eocene Ainsa Basin, Spanish Pyrenees. Marine and Petroleum Geology 41:62–71. doi: 10.1016/j.marpetgeo.2012.07.007

Daly RA (1936) Origin of submarine canyons. Am J Sci Series 5 Vol. 31:401–420. doi: 10.2475/ajs.s5-31.186.401

Damuth JE, Flood RD (1985) Amazon Fan, Atlantic Ocean. In: Submarine Fans and Related Turbidite Systems. Springer, New York, NY, pp 97–106

de Capoa P, Di Staso A, Perrone V, Zaghloul MN (2007) The age of the foredeep sedimentation in the Betic–Rifian Mauretanian Units: A major constraint for the reconstruction of the tectonic evolution of the Gibraltar Arc. Comptes Rendus Geoscience 339:161–170. doi: 10.1016/j.crte.2007.01.003

Dercourt J, Zonenshain LP, Ricou L-E, et al (1986) Geological evolution of the tethys belt from the atlantic to the pamirs since the LIAS. Tectonophysics 123:241–315. doi: 10.1016/0040-1951(86)90199-X

Di Iorio D, Akal T, Guerrini P, et al (1999) Oceanographic Measurements of the West Black Sea: June 15 to July 5, 1996. 60

Di Staso A, Perrone V, Perrotta S, et al (2010) Stratigraphy, age and petrography of the Beni Issef successions (External Rif; Morocco): Insights for the evolution of the Maghrebian Chain. Comptes Rendus Geoscience 342:718–730. doi: 10.1016/j.crte.2010.05.001

Dickinson WR (1970) Interpreting detrital modes of graywacke and arkose. Journal of Sedimentary Research 40:695–707. doi: 10.1306/74D72018-2B21-11D7-8648000102C1865D

Dickinson WR, Suczek CA (1979) Plate Tectonics and Sandstone Compositions. AAPG Bulletin 63:2164–2182

Dickinson WR, Valloni R (1980) Plate settings and provenance of sands in modern ocean basins. Geology 8:82–86. doi: 10.1130/0091-7613(1980)8<82:PSAPOS>2.0.CO;2

Dickinson WR (1982) Compositions of Sandstones in Circum-Pacific Subduction Complexes and Fore-Arc Basins. AAPG Bulletin 66:121–137

Dickinson WR, Beard LS, Brakenridge GR, et al (1983) Provenance of North American Phanerozoic sandstones in relation to tectonic setting. GSA Bulletin 94:222–235. doi: 10.1130/0016-7606(1983)94<222:PONAPS>2.0.CO;2

Dickinson WR (1985) Interpreting Provenance Relations from Detrital Modes of Sandstones. In: Provenance of Arenites. Springer, Dordrecht, pp 333–361

Didon J, Durand-Delga M, Kornprobst J (1973) Homologies geologiques entre les deux rives du detroit de Gibraltar. Bulletin de la Société Géologique de France S7-XV:77–105. doi: 10.2113/gssgfbull.S7-XV.2.77

Dowdeswell JA, Cofaigh CÓ (2002) Glacier-influenced sedimentation on high-latitude continental margins: introduction and overview. Geological Society, London, Special Publications 203:1–9. doi: 10.1144/GSL.SP.2002.203.01.01

Doyle LJ, Pilkey OH (eds) (1979) Geology of Continental Slopes. SEPM (Society for Sedimentary Geology)

Drummond CN, Wilkinson BH (1996) Stratal Thickness Frequencies and the Prevalence of Orderedness in Stratigraphic Sequences. The Journal of Geology 104:1–18

Durand-Delga M, Hottinger L, Marcais J, et al (1960) Données Actuelles Sur La Structure du Rif. Mémoire Hors Serie Société Géologique France (Livre Mém. P. Fallot) T1:399–422

Durand-Delga M, Kornprobst J (1963) Esquisse geologique de la region de Ceuta (Maroc). Bulletin de la Société Géologique de France S7-V:1049–1057. doi: 10.2113/gssgfbull.S7-V.7.1049

Durand-Delga M (1980) La Méditerranée occidentale : étapes de sa genèse et problèmes structuraux liés à celle-ci. Mémoire Hors Serie Société Géologique France 10:203–224

Durand-Delga M, Fontboté JM (1980) Le cadre structural de la Méditerranée occidentale. Mémoires du Bureau de Recherches Géologiques et Minières 115:67–85

Durand-Delga M (2006) Geological adventures and misadventures of the Gibraltar Arc. Zeitschrift der Deutschen Gesellschaft für Geowissenschaften (ZDGG) 687–716. doi: 10.1127/1860-1804/2006/0157-0687

Ediger V, Okyar M, Ergin M (1993) Seismic stratigraphy of the fault-controlled submarine canyon/valley system on the shelf and upper slope of Anamur Bay, Northeastern Mediterranean Sea. Marine Geology 115:129–142. doi: 10.1016/0025-3227(93)90078-A

Eggenhuisen JT, McCAFFREY WD (2012) The vertical turbulence structure of experimental turbidity currents encountering basal obstructions: implications for vertical suspended sediment distribution in non-equilibrium currents. Sedimentology 59:1101–1120. doi: 10.1111/j.1365-3091.2011.01297.x

El Hatimi N, Duee G (1991) La Dorsale calcaire du Haouz: ancienne marge continentale passive téthysienne (Rif, Maroc). Bulletin de la Société Géologique de France 162:79–90

El Kadiri K, Linares A, Oloriz F (1992) La Dorsale calcaire rifaine (Maroc septentrional): Evolution stratigraphique et géodynamique durant le Jurassique-Crétacé. Notes et Mémoires du Service géologique du Maroc 336:217–265

El Mourabet M (1996) Evolution structurale des Rides Prerifaines et du Bassin du Rharb du Trias au Néogène, basée sur les données de subsurface (sismique reflexion et gravimétrie). Thèse 3ème cycle, Université Mohammed V

El Mourabet M, Barakat A, El Baghdadi M, Zaghloul MN (2017a) Geochemistry of fine-grained syn-orogenic Zoumi Flysch (External Rif, Mesorif sub-domain, Morocco): new constraints for paleoweathering, geological processes and geodynamic setting. Oral Communication The First International ASRO, Geological Congress [ASRO – GC- 2017]

El Mourabet M, Barakat A, Rais J, Zaghloul MN (2017b) New petrographic constraints for a mixed mode provenance of Middle Miocene syn-orogenic Zoumi Sandstone suites (External Rif, Mesorif sub-domain, Morocco): implication for paleoclimate and geodynamic context. Oral Communication The First International ASRO, Geological Congress [ASRO – GC- 2017]

El Mourabet M, Barakat A, Rais J, Zaghloul MN (2017c) Sedimentology and lithostratigraphy of Middle Miocene syn-orogenic Zoumi Flysch (External Rif, Mesorif Sub-Domain, Morocco): Depositional processes and palaeoenvironments. Oral Communication The First International ASRO, Geological Congress [ASRO – GC- 2017]

El Mourabet M, Barakat A, Rais J, et al (2018a) Petrology of lower-middle Miocene Zoumi Flysch Fm. (Mesorif sub-domain, Rif belt, Morocco): first evidence of mixed mode provenance and geodynamic setting. Arab J Geosci 11:209. doi: 10.1007/s12517-018-3485-7

El Mourabet M, Barakat A, Zaghloul MN, Baghdadi ME (2018b) Geochemistry of the Miocene Zoumi flysch thrust-top basin (External Rif, Morocco): new constraints on source area weathering, recycling processes, and paleoclimate conditions. Arab J Geosci 11:126. doi: 10.1007/s12517-018-3465-y

El Ouaragli B, Zaghloul MN, Talibi HE, Somma R (2016) Tectono-sedimentary evolution of the

Miocene Oued Dayr Formation (Ghomaride Complex, Internal Domain of the Maghrebian Rif Belt, Morocco). Arab J Geosci 9:660. doi: 10.1007/s12517-016-2663-8

Embley RW (1980) The role of mass transport in the distribution and character of deep-ocean sediments with special reference to the North Atlantic. Marine Geology 38:23–50. doi: 10.1016/0025-3227(80)90050-X

Enos P (1977) Flow regimes in debris flow. Sedimentology 24:133–142. doi: 10.1111/j.1365-3091.1977.tb00123.x

Enos P (2009) Flow Regimes in Debris Flow. In: Deep-Water Turbidite Systems. Wiley-Blackwell, pp 79–88

Ewing M, Thorndike EM (1965) Suspended Matter in Deep Ocean Water. Science 147:1291–1294. doi: 10.1126/science.147.3663.1291

Fallot P (1937) Essai sur la géologie du Rif septentrional. Notes et Mémoires du Service géologique du Maroc 40:548p

Favre P, Stampfli GM (1992) From rifting to passive margin: the examples of the Red Sea, Central Atlantic and Alpine Tethys. Tectonophysics 215:69–97. doi: 10.1016/0040-1951(92)90075-H

Favre P (1995) Analyse quantitative du rifting et de la relaxation thermique de la partie occidentale de la marge transformante nord-africaine: le Rif externe (Maroc). Geodinamica Acta 8:59–81. doi: 10.1080/09853111.1995.11105275

Fedo CM, Nesbitt HW, Young GM (1995) Unraveling the effects of potassium metasomatism in sedimentary rocks and paleosols, with implications for paleoweathering conditions and provenance. Geology 23:921–924. doi: 10.1130/0091-7613(1995)023<0921:UTEOPM>2.3.CO;2

Fedo CM, Eriksson KA, Krogstad EJ (1996) Geochemistry of shales from the Archean (~3.0 Ga) Buhwa Greenstone Belt, Zimbabwe: Implications for provenance and source-area weathering. Geochimica et Cosmochimica Acta 60:1751–1763. doi: 10.1016/0016-7037(96)00058-0

Felix M (2001) A two-dimensional numerical model for a turbidity current. In: Particulate Gravity Currents (Eds W.D. McCaffrey, B.C. Kneller and J. Peakall). IAS Spec. Publ., pp 71–81

Felix M (2004) The significance of single value variables in turbidity currents. Journal of Hydraulic Research 42:323–330. doi: 10.1080/00221686.2004.9728398

Felix M, Peakall J, McCaffrey WD (2006) Relative Importance of Processes That Govern the Generation of Particulate Hyperpycnal Flows. Journal of Sedimentary Research 76:382–387. doi: 10.2110/jsr.2006.022

Fisher RV (1983) Flow transformations in sediment gravity flows. Geology 11:273–274. doi: 10.1130/0091-7613(1983)11<273:FTISGF>2.0.CO;2

Flanagan FJ (1976) Descriptions and analyses of eight new USGS rock standards. Washington : U.S. Govt. Print. Off

Flinch JF (1993) Tectonic evolution of the Gibraltar Arc. PHD Thesis, Rice University

Flinch JF (1996) Accretion and extensional collapse of the external western Rif (northern Morocco). In: P.A. ZIEGLER AND F. HORVATH(Eds) Peri-Tethys memoir 2 Structure and prospects of the Alpine basins and forelands. pp 61–85

Flood RD, Piper DJW, Klaus A, Peterson LC (1997) Proceedings Ocean Drilling Program, Scientific Results, 155. College Station, Texas, USA: Ocean Drilling Program

Floyd PA, Winchester JA, Park RG (1989) Geochemistry and tectonic setting of Lewisian clastic metasediments from the Early Proterozoic Loch Maree Group of Gairloch, NW Scotland. Precambrian Research 45:203–214. doi: 10.1016/0301-9268(89)90040-5

Folk RL, Andrews PB, Lewis DW (1970) Detrital sedimentary rock classification and nomenclature for use in New Zealand. New Zealand Journal of Geology and Geophysics 13:937–968. doi: 10.1080/00288306.1970.10418211

Folk RL (1980) Classification of sedimentary rocks

Frizon de Lamotte D, Leikine M (1982) Les massifs externes à schistosité du Rif (Maroc): une zone de coulissement synmetamorphe. Comptes rendus de l'Académie des sciences Série II, Mécanique, physique, chimie, sciences de l'univers, sciences de la terre 293:1285–1290

Frizon de Lamotte D (1985a) La structure du Rif oriental (Maroc), rôle de la tectonique longitudinale et importance des fluides. Thèse Es-Sciences, Université Paris VI

Frizon de Lamotte D (1985b) La structure du rif oriental (Maroc): Rôle de la tectonique longitudinale et importance des fluides. Doctorat d'Etat, Université Pierre et Marie Curie

Frizon de Lamotte D, Crespo-Blanc A, Saint-Bézar B, et al (2004) TRANSMED-transect I (Betics, Alboran Sea, Rif, Moroccan Meseta, High Atlas, Jbel Saghro, Tindouf basin. In : W. Cavazza, F. Roure, W. Spakman, G.M. Stampfli and P. A. Ziegler (eds). The TRANSMED Atlas : the Mediterranean region from crust to mantle

Frizon de Lamotte D, Zaghloul MN, Haissen F, et al (2017) Rif externe: comment comprendre le chaos apparent? 194:13–15

Fukushima Y, Parker G, Pantin HM (1985) Prediction of ignitive turbidity currents in Scripps Submarine Canyon. Marine Geology 67:55–81. doi: 10.1016/0025-3227(85)90148-3

Gandolfi G, Paganelli L, Zuffa GG (1983) Petrology and dispersal pattern in the Marnoso-arenacea Formation (Miocene, Northern Apennines). Journal of Sedimentary Research 53:493–507. doi: 10.1306/212F8215-2B24-11D7-8648000102C1865D

Garcia M, Parker G (1989) Experiments on Hydraulic Jumps in Turbidity Currents Near a

Canyon-Fan Transition. Science 245:393–396. doi: 10.1126/science.245.4916.393

Garcia D, Fonteilles M, Moutte J (1994) Sedimentary Fractionations between Al, Ti, and Zr and the Genesis of Strongly Peraluminous Granites. Journal of Geology - J GEOL 102:411–422. doi: 10.1086/629683

Gazzi P (1966) Le arenarie del flysch sopracretaceo dell'Appenino modenese: correlazione con il flysch di Monghidoro. 12:69–97

Gee MJR, Gawthorpe RL, Friedmann SJ (2006) Triggering and Evolution of a Giant Submarine Landslide, Offshore Angola, Revealed by 3D Seismic Stratigraphy and Geomorphology. Journal of Sedimentary Research 76:9–19. doi: 10.2110/jsr.2006.02

Ghibaudo G (1992) Subaqueous sediment gravity flow deposits: practical criteria for their field description and classification. Sedimentology 39:423–454. doi: 10.1111/j.1365-3091.1992.tb02126.x

Gladstone C, Ritchie LJ, Sparks RSJ, Woods AW (2004) An experimental investigation of density-stratified inertial gravity currents. Sedimentology 51:767–789. doi: 10.1111/j.1365-3091.2004.00650.x

Guerrera F, Martin-Algarra A, Perrone V (1993) Late Oligocene-Miocene syn-/-late-orogenic successions in Western and Central Mediterranean Chains from the Betic Cordillera to the Southern Apennines*. Terra Nova 5:525–544. doi: 10.1111/j.1365-3121.1993.tb00302.x

Guerrera F, Martín-Martín M, Perrone V, Tramontana M (2005) Tectono-sedimentary evolution of the southern branch of the Western Tethys (Maghrebian Flysch Basin and Lucanian Ocean): Consequences for Western Mediterranean geodynamics. Terra Nova 17:358–367. doi: 10.1111/j.1365-3121.2005.00621.x

Hampton MA (1972) The Role of Subaqueous Debris Flow in Generating Turbidity Currents. Journal of Sedimentary Research 42:775–793

Hampton M (1975) Competence of fine-grained debris flows. Journal of Sedimentary Research 45:834–844. doi: 10.1306/212F6E5B-2B24-11D7-8648000102C1865D

Hand BM, Ellison JB (1985) Inverse Grading in Density-current Deposits. Abstracts, 1985 Mid-year meeting, Society of Economic Paleontologists and Mineralogists, Golden, Colorado

Hand BM (1997) Inverse grading resulting from coarse-sediment transport lag. Journal of Sedimentary Research 67:124–129. doi: 10.1306/D426850E-2B26-11D7-8648000102C1865D

Harms JC, Fahnestock RK (1965) Stratification, bed forms, and flow phenomena (with an example from the Rio Grande). Primary Sedimentary Structures and Their Hydrodynamic Interpretation 12:84–115. doi: 10.2110/pec.65.08.0084

Harnois L (1988) The CIW index: A new chemical index of weathering. Sedimentary Geology

55:319–322. doi: 10.1016/0037-0738(88)90137-6

Harris P, Barrie J, W. Conway K, Greene H (2014) Hanging canyons of Haida Gwaii, British Columbia, Canada: Fault-control on submarine canyon geomorphology along active continental margins. Deep Sea Research Part II: Topical Studies in Oceanography 104:83–92. doi: 10.1016/j.dsr2.2013.06.017

Hassan S, Ishiga H, Roser BP, et al (1999) Geochemistry of Permian–Triassic shales in the Salt Range, Pakistan: implications for provenance and tectonism at the Gondwana margin. Chemical Geology 158:293–314. doi: 10.1016/S0009-2541(99)00057-1

Haughton P, Davis C, McCaffrey W, Barker S (2009) Hybrid sediment gravity flow deposits – Classification, origin and significance. Marine and Petroleum Geology 26:1900–1918. doi: 10.1016/j.marpetgeo.2009.02.012

Haughton P, Davis C, McCaffrey W, Barker S (2010) Reply to Comment by R. Higgs on 'Hybrid sediment gravity flows-classification, origin and significance.' Marine and Petroleum Geology 27:2066–2069

Heezen BC, Menzies RG, Schneider ED, et al (1964) Congo submarine canyon. AAPG Bulletin 48:1126–1149

Hein FJ (1982) Depositional mechanisms of deep-sea coarse clastic sediments, Cap Enragé Formation, Quebec. Can J Earth Sci 19:267–287. doi: 10.1139/e82-020

Heller PL, Ryberg PT (1983) Sedimentary record of subduction to forearc transition in the rotated Eocene basin of western Oregon. Geology 11:380–383. doi: 10.1130/0091-7613(1983)11<380:SROSTF>2.0.CO;2

Herron MM (1988) Geochemical Classification of Terrigenous Sands and Shales from Core or Log Data. Journal of Sedimentary Research 58:820–829

Hieronymus B, Kotschoubey B, Boulègue J (2001) Gallium behaviour in some contrasting lateritic profiles from Cameroon and Brazil. Journal of Geochemical Exploration 72:147–163. doi: 10.1016/S0375-6742(01)00160-1

Hill PR, Moran KM, Blasco SM (1982) Creep deformation of slope sediments in the Canadian Beaufort Sea. Geo-Marine Letters 2:163–170. doi: 10.1007/BF02462758

Hill PR (1984a) Facies and sequence analysis of Nova Scotian Slope muds: turbidite vs 'hemipelagic' deposition. Geological Society, London, Special Publications 15:311–318. doi: 10.1144/GSL.SP.1984.015.01.20

Hill PR (1984b) Sedimentary facies of the Nova Scotian upper and middle continental slope, offshore eastern Canada. Sedimentology 31:293–309. doi: 10.1111/j.1365-3091.1984.tb00861.x

Hiscott R, Middleton GV (1979) Depositional mechanics of thick-bedded sandstones at the base of a submarine slope, Tourelle Formation (Lower Ordovician) Quebec, Canada. SEPM (Society for Sedimentary Geology), pp 307–326

Hiscott RN, Middleton GV (1980) Fabric of coarse deep-water sandstones, Tourelle Formation, Quebec, Canada. Journal of Sedimentary Research 50:703–721. doi: 10.1306/212F7AC7-2B24-11D7-8648000102C1865D

Hiscott RN (1984) Ophiolitic source rocks for Taconic-age flysch: Trace-element evidence. GSA Bulletin 95:1261–1267. doi: 10.1130/0016-7606(1984)95<1261:OSRFTF>2.0.CO;2

Hiscott RN, James NP (1985) Carbonate debris flows, Cow Head Group, western Newfoundland. Journal of Sedimentary Research 55:735–745. doi: 10.1306/212F87D3-2B24-11D7-8648000102C1865D

Hiscott RN, Colella A, Pezard P, et al (1993) Basin plain turbidite succession of the Oligocene Izu-Bonin intraoceanic forearc basin. Marine and Petroleum Geology 10:450–466. doi: 10.1016/0264-8172(93)90047-V

Hiscott RN (1994a) Loss of capacity, not competence, as the fundamental process governing deposition from turbidity currents. Journal of Sedimentary Research 64:209–214. doi: 10.2110/jsr.64.209

Hiscott RN (1994b) Traction-carpet stratification in turbidites; fact or fiction? Journal of Sedimentary Research 64:204–208. doi: 10.1306/D4267D57-2B26-11D7-8648000102C1865D

Hiscott RN, Aksu AE (1994) Submarine debris flows and continental slope evolution in front of Quaternary ice sheets, Baffin Bay, Canadian Arctic. Aapg Bulletin - AAPG BULL 78:445–460

Hiscott RN, DeVries M (1995) Internal characteristics of sandbodies of the Ordovician Tourelle Formation, Quebec, Canada. In: Atlas of Deep Water Environments. Springer, Dordrecht, pp 207–211

Hiscott RN, Pickering KT, Bouma AH, et al (1997) Basin-Floor Fans in the North Sea: Sequence Stratigraphic Models vs. Sedimentary Facies: Discussion. AAPG Bulletin 81:662–665

Hiscott RN, Aksu AE, Flood RD, et al (2013) Widespread overspill from a saline density-current channel and its interaction with topography on the south-west Black Sea shelf. Sedimentology 60:1639–1667. doi: 10.1111/sed.12071

Hlila R, Sanz de Galdeano C (1994) Structure, cinématique et chronologie des déformations dans la dorsale du Haouz (Rif, Maroc). Geogaceta 17:95–97

Hofer G, Wagreich M, Neuhuber S (2013) Geochemistry of fine-grained sediments of the upper Cretaceous to Paleogene Gosau Group (Austria, Slovakia): Implications for paleoenvironmental and provenance studies. Geoscience Frontiers 4:449–468. doi: 10.1016/j.gsf.2012.11.009

Hofmann P, Ricken W, Schwark L, Leythaeuser D (2001) Geochemical signature and related climatic-oceanographic processes for early Albian black shales: Site 417D, North

Atlantic Ocean. Cretaceous Research 22:243–257. doi: 10.1006/cres.2001.0253

Hollister CD, McCave IN (1984) Sedimentation under deep-sea storms. Nature 309:220–225. doi: 10.1038/309220a0

Hoyez B (1989) Le Numidien et les flyschs oligo-miocènes de la bordure sud de la Méditerranée occidentale. Unpublished thesis, University of Lille

Hubert JF, Neal WJ (1967) Mineral Composition and Dispersal Patterns of Deep-Sea Sands in the Western North Atlantic Petrologic Province. GSA Bulletin 78:749–772. doi: 10.1130/0016-7606(1967)78[749:MCADPO]2.0.CO;2

Hughes CJE, Shor AN, Piper DJW, Mayer LA (1990) Large-scale current-induced erosion and deposition in the path of the 1929 Grand Banks turbidity current. Sedimentology 37:613–629. doi: 10.1111/j.1365-3091.1990.tb00625.x

Ilstad T, De Blasio FV, Elverhøi A, et al (2004a) On the frontal dynamics and morphology of submarine debris flows. Marine Geology 213:481–497. doi: 10.1016/j.margeo.2004.10.020

Ilstad T, Marr JG, Elverhøi A, Harbitz C (2004b) Laboratory studies of subaqueous debris flows by measurements of pore-fluid pressure and total stress. Marine Geology 213:403–414. doi: 10.1016/j.margeo.2004.10.016

Ingersoll RV, Suczek CA (1979) Petrology and provenance of Neogene sand from Nicobar and Bengal fans, DSDP sites 211 and 218. Journal of Sedimentary Research 49:1217–1228. doi: 10.1306/212F78F1-2B24-11D7-8648000102C1865D

Ingersoll RV, Bullard TF, Ford RL, et al (1984) The effect of grain size on detrital modes: a test of the Gazzi-Dickinson point-counting method. Journal of Sedimentary Research 54:103–116. doi: 10.1306/212F83B9-2B24-11D7-8648000102C1865D

Inman DL, Nordstrom CE, Flick RE (1976) Currents in Submarine Canyons: An Air-Sea-Land Interaction. Annual Review of Fluid Mechanics 8:275–310. doi: 10.1146/annurev.fl.08.010176.001423

Jabaloy-Sánchez A, Azdimousa A, Booth-Rea G, et al (2015) The structure of the Temsamane fold-and-thrust stack (eastern Rif, Morocco): Evolution of a transpressional orogenic wedge. Tectonophysics 663:150–176. doi: 10.1016/j.tecto.2015.02.003

Jacka AD, Beck RH, Germain LSC (1968) Permian deep-sea fans of the Delaware Mountain Group (Guadalupian), Delaware Basin. In: Silver, B.A. (ed.), Guadalupian Facies, Apache Mountain Area, West Texas. pp 49–90

Jobe ZR, Lowe DR, Morris WR (2012) Climbing-ripple successions in turbidite systems: depositional environments, sedimentation rates and accumulation times. Sedimentology 59:867–898. doi: 10.1111/j.1365-3091.2011.01283.x

John CM, Mutti M, Adatte T (2003) Mixed carbonate-siliciclastic record on the North African margin (Malta)—coupling of weathering processes and mid Miocene climate. GSA

Bulletin 115:217–229. doi: 10.1130/0016-7606(2003)115<0217:MCSROT>2.0.CO;2

Johnson DW (1967) The New England-Acadian Shoreline. New York, Hafner Pub Co 608p

Johnson AM (1970) Physical processes in geology;: A method for interpretation of natural phenomena; intrusions in igneous rocks, fractures, and folds, flow of debris and ice, First Edition. Freeman, Cooper, San Francisco

Johnsson MJ, Stallard RF, Meade RH (1988) First-Cycle Quartz Arenites in the Orinoco River Basin, Venezuela and Colombia. The Journal of Geology 96:263–277

Johnsson MJ, Stallard RF (1989) Physiographic controls on the composition of sediments derived from volcanic and sedimentary terrains on Barro Colorado Island, Panama. Journal of Sedimentary Research 59:768–781. doi: 10.1306/212F906B-2B24-11D7-8648000102C1865D

Johnsson MJ (1993) The system controlling the composition of clastic sediments. In: Johnsson MJ and Basu A, eds., Processes Controlling the Composition of Clastic Sediments. Geological Society of America Special Papers. Geological Society of America 284, pp 1–20

Jones KPN, McCave IN, Weaver PPE (1992) Textural and dispersal patterns of thick mud turbidites from the Madeira Abyssal plain. Marine Geology 107:149–173. doi: 10.1016/0025-3227(92)90165-E

Keefer DK (1984) Landslides caused by earthquake. Geological Society of America Bulletin 95:406–421. doi: 10.1130/0016-7606(1984)95<406:LCBE>2.0.CO

Kenyon N, Belderson R, Stride A (1978) Channels, canyons and slump folds on continental slope between southwest ireland and spain. Oceanologica Acta 1:369–380

Kenyon NH, Akhmetzhanov AM, Twichell DC (2002) Sand wave fields beneath the Loop Current, Gulf of Mexico: reworking of fan sands. Marine Geology 192:297–307. doi: 10.1016/S0025-3227(02)00560-1

Kneller BC, Branney MJ (1995) Sustained high-density turbidity currents and the deposition of thick massive sands. Sedimentology 42:607–616. doi: 10.1111/j.1365-3091.1995.tb00395.x

Knudson KP, Hendy IL (2009) Climatic influences on sediment deposition and turbidite frequency in the Nitinat Fan, British Columbia. Marine Geology 262:29–38. doi: 10.1016/j.margeo.2009.03.002

Komar PD (1971) Hydraulic Jumps in Turbidity Currents. GSA Bulletin 82:1477–1488. doi: 10.1130/0016-7606(1971)82[1477:HJITC]2.0.CO;2

Kornprobst J (1974) Contribution à l'étude pétrographique et structurale de la zone interne du Rif (Maroc septentrional). Ed. du service géologique du Maroc, Rabat, Maroc

Kuenen PH (1951) Properties of turbidity currents of high density. In: Hough, J.L. (ed.), Turbidity Currents. SEPM (Society for Sedimentary Geology), pp 14–33

Kuribayashi E, Tatsuoka F (1977) History of earthquake-induced soil liquefaction in Japan. Public Works Research Bulletin (Japan Ministry of Construction) 31:1–26

Lacoste JC, Maroc. Service des mines et de la carte géologique (1934) Carte géologique provisoire de la région rifaine méridionale: Feuille ouest, feuille est, échelle 1/100 000

Lacoste J, Marcais J (1938) Sur la nature et l'importance des chevauchements entre le Haut-Ouergha et le Haut Leben (Nord Marocain). C R somm séances Soc géol Fr 7:112–113

Lavier LL, Steckler MS, Brigaud F (2001) Climatic and tectonic control on the Cenozoic evolution of the West African margin. Marine Geology 178:63–80. doi: 10.1016/S0025-3227(01)00175-X

Le Pera E, Mongelli G, Chough S (2000) Compositional and Geochemical Signature of Provenance in Modern Sediments from the Tyrrhenian Continental Shelf, Calabria, Italy. Giornale di Geologia 49–67

Leblanc D (1979) Etude géologique du Rif externe oriental au Nord de Taza (Maroc). Notes Mem Serv Geol Maroc 281:160p

Leblanc D (1983) Carte géologique du Maroc au 1/50 000, feuille de Taïneste. Notes et Mémoires du Service géologique du Maroc 305p

Leblanc D, Olivier P (1984) Role of strike-slip faults in the Betic-Rifian orogeny. Tectonophysics 101:345–355. doi: 10.1016/0040-1951(84)90120-3

Leeder MR (1983) On the dynamics of sediment suspension by residual Reynolds stresses—confirmation of Bagnold's theory. Sedimentology 30:485–491. doi: 10.1111/j.1365-3091.1983.tb00687.x

Legros F (2002) Can Dispersive Pressure Cause Inverse Grading in Grain Flows? Journal of Sedimentary Research 72:166–170. doi: 10.1306/041301720166

Lepera E, Mongelli G, Critelli S (2000) Compositional and geochemical signature of provenance in modern sediments from the tyrrhenian continental shelf, Calabria, Italy. Giornale di Geologia 62:49–67

Lespinasse P (1975) Géologie des zones externes et des flyschs entre Chaouen et Zoumi (centre de la chaîne rifaine, Maroc). Université Pierre et Marie Curie-Paris VI

Long X, Yuan C, Sun M, et al (2012) Geochemistry and Nd isotopic composition of the Early Paleozoic flysch sequence in the Chinese Altai, Central Asia: Evidence for a northward-derived mafic source and insight into Nd model ages in accretionary orogen. Gondwana Research 22:554–566. doi: 10.1016/j.gr.2011.04.009

Lowe DR, LoPiccolo RD (1974) The characteristics and origins of dish and pillar structures. Journal of Sedimentary Research 44:484–501. doi: 10.1306/74D72A68-2B21-11D7-

8648000102C1865D

Lowe DR (1976) Grain flow and grain flow deposits. Journal of Sedimentary Research 46:188–199. doi: 10.1306/212F6EF1-2B24-11D7-8648000102C1865D

Lowe DR (1982) Sediment gravity flows; II, Depositional models with special reference to the deposits of high-density turbidity currents. Journal of Sedimentary Research 52:279–297. doi: 10.1306/212F7F31-2B24-11D7-8648000102C1865D

Lowe DR (1988) Suspended-load fallout rate as an independent variable in the analysis of current structures. Sedimentology 35:765–776. doi: 10.1111/j.1365-3091.1988.tb01250.x

Lowe DR, Guy M, Palfrey A (2003) Facies of slurry-flow deposits, Britannia Formation (Lower Cretaceous), North Sea: implications for flow evolution and deposit geometry. Sedimentology 50:45–80. doi: 10.1046/j.1365-3091.2003.00507.x

Lowe DR (2006) Subaqueous liquefied and fluidized sediment flows and their deposits. Sedimentology 23:285–308. doi: 10.1111/j.1365-3091.1976.tb00051.x

Maate A (1996) Estratigrafía y evolución palaeogeográfica alpina del Dominio Gomáride (Rif Interno, Marruecos). PHD Thesis, Univ. Granada

Madhavaraju J, Ramasamy S, Ruffell A, Mohan SP (2002) Clay mineralogy of the Late Cretaceous and early Tertiary successions of the Cauvery Basin (southeastern India): implications for sediment source and palaeoclimates at the K/T boundary. Cretaceous Research 23:153–163. doi: 10.1006/cres.2002.0310

Marbut CF (1935) Atlas of American agriculture, part III, soils of the United States. In: United States department of agriculture advance sheets 8. US Government Printing Office, Washington (DC).

Marcais J (1938) Sur l'âge et le style des plissements dans la partie orientale de la chaîne du Rif. Comptes Rendus sommaires des séances de la Société géologique de France 330–331

Marr JG, Harff PA, Shanmugam G, Parker G (2001) Experiments on subaqueous sandy gravity flows: The role of clay and water content in flow dynamics and depositional structures. GSA Bulletin 113:1377–1386. doi: 10.1130/0016-7606(2001)113<1377:EOSSGF>2.0.CO;2

Masson DG, Huggett QJ, Brunsden D (1993) The surface texture of the Saharan Debris Flow deposit and some speculations on submarine debris flow processes. Sedimentology 40:583–598. doi: 10.1111/j.1365-3091.1993.tb01351.x

Mastbergen DR, Berg JHVD (2003) Breaching in fine sands and the generation of sustained turbidity currents in submarine canyons. Sedimentology 50:625–637. doi: 10.1046/j.1365-3091.2003.00554.x

Mattauer M (1960) Nouvelles données sur la « Dorsale calcaire » du Rif. Comptes rendus de l'Académie des sciences Série II, Mécanique, physique, chimie, sciences de l'univers, sciences de la terre 250:374–376

Maynard JB (1992) Chemistry of Modern Soils as a Guide to Interpreting Precambrian Paleosols. The Journal of Geology 100:279–289

McCaffrey W, Kneller B, Peakall J (2001) Particulate Gravity Currents. International Association of Sedimentologists, Special Publication 31

McCave IN, Lonsdale PF, Hollister CD, Gardner WD (1980) Sediment transport over the Hatton and Gardar contourite drifts. Journal of Sedimentary Research 50:1049–1062. doi: 10.1306/212F7B76-2B24-11D7-8648000102C1865D

McCave IN, Jones KPN (1988) Deposition of ungraded muds from high-density non-turbulent turbidity currents. Nature 333:250–252. doi: 10.1038/333250a0

McLennan SM, Taylor SR, McCulloch MT, Maynard JB (1990) Geochemical and Nd/Sr isotopic composition of deep-sea turbidites: Crustal evolution and plate tectonic associations. Geochimica et Cosmochimica Acta 54:2015–2050. doi: 10.1016/0016-7037(90)90269-Q

McLennan SM, Taylor SR (1991) Sedimentary Rocks and Crustal Evolution: Tectonic Setting and Secular Trends. The Journal of Geology 99:1–21. doi: 10.1086/629470

McLennan SM, Hemming S, McDaniel DK, Hanson GN (1993) Geochemical approaches to sedimentation, provenance, and tectonics. In: Johnson MJ, Basu A (Eds.), Processes Controlling the Composition of Clastic Sediments. pp 21–40

McLennan SM, Taylor SR, Hemming S (2006) Composition, differentiation, and evolution of continental crust: constrains from sedimentary rocks and heat flow. In: Evolution and Differentiation of the Continental Crust. Cambridge University Press, pp 92–134

Michard A, Goffe B, Chalouan A, Saddiqi O (1991) Les Correlations entre les chaines Betico-Rifaines et les Alpes et leurs consequences. Bulletin de la Société Géologique de France 162:1151–1160

Michard A, Feinberg H, El-Azzab D, et al (1992) A serpentinite ridge in a collisional paleomargin setting: the Beni Malek massif, External Rif, Morocco. Earth and Planetary Science Letters 113:435–442. doi: 10.1016/0012-821X(92)90144-K

Michard A, Chalouan A, Feinberg H, et al (2002) How does the Alpine belt end between Spain and Morocco ? Bulletin de la Société Géologique de France 173:3–15. doi: 10.2113/173.1.3

Michard A, Negro F, Saddiqi O, et al (2006) Pressure–temperature–time constraints on the Maghrebide mountain building: evidence from the Rif–Betic transect (Morocco, Spain), Algerian correlations, and geodynamic implications. Comptes Rendus Geoscience 338:92–114. doi: 10.1016/j.crte.2005.11.011

Michard A, Negro F, Frizon de Lamotte D, Saddiqi O (2007) Serpentinite slivers and metamorphism in the External Maghrebides: arguments for an intracontinental suture in the African paleomargin (Morocco, Algeria). Rev Soc Geol Espana 20:173–185

Michard A, Mokhtari A, Chalouan A, et al (2014) New ophiolite slivers in the External Rif belt, and tentative restoration of a dual Tethyan suture in the western Maghrebides. Bulletin de la Societe Geologique de France 185:313–328. doi: 10.2113/gssgfbull.185.5.313

Middleton GV (1967) Experiments on Density and Turbidity Currents: Iii. Deposition of Sediment. Can J Earth Sci 4:475–505. doi: 10.1139/e67-025

Middleton GV (1970) Experimental studies related to problems of flysch sedimentation. In: Lajoie, J. (ed.), Flysch sedimentology in North America. The Geological Association of Canada Special paper, pp 405–426

Middleton GV, Bouma AH (1973) Turbidites and Deep Water Sedimentation: Frontmatter. i–iii

Middleton GV, Hampton M (1973) Sediment gravity flows: mechanics of flow and deposition. In: Middleton, G.V. & Bouma, A.H. (eds), Turbidites and Deep Water Sedimentation. Short course notes, Pacific Section of The Society of Economic Paleontologists and Mineralogists. pp 1–38

Middleton GV (1976) Hydraulic Interpretation of Sand Size Distributions. The Journal of Geology 84:405–426

Middleton GV, Hampton MA (1976) Subaqueous sediment transport and deposition by sediment gravity flows. In: Stanley, D.J. & Swift, D.J.W. (eds), Marine Sediment Transport and Environmental Management. New York: Wiley, pp 197–218

Middleton GV, Southard BJ (1984) Mechanics of Sediment Transport, 2nd ed. Society of Economic Paleontologists and Mineralogists Eastern Section Short Course No 3, Providence

Middleton GV (1993) Sediment Deposition from Turbidity Currents. Annual Review of Earth and Planetary Sciences 21:89–114. doi: 10.1146/annurev.ea.21.050193.000513

Middleton GV, Wilcock PR (1994) Mechanics in the Earth and Environmental Sciences. Cambridge University Press

Miller KG, Wright JD, Fairbanks RG (1991) Unlocking the Ice House: Oligocene-Miocene oxygen isotopes, eustasy, and margin erosion. Journal of Geophysical Research: Solid Earth 96:6829–6848. doi: 10.1029/90JB02015

Milliard Y (1959) Sur l'existence du Permien dans le massif paléozoique interne du Rif (Maroc). Comptes rendus de l'Académie des sciences Série II, Mécanique, physique, chimie, sciences de l'univers, sciences de la terre 249:1051–1052

Mitchell RL, Sheldon ND (2009) Weathering and paleosol formation in the 1.1Ga

Keweenawan Rift. Precambrian Research 168:271–283. doi: 10.1016/j.precamres.2008.09.013

Mohrig D, Ellis C, Parker G, et al (1998) Hydroplaning of subaqueous debris flows. GSA Bulletin 110:387–394. doi: 10.1130/0016-7606(1998)110<0387:HOSDF>2.3.CO;2

MMongelli G, Cullers RL, Dinelli E, Rottura A (1998) Elemental mobility during the weathering of exposed lower crust: the kinzigitic paragneisses from the Serre, Calabria, southern Italy. Terra Nova 10:190–195. doi: 10.1046/j.1365-3121.1998.104188.x

Mongelli G, Cullers RL, Muelheisen S (1996) Geochemistry of Late Cretaceous-Oligocenic shales from the Varicolori Formation, Southern Apennines, Italy; implications for mineralogical, grain-size control and provenance. European Journal of Mineralogy 8:733–754

ongelli G, Critelli S, Perri F, et al (2006) Sedimentary recycling, provenance and paleoweathering from chemistry and mineralogy of Mesozoic continental redbed mudrocks, Peloritani mountains, southern Italy. Geochem J 40:197–209. doi: 10.2343/geochemj.40.197

Morley CK (1988) The tectonic evolution of the Zoumi Sandstone, western Moroccan Rif. Journal of the Geological Society 145:55–63. doi: 10.1144/gsjgs.145.1.0055

Mulder T, Syvitski JPM (1995) Turbidity Currents Generated at River Mouths during Exceptional Discharges to the World Oceans. The Journal of Geology 103:285–299

Mulder T, Cochonant H. (1996) Classification of offshore mass movement. Journal of Sedimentary Research 66:43–57. doi: 10.1306/D42682AC-2B26-11D7-8648000102C1865D

Mulder T, Savoye B, Syvitski JPM (1997) Numerical modelling of a mid-sized gravity flow: the 1979 Nice turbidity current (dynamics, processes, sediment budget and seafloor impact). Sedimentology 44:305–326. doi: 10.1111/j.1365-3091.1997.tb01526.x

Mulder T, Alexander J (2001) The physical character of subaqueous sedimentary density flows and their deposits. Sedimentology 48:269–299. doi: 10.1046/j.1365-3091.2001.00360.x

Mulder T, Syvitski JPM, Migeon S, et al (2003) Marine hyperpycnal flows: initiation, behavior and related deposits. A review. Marine and Petroleum Geology 20:861–882. doi: 10.1016/j.marpetgeo.2003.01.003

Mutti E, Ricci Lucchi F (1972) Le torbiditi dell'Appennino settentrionale: introduzione all'analisi di facies. Memorie della Società geologica italiana 11:161–199

Mutti E, Ghibaudo G (1972) Un Esempio di torbiditi di conoide sottomarina esterna: le Arenarie di San Salvatore (formazione di Bobbio, Miocene) nell'Appennino di Piacenza: memoria di Emiliano Mutti e Guido Ghibaudo. Accademia delle scienze, Torino

Mutti E, Ricci Lucchi F (1975) Turbidite Facies and Facies Associations. In: Examples of Turbidite Facies and Facies Associations from Selected Formations of the Northern Apennines, Field Trip Guidebook. IX International Congress of Sedimentologists, Nice, France. pp 21–36

Mutti E (1977) Distinctive thin-bedded turbidite facies and related depositional environments in the Eocene Hecho Group (South-central Pyrenees, Spain). Sedimentology 24:107–131. doi: 10.1111/j.1365-3091.1977.tb00122.x

Mutti E (1979) Turbidites et cônes sous-marins profonds. In: Homewood, P. (ed.), Sedimentation détritique (fluviatile, littorale et marine). Switzerland: Institut Geologique, Université de Fribourg, pp 353–419

Mutti E, Johns D (1979) The role of sedimentary by-passing in the genesis of fan fringe and basin plain turbidites in the Hecho Group System (South-Central Pyrenees). Memoria Geological Society of Italy Mem. Geol.Soc.It:15–22

Mutti E, Normark WR (1987) Comparing Examples of Modern and Ancient Turbidite Systems: Problems and Concepts. In: Marine Clastic Sedimentology. Springer, Dordrecht, pp 1–38

Mutti E, Normark WR (1991) An Integrated Approach to the Study of Turbidite Systems. In: Seismic Facies and Sedimentary Processes of Submarine Fans and Turbidite Systems. Springer, New York, NY, pp 75–106

Mutti E (1992) Turbidite sandstones. Agip, Instituto di geologia, Università di Parma

Nakajima T, Satoh M, Okamura Y (1998) Channel-levee complexes, terminal deep-sea fan and sediment wave fields associated with the Toyama Deep-Sea channel system in the Japan Sea. Marine Geology 147:25–41. doi: 10.1016/S0025-3227(97)00137-0

Naylor MA (1980) The origin of inverse grading in muddy debris flow deposits; a review. Journal of Sedimentary Research 50:1111–1116. doi: 10.1306/212F7B8F-2B24-11D7-8648000102C1865D

Negró F (2005) Exhumation des roches métamorphiques du domaine d'Alboran: étude de la chaîne rifaine (Maroc) et corrélation avec les cordillères bétiques (Espagne). Thèse de doctorat Université, Paris XI, Orsay

Negro F, Agard P, Goffé B, Saddiqi O (2007) Tectonic and metamorphic evolution of the Temsamane units, External Rif (northern Morocco): implications for the evolution of the Rif and the Betic–Rif arc. Journal of the Geological Society 164:829–842. doi: 10.1144/0016-76492006-112

Nelson CH, Twichell DC, Schwab WC, et al (1992) Upper Pleistocene turbidite sand beds and chaotic silt beds in the channelized, distal, outer-fan lobes of the Mississippi fan. Geology 20:693–696. doi: 10.1130/0091-7613(1992)020<0693:UPTSBA>2.3.CO;2

Nesbitt HW, Markovics G, price RC (1980) Chemical processes affecting alkalis and alkaline earths during continental weathering. Geochimica et Cosmochimica Acta 44:1659–1666. doi: 10.1016/0016-7037(80)90218-5

Nesbitt HW, Young GM (1982) Early Proterozoic climates and plate motions inferred from major element chemistry of lutites. Nature 299:715–717. doi: 10.1038/299715a0

Nesbitt HW, Young GM (1984) Prediction of some weathering trends of plutonic and volcanic rocks based on thermodynamic and kinetic considerations. Geochimica et Cosmochimica Acta 48:1523–1534. doi: 10.1016/0016-7037(84)90408-3

Nesbitt HW, Young GM (1989) Formation and Diagenesis of Weathering Profiles. The Journal of Geology 97:129–147

Nesbitt HW (1992) Diagenesis and metasomatism of weathering profiles, with emphasis on Precambrian paleosols. In: Martini IP, Chesworth W (eds) Developments in Earth Surface Processes. Elsevier, pp 127–152

Nesbitt HW, Young GM, McLennan SM, Keays RR (1996) Effects of Chemical Weathering and Sorting on the Petrogenesis of Siliciclastic Sediments, with Implications for Provenance Studies. The Journal of Geology 104:525–542

Nesbitt WH, Fedo C, Young G (1997) Quartz and Feldspar Stability, Steady and Non-Steady-State Weathering, and Petrogenesis of Siliciclastic Sands and Muds. The Journal of Geology 105:173–191. doi: 10.1086/515908

Nold M, Uttinger J, Wildi W (1981) Géologie de la dorsale calcaire entre Tétouan et Assifane (Rif interne, Maroc). Notes et Mémoires du Service géologique du Maroc 233:1–233

Normark WR (1970) Growth Patterns of Deep-Sea Fans. AAPG Bulletin 54:2170–2195

Normark WR, Piper DJW (1984) Navy Fan, California Borderland: Growth pattern and depositional processes. Geo-Marine Letters 3:101–108. doi: 10.1007/BF02462454

Normark WR, Piper D (1991) Initiation processes and flow evolution of turbidity currents: Implications for the depositional record. From shoreline to abyss: contributions in marine geology in honor of Francis Parker Shepard 46:207–230

Normark WR, Posamentier H, Mutti E (1993a) Turbidite systems: State of the art and future directions. Reviews of Geophysics 31:91–116. doi: 10.1029/93RG02832

Normark WR, Wilde P, Campbell JF, et al (1993b) Submarine slope failures initiated by Hurricane Iwa, Kahe Point, Oahu, Hawaii. Bulletin of the US Geological Survey 202:197–204

Normark, Piper, Hiscott (1998) Sea level controls on the textural characteristics and depositional architecture of the Hueneme and associated submarine fan systems, Santa Monica Basin, California. Sedimentology 45:53–70. doi: 10.1046/j.1365-3091.1998.00139.x

Normark WR, Piper DJW, Sliter R (2006) Sea-level and tectonic control of middle to late Pleistocene turbidite systems in Santa Monica Basin, offshore California. Sedimentology 53:867–897. doi: 10.1111/j.1365-3091.2006.00797.x

Olivier P (1984) Evolution de la limite entre zones internes et zones externes dans l'arc de Gibraltar (Maroc-Espagne). Thése d'Etat, Université de Toulouse

Ori GG, Friend PF (1984) Sedimentary basins formed and carried piggyback on active thrust sheets. Geology 12:475–478. doi: 10.1130/0091-7613(1984)12<475:SBFACP>2.0.CO;2

Ouaragli BE, Zaghloul MN, Talibi HE, Somma R (2016) Tectono-sedimentary evolution of the Miocene Oued Dayr Formation (Ghomaride Complex, Internal Domain of the Maghrebian Rif Belt, Morocco). Arab J Geosci 9:660. doi: 10.1007/s12517-016-2663-8

Pantin HM (1979) Interaction between velocity and effective density in turbidity flow: Phase-plane analysis, with criteria for autosuspension. Marine Geology 31:59–99. doi: 10.1016/0025-3227(79)90057-4

Parker G (1982) Conditions for the ignition of catastrophically erosive turbidity currents. Marine Geology 46:307–327. doi: 10.1016/0025-3227(82)90086-X

Peakall J, Felix M, Mccaffrey B, Kneller B (2001) Particulate gravity currents: Perspectives. Particulate Gravity Currents 31:1–8

Peltola P, Brun C, Astrom M, Tomilina O (2008) High K/Rb ratios in stream waters — Exploring plant litter decay, ground water and lithology as potential controlling mechanisms. Chemical Geology 257:92–100. doi: 10.1016/j.chemgeo.2008.08.009

Perri F, Cirrincione R, Critelli S, et al (2008) Clay Mineral Assemblages and Sandstone Compositions of the Mesozoic Longobucco Group, Northeastern Calabria: Implications for Burial History and Diagenetic Evolution. International Geology Review 50:1116–1131. doi: 10.2747/0020-6814.50.12.1116

Perri F, Critelli S, Mongelli G, Cullers R (2011) Sedimentary evolution of the Mesozoic continental redbeds using geochemical and mineralogical tools: The case of Upper Triassic to Lowermost Jurassic Monte di Gioiosa mudrocks (Sicily, southern Italy). International Journal of Earth Sciences 100:1569–1587. doi: 10.1007/s00531-010-0602-6

Perri F, Critelli S, Dominici R, et al (2012) Provenance and accommodation pathways of late Quaternary sediments in the deep-water northern Ionian Basin, southern Italy. Sedimentary Geology 280:244–259. doi: 10.1016/j.sedgeo.2012.01.007

Perri F (2014) Composition, provenance and source weathering of Mesozoic sandstones from Western-Central Mediterranean Alpine Chains. Journal of African Earth Sciences 91:32–43. doi: 10.1016/j.jafrearsci.2013.12.002

Perri F, Caracciolo L, Cavalcante F, et al (2016) Sedimentary and thermal evolution of the

Eocene-Oligocene mudrocks from the southwestern Thrace Basin (NE Greece). Basin Research 28:1–21. doi: 10.1111/bre.12112

Perrone V, Martín-Algarra A, Critelli S, et al (2006) 'Verrucano' and 'Pseudoverrucano' in the Central-Western Mediterranean Alpine Chains: palaeogeographical evolution and geodynamic significance. Geological Society, London, Special Publications 262:1–43. doi: 10.1144/GSL.SP.2006.262.01.01

Petrelli M, Poli G, Perugini D, Peccerillo A (2005) PetroGraph: A new software to visualize, model, and present geochemical data in igneous petrology. Geochemistry, Geophysics, Geosystems 6:1–15. doi: 10.1029/2005GC000932

Pettijohn FJ, Potter PE, Siever R (1972) Sand and Sandstone, 2nd edn. Springer-Verlag, New York, Heidelberg, Berlin

Pickering KT (1979) Possible retrogressive flow slide deposits from the Kongsfjord Formation: a Precambrian submarine fan, Finnmark, N. Norway. Sedimentology 26:295–306. doi: 10.1111/j.1365-3091.1979.tb00356.x

Pickering KT (1982) The shape of deep-water siliciclastic systems: A discussion. Geo-Marine Letters 2:41–46. doi: 10.1007/BF02462798

Pickering KT (1985) Kongsfjord Turbidite System, Norway. In: Submarine Fans and Related Turbidite Systems. Springer, New York, NY, pp 237–244

Pickering KT, Hiscott RN (1985) Contained (reflected) turbidity currents from the Middle Ordovician Cloridorme Formation, Quebec, Canada: an alternative to the antidune hypothesis. Sedimentology 32:373–394. doi: 10.1111/j.1365-3091.1985.tb00518.x

Pickering K, Stow D, Watson M, Hiscott R (1986) Deep-water facies, processes and models: a review and classification scheme for modern and ancient sediments. Earth-Science Reviews 23:75–174. doi: 10.1016/0012-8252(86)90001-2

Pickering KT, Hiscott RN, Hein FJ (1989) Deep-marine environments: Clastic Sedimentation and Tectonics. Allen & Unwin Australia

Pickering KT, Corregidor J (2005) Mass transport complexes and tectonic control on confined basin-floor submarine fans, Middle Eocene, south Spanish Pyrenees. Geological Society, London, Special Publications 244:51–74. doi: 10.1144/GSL.SP.2005.244.01.04

Pickering KT, Hiscott RN (2015) Deep Marine Systems: Processes, Deposits, Environments, Tectonics and Sedimentation, Har/Psc edition. Wiley-Blackwell, Chichester, West Sussex ; Hoboken, NJ

Pierson TC (1981) Dominant particle support mechanisms in debris flows at Mt Thomas, New Zealand, and implications for flow mobility. Sedimentology 28:49–60. doi: 10.1111/j.1365-3091.1981.tb01662.x

Piper DJW (1978) Turbidite muds and silts on deep-sea fans and abyssal plains. In: Stanley, D.J. &Kelling, G. (eds), Sedimentation in Submarine Canyons, Fans, and Trenches.

Stroudsburg, PA: Dowden, Hutchinson & Ross., 1st Edition. Dowden,Hutchinson & Ross Inc., Stroudsburg, Pa, pp 163–176

Piper DJW, Stow DAV (1991) Fine-grained turbidites. In: Einsele, G., Ricken, W. & Seilacher, A. (eds), Cycles and Events in Stratigraphy. Berlin: Springer-Verlag, pp 360–376

Piper DJ, Deptuck M (1997) Fined-grained turbidites of the Amazon Fan: facies characterization and interpretation. In: Flood, R.D., Piper, D.J.W., Klaus, A. et al., Proceedings Ocean Drilling Program, Scientific Result. College Station, Texas, USA: Ocean Drilling Program. NATIONAL SCIENCE FOUNDATION, pp 79–108

Popescu I, Lericolais G, Panin N, et al (2004) The Danube submarine canyon (Black Sea): morphology and sedimentary processes. Marine Geology 206:249–265. doi: 10.1016/j.margeo.2004.03.003

Postma G, Nemec W, Kleinspehn KL (1988) Large floating clasts in turbidites: a mechanism for their emplacement. Sedimentary Geology 58:47–61. doi: 10.1016/0037-0738(88)90005-X

Potter PE (1978) Significance and Origin of Big Rivers. The Journal of Geology 86:13–33

Pratson FL, Imran J, Parker G, et al (2000) Debris flows vs. turbidity currents: A modeling comparison of their dynamics and deposits. In: Bouma, A.H. & Stone, C.G. (eds), Fine-Grained Turbidite Systems, American Association of Petroleum Geologists. Memoir, 72 & Society of Sedimentary Geologists, Special Publication, 68. Joint publication, Tulsa, Oklahoma. pp 55–72

Prave AR, Duke WL (1990) Small-scale hummocky cross-stratification in turbidites: a form of antidune stratification? Sedimentology 37:531–539. doi: 10.1111/j.1365-3091.1990.tb00152.x

Prior DB, Coleman JM (1982) Active Slides and Flows in Underconsolidated Marine Sediments on the Slopes of the Mississippi Delta. In: Saxov, S. &Nieuwenhuis, J.K. (eds), Marine Slides and Other Mass Movements. Springer, Boston, MA, pp 21–49

Ratcliffe K, Wright M, Montgomery P, et al (2010) Application of chemostratigraphy to the Mungaroo Formation, the Gorgon field, offshore northwest Australia. The APPEA Journal 50:371–388. doi: 10.1071/AJ09022

Ratcliffe K, M. Wright A, Hallsworth C, et al (2004) An example of alternative correlation techniques in a low-accommodation setting, nonmarine hydrocarbon system: The (Lower Cretaceous) Mannville Basal Quartz succession of southern Alberta. AAPG Bulletin 88:1419–1432. doi: 10.1306/05100402035

Reading HG, Richards M (1994) Turbidite Systems in Deep-Water Basin Margins Classified by Grain Size and Feeder System. AAPG Bulletin 78:792–822

Retallack GJ (1990) Soils of the Past: An introduction to paleopedology. Springer Netherlands

Retallack GJ (2001) Cenozoic Expansion of Grasslands and Climatic Cooling. The Journal of

Geology 109:407–426. doi: 10.1086/320791

Ricci L (1975a) Miocene palaeogeography and basin analysis in the Periadriatic Apennines. In: Squyres, C. (ed.), Geology of Italy. pp 5–111

Ricci-Lucchi F (1975b) Depositional cycles in two turbidite formations of northern Apennines. Journal of Sedimentary Research 45:3–43. doi: 10.1306/212F6CB7-2B24-11D7-8648000102C1865D

Ricci Lucchi F (1995) Sedimentographica : photographic atlas of sedimentary structures, 2nd ed. New York : Columbia University Press

Richards M, Bowman M, Reading H (1998) Submarine-fan systems i: characterization and stratigraphic prediction. Marine and Petroleum Geology 15:689–717. doi: 10.1016/S0264-8172(98)00036-1

Rieu R, Allen PA, Plötze M, Pettke T (2007) Climatic cycles during a Neoproterozoic “snowball” glacial epoch. Geology 35:299–302. doi: 10.1130/G23400A.1

Roddaz M, Viers J, Brusset S, et al (2006) Controls on weathering and provenance in the Amazonian foreland basin: Insights from major and trace element geochemistry of Neogene Amazonian sediments. Chemical Geology 226:31–65. doi: 10.1016/j.chemgeo.2005.08.010

Roser BP, Korsch RJ (1986) Determination of Tectonic Setting of Sandstone-Mudstone Suites Using \$ SiO_{2}\$ Content and \$K_{2}O/Na_{2}O\$ Ratio. The Journal of Geology 94:635–650

Roser BP, Korsch RJ (1988) Provenance signatures of sandstone-mudstone suites determined using discriminant function analysis of major-element data. Chemical Geology 67:119–139. doi: 10.1016/0009-2541(88)90010-1

Rothman DH, Grotzinger JP, Flemings P (1994) Scaling in turbidite deposition. Journal of Sedimentary Research 64:59–67. doi: 10.1306/D4267D07-2B26-11D7-8648000102C1865D

Roy PD, Caballero M, Lozano R, Smykatz-Kloss W (2008) Geochemistry of late quaternary sediments from Tecocomulco lake, central Mexico: Implication to chemical weathering and provenance. Chemie der Erde - Geochemistry 68:383–393. doi: 10.1016/j.chemer.2008.04.001

Roy DK, Roser BP (2013) Climatic control on the composition of Carboniferous–Permian Gondwana sediments, Khalaspir basin, Bangladesh. Gondwana Research 23:1163–1171. doi: 10.1016/j.gr.2012.07.006

Sadler PM (1982) Bed-thickness and grain size of turbidites. Sedimentology 29:37–51. doi: 10.1111/j.1365-3091.1982.tb01707.x

Sadler MP (2006) Bed Thickness and Grain Size of Turbidites. Sedimentology 29:37–51. doi: 10.1111/j.1365-3091.1982.tb01707.x

Salaheldin TM, Imran J, Chaudhry MH, Reed C (2000) Role of fine-grained sediment in turbidity current flow dynamics and resulting deposits. Marine Geology 171:21–38. doi: 10.1016/S0025-3227(00)00114-6

SamaKa F, Benyaich A, Dakki M, et al (1997) Origine et inversion des bassins miocènes supra-nappes du Rif Central (Maroc) Étude de surface et de subsurface. Geodinamica Acta 10:30–40. doi: 10.1080/09853111.1997.11105291

Schneider RR, Muller PJ, Kroon D, Alexander I (1997) Monsoon related variations in Zaire (Congo) sediment load and influence of fluvial silicate supply on marine productivity in the east equatorial Atlantic during the last 200,000 years. Paleoceanography 12:463–481. doi: 10.1029/96PA03640

Schwab W, C. Twichell D, Lee H, et al (1996) Sediment mass-flow processes on a depositional lobe, outer Mississippi Fan. Journal of Sedimentary Research 66:916–927. doi: 10.1306/D426843C-2B26-11D7-8648000102C1865D

Seed HB, Lee KL (1966) Liquefaction of Saturated Sands During Cyclic Loading. Journal of the Soil Mechanics and Foundations Division 92:105–134

Shanmugam G, Moiola RJ (1988) Submarine fans: Characteristics, models, classification, and reservoir potential. Earth-Science Reviews 24:383–428. doi: 10.1016/0012-8252(88)90064-5

Shanmugam G, D. Spalding T, H. Rofheart D (1993a) Process sedimentology and reservoir quality of deep-marine bottom-current reworked sands (sandy contourites): An example from the Gulf of Mexico. AAPG Bull 77:1241–1259

Shanmugam G, Spalding TD, Rofheart DH (1993b) Traction structures in deep-marine, bottom-current-reworked sands in the Pliocene and Pleistocene, Gulf of Mexico. Geology 21:929–932. doi: 10.1130/0091-7613(1993)021<0929:TSIDMB>2.3.CO;2

Shanmugam G, Bloch RB, Mitchell SM, et al (1995) Basin-Floor Fans in the North Sea: Sequence Stratigraphic Models vs. Sedimentary Facies. AAPG Bulletin 79:477–511

Shanmugam G, Moiola RJ (1995) Reinterpretation of Depositional Processes in a Classic Flysch Sequence (Pennsylvanian Jackfork Group), Ouachita Mountains, Arkansas and Oklahoma. AAPG Bulletin 79:672–695

Shanmugam G (2000) 50 years of the turbidite paradigm (1950s—1990s): deep-water processes and facies models—a critical perspective. Marine and Petroleum Geology 17:285–342. doi: 10.1016/S0264-8172(99)00011-2

Shanmugam G (2008) Deep-water Bottom Currents and their Deposits. In: Rebesco, M. & Camerlenghi, A. (eds), Contourites, 59–81. Developments in Sedimentology. Elsevier, pp 59–81

Sheldon ND, Retallack GJ, Tanaka S (2002) Geochemical Climofunctions from North American Soils and Application to Paleosols across the Eocene-Oligocene Boundary in Oregon.

The Journal of Geology 110:687–696. doi: 10.1086/342865

Shepard FP (1977) Geological oceanography: Evolution of coasts, continental margins & the deep-sea floor, First Edition edition. Crane, Russak, New York, 214p

Shepard FP (1933) Canyons beneath the seas. Scientific Monthly 37:31–39

Shultz AW (1984) Subaerial Debris-Flow Deposition in the Upper Paleozoic Cutler Formation, Western Colorado. Journal of Sedimentary Research 54:759–772

Simm RW, Kidd RB (1983) Submarine debris flow deposits detected by long-range side-scan sonar 1,000-kilometers from source. Geo-Marine Letters 3:13–16. doi: 10.1007/BF02463436

Skipper K (1971) Antidune cross-stratification in a turbidite sequence, Cloridrome Formation, Gaspé, Quebec. Sedimentology 17:51–68. doi: 10.1111/j.1365-3091.1971.tb01130.x

Slack JF, Stevens BPJ (1994) Clastic metasediments of the Early Proterozoic Broken Hill Group, New South Wales, Australia: Geochemistry, provenance, and metallogenic significance. Geochimica et Cosmochimica Acta 58:3633–3652. doi: 10.1016/0016-7037(94)90155-4

Sohn YK (1997) On traction-carpet sedimentation. Journal of Sedimentary Research 67:502–509. doi: 10.1306/D42685AE-2B26-11D7-8648000102C1865D

Southard BJ, Mackintosh EM (1981) Experimental test of autosuspension. Earth Surface Processes and Landforms 6:103–111. doi: 10.1002/esp.3290060204

Spencer JW (1903) Submarine valleys off the American coast and in the north Atlantic. GSA Bulletin 14:207–226. doi: 10.1130/GSAB-14-207

Stacey MW, Bowen AJ (1988) The vertical structure of density and turbidity currents: Theory and observations. Journal of Geophysical Research: Oceans 93:3528–3542. doi: 10.1029/JC093iC04p03528

Stanley DJ, Swift DJP, American Geological Institute (eds) (1976) Marine sediment transport and environmental management. Wiley, New York

Stanley DJ, Maldonado A (1981) Depositional models for fine-grained sediment in the western Hellenic Trench, Eastern Mediterranean. Sedimentology 28:273–290. doi: 10.1111/j.1365-3091.1981.tb01680.x

Stanley J-D, Kelling G (2018) Sedimentation in submarine canyons, fans, and trenches / edited by Daniel Jean Stanley and Gilbert Kelling. SERBIULA (sistema Librum 20)

Stevenson RK, Whittaker S, Mountjoy EW (2000) Geochemical and Nd isotopic evidence for sedimentary-source changes in the Devonian miogeocline of the southern Canadian Cordillera. GSA Bulletin 112:531–539. doi: 10.1130/0016-7606(2000)112<531:GANIEF>2.0.CO;2

Stevenson CJ, Talling PJ, Wynn RB, et al (2013) The flows that left no trace: Very large-volume turbidity currents that bypassed sediment through submarine channels without eroding the sea floor. Marine and Petroleum Geology 41:186–205. doi: 10.1016/j.marpetgeo.2012.02.008

Stow D a. V (1979) Distinguishing between fine-grained turbidites and contourites on the Nova Scotian deep water margin. Sedimentology 26:371–387. doi: 10.1111/j.1365-3091.1979.tb00915.x

Stow D a. V, Bowen AJ (1980) A physical model for the transport and sorting of fine-grained sediment by turbidity currents. Sedimentology 27:31–46. doi: 10.1111/j.1365-3091.1980.tb01156.x

Stow DAV, Shanmugam G (1980) Sequence of structures in fine-grained turbidites: Comparison of recent deep-sea and ancient flysch sediments. Sedimentary Geology 25:23–42. doi: 10.1016/0037-0738(80)90052-4

Stow D a. V, Piper DJW (1984) Deep-water fine-grained sediments: facies models. Geological Society, London, Special Publications 15:611–646. doi: 10.1144/GSL.SP.1984.015.01.38

Stow DAV, Faugères J-C (2008) Contourite Facies and the Facies Model. In: Rebesco M, Camerlenghi A (eds) Developments in Sedimentology. Elsevier, pp 223–256

Strachan LJ (2008) Flow transformations in slumps: a case study from the Waitemata Basin, New Zealand. Sedimentology 55:1311–1332. doi: 10.1111/j.1365-3091.2007.00947.x

Stromberg SG, Bluck B (1998) Turbidite facies, fluid-escape structures and mechanisms of emplacement of the Oligo-Miocene Aljibe Flysch, Gibraltar Arc, Betics, southern Spain. Sedimentary Geology 115:267–288. doi: 10.1016/S0037-0738(97)00096-1

Sumner EJ, Talling PJ, Amy LA (2009) Deposits of flows transitional between turbidity current and debris flow. Geology 37:991–994. doi: 10.1130/G30059A.1

Surlyk F (1978) Submarine fan sedimentation along fault scarps on tilted fault blocks (Jurassic-Cretaceous boundary, East Greenland). Grønlands Geologiske Undersøgelse, 142p

Suter G (1965) La région du Moyen Ouerrha (Rif, Maroc): étude préliminaire sur la tectonique et la stratigraphie. Notes et Mémoires du Service géologique du Maroc 24:7–1

Suter G (1980a) Carte géologique du Rif Echelle 1: 500.000. Notes et Mémoires du Service géologique du Maroc 245a:21–35

Suter G (1980b) Carte structurale du Rif, 1/500 000. Notes et Mémoires du Service géologique du Maroc 245b:

Suttner LJ (1974) Sedimentary petrographic provinces: An evaluation. In: Paleogeographic Provinces and Provinciality. pp 75–84

Suttner LJ, Dutta PK (1986) Alluvial sandstone composition and paleoclimate; I, Framework mineralogy. Journal of Sedimentary Research 56:329–345. doi: 10.1306/212F8909-2B24-11D7-8648000102C1865D

Takahashi T (1981) Debris Flow. Annu Rev Fluid Mech 13:57–77. doi: 10.1146/annurev.fl.13.010181.000421

Talling PJ, Peakall J, Sparks RSJ, et al (2002) Experimental constraints on shear mixing rates and processes: implications for the dilution of submarine debris flows. Geological Society, London, Special Publications 203:89–103. doi: 10.1144/GSL.SP.2002.203.01.06

Talling PJ, Amy LA, Wynn RB, et al (2004) Beds comprising debrite sandwiched within co-genetic turbidite: origin and widespread occurrence in distal depositional environments. Sedimentology 51:163–194. doi: 10.1111/j.1365-3091.2004.00617.x

Talling PJ, Wynn RB, Rixon R, Schmmidt DN (2010a) How did submarine flows transport boulder sized mud clasts to the fringes of the Mississippi Fan? Journal of Sedimentary Research 80:829–851

Talling PJ, Wynn RB, Schmmidt DN, et al (2010b) How Did Thin Submarine Debris Flows Carry Boulder-Sized Intraclasts for Remarkable Distances Across Low Gradients to the Far Reaches of the Mississippi Fan? Journal of Sedimentary Research 80:829–851. doi: 10.2110/jsr.2010.076

Talling PJ, Masson DG, Sumner EJ, Malgesini G (2012) Subaqueous sediment density flows: Depositional processes and deposit types. Sedimentology 59:1937–2003. doi: 10.1111/j.1365-3091.2012.01353.x

Taylor SR, McLennan SM (1985) The Continental Crust: Its Composition and Evolution, Blackwell, London, 312p

Tejera de Leon J (1993) Les bassins néogènes d'avant-pays du Rif externe occidental liés à la transformante Jebha-Arbaoua (Maroc). Thése d'Etat es-Sciences, Université de Pau et des Pays de l'Adour

Tejera de Leon J, Duee G (2003) Relationships between the Neogene foredeep basins of the western external Riffian belt related to the Arbaoua-Jebha transform fault. Consequence for the interpretation of the evolution of the riffian belt. Travaux Institut Scientifique de Rabat, Série Géologie, Géographie & Physique 21:47–67

Tennyson ME, Cole MR (1978) Tectonic Significance of Upper Mesozoic Methow-Pasayten Sequence, Northeastern Cascade Range, Washington and British Columbia. 499–508

Thomas MFH, Bodin S, Redfern J, Irving DHB (2010) A constrained African craton source for the Cenozoic Numidian Flysch: Implications for the palaeogeography of the western Mediterranean basin. Earth-Science Reviews 101:1–23. doi: 10.1016/j.earscirev.2010.03.003

Thornton SE (1984) Basin model for hemipelagic sedimentation in a tectonically active continental margin: Santa Barbara Basin, California Continental Borderland. Geological Society, London, Special Publications 15:377–394. doi: 10.1144/GSL.SP.1984.015.01.25

Totten MW, Hanan MA, Weaver BL (2000) Beyond whole-rock geochemistry of shales: The importance of assessing mineralogic controls for revealing tectonic discriminants of multiple sediment sources for the Ouachita Mountain flysch deposits. GSA Bulletin 112:1012–1022. doi: 10.1130/0016-7606(2000)112<1012:BWGOST>2.0.CO;2

Vai GB, Martini P, service) S (2001) Anatomy of an orogen : the Apennines and adjacent Mediterranean basins. Dordrecht ; Boston : Kluwer Academic Publishers

Van de Kamp PC, Leake BE (1985) Petrography and geochemistry of feldspathic and mafic sediments of the northeastern Pacific margin. Earth and Environmental Science Transactions of The Royal Society of Edinburgh 76:411–449. doi: 10.1017/S0263593300010646

Van Den Berg JH, Van Gelder A, Mastbergen DR (2004) The importance of breaching as a mechanism of subaqueous slope failure in fine sand. Sedimentology 49:81–95. doi: 10.1111/j.1525-139X.2006.00168.x-i1

van der Lingen GJ (1969) The Turbidite Problem. New Zealand Journal of Geology and Geophysics 12:7–50. doi: 10.1080/00288306.1969.10420225

Van Hinsbergen DJJ, Vissers RLM, Spakman W (2014) Origin and consequences of western Mediterranean subduction, rollback, and slab segmentation. Tectonics 33:393–419. doi: 10.1002/2013TC003349

Verma SP, Armstrong-Altrin JS (2013) New multi-dimensional diagrams for tectonic discrimination of siliciclastic sediments and their application to Precambrian basins. Chemical Geology 355:117–133. doi: 10.1016/j.chemgeo.2013.07.014

Verma SP, Pandarinath K, Verma SK, Agrawal S (2013) Fifteen new discriminant-function-based multi-dimensional robust diagrams for acid rocks and their application to Precambrian rocks. Lithos 168–169:113–123. doi: 10.1016/j.lithos.2013.01.014

Vicente Bravo JC, Robles S (eds) (1995) Large-scale mesotopographic bedforms from the Albion Black Flysch, northern Spain: characterization, setting and comparison with recent channel-lobe transition zone analogues. In: Pickering, K.T., Hiscott, R.N., Kenyon, N.H., Ricci Lucchi, F. & Smith, R.D.A. (eds), Atlas of Deep Water Environments: Architectural Style in Turbidite Systems. London: Chapman and Hall. Springer Netherlands, pp 216–226

Vidal JC (1977) Present structure and evolution of the Rif chain (southern part of the arc of Gibraltar) since the Miocene. Bulletin de la Societe Geologique de France 1:789–796

Vidal JC (1983) Carte géologique du Rif à 1/50000, feuille Dahar Souk. Notes et Mémoires du Service géologique du Maroc 298:

Vital H, Stattegger K (2000) Major and trace elements of stream sediments from the lowermost Amazon River. Chemical Geology 168:151–168. doi: 10.1016/S0009-2541(00)00191-1

Vitale S, Ciarcia S (2013) Tectono-stratigraphic and kinematic evolution of the southern Apennines/Calabria–Peloritani Terrane system (Italy). Tectonophysics 583:164–182. doi: 10.1016/j.tecto.2012.11.004

Vitale S, Zaghloul MN, Tramparulo FD, et al (2014) From Jurassic extension to Miocene shortening: An example of polyphasic deformation in the External Dorsale Calcaire Unit (Chefchaouen, Morocco). Tectonophysics 633:63–76. doi: 10.1016/j.tecto.2014.06.028

Vitale S, Zaghloul MN, El Ouaragli B, et al (2015) Polyphase deformation of the Dorsale Calcaire Complex and the Maghrebian Flysch Basin Units in the Jebha area (Central Rif, Morocco): New insights into the Miocene tectonic evolution of the Central Rif belt. Journal of Geodynamics 90:14–31. doi: 10.1016/j.jog.2015.07.002

Von Rad U, Tahir M (1997) Late Quaternary sedimentation on the outer Indus shelf and slope (Pakistan): evidence from high-resolution seismic data and coring. Marine Geology 138:193–236. doi: 10.1016/S0025-3227(96)00090-4

Walker RG (1965) The Origin and Significance of the Internal Sedimentary Structures of Turbidites. Proceedings of the Yorkshire Geological Society 35:1–32. doi: 10.1144/pygs.35.1.1

Walker RG (1975a) Upper Cretaceous resedimented conglomerates at Wheeler Gorge, California; description and field guide. Journal of Sedimentary Research 45:105–112. doi: 10.1306/212F6CD5-2B24-11D7-8648000102C1865D

Walker RG (1975b) Generalized Facies Models for Resedimented Conglomerates of Turbidite Association. GSA Bulletin 86:737–748. doi: 10.1130/0016-7606(1975)86<737:GFMFRC>2.0.CO;2

Walker RG (1978) Deep-Water Sandstone Facies and Ancient Submarine Fans: Models for Exploration for Stratigraphic Traps. AAPG Bulletin 62:932–966

Walker RG (1985) Mudstones and thin-bedded turbidites associated with the Upper Cretaceous Wheeler Gorge conglomerates, California; a possible channel-levee complex. Journal of Sedimentary Research 55:279–290. doi: 10.1306/212F869D-2B24-11D7-8648000102C1865D

Weaver PPE (1994) Determination of turbidity current erosional characteristics from reworked coccolith assemblages, Canary Basin, north-east Atlantic. Sedimentology 41:1025–1038. doi: 10.1111/j.1365-3091.1994.tb01438.x

Wedepohl KH (1969) Handbook of Geochemistry. Springer-Verlag, Berlin Heidelberg

Weirich FH (1988) Field evidence for hydraulic jumps in subaqueous sediment gravity flows.

Nature 332:626–629. doi: 10.1038/332626a0

Weltje GJ (2006) Ternary sandstone composition and provenance: an evaluation of the 'Dickinson model.' Geological Society, London, Special Publications 264:79–99. doi: 10.1144/GSL.SP.2006.264.01.07

Wetzel A (1993) The Transfer of River Load to Deep-Sea Fans: A Quantitative Approach. AAPG Bulletin 77:1679–1692

Wildi W (1979) Evolution de la plate-forme carbonatee de type austro-alpin de la Dorsale calcaire (Rif interne, Maroc septentrional) au Mesozoique. Bulletin de la Société Géologique de France S7-XXI:49–56. doi: 10.2113/gssgfbull.S7-XXI.1.49

Wildi W, Nold M, Uttinger J (1977) La Dorsale calcaire entre Tetouan et Assifane (Rif interne, Maroc). Eclogae Geologicae Helvetiae 70:371–415

Wildi W (1983) La chaîne tello-rifaine (Algérie, Maroc, Tunisie): structure, stratigraphie et évolution du Trias au Miocène. Revue de géographie physique et de géologie dynamique 24:201–297

Wonham JP, Jayr S, Mougamba R, Chuilon P (2000) 3D sedimentary evolution of a canyon fill (Lower Miocene-age) from the Mandorove Formation, offshore Gabon. Marine and Petroleum Geology 17:175–197. doi: 10.1016/S0264-8172(99)00033-1

Worthington LV (1976) On the North American Circulation. Baltimore: Johns Hopkins University Press

Wrafter JP, Graham JR (1989) Ophiolitic detritus in the Ordovician sediments of South Mayo, Ireland. Journal of the Geological Society 146:213–215. doi: 10.1144/gsjgs.146.2.0213

Wronkiewicz DJ, Kent C C (1989) Geochemistry and provenance of sediments from the Pongola Supergroup, South Africa: Evidence for a 3.0-Ga-old continental craton. Geochimica et Cosmochimica Acta 53:1537–1549. doi: 10.1016/0016-7037(89)90236-6

Yagishita K (1994) Antidunes and traction-carpet deposits in deep-water channel sandstones, Cretaceous, British Columbia, Canada. Journal of Sedimentary Research 64:34–41. doi: 10.1306/D4267CF8-2B26-11D7-8648000102C1865D

Young SW (1976) Petrographic textures of detrital polycrystalline quartz as an aid to interpreting crystalline source rocks. Journal of Sedimentary Research 46:595–603. doi: 10.1306/212F6FFA-2B24-11D7-8648000102C1865D

Zaghloul MN, Di Staso A, El Moutchou B, et al (2005a) Sedimentology, provenance and biostratigraphy of the Upper Oligocene-Lower Miocene terrigenous deposits of the internal «dorsale calcaire« (Rif, Morocco): Palaeogeographic and geodynamic implications. Bollettino della Societa Geologica Italiana 124:437–454

Zaghloul MN, Di Staso A, Gigliuto LG, et al (2005b) Stratigraphy and provenance of Lower and Middle Miocene strata within the External Tanger Unit (Intrarif sub-domain, External domain, Rif, Morocco): first evidence. Geol Carpathica 56:517–530

Zaghloul MN, Di Staso A, De Capoa P, Perrone V (2007) Occurrence of upper Burdigalian silexite beds within the Beni Ider Flysch Fm. in the Ksar-es-Seghir area (Maghrebian Flysch Basin, Northern Rif, Morocco): Stratigraphic correlations and geodynamic implications. Bollettino della Societa Geologica Italiana 126:223–239

Zaghloul MN, Critelli S, Perri F, et al (2010) Depositional systems, composition and geochemistry of Triassic rifted-continental margin redbeds of the Internal Rif Chain, Morocco. Sedimentology 57:312–350. doi: 10.1111/j.1365-3091.2009.01080.x

Zakir A, Chalouan A, Feinberg H (2004) Tectono-sedimentary evolution of a fore-chain domain : example of the Habt and Sidi Mrayt basins, northwestern external Moroccan Rif ; stratigraphic precisions and tectonic modelling. Bulletin de la Société Géologique de France 175:383–397. doi: 10.2113/175.4.383

Zizi M (2002) Triassic-Jurassic extensional systems and their Neogene reactivation in northern Morocco; the “Rides Prérifaines” and Guercif Basin. Notes Mém Serv Géol Maroc 146:1–138

Zuffa GG, Gaudio W, Rovito S (1980) Detrital mode evolution of the rifted continental-margin Longobucco Sequence (Jurassic), Calabrian Arc, Italy. Journal of Sedimentary Research 50:51–61. doi: 10.1306/212F795F-2B24-11D7-8648000102C1865D

Zuffa GG (1985) Optical Analyses of Arenites: Influence of Methodology on Compositional Results. In: Provenance of Arenites, NATO ASI Series. Springer, Dordrecht, pp 165–189

# TABLES

**Table 1** Planktonic Foraminifers data (Ben Yaich 1991) used in this work.

| Planktonic Foraminifers | | Burdigalian | | Langhian | Serravallian |
|---|---|---|---|---|---|
| Ben-Yaich Intervals (1991) | | A | B | C | D |
| Present work intervals | | I | II | III | IV |
| Markers | *Globigerinita stainforthi* | | | | |
| | *Globorotalia acrostoma* | | | | |
| | *Globigerina woodi* | | | | |
| | *Globigerina cipercensis* | | | | |
| | *Globigerinoides sicanus* | | | | |
| | *Praeorbulina glomerosa* | | | | |
| | *Globorotalia gr. miozea* | | | | |
| | *Orbiluna suturalis* | | | | |
| Associations | *Globigerinoides immaturus* | | | | |
| | *Globigerinoides bisphaericus* | | | | |
| | *Globigerinoides sacculifer subsacculifer* | | | | |
| | *Globorotalia scitula praescitula* | | | | |
| | *Globigerina praebulloides* | | | | |
| | *Globigerinoides subquadratus* | | | | |
| | *Globigerinoides trilobus* | | | | |
| | *Globoquadrina baroemcenensis* | | | | |
| | *Globoquadrina dehiscens* | | | | |
| | *Globorotalia mayeri* | | | | |
| | *Globorotalia obesa* | | | | |
| | *Globorotalia forsi peripheroronda* | | | | |

**Table 2** Point count modal analysis data.

| | Localities | Zoumi | | | | | | | | | | | | | | | | | | | | |
|---|---|---|---|---|---|---|---|---|---|---|---|---|---|---|---|---|---|---|---|---|---|---|
| | **Samples** | **Z3** | **Z4** | **Z8** | **Z10** | **Z11** | **Z12** | **Z13** | **Z15** | **Z17** | **Z23** | **Z25** | **Z27** | **Z29** | **Z32** | **Z33** | **Z36** | **Z37** | **Z40** | **Z42** | **Z43** | **Z47** |
| **NCE** | Quartz (Single Crystal) | 267 | 330 | 320 | 233 | 302 | 316 | 311 | 259 | 289 | 300 | 318 | 316 | 332 | 355 | 356 | 282 | 339 | 336 | 338 | 264 | 287 |
| | Quartz (2Gr-3Gr) | 7 | 16 | 11 | 74 | 36 | 38 | 26 | 29 | 42 | 35 | 14 | 6 | 11 | 5 | 11 | 51 | 10 | 23 | 4 | 10 | 7 |
| | Quartz(>3Gr) | 1 | 11 | 1 | 37 | 4 | 10 | 8 | 11 | 20 | 11 | 3 | 1 | 3 | 4 | 4 | 21 | 1 | 7 | 0 | 4 | 3 |
| | Quartz (fine grains polycrystalline) | 3 | | 4 | 3 | 1 | 5 | 1 | 1 | 13 | 7 | 8 | 5 | 9 | 1 | 3 | 5 | 6 | 14 | 6 | 4 | 4 |
| | Impur Chert | 0 | 1 | 1 | 7 | 0 | 0 | 1 | 0 | 3 | 1 | 0 | 0 | 0 | 1 | 1 | 3 | 0 | 0 | 0 | 2 | 1 |
| | K-feldspar (single crystal) | 0 | 5 | 26 | 15 | 14 | 11 | 9 | 4 | 4 | 4 | 4 | 3 | 2 | 1 | 2 | 5 | 3 | 1 | 3 | 8 | 1 |
| | Plagioclase (single crystal) | 0 | 1 | 0 | 0 | 0 | 2 | 0 | 0 | 2 | 0 | 0 | 0 | 3 | 1 | 2 | 1 | 2 | 0 | 3 | 1 | |
| | Mica and Chlorites (single crystal) | 0 | 0 | 0 | 0 | 0 | 0 | 0 | 0 | 0 | 2 | 0 | 4 | 0 | 0 | 0 | 0 | 0 | 0 | 0 | 0 | 0 |
| | Ls | 2 | 3 | | 29 | 20 | 4 | 24 | 43 | 11 | 19 | 24 | 5 | 27 | 16 | 16 | 3 | 18 | 8 | 14 | 49 | 47 |
| | Lm | 0 | 0 | 0 | 0 | 1 | 0 | 0 | 0 | 0 | 0 | 0 | 0 | 1 | 4 | 1 | 0 | 0 | 0 | 1 | 1 | 0 |
| | Lv | 0 | 0 | 0 | 0 | 4 | 1 | 2 | 3 | 0 | 2 | 0 | 0 | 0 | 1 | 1 | 0 | 0 | 0 | 0 | 0 | 1 |
| | Slates | 0 | 9 | 0 | 1 | 2 | 1 | 0 | 0 | 1 | 2 | 1 | 0 | 0 | 0 | 0 | 0 | 1 | 0 | 2 | 0 | 0 |
| **CE** | CE limestones | 1 | 5 | 28 | 4 | 4 | 3 | 7 | 27 | 2 | 11 | 12 | 2 | 4 | 1 | 0 | 2 | 4 | 4 | 5 | 52 | 27 |
| **CI** | CI Bioclast | 42 | 28 | 0 | 5 | 4 | 6 | 16 | 3 | 5 | 2 | 8 | 27 | 11 | 5 | 2 | 3 | 9 | 6 | 19 | 1 | 11 |
| **NCI** | NCI Glauconite | 25 | 1 | 0 | 0 | 0 | 0 | 0 | 1 | 2 | 0 | 1 | 1 | 0 | 1 | 0 | 0 | 1 | 0 | 5 | 0 | 2 |
| **Monocystalline dense minerals** | | | | | | | | | | | | | | | | | | | | | | |
| | Zircon | 1 | 0 | 0 | 1 | 1 | 1 | 3 | 4 | 4 | 0 | 2 | 5 | 0 | 2 | 0 | 5 | 0 | 0 | 0 | 1 | 1 |
| | Staurolite | 0 | 0 | 0 | 0 | 0 | 0 | 1 | 0 | 0 | 0 | 0 | 0 | 0 | 0 | 0 | 0 | 0 | 0 | 0 | 0 | 0 |
| | Tourmaline | 0 | 0 | 0 | 1 | 1 | 0 | 0 | 2 | 0 | 0 | 0 | 0 | 0 | 0 | 0 | 0 | 1 | 0 | 0 | 0 | 0 |
| | Opaque Minerals | 29 | 12 | 8 | 1 | 0 | 2 | 2 | 12 | 2 | 3 | 2 | 25 | 0 | 1 | 1 | 19 | 3 | 1 | 0 | 0 | 8 |
| **Unknown minerals** | | 1 | 2 | 1 | 0 | 0 | 0 | 0 | 1 | 0 | 1 | 3 | 0 | 0 | 1 | 0 | 0 | 2 | 0 | 0 | 3 | 0 |

**Table 2** Point count modal analysis data (continued).

| | Localities | | | | | | | Dmani | | | | | | | | | Khakha | | | | | Taourda | |
|---|---|---|---|---|---|---|---|---|---|---|---|---|---|---|---|---|---|---|---|---|---|---|---|
| | **Samples** | **Z50** | **Z51** | **Z52** | **Z53** | **Z55** | **Z56** | **Z58** | **Z60** | **Z63** | **Z64** | **Z67** | **Z68** | **Z71** | **Z75** | **Z78** | **Z80** | **Z81** | **Z84** | **Z87** | **Z118** | **Z127** | **Z131** |
| **NCE** | Quartz (Single Crystal) | 305 | 270 | 303 | 290 | 254 | 291 | 301 | 292 | 287 | 287 | 310 | 279 | 221 | 256 | 302 | 313 | 330 | 175 | 298 | 296 | 202 | 237 |
| | Quartz (2Gr-3Gr) | 12 | 21 | 12 | 5 | 39 | 15 | 11 | 3 | 5 | 36 | 6 | 19 | 71 | 51 | 19 | 7 | 25 | 84 | 8 | 10 | 94 | 53 |
| | Quartz(>3Gr) | 0 | 1 | 2 | 3 | 32 | 2 | 1 | 1 | 4 | 6 | 0 | 1 | 36 | 22 | 9 | 0 | 2 | 5 | 0 | 8 | 36 | 18 |
| | Quartz (fine grains polycrystalline) | 2 | 6 | 8 | 3 | 8 | 7 | 3 | 1 | 6 | 1 | 6 | 4 | 5 | 2 | 0 | 0 | 1 | 3 | 2 | 2 | 5 | 2 |
| | Impur Chert | 1 | 0 | 0 | 0 | 0 | 1 | 2 | 0 | 1 | 1 | 1 | 0 | 1 | 0 | 0 | 0 | 0 | 0 | 0 | 0 | 0 | 0 |
| | K-feldspar (single crystal) | 4 | 16 | 12 | 8 | 6 | 22 | 6 | 8 | 6 | 19 | 4 | 1 | 7 | 6 | 10 | 14 | 10 | 23 | 14 | 16 | 19 | 23 |
| | Plagioclase (single crystal) | 1 | 2 | 2 | 2 | 0 | 1 | 1 | 1 | 0 | 2 | 0 | 0 | 0 | 1 | 0 | 1 | 1 | 1 | 0 | 0 | 0 | 0 |
| | Mica and Chlorites (single crystal) | 0 | 1 | 0 | 0 | 0 | 0 | 0 | 0 | 0 | 0 | 0 | 1 | 0 | 0 | 0 | 1 | 0 | 0 | 0 | 0 | 1 | 0 |
| | Ls | 42 | 31 | 26 | 41 | 38 | 15 | 47 | 50 | 54 | 32 | 51 | 45 | 41 | 37 | 38 | 26 | 20 | 25 | 31 | 25 | 14 | 35 |
| | Lm | 0 | 0 | 0 | 1 | 3 | 0 | 0 | 0 | 0 | 0 | 0 | 10 | 0 | 0 | 0 | 0 | 0 | 0 | 0 | 0 | 0 | 0 |
| | Lv | 0 | 1 | 0 | 0 | 1 | 0 | 0 | 0 | 0 | 0 | 0 | 7 | 0 | 0 | 0 | 0 | 0 | 0 | 0 | 0 | 0 | 1 |
| | Slates | 0 | 0 | 0 | 0 | 1 | 0 | 0 | 1 | 0 | 0 | 0 | 0 | 1 | 0 | 0 | 0 | 0 | 0 | 0 | 7 | 1 | 3 |
| **CE** | CE limestones | 19 | 13 | 27 | 2 | 11 | 39 | 20 | 5 | 3 | 2 | 15 | 2 | 6 | 11 | 2 | 30 | 2 | 17 | 22 | 19 | 7 | 10 |
| **CI** | CI Bioclast | 1 | 22 | 5 | 20 | 3 | 6 | 0 | 25 | 19 | 7 | 2 | 16 | 8 | 2 | 7 | 1 | 1 | 7 | 4 | 1 | 2 | 2 |
| **NCI** | NCI Glauconite | 1 | 10 | 2 | 1 | 0 | 0 | 5 | 6 | 13 | 2 | 2 | 2 | 0 | 0 | 0 | 1 | 1 | 0 | 5 | 0 | 9 | 3 |
| **Monocystalline dense minerals** | | | | | | | | | | | | | | | | | | | | | | | |
| | Zircon | 2 | 0 | 0 | 0 | 0 | 0 | 2 | 1 | 0 | 0 | 0 | 3 | 0 | 2 | 0 | 0 | 1 | 1 | 0 | 0 | 0 | 0 |
| | Staurolite | 0 | 0 | 0 | 0 | 0 | 0 | 0 | 0 | 0 | 0 | 0 | 0 | 0 | 0 | 0 | 0 | 0 | 0 | 0 | 1 | 0 | 0 |
| | Tourmaline | 0 | 0 | 0 | 0 | 0 | 0 | 0 | 0 | 0 | 0 | 0 | 0 | 1 | 0 | 0 | 0 | 0 | 0 | 0 | 0 | 0 | 0 |
| | Opaque Minerals | 10 | 6 | 1 | 24 | 2 | 1 | 1 | 6 | 2 | 5 | 3 | 10 | 2 | 7 | 13 | 6 | 6 | 6 | 16 | 16 | 9 | 13 |
| **Unknown Minerals** | | 0 | 0 | 0 | 0 | 2 | 0 | 0 | 0 | 0 | 0 | 0 | 0 | 0 | 0 | 0 | 0 | 0 | 0 | 0 | 0 | 1 | 0 |

**Table 3** Recalculated modal point count data.

| Sample | % | | | % | | | % | | | % | | | % | | | Index | | | |
|---|---|---|---|---|---|---|---|---|---|---|---|---|---|---|---|---|---|---|---|
| | Qm | F | Lt | Qt | F | L | Qp | Lvm | Lsm | Lm | Lv | Ls | Qm | P | K | Lv/L | P/F | Q/F | F/L |
| Z3 | 98.85 | 0 | 1.145 | 99.26 | 0 | 0.743 | 80 | 0 | 20 | 0 | 0 | 100 | 100 | 0 | 0 | 0 | - | - | 0 |
| Z4 | 95.93 | 1.744 | 2.326 | 97.55 | 1.635 | 0.817 | 90 | 0 | 10 | 0 | 0 | 100 | 98.21 | 0.3 | 1.49 | 0 | 0.17 | 59.67 | 2 |
| Z8 | 85.56 | 6.952 | 7.487 | 92.84 | 7.163 | 0 | 100 | 0 | 0 | - | - | - | 92.49 | 0 | 7.51 | - | 0 | 12.96 | - |
| Z10 | 82.73 | 5.396 | 11.87 | 88.63 | 3.876 | 7.494 | 79.14 | 0 | 20.86 | 0 | 0 | 100 | 93.88 | 0 | 6.12 | 0 | 0 | 22.87 | 0.52 |
| Z11 | 87.5 | 4.07 | 8.43 | 89.95 | 3.608 | 6.443 | 62.5 | 6.25 | 31.25 | 4 | 16 | 80 | 95.56 | 0 | 4.44 | 0.16 | 0 | 24.93 | 0.56 |
| Z12 | 93.77 | 3.858 | 2.374 | 95.35 | 3.359 | 1.292 | 90.57 | 1.887 | 7.547 | 0 | 20 | 80 | 96.05 | 0.61 | 3.34 | 0.2 | 0.15 | 28.38 | 2.6 |
| Z13 | 87.76 | 2.624 | 9.621 | 90.57 | 2.426 | 7.008 | 55.93 | 3.39 | 40.68 | 0 | 7.69 | 92.31 | 97.1 | 0 | 2.9 | 0.08 | 0 | 37.33 | 0.35 |
| Z15 | 77.08 | 1.19 | 21.73 | 85.71 | 1.143 | 13.14 | 46.51 | 3.488 | 50 | 0 | 6.52 | 93.48 | 98.48 | 0 | 1.52 | 0.07 | 0 | 75 | 0.09 |
| Z17 | 93.83 | 1.948 | 4.221 | 95.57 | 1.563 | 2.865 | 84.93 | 0 | 15.07 | 0 | 0 | 100 | 97.97 | 0.68 | 1.36 | 0 | 0.33 | 61.17 | 0.55 |
| Z23 | 89.29 | 1.19 | 9.524 | 93.4 | 1.055 | 5.541 | 68.66 | 2.985 | 28.36 | 0 | 9.52 | 90.48 | 98.68 | 0 | 1.32 | 0.1 | 0 | 88.5 | 0.19 |
| Z25 | 88.83 | 1.117 | 10.06 | 92.45 | 1.078 | 6.469 | 41.46 | 0 | 58.54 | 0 | 0 | 100 | 98.76 | 0 | 1.24 | 0 | 0 | 85.75 | 0.17 |
| Z27 | 96.93 | 0.92 | 2.147 | 97.62 | 0.893 | 1.488 | 58.33 | 0 | 41.67 | 0 | 0 | 100 | 99.06 | 0 | 0.94 | 0 | 0 | 109.33 | 0.6 |
| Z29 | 90.16 | 1.366 | 8.47 | 91.69 | 1.299 | 7.013 | 35 | 0 | 65 | 3.7 | 0 | 96.3 | 98.51 | 0.9 | 0.6 | 0 | 0.6 | 70.6 | 0.19 |
| Z32 | 93.67 | 0.528 | 5.805 | 94.09 | 0.514 | 5.398 | 31.03 | 3.448 | 65.52 | 4.76 | 4.76 | 90.48 | 99.44 | 0.28 | 0.28 | 0.05 | 0.5 | 183 | 0.1 |
| Z33 | 94.18 | 1.058 | 4.762 | 94.46 | 1.008 | 4.534 | 46.88 | 3.125 | 50 | 5.56 | 5.56 | 88.89 | 98.89 | 0.56 | 0.56 | 0.06 | 0.5 | 93.75 | 0.22 |
| Z36 | 96.25 | 2.048 | 1.706 | 97.57 | 1.617 | 0.809 | 96 | 0 | 4 | 0 | 0 | 100 | 97.92 | 0.35 | 1.74 | 0 | 0.17 | 60.33 | 2 |
| Z37 | 92.62 | 1.366 | 6.011 | 93.93 | 1.319 | 4.749 | 36.67 | 3.333 | 60 | 5 | 5 | 90 | 98.55 | 0.58 | 0.87 | 0.06 | 0.4 | 71.2 | 0.28 |
| Z40 | 96.28 | 0.287 | 3.438 | 97.69 | 0.257 | 2.057 | 78.95 | 0 | 21.05 | 0 | 0 | 100 | 99.7 | 0 | 0.3 | 0 | 0 | 380 | 0.13 |
| Z42 | 92.86 | 1.648 | 5.495 | 94.31 | 1.626 | 4.065 | 22.22 | 0 | 77.78 | 6.67 | 0 | 93.33 | 98.26 | 0.87 | 0.87 | 0 | 0.5 | 58 | 0.4 |
| Z43 | 71.02 | 2.35 | 26.63 | 82.8 | 2.624 | 14.58 | 22.22 | 0 | 77.78 | 2 | 0 | 98 | 96.8 | 0.36 | 2.85 | 0 | 0.11 | 31.56 | 0.18 |
| Z47 | 78.53 | 0.282 | 21.19 | 86.04 | 0.285 | 13.68 | 17.24 | 1.724 | 81.03 | 0 | 2.08 | 97.92 | 99.64 | 0 | 0.36 | 0.02 | 0 | 302 | 0.02 |
| Z50 | 82.31 | 1.34 | 16.35 | 87.19 | 1.362 | 11.44 | 22.22 | 0 | 77.78 | 0 | 0 | 100 | 98.4 | 0.32 | 1.28 | 0 | 0.2 | 64 | 0.12 |
| Z51 | 81.19 | 5.373 | 13.43 | 85.63 | 5.172 | 9.195 | 40.74 | 1.852 | 57.41 | 0 | 3.13 | 96.88 | 93.79 | 0.69 | 5.52 | 0.03 | 0.11 | 16.56 | 0.56 |
| Z52 | 81.74 | 3.815 | 14.44 | 89.04 | 3.836 | 7.123 | 35 | 0 | 65 | 0 | 0 | 100 | 95.54 | 0.64 | 3.82 | 0 | 0.14 | 23.21 | 0.54 |

**Table 3** Recalculated modal point count data (continued).

| Sample | % | | | % | | | % | | | % | | | % | | | Index | | | |
|---|---|---|---|---|---|---|---|---|---|---|---|---|---|---|---|---|---|---|---|
| | Qm | F | Lt | Qt | F | L | Qp | Lvm | Lsm | Lm | Lv | Ls | Qm | P | K | Lv/L | P/F | Q/F | F/L |
| Z53 | 83.78 | 3.003 | 13.21 | 85.27 | 2.833 | 11.9 | 16.33 | 0 | 83.67 | 2.38 | 0 | 97.62 | 96.54 | 0.69 | 2.77 | 0 | 0.2 | 30.1 | 0.24 |
| Z55 | 81.15 | 1.917 | 16.93 | 87.4 | 1.575 | 11.02 | 64.55 | 0.909 | 34.55 | 7.14 | 2.38 | 90.48 | 97.69 | 0 | 2.31 | 0.02 | 0 | 55.5 | 0.14 |
| Z56 | 77.01 | 6.866 | 16.12 | 89.27 | 6.497 | 4.237 | 51.52 | 3.03 | 45.45 | 5.88 | 5.88 | 88.24 | 91.81 | 0.36 | 7.83 | 0.07 | 0.04 | 13.74 | 1.53 |
| Z58 | 79.84 | 1.907 | 18.26 | 85.48 | 1.882 | 12.63 | 20.34 | 0 | 79.66 | 0 | 0 | 100 | 97.67 | 0.33 | 2 | 0 | 0.14 | 45.43 | 0.15 |
| Z60 | 81.87 | 2.55 | 15.58 | 83.43 | 2.528 | 14.04 | 7.407 | 0 | 92.59 | 0 | 0 | 100 | 96.98 | 0.34 | 2.68 | 0 | 0.11 | 33 | 0.18 |
| Z63 | 81.95 | 1.719 | 16.33 | 83.47 | 1.653 | 14.88 | 14.29 | 0 | 85.71 | 0 | 0 | 100 | 97.95 | 0 | 2.05 | 0 | 0 | 50.5 | 0.11 |
| Z64 | 83.87 | 6.158 | 9.971 | 86.2 | 5.469 | 8.333 | 56.76 | 0 | 43.24 | 0 | 0 | 100 | 93.16 | 0.65 | 6.19 | 0 | 0.1 | 15.76 | 0.66 |
| Z67 | 81.43 | 1.061 | 17.51 | 85.45 | 1.058 | 13.49 | 10.53 | 0 | 89.47 | 0 | 0 | 100 | 98.71 | 0 | 1.29 | 0 | 0 | 80.75 | 0.08 |
| Z68 | 80.94 | 0.293 | 18.77 | 82.79 | 0.273 | 16.94 | 27.78 | 9.722 | 62.5 | 16.13 | 11.29 | 72.58 | 99.64 | 0 | 0.36 | 0.11 | 0 | 303 | 0.02 |
| Z71 | 80.36 | 2.545 | 17.09 | 87.43 | 1.832 | 10.73 | 72.3 | 0 | 27.7 | 0 | 0 | 100 | 96.93 | 0 | 3.07 | 0 | 0 | 47.71 | 0.17 |
| Z75 | 81.53 | 3.185 | 15.29 | 87.57 | 2.646 | 9.788 | 66.36 | 0 | 33.64 | 0 | 0 | 100 | 96.24 | 0.38 | 3.38 | 0 | 0.1 | 33.1 | 0.27 |
| Z78 | 85.75 | 2.849 | 11.4 | 87.3 | 2.646 | 10.05 | 42.42 | 0 | 57.58 | 0 | 0 | 100 | 96.78 | 0 | 3.22 | 0 | 0 | 33 | 0.26 |
| Z80 | 81.56 | 3.896 | 14.55 | 88.64 | 4.155 | 7.202 | 21.21 | 0 | 78.79 | 0 | 0 | 100 | 95.44 | 0.3 | 4.26 | 0 | 0.07 | 21.33 | 0.58 |
| Z81 | 88.21 | 3.929 | 7.857 | 92.03 | 2.828 | 5.141 | 57.45 | 0 | 42.55 | 0 | 0 | 100 | 95.74 | 0.39 | 3.88 | 0 | 0.09 | 32.55 | 0.55 |
| Z84 | 72.73 | 9.917 | 17.36 | 86.72 | 6.504 | 6.775 | 85.03 | 0 | 14.97 | 0 | 0 | 100 | 88 | 0.5 | 11.5 | 0 | 0.04 | 13.33 | 0.96 |
| Z87 | 81.64 | 3.836 | 14.52 | 87.25 | 3.966 | 8.782 | 20.51 | 0 | 79.49 | 0 | 0 | 100 | 95.51 | 0 | 4.49 | 0 | 0 | 22 | 0.45 |
| Z118 | 85.79 | 4.63 | 9.56 | 88.45 | 4.50 | 7.04 | 41.86 | 0 | 58.13 | 0 | 0 | 100 | 94.87 | 0 | 5.12 | 0 | 0 | 19.62 | 0.64 |
| Z127 | 83.81 | 7.88 | 8.29 | 90.95 | 5.20 | 3.83 | 90.27 | 0 | 9.72 | 0 | 0 | 100 | 91.40 | 0 | 8.59 | 0 | 0 | 17.47 | 1.35 |
| Z131 | 78.73 | 7.64 | 13.62 | 84.23 | 6.25 | 9.51 | 66.35 | 0.93 | 32.71 | 0 | 2.77 | 97.22 | 91.15 | 0 | 8.84 | 0.02 | 0 | 13.39 | 0.65 |

**Table 4** Mineralogical composition of the bulk mudrocks (wt %)

| Sample | Illite | Chl | Micas | Kao | Smect. | Verm | ∑ Phyll. | Qtz | Plag. | K-feldsp. | Cal | Dol | Sid | Hem | Goet |
|---|---|---|---|---|---|---|---|---|---|---|---|---|---|---|---|
| Z1 | 12.32 | 2.56 | 16.51 | 2.62 | 1.32 | 3.75 | 39.08 | 5.92 | 15.95 | 24.05 | 14.41 | 1.01 | 0.15 | 0.1 | 0.56 |
| Z2 | 15.79 | 1.39 | 11.52 | 4.57 | 0.02 | 0 | 33.29 | 0.65 | 6.89 | 51.85 | 5.52 | 0.25 | 0.14 | 0.15 | 1.27 |
| Z4 | 12.93 | 1.24 | 17.13 | 2.2 | 0.01 | 0.03 | 33.54 | 7.67 | 17.67 | 25.41 | 14.73 | 0.2 | 0.13 | 0.08 | 0.56 |
| Z5 | 9.79 | 1.66 | 14.79 | 2.08 | 0.02 | 0.08 | 28.42 | 5.54 | 14.8 | 35.17 | 15.04 | 0.26 | 0.1 | 0.08 | 0.6 |
| Z6 | 10.93 | 1.36 | 15.43 | 2.18 | 0.02 | 0.05 | 29.97 | 5.86 | 13.33 | 34.17 | 15.77 | 0.1 | 0.1 | 0.08 | 0.64 |
| Z7 | 11 | 1.19 | 14.26 | 2.24 | 0.03 | 0.05 | 28.77 | 7.14 | 15.26 | 19.05 | 28.96 | 0.06 | 0.09 | 0.08 | 0.59 |
| Z16 | 9.13 | 1.61 | 14.1 | 1.98 | 1.59 | 0.36 | 28.77 | 3.79 | 18 | 37.28 | 11.26 | 0.25 | 0.12 | 0.09 | 0.46 |
| Z18 | 15.23 | 1.47 | 22.38 | 1.95 | 1.49 | 0.39 | 42.91 | 9 | 11.53 | 20.13 | 15.49 | 0.1 | 0.11 | 0.06 | 0.65 |
| Z19 | 11.72 | 1.46 | 18.06 | 1.93 | 1.14 | 0.02 | 34.33 | 7.69 | 19.2 | 27.41 | 10.35 | 0.16 | 0.13 | 0.08 | 0.65 |
| Z20 | 11.66 | 1.38 | 15.95 | 2.08 | 1.95 | 3.41 | 36.43 | 6.72 | 14.38 | 21.55 | 20.18 | 0.03 | 0.11 | 0.06 | 0.55 |
| Z22 | 9.95 | 2.07 | 14.97 | 2.28 | 1.7 | 0.61 | 31.58 | 2.21 | 15.95 | 43.97 | 5.24 | 0.24 | 0.12 | 0.09 | 0.6 |
| Z26 | 9.92 | 2.07 | 14.08 | 2.97 | 1.97 | 1.89 | 32.9 | 0.45 | 12.52 | 48.94 | 3.79 | 0.2 | 0.1 | 0.13 | 0.98 |
| Z28 | 13.37 | 1.13 | 19.86 | 1.88 | 1.32 | 2.1 | 39.66 | 9.06 | 15.87 | 23.14 | 11.5 | 0.03 | 0.09 | 0.05 | 0.58 |
| Z30 | 11.02 | 2.12 | 16.86 | 2.39 | 1.04 | 1.35 | 34.78 | 3.04 | 18.29 | 36.88 | 5.35 | 0.41 | 0.21 | 0.13 | 0.92 |
| Z31 | 16.72 | 3.02 | 12.16 | 4.16 | 1.01 | 4.29 | 41.36 | 0.23 | 5.06 | 49.24 | 0.31 | 0.44 | 0.1 | 0.09 | 3.19 |
| Z34 | 10.93 | 3.29 | 10.26 | 4.89 | 0.57 | 5.61 | 35.55 | 0.51 | 7.2 | 52.75 | 2.49 | 0.31 | 0.25 | 0.13 | 0.72 |
| Z38 | 9.88 | 2.47 | 19.09 | 2.06 | 2.45 | 0.69 | 36.64 | 3.22 | 15.25 | 29.11 | 14.35 | 0.15 | 0.13 | 0.15 | 1.02 |
| Z39 | 9.76 | 2.65 | 15.45 | 2.5 | 2.97 | 0.13 | 33.46 | 1.78 | 9.37 | 48.67 | 5.42 | 0.23 | 0.19 | 0.09 | 0.79 |
| Z41 | 14.83 | 2.08 | 21.05 | 1.62 | 2.82 | 0.45 | 42.85 | 5.7 | 14.24 | 23.54 | 12.53 | 0.15 | 0.11 | 0.08 | 0.81 |
| Z44 | 12.24 | 5.01 | 13.75 | 4.04 | 1.52 | 0.65 | 37.21 | 3.65 | 23.36 | 25.34 | 7.95 | 0.3 | 0.19 | 0.18 | 1.82 |
| Z46 | 12.76 | 4.06 | 14.07 | 4.26 | 2.03 | 4.65 | 41.83 | 0.96 | 8 | 45.84 | 1.27 | 0.41 | 0.3 | 0.32 | 1.09 |
| Z48 | 13.08 | 2.19 | 22.91 | 1.72 | 2.64 | 0.18 | 42.72 | 4.5 | 11.52 | 28.49 | 11.37 | 0.33 | 0.11 | 0.08 | 0.88 |
| Z54 | 15.12 | 1.83 | 23.78 | 1.41 | 2.72 | 0.18 | 45.04 | 6.64 | 12.25 | 27.2 | 7.77 | 0.06 | 0.13 | 0.08 | 0.81 |
| Z59 | 7.93 | 2.33 | 13.69 | 2.4 | 1.81 | 0.57 | 28.73 | 1.65 | 12.13 | 46.36 | 9.95 | 0.12 | 0.15 | 0.18 | 0.72 |
| Z61 | 8.9 | 2.36 | 14.38 | 1.99 | 2.77 | 4.61 | 35.01 | 1.92 | 12.66 | 41.18 | 7.91 | 0.27 | 0.13 | 0.14 | 0.79 |
| Z62 | 7.03 | 1.67 | 15.04 | 1.67 | 1.2 | 5 | 31.61 | 2.04 | 10.16 | 50.05 | 5.14 | 0.08 | 0.09 | 0.08 | 0.75 |
| Z65 | 9.09 | 2.86 | 12.06 | 3.07 | 2.42 | 2.32 | 31.82 | 0.86 | 11.15 | 53.68 | 1.45 | 0.29 | 0.11 | 0.19 | 0.47 |
| Z66 | 15.66 | 1.43 | 20.97 | 1.26 | 2.09 | 0.1 | 41.51 | 8.44 | 13.69 | 27.84 | 7.63 | 0.05 | 0.09 | 0.05 | 0.69 |
| Z69 | 10.38 | 3.72 | 13.69 | 2.74 | 0.01 | 0.21 | 30.75 | 2.25 | 14.18 | 45.628 | 6.02 | 0.24 | 0.04 | 0.09 | 0.74 |
| Z73 | 6.79 | 4.31 | 7.01 | 3.11 | 0.06 | 0.26 | 21.54 | 0.6 | 5.63 | 70.78 | 0.48 | 0.22 | 0.03 | 0.02 | 0.69 |
| Z74 | 13.07 | 2.92 | 9.69 | 3.7 | 0 | 0.11 | 29.49 | 0.4 | 9.26 | 57.52 | 0.36 | 0.35 | 0.05 | 0.09 | 2.49 |
| Z76 | 14.16 | 1.21 | 18.97 | 2.17 | 0 | 0.02 | 36.53 | 9.02 | 16.91 | 22.06 | 14.59 | 0.09 | 0.15 | 0.08 | 0.58 |
| Z86 | 13.53 | 2.81 | 17.86 | 1.91 | 0.04 | 0.18 | 36.33 | 7.06 | 13.41 | 30.82 | 11.4 | 0.09 | 0.12 | 0.06 | 0.68 |
| ***Mean*** | ***11.72*** | ***2.27*** | ***15.81*** | ***2.55*** | ***1.30*** | ***1.34*** | ***34.98*** | ***4.13*** | ***13.18*** | ***37.12*** | ***9.27*** | ***0.23*** | ***0.13*** | ***0.10*** | ***0.89*** |
| ***SD*** | ***2.58*** | ***0.98*** | ***3.88*** | ***0.94*** | ***1.02*** | ***1.78*** | ***5.38*** | ***3.00*** | ***4.10*** | ***13.17*** | ***6.36*** | ***0.18*** | ***0.05*** | ***0.06*** | ***0.57*** |

**Table 5** Major elements concentrations with some important geochemical indices and ratios in the studied mudrock samples.

| Localities | Sample | $SiO_2$ | $TiO_2$ | $Al_2O_3$ | $Fe_2O_3(T)$ | MgO | MnO | CaO | $Na_2O$ | $K_2O$ | $P_2O_5$ | LOI | ICV | CIA | PIA | CIW |
|---|---|---|---|---|---|---|---|---|---|---|---|---|---|---|---|---|
| **Zoumi** | Z2 | 32,24 | 0,44 | 8,84 | 3,08 | 1,13 | 0,05 | 26,38 | 1,61 | 1,68 | 0,17 | 25,8 | 1,8 | 54,45 | 55,74 | 61,32 |
| | Z4 | 42,24 | 0,66 | 10,56 | 3,55 | 1,2 | 0,01 | 18,35 | 2,82 | 2,33 | 0,09 | 24,2 | 2,07 | 46,22 | 45,15 | 51,95 |
| | Z5 | 40,6 | 0,27 | 10,09 | 1,9 | 1,76 | 0 | 18,4 | 0,46 | 1,36 | 0,22 | 23,9 | 2,39 | 72,57 | 81,95 | 87,25 |
| | Z6 | 36,54 | 0,48 | 9,13 | 2,93 | 1,14 | 0,01 | 24,11 | 2,21 | 1,91 | 0,13 | 24,6 | 2,19 | 48,43 | 48 | 54,4 |
| | Z7 | 29,4 | 0,21 | 7,34 | 1,71 | 1,2 | 0,05 | 27,2 | 0,27 | 0,93 | 0,19 | 31,4 | 4,3 | 69,5 | 76,01 | 88,7 |
| | Z16 | 31,7 | 0,25 | 8,81 | 1,82 | 1,41 | 0,02 | 24,6 | 0,35 | 1,22 | 0,19 | 29,4 | 3,36 | 77,67 | 86,1 | 87,91 |
| | Z18 | 41,9 | 0,36 | 11,6 | 2,85 | 1,69 | 0,03 | 17 | 0,25 | 1,68 | 0,16 | 22,3 | 2,05 | 81,21 | 91,9 | 93,05 |
| | Z19 | 43,7 | 0,4 | 11,5 | 2,71 | 1,74 | 0 | 16,6 | 0,46 | 1,49 | 0,17 | 21 | 2,03 | 78,2 | 86,1 | 87,83 |
| | Z20 | 33,4 | 0,27 | 10,3 | 1,91 | 1,5 | 0,04 | 22,1 | 0,38 | 1,37 | 0,2 | 28,4 | 2,67 | 78,63 | 87 | 88,67 |
| | Z22 | 45,1 | 0,37 | 15,5 | 7,65 | 1,96 | 0 | 7,87 | 0,43 | 1,55 | 0,14 | 19,4 | 1,27 | 83,03 | 90,3 | 91,23 |
| | Z26 | 45,4 | 0,49 | 14 | 3,94 | 1,92 | 0,03 | 12,3 | 0,31 | 2,07 | 0,15 | 19,2 | 1,5 | 80,86 | 91,6 | 92,88 |
| | Z28 | 45,5 | 0,44 | 12,8 | 2,87 | 1,78 | 0,04 | 14,3 | 0,44 | 1,68 | 0,14 | 19,8 | 1,68 | 79,29 | 87,8 | 89,36 |
| | Z30 | 45,3 | 0,48 | 13,4 | 2,94 | 2,09 | 0 | 13,2 | 0,26 | 2,03 | 0,13 | 20 | 1,56 | 81,22 | 92,6 | 93,7 |
| | Z31 | 44,3 | 0,42 | 14,4 | 6,89 | 1,81 | 0 | 10,02 | 0,35 | 1,4 | 0,16 | 19,9 | 1,45 | 84,07 | 91,4 | 92,24 |
| | Z34 | 32,4 | 0,28 | 9,75 | 1,56 | 1,53 | 0 | 23,4 | 0,29 | 1,21 | 0,16 | 29,3 | 2,89 | 80,82 | 89,4 | 90,66 |
| | Z38 | 41,4 | 0,4 | 12,5 | 2,37 | 1,87 | 0 | 16 | 0,48 | 1,71 | 0,14 | 22,9 | 1,82 | 75,97 | 86,92 | 88,26 |
| | Z39 | 46 | 0,49 | 13,4 | 2,75 | 2,06 | 0 | 13,4 | 0,29 | 2,01 | 0,12 | 19,2 | 1,56 | 76,6 | 90,67 | 93,03 |
| | Z41 | 46,8 | 0,39 | 15 | 2,48 | 2,21 | 0 | 11,1 | 0,52 | 1,81 | 0,14 | 19,4 | 1,23 | 75,36 | 87,24 | 89,28 |
| | Z44 | 37,1 | 0,34 | 10,5 | 1,97 | 1,66 | 0 | 21,1 | 0,52 | 1,37 | 0,16 | 25,2 | 2,56 | 75,59 | 84,79 | 85,36 |
| | Z46 | 24,7 | 0,15 | 7,97 | 1,2 | 1,2 | 0 | 4,74 | 0,22 | 0,82 | 0,06 | 24,7 | 1,04 | 51,24 | 51,4 | 91,27 |
| **Dmani** | Z48 | 47,6 | 0,4 | 14,9 | 6,79 | 2,17 | 0 | 8,42 | 0,51 | 1,71 | 0,08 | 17,3 | 1,34 | 71,85 | 85,47 | 89,4 |
| | Z54 | 52,15 | 0,62 | 11,46 | 4,1 | 1,35 | 0,01 | 11,8 | 3,31 | 2,33 | 0,09 | 14,5 | 1,13 | 45,04 | 43,8 | 49,99 |
| | Z59 | 37,7 | 0,28 | 9,92 | 2,12 | 1,54 | 0,02 | 21,7 | 0,49 | 1,33 | 0,17 | 24,6 | 2,77 | 75,98 | 83,3 | 85,39 |
| | Z61 | 41,9 | 0,4 | 12,4 | 2,88 | 1,98 | 0 | 16 | 0,38 | 1,94 | 0,13 | 21,7 | 1,9 | 73,16 | 86,73 | 90,4 |
| | Z62 | 46,4 | 0,43 | 12,9 | 3,4 | 1,92 | 0,04 | 13,5 | 0,56 | 1,81 | 0,18 | 18,7 | 1,67 | 71,77 | 82,07 | 86,93 |
| | Z65 | 47 | 0,5 | 15 | 3,48 | 2,19 | 0,03 | 11,1 | 0,69 | 2,22 | 0,13 | 17,4 | 1,34 | 75,33 | 87,66 | 86,26 |
| | Z66 | 50,8 | 0,52 | 14,4 | 3,07 | 1,98 | 0 | 11 | 0,94 | 1,73 | 0,2 | 15,2 | 1,33 | 73,74 | 79,4 | 81,56 |
| | Z69 | 44,4 | 0,48 | 13,6 | 3,57 | 2,01 | 0 | 13 | 0,45 | 1,94 | 0,13 | 20,1 | 1,57 | 75,07 | 88,51 | 89,72 |
| | Z70 | 50,86 | 0,79 | 15,6 | 5,51 | 1,66 | 0 | 8,17 | 0,28 | 2,6 | 0,15 | 15,1 | 1,52 | 80,48 | 92,95 | 94,15 |
| | Z72 | 49,5 | 0,48 | 14,4 | 4,46 | 1,96 | 0,03 | 9,27 | 0,42 | 1,81 | 0,13 | 17,3 | 1,27 | 76,86 | 89,2 | 90,83 |
| | Z73 | 49,8 | 0,48 | 13,9 | 3,44 | 1,79 | 0,03 | 10,7 | 0,51 | 1,54 | 0,19 | 17,5 | 1,33 | 77,26 | 85,73 | 88,73 |
| | Z74 | 48 | 0,47 | 13,8 | 3,62 | 1,96 | 0,03 | 11 | 0,49 | 1,83 | 0,17 | 18,4 | 1,4 | 76,64 | 88,47 | 89,05 |
| **Khakha** | Z76 | 38,8 | 0,41 | 12,1 | 2,83 | 1,91 | 0,04 | 17,6 | 0,53 | 1,82 | 0,17 | 23,2 | 2,07 | 72,42 | 83,72 | 86,83 |
| | Z78 | 34,5 | 0,34 | 11,2 | 2,63 | 1,7 | 0,05 | 20,7 | 0,43 | 1,77 | 0,15 | 26,3 | 2,46 | 76,69 | 86,2 | 88,26 |
| | Z83 | 39,4 | 0,46 | 12,4 | 3,27 | 1,76 | 0,06 | 17,9 | 0,57 | 1,9 | 0,12 | 21,8 | 2,09 | 74,28 | 84,69 | 86,27 |
| | Z85 | 45,4 | 0,57 | 14,6 | 3,83 | 2,11 | 0,04 | 12,2 | 0,55 | 2,32 | 0,15 | 18 | 1,48 | 76,78 | 85,8 | 88,46 |
| | Z86 | 45,9 | 0,56 | 14,1 | 3,85 | 2,01 | 0,05 | 12,1 | 0,56 | 2,24 | 0,17 | 18,3 | 1,51 | 75,88 | 87,15 | 87,91 |
| | Z101 | 48,51 | 0,76 | 13,06 | 3,96 | 1,57 | 0,01 | 13,26 | 0,39 | 3,15 | 0,04 | 15,6 | 1,76 | 73,29 | 87,72 | 90,63 |
| | Z104 | 32,85 | 0,58 | 11,97 | 3,33 | 1,42 | 0,02 | 23,38 | 0,72 | 2,96 | 0,08 | 22,74 | 2,71 | 67,75 | 77,85 | 82,76 |
| | Z120 | 49,15 | 0,68 | 12,24 | 4,07 | 1,64 | 0,01 | 14,23 | 0,47 | 2,77 | 0,08 | 15,18 | 1,93 | 72,57 | 85,02 | 88,26 |
| | Z124 | 43,61 | 0,62 | 12,57 | 3,87 | 1,73 | 0,01 | 16,83 | 0,53 | 2,82 | 0,09 | 17,72 | 2,09 | 72 | 83,83 | 87,26 |
| **Taourda** | Z126 | 45,9 | 0,61 | 11,75 | 3,77 | 1,43 | 0,01 | 16,32 | 0,5 | 2,56 | 0,08 | 17,04 | 2,17 | 72,3 | 83,83 | 87,16 |
| | Z133 | 52,15 | 0,8 | 14,56 | 4,75 | 1,65 | 0,02 | 9,75 | 0,43 | 3,12 | 0,12 | 13,17 | 1,39 | 74,95 | 88,25 | 90,72 |

| | | | | | | | | | | | | | | | |
|---|---|---|---|---|---|---|---|---|---|---|---|---|---|---|---|
| Z135 | 42,97 | 0,59 | 11,59 | 3,56 | 1,33 | 0,03 | 18,81 | 0,52 | 2,36 | 0,08 | 18,7 | 2,07 | 72,69 | 83,38 | 86,55 |
| Z141 | 41,95 | 0,61 | 12,87 | 4,07 | 1,45 | 0,02 | 15,13 | 0,39 | 2,27 | 0,08 | 20,28 | 2,46 | 77,48 | 89,03 | 90,93 |

**Table 6** Trace elements geochemistry (in ppm) and selected elemental ratios of the Zoumi mudrock samples.

| Sample | Z18 | Z20 | Z38 | Z41 | Z46 | Z48 | Z62 | Z65 | Z69 | Z73 | Z83 | Z86 | Z106 | Z120 | Z128 | Z132 | Z135 | *Mean* | *SD* |
|---|---|---|---|---|---|---|---|---|---|---|---|---|---|---|---|---|---|---|---|
| ***Trace elements (ppm)*** | | | | | | | | | | | | | | | | | | | |
| Ba | 231 | 237 | 282 | 302 | 269 | 271 | 202 | 277 | 313 | 255 | 179 | 269 | 238 | 213 | 224 | 236 | 550 | ***267.53*** | ***80.87*** |
| Co | 6 | 10 | 1 | 2 | 1 | 2 | 4 | 1 | 2 | 1 | 1 | 7 | 2 | 1 | 1 | 4 | 4 | ***2.94*** | ***2.61*** |
| Nb | 8 | 5 | 16 | 7 | 22 | 13 | 9 | 3 | 12 | 8 | 11 | 5 | 4 | 14 | 16 | 3 | 13 | ***9.94*** | ***5.34*** |
| Ni | 42 | 38 | 65 | 42 | 48 | 36 | 43 | 42 | 45 | 42 | 42 | 62 | 41 | 43 | 30 | 45 | 40 | ***43.88*** | ***8.39*** |
| Cr | 56 | 53 | 97 | 68 | 94 | 71 | 54 | 80 | 76 | 76 | 65 | 84 | 89 | 76 | 60 | 95 | 70 | ***74.35*** | ***14.24*** |
| Pb | 6 | 46 | 51 | 79 | 73 | 53 | 59 | 58 | 79 | 68 | 18 | 18 | 90 | 82 | 88 | 44 | 73 | ***57.94*** | ***25.31*** |
| Sr | 404 | 646 | 331 | 266 | 322 | 253 | 288 | 246 | 350 | 175 | 502 | 381 | 213 | 190 | 508 | 180 | 314 | ***327.59*** | ***129.54*** |
| V | 86 | 61 | 110 | 100 | 104 | 80 | 66 | 106 | 109 | 81 | 75 | 96 | 117 | 97 | 83 | 114 | 88 | ***92.53*** | ***16.74*** |
| Zn | 123 | 57 | 79 | 66 | 79 | 51 | 76 | 76 | 111 | 69 | 49 | 81 | 128 | 112 | 47 | 77 | 76 | ***79.82*** | ***24.92*** |
| Zr | 56 | 54 | 75 | 73 | 86 | 79 | 44 | 78 | 67 | 80 | 57 | 63 | 105 | 67 | 61 | 63 | 62 | ***68.82*** | ***14.35*** |
| Sc | 8.45 | 6.48 | 9.66 | 9.92 | 10.36 | 8.26 | 6.09 | 10.54 | 10.58 | 7.39 | 7.73 | 10.89 | 10.62 | 8.61 | 8.74 | 12.09 | 9.68 | ***9.18*** | ***1.65*** |
| Y | 13.75 | 11.80 | 14.38 | 13.06 | 13.27 | 13.15 | 12.25 | 13.92 | 13.92 | 13.70 | 12.57 | 17.57 | 12.75 | 11.18 | 14.15 | 12.46 | 14.50 | ***13.43*** | ***1.41*** |
| La | 20.11 | 15.10 | 24.19 | 22.30 | 23.75 | 21.45 | 16.11 | 23.26 | 23.52 | 21.75 | 19.85 | 25.88 | 26.44 | 20.68 | 22.50 | 25.68 | 22.75 | ***22.08*** | ***3.10*** |
| Ce | 35.46 | 26.97 | 45.74 | 41.00 | 44.61 | 40.89 | 28.98 | 43.90 | 43.80 | 42.88 | 37.77 | 49.93 | 50.47 | 39.57 | 40.80 | 49.43 | 43.05 | ***41.49*** | ***6.52*** |
| Nd | 18.18 | 13.57 | 22.04 | 20.10 | 20.78 | 19.20 | 15.07 | 20.67 | 20.46 | 20.31 | 18.14 | 23.78 | 22.30 | 18.44 | 19.47 | 22.53 | 20.20 | ***19.72*** | ***2.57*** |
| Sm | 3.52 | 2.65 | 4.33 | 3.83 | 3.93 | 3.66 | 2.99 | 3.93 | 3.88 | 4.04 | 3.51 | 4.65 | 4.01 | 3.54 | 3.70 | 4.18 | 3.93 | ***3.78*** | ***0.47*** |
| Eu | 0.77 | 0.60 | 0.90 | 0.83 | 0.85 | 0.75 | 0.65 | 0.83 | 0.83 | 0.87 | 0.72 | 0.99 | 0.76 | 0.70 | 0.78 | 0.87 | 1.20 | ***0.82*** | ***0.14*** |
| Gd | 3.48 | 2.65 | 4.13 | 3.65 | 3.70 | 3.52 | 2.98 | 3.73 | 3.65 | 3.91 | 3.37 | 4.53 | 3.70 | 3.34 | 3.57 | 3.83 | 3.73 | ***3.62*** | ***0.42*** |
| Er | 1.48 | 1.21 | 1.65 | 1.46 | 1.47 | 1.48 | 1.24 | 1.55 | 1.50 | 1.44 | 1.37 | 1.88 | 1.56 | 1.33 | 1.51 | 1.41 | 1.53 | ***1.47*** | ***0.15*** |
| Yb | 1.37 | 1.11 | 1.54 | 1.42 | 1.39 | 1.39 | 1.15 | 1.48 | 1.41 | 1.29 | 1.26 | 1.75 | 1.57 | 1.25 | 1.44 | 1.36 | 1.51 | ***1.39*** | ***0.16*** |
| Th | 4.55 | 3.41 | 5.94 | 5.54 | 5.64 | 5.16 | 3.42 | 5.58 | 5.43 | 5.38 | 4.46 | 6.00 | 6.71 | 5.24 | 5.35 | 6.01 | 5.16 | ***5.23*** | ***0.87*** |
| Ga | 16.08 | 13.80 | 18.67 | 18.44 | 19.30 | 16.56 | 12.75 | 18.98 | 20.82 | 16.13 | 12.66 | 18.92 | 19.08 | 15.12 | 16.93 | 20.51 | 87.90 | ***21.33*** | ***17.34*** |
| Rb | 66.85 | 53.25 | 82.15 | 77.23 | 82.68 | 79.74 | 49.45 | 88.76 | 87.38 | 51.27 | 62.56 | 85.82 | 98.00 | 74.72 | 87.27 | 100.40 | 78.50 | ***76.83*** | ***15.39*** |
| ***Ratios*** | | | | | | | | | | | | | | | | | | | |
| Eu/Eu* | 0.67 | 0.69 | 0.64 | 0.67 | 0.67 | 0.63 | 0.66 | 0.66 | 0.67 | 0.66 | 0.64 | 0.65 | 0.60 | 0.62 | 0.65 | 0.66 | 0.94 | ***0.67*** | ***0.07*** |
| $La_N/Yb_N$ | 9.96 | 9.18 | 10.65 | 10.58 | 11.55 | 10.45 | 9.47 | 10.62 | 11.26 | 11.36 | 10.64 | 9.99 | 11.35 | 11.14 | 10.60 | 12.79 | 10.21 | ***10.69*** | ***0.85*** |
| $Gd_N/Yb_N$ | 2.07 | 1.93 | 2.18 | 2.08 | 2.16 | 2.06 | 2.10 | 2.04 | 2.10 | 2.45 | 2.17 | 2.10 | 1.91 | 2.16 | 2.02 | 2.29 | 2.01 | ***2.11*** | ***0.13*** |
| Sm/Nd | 0.19 | 0.19 | 0.20 | 0.19 | 0.19 | 0.19 | 0.20 | 0.19 | 0.19 | 0.20 | 0.19 | 0.20 | 0.18 | 0.19 | 0.19 | 0.19 | 0.19 | ***0.19*** | ***0.00*** |
| La/Sc | 2.38 | 2.33 | 2.50 | 2.25 | 2.29 | 2.60 | 2.64 | 2.21 | 2.22 | 2.94 | 2.57 | 2.38 | 2.49 | 2.40 | 2.57 | 2.12 | 2.35 | ***2.43*** | ***0.20*** |
| Th/Sc | 0.54 | 0.53 | 0.62 | 0.56 | 0.54 | 0.62 | 0.56 | 0.53 | 0.51 | 0.73 | 0.58 | 0.55 | 0.63 | 0.61 | 0.61 | 0.50 | 0.53 | ***0.57*** | ***0.06*** |
| Zr/Sc | 6.63 | 8.33 | 7.76 | 7.36 | 8.30 | 9.56 | 7.22 | 7.40 | 6.33 | 10.82 | 7.37 | 5.79 | 9.89 | 7.79 | 6.98 | 5.21 | 6.40 | ***7.60*** | ***1.46*** |
| La/Co | 3.35 | 1.51 | 24.19 | 11.15 | 23.75 | 10.73 | 4.03 | 23.26 | 11.76 | 21.75 | 19.85 | 3.70 | 13.22 | 20.68 | 22.50 | 6.42 | 5.69 | ***13.38*** | ***8.35*** |
| Th/Co | 0.76 | 0.34 | 5.94 | 2.77 | 5.64 | 2.58 | 0.85 | 5.58 | 2.71 | 5.38 | 4.46 | 0.86 | 3.36 | 5.24 | 5.35 | 1.50 | 1.29 | ***3.21*** | ***2.04*** |
| La/Cr | 0.36 | 0.28 | 0.25 | 0.33 | 0.25 | 0.30 | 0.30 | 0.29 | 0.31 | 0.29 | 0.31 | 0.31 | 0.30 | 0.27 | 0.38 | 0.27 | 0.33 | ***0.30*** | ***1.13*** |
| Th/Cr | 0.08 | 0.06 | 0.06 | 0.08 | 0.06 | 0.07 | 0.06 | 0.07 | 0.07 | 0.07 | 0.07 | 0.07 | 0.08 | 0.07 | 0.09 | 0.06 | 0.07 | ***0.07*** | ***0.01*** |
| Cr/Th | 12.32 | 15.55 | 16.32 | 12.27 | 16.66 | 13.77 | 15.81 | 14.34 | 14.00 | 14.14 | 14.56 | 13.99 | 13.26 | 14.50 | 11.21 | 15.81 | 13.57 | ***14.24*** | ***1.49*** |
| Cr/Ni | 1.33 | 1.39 | 1.49 | 1.62 | 1.96 | 1.97 | 1.26 | 1.90 | 1.69 | 1.81 | 1.55 | 1.35 | 2.17 | 1.77 | 2.00 | 2.11 | 1.75 | ***1.71*** | ***0.28*** |
| Y/Ni | 0.33 | 0.31 | 0.22 | 0.31 | 0.28 | 0.37 | 0.28 | 0.33 | 0.31 | 0.33 | 0.30 | 0.28 | 0.31 | 0.26 | 0.47 | 0.28 | 0.36 | ***0.31*** | ***0.05*** |
| Cr/V | 0.65 | 0.87 | 0.88 | 0.68 | 0.90 | 0.89 | 0.82 | 0.75 | 0.70 | 0.94 | 0.87 | 0.88 | 0.76 | 0.78 | 0.72 | 0.83 | 0.80 | ***0.81*** | ***0.09*** |
| La+Ce/Co | 9.26 | 4.21 | 69.93 | 31.65 | 68.36 | 31.17 | 11.27 | 67.16 | 33.66 | 64.63 | 57.62 | 10.83 | 38.46 | 60.25 | 63.30 | 18.78 | 16.45 | ***38.65*** | ***24.20*** |
| La+Ce/Cr | 0.99 | 0.79 | 0.72 | 0.93 | 0.73 | 0.88 | 0.84 | 0.84 | 0.89 | 0.85 | 0.89 | 0.90 | 0.86 | 0.79 | 1.06 | 0.79 | 0.94 | ***0.86*** | ***0.09*** |
| La+Ce/Ni | 1.32 | 1.11 | 1.08 | 1.51 | 1.42 | 1.73 | 1.05 | 1.60 | 1.50 | 1.54 | 1.37 | 1.22 | 1.88 | 1.40 | 2.11 | 1.67 | 1.65 | ***1.48*** | ***0.28*** |

**Table 7** Mean Annual Precipitation (MAP) and Mean Annual Temperature (MAT) Estimated From Major Oxides Sample Compositions.

| Sample | MAP1 (mm/y) | MAP2 (mm/y) | MAP3 (mm/y) | MAT (°C) |
|---|---|---|---|---|
| Z2 | 1159,04 | 485,55 | 360,90 | 13,19 |
| Z4 | 1243,46 | 499,05 | 366,57 | 13,72 |
| Z5 | 1206,96 | 479,18 | 356,69 | 13,51 |
| Z6 | 1214,62 | 486,66 | 360,59 | 13,43 |
| Z7 | 1227,67 | 330,16 | 267,15 | 13,64 |
| Z17 | 1216,34 | 378,06 | 295,22 | 13,31 |
| Z18 | 1289,79 | 508,63 | 372,42 | 13,74 |
| Z19 | 1215,30 | 505,62 | 372,26 | 13,48 |
| Z20 | 1227,25 | 444,64 | 333,14 | 13,51 |
| Z22 | 805,19 | 707,91 | 506,09 | 14,45 |
| Z26 | 1287,26 | 602,17 | 434,29 | 13,66 |
| Z28 | 1237,11 | 557,50 | 403,85 | 13,62 |
| Z30 | 1299,04 | 577,61 | 421,26 | 13,67 |
| Z31 | 1278,11 | 655,13 | 463,57 | 14,61 |
| Z34 | 1255,65 | 422,46 | 320,06 | 13,91 |
| Z37 | 1221,42 | 534,26 | 391,21 | 13,39 |
| Z39 | 1289,40 | 572,70 | 417,44 | 13,63 |
| Z41 | 1235,96 | 630,23 | 456,96 | 13,83 |
| Z44 | 1180,02 | 445,19 | 335,83 | 13,18 |
| Z46 | 729,97 | 681,10 | 494,51 | 14,40 |
| Z48 | 1237,69 | 672,20 | 488,86 | 13,96 |
| Z54 | 1162,41 | 655,71 | 478,63 | 13,11 |
| Z59 | 1180,48 | 425,93 | 323,83 | 13,11 |
| Z61 | 1251,99 | 526,17 | 388,21 | 13,23 |
| Z62 | 1202,43 | 561,29 | 410,53 | 13,17 |
| Z65 | 1192,84 | 619,45 | 453,99 | 12,93 |
| Z66 | 1125,83 | 612,27 | 446,19 | 12,90 |
| Z69 | 1242,20 | 583,66 | 424,87 | 13,43 |
| Z70 | 997,04 | 835,00 | 605,28 | 15,12 |
| Z72 | 1257,99 | 655,01 | 472,04 | 13,89 |
| Z73 | 1228,04 | 627,78 | 448,77 | 13,96 |
| Z74 | 1232,66 | 615,32 | 445,81 | 13,56 |
| Z76 | 1200,97 | 506,33 | 375,63 | 12,95 |
| Z80 | 1221,45 | 466,71 | 349,07 | 12,96 |
| Z83 | 1192,96 | 506,93 | 373,86 | 12,83 |
| Z85 | 1224,24 | 600,64 | 438,99 | 12,97 |
| Z86 | 1216,38 | 596,69 | 435,87 | 12,91 |
| Z101 | 1255,16 | 525,56 | 387,13 | 11,56 |
| Z104 | 1142,93 | 385,76 | 301,47 | 10,51 |
| Z120 | 1221,43 | 495,67 | 369,40 | 11,60 |
| Z124 | 1207,10 | 466,07 | 350,91 | 11,52 |
| Z126 | 1205,64 | 462,38 | 346,11 | 11,64 |
| Z133 | 1256,50 | 608,81 | 441,63 | 12,11 |
| Z135 | 1197,02 | 431,55 | 325,72 | 11,85 |
| Z141 | 1259,54 | 505,01 | 367,94 | 12,84 |
| ***Sum*** | ***53932,49*** | ***24451,72*** | ***17980,73*** | ***594,51*** |
| ***Mean*** | ***1172,45*** | ***531,56*** | ***390,89*** | ***12,92*** |
| ***SD*** | ***106,96*** | ***99,14*** | ***65,61*** | ***0,89*** |

**Table 8** Range of trace elements ratios of the Zoumi mudrock samples compared to the ratios of sediments derived from felsic and mafic rocks (Cullers 1994, 2000; Cullers and Podkovyrov 2000), Upper Continental Crust (UCC; McLennan et al. 2006), and Post-Archaean Australian shale (PAAS; Taylor and McLennan 1985).

| Elemental ratio | Zoumi sandstones (Present study) | | Range of sediments (Cullers 1994, 2000; Cullers and Podkovyrov 2000) | | UCC (McLennan et al. 2006) | PAAS (Taylor and McLennan 1985) |
|---|---|---|---|---|---|---|
| | Range | Average | Felsic rocks | Mafic rocks | | |
| Eu/Eu* | 0.60-0.94 | 0.67 | 0.32-0.83 | 0.70-1.02 | 0.65 | 0.66 |
| La/Sc | 2.12–2.94 | 2.43 | 2.5–16.3 | 0.43–0.86 | 2.21 | 2.4 |
| Th/Sc | 0.49–0.72 | 0.57 | 0.84–20.5 | 0.05–0.22 | 0.79 | 0.9 |
| Th/Co | 0.34–5.94 | 3.21 | 0.67–19.4 | 0.04–1.4 | 0.63 | 0.63 |
| Th/Cr | 0.06–0.08 | 0.07 | 0.13–2.7 | 0.43–0.86 | 2.21 | 2.4 |
| Cr/Th | 11.21–16.66 | 14.24 | 4.00–15 | 25–500 | 7.76 | 7.53 |

# PLATES

## PLATE DISPLAYING MAJOR FIELD SEDIMENTARY LITHOFACIES

**Plate 1**: Panoramic view of Basin Plain outcrop with thin-bedded and fine- to medium-grained sandstones alternating with thick nodular or massif and withish-greyish hemipelagic marls (a) and main basin plain lithofacies: (b) Ta-c Bouma divisions (Ta: ungraded massive level, Tb: parallel lamina, Tc: convoluted lamina); (c) nodular greyish marls; (d) thin-bedded fine-grained lenticular beds; (e) Tb-c Bouma divisions (Tb: parallel lamina; Tc: convoluted lamina).

**Plate 2**: Panoramic view of Fringe Lobe deposits with thin- to thick-bedded and fine- to medium-grained sandstones alternating with thick nodular or massif and greyish marls (a) and main fringe-lobe lithofacies: (b) Ta-c/Ta/e Bouma divisions (Ta: normal-graded level, Tb: parallel lamina, Tc: parallel cross lamina and wavy ripples, Ta: ungraded level, Te: massive whitish-greyish marls); (c) Tb-e Bouma divisions, Tb: parallel lamina, Tc: wavy ripples, convoluted lamina, parallel cross lamina, wavy ripples, Td: fine-grained silty marly, Te: massive whitish-greyish marls level), (d) normal graded bed : Tb/Ta Bouma divisions, Tb: coarse- to medium-grained parallel strata, Ta: massive sandstone level with water escape structure); (e) Tb-c/e fine-grained Bouma divisions (Tb: parallel lamina, Tc: convoluted lamina, Te: massive whitish-greyish marls).

**Plate 3:** Panoramic view of Lobe deposits with thick-bedded and medium- to coarse-grained sandstones alternating with thin witish marls (a) and main lobe lithofacies: (b) medium- to coarse-grained thick-bedded sandstone with decimetric mudclasts, (c) medium- to coarse-grained thick-bedded sandstone with basal load structures (gutters), (d) medium-grained thick-bedded sandstone bed with secondary sedimentary structures (dishs and pillars), (e) normal-gradded coarse- to medium-grained Ta-b Bouma divisions and reverse-gradded medium- to coarse-grained Ta-b/Ta Bouma divisions.

**Plate 4:** Channel fill lithofacies with Sandy debris flow deposits with fine-grained sandstone matrix bearing centimetric to decimetric medium-grained sandstone boulders (a, b); irregular and highly erosive beds (c, d) and slumped levels (d).

**Plate 5:** Matrix-supported conglomerates occurring as singular events through the Zoumi basin. Sandy- marly-matrix bearing centimetric to decimetric sandstones pebbles and boulders.

Plate 1: Panoramic view of Basin Plain outcrop with thin-bedded and fine- to medium-grained sandstones alternating with thick nodular or massif and withish-greyish hemipelagic marls (a) and main basin plain lithofacies (b, c, d, e).

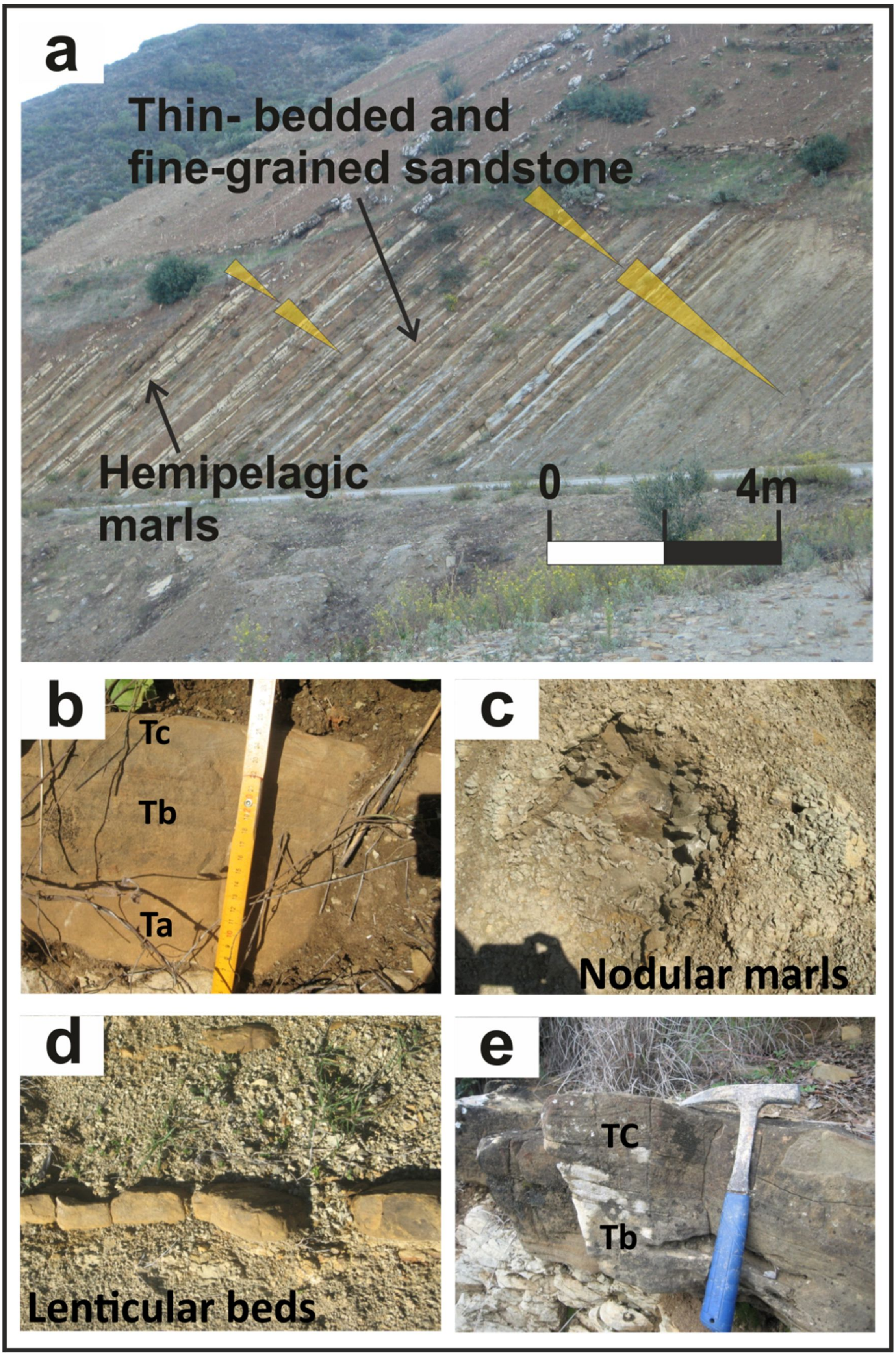

Plate 2: Panoramic view of Fringe Lobe deposits with thin- to thick-bedded and fine- to medium-grained sandstones alternating with thick nodular or massif and greyish marls (a) and main fringe-lobe lithofacies (b, c, d, e).

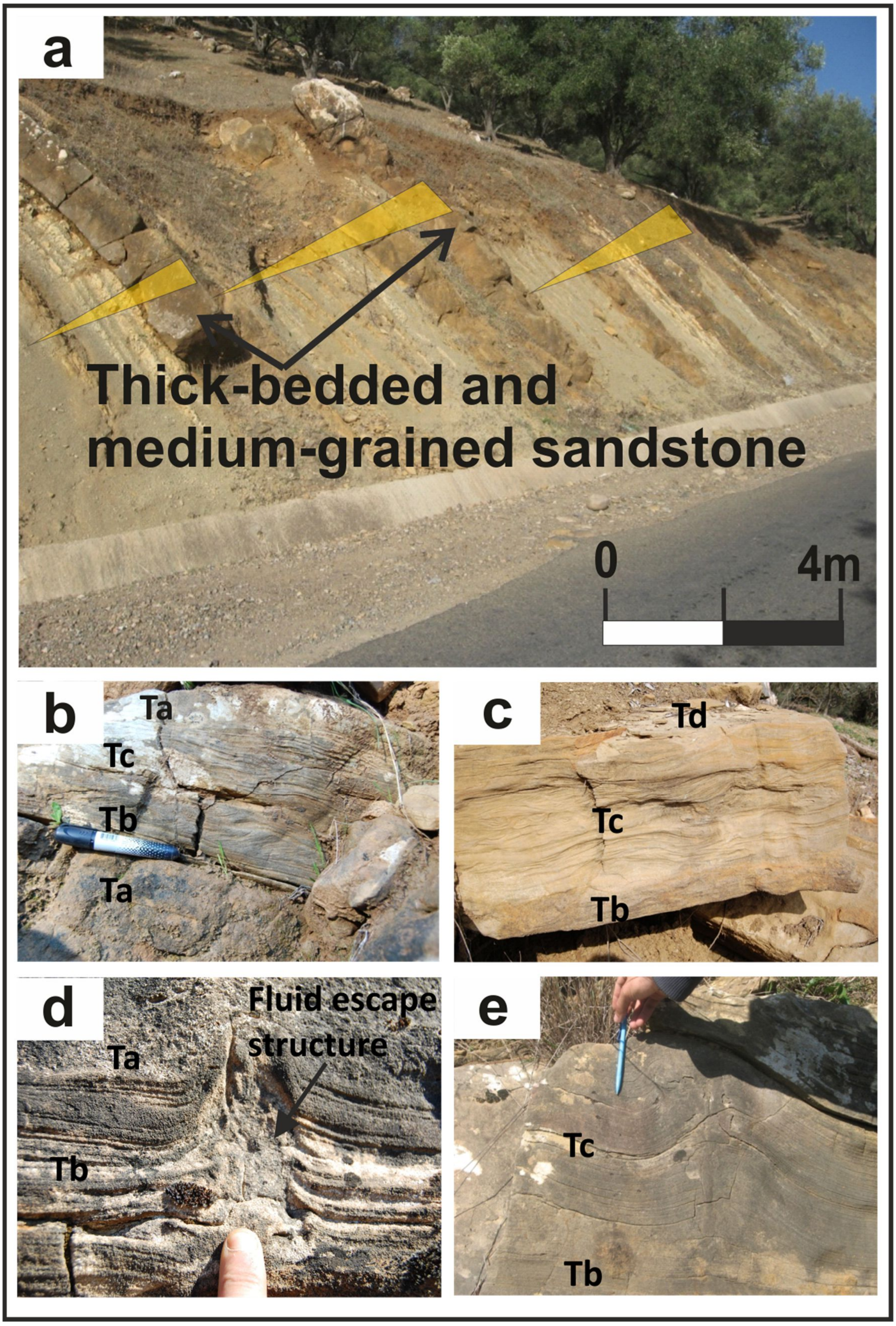

Plate 3: Panoramic view of Lobe deposits with thick-bedded and medium- to coarse-grained sandstones alternating with thin witish marls (a) and main lobe lithofacies (b, c, d, e).

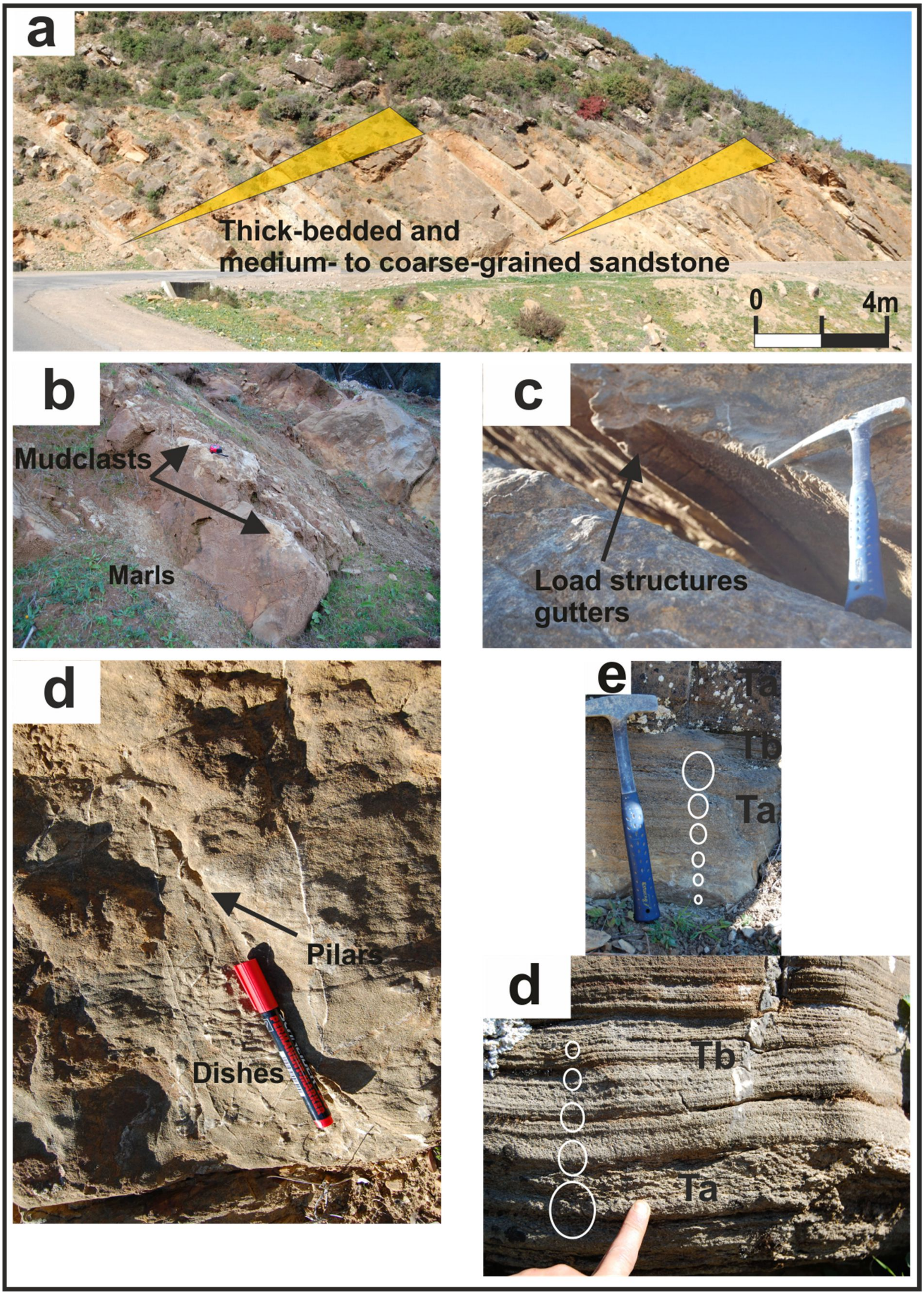

Plate 4: Channel fill lithofacies with Sandy debris flow deposits (a, b); irregular and highly erosive beds (c, d) and slumped levels (d).

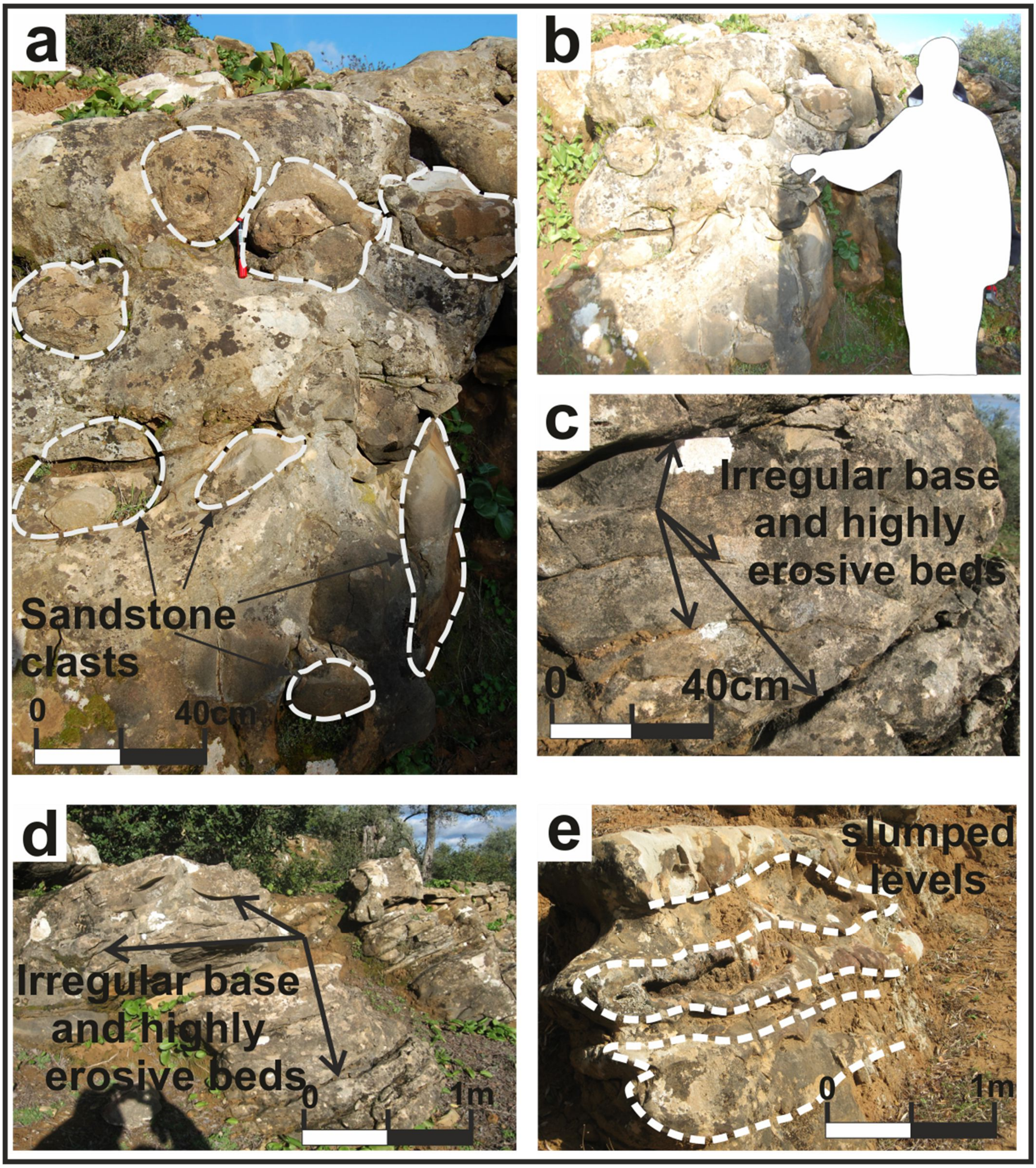

Plate 5: Matrix-supported conglomerates occurring as singular events through the Zoumi basin.

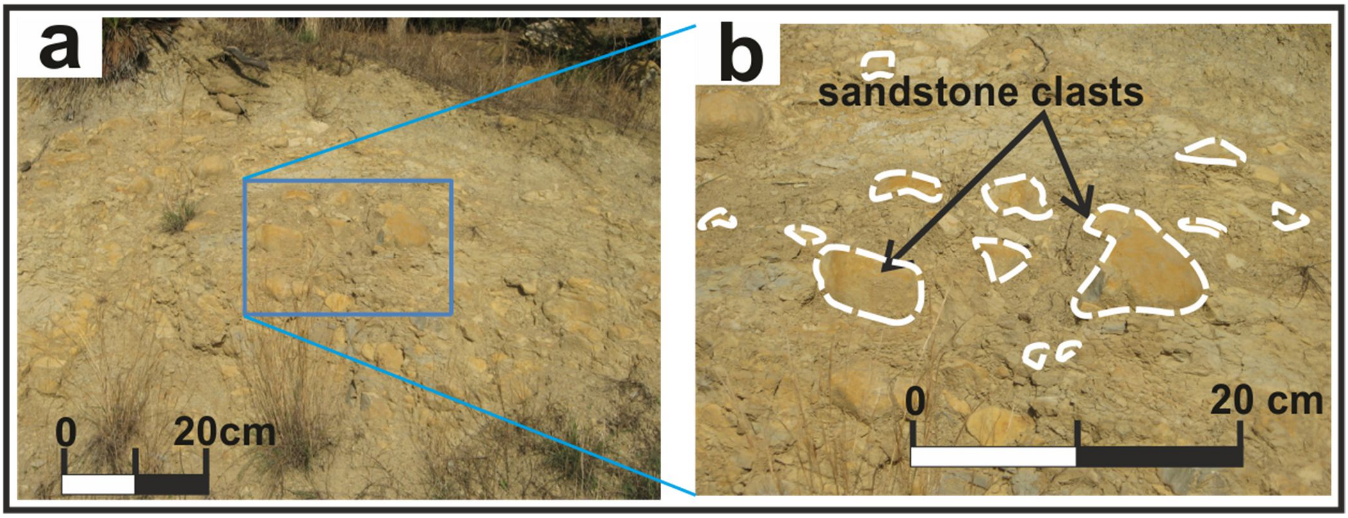

# APPENDIX 1

## Samples for Petrography

| Samples | Geographic coordinates | |
|---|---|---|
| | X | Y |
| Z3 | 34°47'857'' | 5°21'135'' |
| Z4 | 34°47'857'' | 5°21'136'' |
| Z8 | 34°48'006'' | 5°21'301'' |
| Z10 | 34°48'076'' | 5°21'337'' |
| Z11 | 34°48'107'' | 5°21'364'' |
| Z12 | 34°48'235'' | 5°21'446'' |
| Z13 | 34°48'260'' | 5°21'458'' |
| Z15 | 34°48'399'' | 5°21'484'' |
| Z17 | 34°48'008'' | 5°21'110'' |
| Z23 | 34°48'049'' | 5°21'120'' |
| Z25 | 34°48'135'' | 5°21'124'' |
| Z27 | 34°48'155'' | 5°21'133'' |
| Z29 | 34°48'178'' | 5°21'165'' |
| Z32 | 34°48'220'' | 5°21'190'' |
| Z33 | 34°48'223'' | 5°21'217'' |
| Z36 | 34°48'297'' | 5°21'227'' |
| Z37 | 34°48'311'' | 5°21'249'' |
| Z40 | 34°48'393'' | 5°21'307'' |
| Z42 | 34°48'606'' | 5°21'595'' |
| Z43 | 34°48'648'' | 5°21'652'' |
| Z47 | 34°48'824'' | 5°21'464'' |
| Z50 | 34°50'584'' | 5°20'861'' |
| Z51 | 34°50'635'' | 5°20'830'' |
| Z52 | 34°50'870'' | 5°20'820'' |
| Z53 | 34°50'877'' | 5°20'813'' |
| Z55 | 34°50'882'' | 5°20'784'' |
| Z56 | 34°50'823'' | 5°20'788'' |
| Z58 | 34°50'889'' | 5°20'733'' |
| Z60 | 34°50'918'' | 5°20'721'' |
| Z63 | 34°50'931'' | 5°20'700'' |
| Z64 | 34°50'950'' | 5°20'149'' |
| Z67 | 34°50'950'' | 5°20'693'' |
| Z68 | 34°50'967'' | 5°20'620'' |
| Z71 | 34°50'988'' | 5°20'555'' |
| Z75 | 34°56'632'' | 5°23'415'' |
| Z78 | 34°56'601'' | 5°23'385'' |

| Samples | Geographic coordinates | |
|---|---|---|
| | X | Y |
| Z80 | 34°56'517'' | 5°23'373'' |
| Z81 | 34°56'545'' | 5°23'354'' |
| Z84 | 34°56'588'' | 5°23'272'' |
| Z87 | 34°56'574'' | 5°23'250'' |
| Z118 | 34°56'48N | 5°23'41W |
| Z127 | 34°54'52N | 5°21'53W |
| Z131 | 34°54'54N | 5°21'42W |

# APPENDIX 2

## Samples for Geochemistry & Clay Mineralogy analysis

| Samples | Geographic coordinates | |
|---|---|---|
| | X | Y |
| Z1 | 34°47'786'' | 5°21'064'' |
| Z2 | 34°47'790'' | 5°21'161'' |
| Z4 | 34°47'857'' | 5°21'136'' |
| Z5 | 34°47'946'' | 5°21'243'' |
| Z6 | 34°47'975'' | 5°21'263'' |
| Z7 | 34°48'001'' | 5°21'283'' |
| Z16 | 34°48'008'' | 5°21'110'' |
| Z18 | 34°48'067'' | 5°21'127'' |
| Z19 | 34°48'124'' | 5°21'141'' |
| Z20 | 34°48'139'' | 5°21'136'' |
| Z22 | 34°48'071'' | 5°21'115'' |
| Z26 | 34°48'135'' | 5°21'129'' |
| Z28 | 34°48'162'' | 5°21'156'' |
| Z30 | 34°48'188'' | 5°21'187'' |
| Z31 | 34°48'200'' | 5°21'200'' |
| Z34 | 34°48'223'' | 5°21'217'' |
| Z38 | 34°48'311'' | 5°21'249'' |
| Z39 | 34°48'346'' | 5°21'271'' |
| Z41 | 34°48'560'' | 5°21'597'' |
| Z44 | 34°48'771'' | 5°21'615'' |
| Z46 | 34°48'816'' | 5°21'511'' |
| Z48 | 34°50'559'' | 5°20'878'' |
| Z54 | 34°50'877'' | 5°20'813'' |
| Z59 | 34°50'897'' | 5°20'732'' |
| Z61 | 34°50'923'' | 5°20'711'' |
| Z62 | 34°50'928'' | 5°20'706'' |
| Z65 | 34°50'950'' | 5°20'693'' |
| Z66 | 34°50'982'' | 5°20'641'' |
| Z69 | 34°50'992'' | 5°20'604'' |
| Z70 | 34°50'988'' | 5°20'556'' |
| Z72 | 34°51'002'' | 5°20'550'' |
| Z73 | 34°50'988'' | 5°20'510'' |
| Z74 | 34°50'012'' | 5°20'459'' |
| Z76 | 34°56'484'' | 5°23'388'' |
| Z79 | 34°56'517'' | 5°23'373'' |
| Z83 | 34°56'561'' | 5°23'328'' |
| Z85 | 34°56'574'' | 5°23'272'' |

| Samples | Geographic coordinates | |
|---|---|---|
| | X | Y |
| Z86 | 34°56'588'' | 5°23'250'' |
| Z101 | 34°56'450'' | 5°23'456'' |
| Z104 | 34°56'451'' | 5°23'461'' |
| Z106 | 34°56'452'' | 5°23'560'' |
| Z120 | 34°56'473'' | 5°23'400'' |
| Z124 | 34°54'520'' | 5°21'552'' |
| Z126 | 34°54'522'' | 5°21'549'' |
| Z128 | 34°54'523'' | 5°21'537'' |
| Z132 | 34°54'500'' | 5°21'430'' |
| Z133 | 34°54'502'' | 5°21'437 |
| Z135 | 34°54'503'' | 5°21'451'' |
| Z141 | 34°54'504'' | 5°21'480'' |